Modeling and numerical analysis of free surface flows

Pierrick Quemar

THÈSE DE DOCTORAT
DE L'UNIVERSITE PARIS 13

ÉCOLE DOCTORALE SCIENCES, TECHNOLOGIES, SANTÉ "GALILÉE"

SPÉCIALITÉ : MATHÉMATIQUES APPLIQUÉES

Présentée par

Pierrick QUEMAR

pour l'obtention du grade de

DOCTEUR DE L'UNIVERSITÉ PARIS 13

MODÉLISATION ET ANALYSE NUMÉRIQUE DES ÉCOULEMENTS À SURFACE LIBRE

Directeur de thèse :	Olivier LAFITTE	Prof.	Université Paris 13
		Dir. UMI-3457	CRM-Montréal
Co-directeur de thèse :	Emmanuel AUDUSSE	Mcf	Université Paris 13
Encadrants académiques :	Astrid DECOENE	Mcf	Université Paris Sud
Encadrants industriels :	Agnès LEROY	Ing.-Chercheur	EDF R&D | LHSV
	Chi-Tuân PHAM	Ing.-Chercheur	EDF R&D
Rapporteurs :	Miguel A. FERNÁNDEZ	Dr	Inria Paris
	Volker JOHN	Prof.	Weierstrass Institute

Soutenue publiquement le 27 septembre 2019 devant le jury composé de :

Président du jury :	Pascal OMNES	Prof. associé	CEA et Université Paris 13
Directeur de thèse :	Olivier LAFITTE	Prof.	Université Paris 13
		Dir. UMI-3457	CRM-Montréal
Co-directeur :	Emmanuel AUDUSSE	Mcf	Université Paris 13
Encadrants :	Astrid DECOENE	Mcf	Université Paris Sud
	Chi-Tuân PHAM	Ing.-Chercheur	EDF R&D
Rapporteur :	Miguel A. FERNÁNDEZ	Dr	Inria Paris
Examinateurs :	Cindy GUICHARD	Mcf	Sorbonne Université
	Laurence HALPERN	Prof.	Université Paris 13
Invitée :	Agnès LEROY	Ing.-Chercheur	EDF R&D | LHSV

PHD THESIS
OF UNIVERSITÉ PARIS 13

ÉCOLE DOCTORALE SCIENCES, TECHNOLOGIES, SANTÉ "GALILÉE"

ACADEMIC FIELD: APPLIED MATHEMATICS

Defended by

Pierrick QUEMAR

in order to become

DOCTOR FROM UNIVERSITÉ PARIS 13

MODELING AND NUMERICAL ANALYSIS OF FREE SURFACE FLOWS

Thesis supervisor:	Olivier LAFITTE	Prof.	Université Paris 13
		Dir. UMI-3457	CRM-Montréal
Thesis co-supervisor :	Emmanuel AUDUSSE	Mcf	Université Paris 13
Academic advisor:	Astrid DECOENE	Mcf	Université Paris Sud
Industrial advisors:	Agnès LEROY	Ing.-Chercheur	EDF R&D | LHSV
	Chi-Tuân PHAM	Ing.-Chercheur	EDF R&D
Referees:	Miguel A. FERNÁNDEZ	Dr	Inria Paris
	Volker JOHN	Prof.	Weierstrass Institute

Defended in public on September 29^{th}, 2019 in front of the committee members:

Committee president:	Pascal OMNES	Prof. associé	CEA et Université Paris 13
Thesis supervisor:	Olivier LAFITTE	Prof.	Université Paris 13
		Dir. UMI-3457	CRM-Montréal
Thesis co-supervisor:	Emmanuel AUDUSSE	Mcf	Université Paris 13
Advisors:	Astrid DECOENE	Mcf	Université Paris Sud
	Chi-Tuân PHAM	Ing.-Chercheur	EDF R&D
Referee:	Miguel A. FERNÁNDEZ	Dr	Inria Paris
Examiners:	Cindy GUICHARD	Mcf	Sorbonne Université
	Laurence HALPERN	Prof.	Université Paris 13
Guest:	Agnès LEROY	Ing.-Chercheur	EDF R&D | LHSV

Thèse effectuée au sein du
Laboratoire d'Analyse, Géométrie et Application
UMR CNRS 7539, 93430 Villetaneuse, FRANCE

et du

Laboratoire National d'Hydraulique Et Environnement
Division Recherche et Développement
Électricité de France
6 Quai Watier, 78400 Chatou, FRANCE

Financements : ANRT (bourse CIFRE #2015-1385) et EDF R&D

Résumé

Dans cette thèse, nous nous intéressons à la résolution numérique des équations tridimensionnelles de Navier–Stokes à surface libre, écrites sous formalisme ALE, par la méthode des éléments finis. Ces équations permettent la représentation d'écoulements environnementaux. L'objectif initial et principal porte sur une analyse précise des limitations existantes des méthodes numériques et de possibles voies d'amélioration, mathématiquement justifiées, afin de réviser et d'améliorer le cœur numérique du code hydrodynamique Telemac-3D, développé par le Laboratoire National d'Hydraulique et Environnement d'EDF R&D. Nous décrivons ainsi précisément l'algorithme de ce dernier et nous l'évaluons à l'aune des publications les plus récentes. Ainsi, au sein de ce logiciel, les équations de Navier–Stokes à surface libre dans lesquelles la pression a été décomposée en une partie hydrostatique et une partie non-hydrostatique sont résolues. Une des limitations majeures concerne le fait que la vitesse calculée ne satisfait pas l'équation de continuité. De plus, nous avons relevé l'existence d'une restriction sur le pas de temps.
Des voies alternatives sont explorées, et un algorithme très différent est analysé et programmé à des fins de comparaison. La stratégie numérique consiste à convecter la surface libre, à mettre à jour le domaine et à résoudre ensuite les équations de Navier–Stokes. Considérant cette approche, nous analysons un schéma éléments finis explicite d'ordre 1 en temps avec un terme de stabilisation symétrique pour l'équation cinématique de surface libre. Nous montrons que ce schéma permet de satisfaire deux propriétés importantes : la conservation globale de la masse d'eau et la divergence nulle faible. De plus, nous démontrons la stabilité conditionnelle de l'algorithme et nous proposons une nouvelle formulation variationnelle associée aux équations de Navier–Stokes permettant d'aboutir à un schéma éléments finis semi-implicite en temps, qui est stable indépendamment de la vitesse du domaine et d'une vitesse de convection à divergence nulle exacte.
Finalement, certains modèles simplifiés utilisés dans d'autres logiciels développés par EDF R&D, notamment le modèle asymptotique en fréquence de Berkhoff utilisé au sein du logiciel Artemis [51], sont également étudiés afin d'acquérir une vue d'ensemble du domaine. L'équation de Berkhoff est dérivée asymptotiquement des équations de la houle linéaire. Une étude systématique de la dérivation de différents modèles simplifiés (Berkhoff, Shallow water linéaire, Helmholtz) à partir des équations de la houle linéaire est effectuée. Le calcul d'une solution approchée des équations de Berkhoff utilisant des résultats de l'optique géométrique complète ce chapitre.

Mots-clés : équations de Navier–Stokes à surface libre ; méthode Arbitrary Lagrangian-Eulerian ; écoulements tridimensionnels ; Telemac-3D ; méthode des éléments finis ; méthode de stabilisation ; analyse numérique ; équations des vagues ; modèles asymptotiques.

Abstract

In this thesis, we are interested by Finite Elements methods for the three-dimensional free surface Navier–Stokes equations under the ALE formulation. They enable to simulate geophysical flows. The initial and main goal is to analyse the existing limitations of these numerical methods and to provide perspectives of improvement, justified mathematically. This purpose helps us to present a review and improvement way for Telemac-3D, which is a hydrodynamics industrial software developed by the Laboratoire National d'Hydraulique et Environnement of EDF R&D. Therefore, we analyse precisely and we evaluate this algorithm, with respect to the recent scientific publications. This software solves the free surface Navier–Stokes equations with the decomposition of the pressure through a hydrostatic part and a dynamic part. A major limitation is that the velocity field of the fluid is not divergence-free. Furthermore, we highlight a time restriction on the time step.

Moreover, alternative approaches are studied and compared. In particular, we focus on a numerical strategy which consists in advecting the free surface, in updating the domain and in solving the Navier–Stokes equations. Based on this strategy, we analyze a first order explicit scheme in time with a Finite Elements stabilization term. The numerical method allows to ensure important properties: the mass conservation of the water quantity and the weak free divergence condition. We demonstrate that this scheme is conditionally stable in time. Besides, we propose a new variational formulation allowing to obtain a semi-implicit scheme in time combined with the Finite Elements method, which is stable independently from the velocity of the mesh and without an exact free divergence velocity.

Finally, in order to expand the hydrodynamic knowledges, some simplified models used in other software developed by EDF R&D are studied. In particular, we focus on the mild-slope equation solved in the software Artemis [51]. It is an asymptotic model derived from the linear water wave equation. As a consequence, we study the hypothesis and the validity of the derivation. An approximate analytical solution is additionally derived for this purpose. Moreover, comparisons with other asymptotic models, such as the linear shallow water equation or the Helmholtz equation, are presented.

Mots-clés : Navier–Stokes equations with free surface; Arbitrary Lagrangian-Eulerian method; three-dimensional flows; Telemac-3D, Finite Elements method; stabilization method; numerical analysis; water waves equation ; asymptotic models.

Remerciements

Au travers de ces quelques lignes, je souhaite remercier vivement toutes les personnes, qui, de près ou de loin, se sont impliquées dans la réalisation de cette thèse, tant par leur soutien personnel, que professionnel.

Mes premiers remerciements vont tout naturellement à mon directeur de thèse, Olivier Lafitte, pour son encadrement. Olivier s'est toujours montré investi et passionné afin de me guider tout au long de cette aventure. Il a aussi fait preuve d'une grande rigueur scientifique, qu'il s'est efforcé de me transmettre. Sa bonne humeur, sa culture, ainsi que son humour, auront fait de chaque réunion un moment spécial.

Je tiens ensuite à remercier Emmanuel Audusse, mon co-directeur de thèse, pour la confiance, la patience et le soutien qu'il m'a accordés. Emmanuel est incontestablement un élément central de la réussite de cette thèse et il a été le lien entre les nombreuses pistes explorées. Je lui suis ainsi très reconnaissant pour avoir toujours répondu avec précision aux diverses questions que je lui posais et pour la richesse professionnelle et culturelle qu'il m'aura transmise. Au-delà du scientifique, je le remercie enfin pour tous les carrés de chocolat partagés et pour m'avoir initié à la douceur des noix de cajou et d'autres condiments...

Parallèlement, je remercie chaleureusement Astrid Decoene, ma co-encadrante académique, pour son investissement scientifique, sa pédagogie et ses nombreuses idées, aussi intéressantes que pertinentes. Au-delà de l'impact inestimable qu'Astrid a eu sur mon travail, je lui suis très reconnaissant pour tous les conseils qu'elle m'a donnés et pour m'avoir également rassuré lorsque les doutes subsistaient. Je la remercie aussi pour les diverses conversations, scientifiques ou non, que nous avons pu avoir.

Je tiens également à remercier mes co-encadrants industriels, Agnès Leroy et Chi-Tuân Pham, pour leurs disponibilités et leurs expertises à la recherche des secrets de Telemac-3D. Je les remercie pour tous les conseils d'orientation et de parcours professionnel afin de suivre la voie la plus appropriée pour de nouvelles aventures. De plus, j'ai pris plaisir à discuter avec eux de sujets divers et variés que ce soit d'énergies, de voyages, de sorties sur Paris, d'alimentations (miam les nougats vietnamiens) ou encore de sports.

A tous mes encadrants cités plus haut : être sous votre encadrement a été très enrichissant et une réel chance. Merci !

Mes remerciements ne seraient pas complets si j'omettais Gabriel Barrenechea et Benjamin Melinand. Ainsi, je tiens à leur exprimer ma profonde gratitude pour la collaboration que j'ai pu avoir avec eux et pour leur apport, scientifique et personnel, substantiel. Je les remercie pour le temps qu'ils m'ont consacré, que ce soit pour répondre à mes

questions, pour me guider ou pour relire ce présent manuscrit et de m'avoir accueilli dans leurs contrées (professionnelles) respectives. Travailler avec eux a été très enrichissant et j'espère sincèrement que cette opportunité se représentera de nouveau.

Je tiens à exprimer ma profonde gratitude à mes rapporteurs Miguel Fernández et Volker John pour avoir accepté de passer du temps à la lecture et à l'évaluation de mon manuscrit. Je remercie également Cindy Guichard et Laurence Halpern d'avoir accepté de faire partie du jury en tant qu'examinatrices. Enfin, je tiens à remercier sincèrement Pascal Omnes pour avoir accepté de présider mon jury de thèse et pour les divers échanges que nous avons pu avoir à l'université Paris 13 ou ailleurs.

Je remercie chaleureusement les membres du Laboratoire Nationale d'Hydraulique et Environnement (LNHE) d'EDF R&D et du Laboratoire d'Hydraulique Saint-Venant (LHSV) que j'ai eu plaisir à côtoyer durant ces 3 années (+ epsilon) de thèse. Je remercie ainsi Nicole Goutal, directrice du LHSV pour l'accueil et pour l'intérêt porté sur le déroulement de la thèse. Je tiens aussi à remercier particulièrement mes collègues (ex)-thésards, sans ordre particulier : Adrien, Florent (Gigi Buffon), Florian, Marina, Sofiane, Sophia, Roberto (numero uno), Thomas ; un long chemin a été parcouru. Je remercie également mes co-bureaux qui auront chaleureusement égayé mes journées : Pat et Max (le Casoar, chut !). De manière plus générale, merci aux membres du LHSV et du LNHE, en particulier des groupes P74 et P73.

Mes remerciements vont également aux membres du Laboratoire Analyse, Géométrie et Applications (LAGA) de l'université Paris 13 avec qui j'aurais discuté à de trop rares occasions. Je tiens aussi à remercier chaleureusement les membres de l'équipe ANGE de l'INRIA pour m'avoir accueilli de temps à autre. Je remercie particulièrement Martin et Yohan pour les discussions échangées tant scientifiques que diverses et variées.

Je remercie mes amis de longue date pour leur soutien inconditionnel : Brice & Anne-Sophie, Alain & Mélissa, Quentin, Wilfried. C'est toujours avec un grand plaisir que je vous retrouve.

Je remercie enfin ma famille pour leur présence et pour leur réconfort. Un grand merci à mes parents et à mon frère qui ont toujours su m'encourager et me guider dans mes études et projets personnels ; les obstacles auraient été bien plus difficiles à franchir si vous n'aviez pas été là. Je remercie également mes grands-parents, mes tantes et mes oncles, ainsi que mes cousins pour leur appui sans faille. Merci enfin à la famille de Sherebanou pour leurs conseils et d'avoir toujours répondu présente malgré la distance.

Mes derniers remerciements vont à Sherebanou pour son sourire, sa bonne humeur et pour m'avoir soutenu, tout en restant patiente dans les moments difficiles ; tout court et tout simplement : *Shukriyaa.*

Contents

List of Figures

List of Tables

Chapter 1

Introduction

Contents

1.1 Motivation et objectif de la thèse

L'étude et la simulation numérique de phénomènes hydrauliques est un enjeu scientifique et industriel majeur. Elles permettent plus généralement de comprendre et de prédire des événements naturels tels que les tsunamis, la montée des eaux, l'érosion... Du point de vue industriel, il s'agit entre autres, pour un producteur d'électricité, de simuler l'évolution des cours d'eau à proximité de ses aménagements afin d'en assurer la performance et la sûreté des ouvrages dans le respect des contraintes environnementales. Par ailleurs, l'industriel doit être capable de prévoir les effets de ses aménagements sur le milieu mais aussi d'anticiper les effets des actions d'autres acteurs, ou de l'évolution naturelle du système. Compte tenu de l'importance de bien appréhender ces problèmes, des études mathématiques et physiques n'ont cessé de se multiplier. Par la suite, de nombreux outils industriels et académiques dédiés à la simulation numérique des écoulements à surface libre ont émergé. Par exemple, nous trouvons dans le milieu académique : Elcom [78], FVCOM [89], MITgcm [99], OpenFOAM [84], POM [12], POP [49, 98], ROMS [87, 121], Selfe [140], Suntans [60]. Par ailleurs, dans le domaine industriel, nous pouvons trouver Adcirc [97], Delft3D [94], flow-3D [120] , Fluent [8], MIKE21 [135], (Un)Trim [30, 33] et Telemac-3D [76]. Ce dernier, appartenant à la suite de logiciels hydrodynamiques Telemac-Mascaret, est un logiciel développé par le Laboratoire National d'Hydraulique et Environnement (LNHE), faisant partie de la division Recherche et Développement (R&D) d'EDF. Celui-ci permet la simulation numérique des écoulements environnementaux 3D à l'échelle locale (kilométrique). Il permet en outre de traiter des écoulements à géométries complexes telles que des vagues non-linéaires. Pour cela, les équations 3D de Navier–Stokes à surface libre pour des écoulements incompressibles, laminaires ou turbulents, sont résolues. La résolution de ces équations est basée sur une méthode éléments finis.

L'objectif initial et principal de cette thèse est de proposer des méthodes numériques pour améliorer le code Telemac-3D afin de simuler des vagues non-linéaires. Telemac-3D est un logiciel libre initialement développé par le Laboratoire National d'Hydraulique et Environnement d'EDF R&D qui est inscrit au sein du système « Telemac-Mascaret ». Il est dédié à la résolution d'écoulements 3D à surface libre à grande échelle, par exemple en milieu océanique, maritime, fluvial... Couplé à d'autres modèles appartenant à la suite Telemac-Mascaret, son domaine d'applications peut être étendu à des problèmes liés à l'environnement tels que l'étude de la qualité de l'eau, la sédimentologie, etc. Afin de réviser le cœur numérique du code, une analyse précise des limitations des méthodes existantes, ainsi que des propositions d'amélioration, mathématiquement justifiées, seront faites. Le chapitre 2 a ainsi pour but de replacer le contexte et d'introduire les différentes formulations et résolutions possibles des équations de Navier–Stokes à surface libre. Il constituera ainsi une base aux chapitres qui suivront. Le chapitre 3 sera dédié à l'algorithme de Telemac-3D qui sera ainsi décrit précisément et évalué à l'aune des publications les plus récentes sur le sujet. Des voies alternatives ont été explorées, et un algorithme très différent a été analysé et programmé en utilisant la bibliothèque FreeFem++ [75] à des fins de comparaison. Cette méthode permettant de conserver la masse de la quantité d'eau est présentée dans le chapitre 4. Pour finir, certains modèles

simplifiés utilisés dans d'autres logiciels développés par EDF, notamment le modèle en fréquence de Berkhoff, ont également été étudiés dans le chapitre 5, afin d'acquérir une vue d'ensemble du domaine. Les hypothèses de dérivation de ce modèle et son domaine de validité ont été revisités.

1.2 Principaux modèles pour les écoulements à surface libre

1.2.1 Équations de Navier–Stokes à surface libre

Le mouvement d'un fluide newtonien et d'un écoulement incompressible est régi par les équations de Navier–Stokes. Il s'agit d'équations aux dérivées partielles posées dans un domaine tridimensionnel $\Omega_t = \{(x, y, z \mid (x, y) \in \omega \text{ and } b(x, y) < z < \eta(x, y, t)\}$, avec ω un domaine fixe horizontal, dont les inconnues sont la vitesse du fluide $\mathbf{u}$, la densité du fluide ρ et la pression p. Nous supposerons dans toute cette thèse que la densité du fluide est constante. Par ailleurs, nous considérerons $\mathcal{D}_T = \{(\boldsymbol{x}, t) \mid t \in]0, T[, \ \boldsymbol{x} \in \Omega_t\}$. Ces équations expriment la conservation de la masse du fluide et la conservation de la quantité de mouvement. La forme non-conservative de ces équations s'écrit à tout instant t sur Ω_t:

$$\begin{cases} \dfrac{\partial \mathbf{u}}{\partial t} + \big(\mathbf{u} \cdot \nabla\big)\mathbf{u} - \nu \Delta \mathbf{u} + \dfrac{1}{\rho}\nabla p = \mathbf{f} + \mathbf{g}, & \text{sur } \ \mathcal{D}_T, \qquad (1.1) \\ \nabla \cdot \mathbf{u} = 0, & \text{sur } \ \mathcal{D}_T. \qquad (1.2) \end{cases}$$

avec ν la viscosité cinématique moléculaire telle que la viscosité dynamique moléculaire μ, supposée constante, satisfait $\mu = \nu\,\rho$. Les forces extérieures pouvant s'appliquer sur le fluide sont représentées par $\mathbf{f}$. La force de gravité est quant à elle notée $\mathbf{g} = (0, 0, -g)$.

Dans le cas d'un écoulement à surface libre, les équations de Navier–Stokes sont couplées à une équation d'advection sur la surface libre η et écrite le domaine horizontal ω tel que:

$$\frac{\partial \eta}{\partial t} + (\boldsymbol{u}^{hor}_{|_{z=\eta}} \cdot \nabla_{hor})\,\eta = w_{|_{z=\eta}}, \quad \text{sur } \ \omega \times]0, T[. \qquad (1.3)$$

avec $\boldsymbol{u}^{hor}_{|_{z=\eta}}$ la composante horizontale de la vitesse du fluide à la surface libre et $w_{|_{z=\eta}}$ la composante verticale. L'opérateur $\nabla_{hor} = (\partial_x, \partial_y)$ désigne le gradient horizontal. Cette équation est la condition cinématique à la surface libre et traduit le fait qu'une particule de fluide ne traverse pas la surface libre. Notons que la surface libre est considérée de façon univoque [1].

Contrairement aux équations simplifiées de Navier–Stokes hydrostatiques à surface libre (introduites dans la section suivante), les équations de Navier–Stokes à surface libre permettent de traiter des écoulements pour lesquels l'approximation hydrostatique ne

[1] Cela implique donc qu'un tel modèle ne peut être utilisé afin de représenter un écoulement présentant un déferlement de la surface libre. Il s'agit d'une limitation importante mais qui se retrouve dans de nombreux modèles dédiés à la simulation des vagues (Berkhoff [10], Zakharoff [138], etc.)

s'applique pas. Ceci à cause d'un fort gradient de surface libre ou de fond, ou de petites longueurs d'onde par rapport à la hauteur d'eau. Ils prennent en compte des phénomènes 3D plus variés, comme les mouvements orbitaux, les recirculations verticales intensives, les écoulements autour d'obstacles, dans lesquels la pression est fortement non-hydrostatique. Des stratégies numériques de résolutions pour ces équations ont été étudiées par différents auteurs tels que Maury [100] et Decoene et Maury [46]. Dans ce travail de thèse, nous proposerons une méthode numérique afin de résoudre ces équations.

1.2.2 Équations de Navier–Stokes hydrostatiques à surface libre

L'approximation hydrostatique consiste à négliger les accélérations de la vitesse verticale, ainsi que les termes de diffusion et les termes sources dans l'équation de quantité de mouvement sur w. Cette dernière équation se réduit ainsi à :

$$\frac{\partial p}{\partial z} = -\rho\, g.$$

Par conséquent, la pression ne varie sur la verticale qu'en fonction du poids de la colonne d'eau et est ainsi appelée pression hydrostatique. Elle correspond à :

$$p = -\rho\, g(z - \eta) + p_{atm}. \tag{1.4}$$

avec p_{atm} la pression atmosphérique. Cette hypothèse est en particulier valable pour un fluide au repos et pour les écoulements en eaux peu profondes, c'est-à-dire pour des écoulements où la dimension horizontale caractéristique est grande par rapport à la profondeur.

Ces approximations sont au cœur de la dérivation de modèles simplifiés, plus facile à résoudre numériquement que le problème de Navier–Stokes complet. L'analyse mathématique du problème simplifié n'en est pas plus aisée pour autant. Dérivées des équations de Navier–Stokes sous l'hypothèse hydrostatique, les équations de Navier–Stokes hydrostatiques à surface libre, parfois appelées équations de « Saint-Venant tridimensionnelles », sont :

$$\begin{cases} \left.\dfrac{\partial \boldsymbol{u}^{hor}}{\partial t}\right|_{\widehat{\Omega}} + (\mathbf{u}\cdot\nabla)\,\boldsymbol{u}^{hor} - \nu\Delta\boldsymbol{u}^{hor} + g\,\nabla_{hor}\eta = \boldsymbol{f}_{xy}, & \text{sur } \mathcal{D}_T, \\ \dfrac{\partial \eta}{\partial t} + \nabla_{hor}\cdot\left(\displaystyle\int_b^\eta \boldsymbol{u}^{hor}\,dz\right) = 0, & \text{sur } \omega\times]0,T[, \\ \nabla_{hor}\cdot\boldsymbol{u}^{hor} + \dfrac{\partial w}{\partial z} = 0, & \text{sur } \mathcal{D}_T, \end{cases}$$

où $\boldsymbol{f}_{xy} \in \mathbb{R}^2$ désigne le terme source horizontal, b la topographie et $\nabla_{hor}\cdot$ les opérateurs horizontaux de gradient et divergence.
L'équation conservative à la surface libre est obtenue en intégrant sur la verticale l'équation de continuité. Cette équation est appelée en anglais « depth-averaged free surface equation ». Remarquons que l'équation de continuité est conservée dans le système afin de

coupler les composantes horizontales et verticale de la vitesse. Les équations de Navier–Stokes hydrostatiques à surface libre sont valides pour des écoulements en eaux peu profondes et à faible accélération de la vitesse verticale, dans lesquels les gradients de pression et de fond restent faibles. Ce modèle a par exemple été adopté par Casulli et Cattani [29], Fontana et al. [56] et Hervouet [76]. Le logiciel Telemac-3D était initialement basé sur les équations 3D de Navier–Stokes hydrostatiques. Ces équations peuvent toujours être résolues au sein de ce logiciel.

1.2.3 Équations de Navier–Stokes à surface libre avec décomposition de pression

La résolution complète des équations 3D de Navier–Stokes a largement été étudiée dans le but d'éviter les restrictions dues à l'approximation hydrostatique et ainsi, étendre les domaines d'applications. Dans le cadre des écoulements à surface libre, il existe différentes formulations des équations 3D de Navier–Stokes à surface libre qui mènent à des résolutions numériques différentes. Comme introduit précédemment, une première approche consiste à considérer directement les équations 3D de Navier–Stokes associées à la condition cinématique à la surface libre. Une seconde formulation consiste à décomposer la pression en une partie hydrostatique p_h et une partie dynamique p_d telle que $p = p_h + p_d$. Cette décomposition permet ainsi de faire apparaître explicitement la surface libre au travers de la pression hydrostatique. Les équations de Navier–Stokes 3D à surface libre avec décomposition de la pression s'écrivent alors à tout instant t:

$$
\begin{cases}
\left.\dfrac{\partial \boldsymbol{u}^{hor}}{\partial t}\right|_{\widehat{\Omega}} + \big(\mathbf{u}\cdot\nabla\big)\boldsymbol{u}^{hor} - \nu\,\Delta\boldsymbol{u}^{hor} + g\,\nabla_{hor}\eta + \dfrac{1}{\rho}\nabla_{hor}p_d = \mathbf{f}_{xy}, \quad \text{sur } \mathcal{D}_T, & (1.5)\\
\left.\dfrac{\partial w}{\partial t}\right|_{\widehat{\Omega}} + (\mathbf{u}\cdot\nabla)w - \nu\,\Delta w + \dfrac{1}{\rho}\dfrac{\partial p_d}{\partial z} = \mathbf{f}_z, \quad \text{sur } \mathcal{D}_T, & (1.6)\\
\nabla\cdot\mathbf{u} = 0, \quad \text{sur } \mathcal{D}_T, & (1.7)\\
\dfrac{\partial \eta}{\partial t} + \nabla_{hor}\cdot\displaystyle\int_b^\eta \boldsymbol{u}^{hor}\,dz = 0, \quad \text{sur } \omega\times]0,T[. & (1.8)
\end{cases}
$$

où $f_z \in \mathbb{R}$ est le terme source vertical.

Mahadevan et al [98] ont développé un modèle océanographique basé sur cette formulation et ont démontré que le problème est bien posé et qu'il permet de traiter les conditions aux limites physiques[2]. Numériquement, ces équations mènent à considérer une étape de prédiction hydrostatique et une étape de correction dynamique. La première étape permet de calculer la surface libre et une vitesse intermédiaire à divergence non nulle. La seconde étape permet quant à elle d'assurer la divergence nulle du vecteur vitesse du fluide en la corrigeant par la pression dynamique. Plusieurs approches numériques ont été développées pour la résolution de ces équations, par exemple par Casulli et Stelling [31],

[2] *i.e.* Non fictives, comme c'est le cas pour des frontières liquides.

Casulli et Zanolli [34], Miglio et al. [102] ou encore Hervouet [76]. Le logiciel Telemac-3D est basé sur cette formulation. Des stratégies numériques basées sur la méthode des éléments finis seront discutées dans le chapitre 2 et une étude détaillée de l'approche numérique effectuée au sein du logiciel Telemac-3D sera discutée dans le chapitre 3.

Le cœur de ce travail de thèse est de comparer les stratégies numériques basées sur les 2 formulations des équations de Navier–Stokes à surface libre, (1.1-1.3) et (1.5-1.8).

1.3 Points clés des méthodes numériques

1.3.1 Approximation spatiale et temporelle

Les méthodes d'approximation spatiale les plus souvent utilisées sont celles basées sur la construction de maillage. Elles correspondent aux méthodes des différences finies, des éléments finis ou des volumes finis. Des alternatives à ces méthodes existent telles que les méthodes Discontinuous Galerkin (DG) [40] ou la méthode Smooth Particle Hydrodynamics (SPH) [104, 133]. Cette dernière est une méthode entièrement Lagrangienne et sans maillage, utilisant des particules qui se déplacent sous l'influence des forces de pression, de viscosité et de pesanteur. Elle permet de simuler des cas d'écoulements complexes, en particulier les écoulements mixtes, le déferlement, et tous les cas où la surface libre ne peut pas être définie de manière univoque. De plus, elle traite avec grande précision les fortes déformations de surface libre.
La méthode des différences finies est la plus simple et permet la construction de schémas peu coûteux. Cependant, elle n'est utilisable qu'avec des maillages structurés et ne s'applique qu'aux problèmes posés sur des géométries simples. Elle pose en particulier des problèmes pour imposer des conditions aux limites et n'assure pas naturellement la conservation de la masse. Cette méthode est principalement utilisée en océanographie où il n'est pas nécessaire de discrétiser finement les frontières latérales du domaine. Dans le cadre des écoulements à surface libre, Casulli [28] et Vitousek et al. [134] ont par exemple proposé des approches numériques basées sur cette méthode.
La méthode des volumes finis est applicable sur des maillages non structurés et permet de discrétiser facilement des géométries complexes. Cette méthode permet d'assurer la conservation de la masse au niveau local. Dans le cadre des écoulements à surface libre, des approches numériques basées sur cette méthode ont par exemple été étudiées par Audusse et al. [5, 6], Marshall et al. [99].
La méthode des éléments finis, qui sera considérée dans ce travail de thèse, est basée sur la formulation variationnelle des équations aux dérivées partielles et s'inscrit dans un cadre théorique rigoureux. Cette méthode est aussi applicable sur des maillages non structurés. Elle offre une grande souplesse pour discrétiser des géométries complexes et imposer les conditions aux limites variées. Cependant, contrairement à la méthode des volumes finis, la conservation de la masse n'est le plus souvent assurée qu'au niveau global. Dans le cadre des écoulements à surface libre, Miglio et al. [102], Fontana et al. [56], Maury [100], Decoene [44, 46] ou encore Hervouet [76] ont proposé des résolutions numériques basées sur cette méthode. Le code Telemac-3D qui sera étudié dans cette thèse est basé

sur cette méthode.
Des études sont menées afin de combiner la méthode des volumes finis et celle des éléments finis afin de tirer parti des avantages de chacune d'entre elles. Les schémas distributifs par exemple, qui connaissent un fort engouement en mécanique des fluides, sont basés sur la méthode des volumes finis mais utilisent la structure de données des éléments finis [1].

Plusieurs choix existent concernant l'approximation temporelle des équations de Navier–Stokes à surface libre. Le traitement de chacun des termes peut être explicite ou implicite menant à la résolution de problèmes linéaires ou non. Différentes stratégies existent quant à la résolution des équations de Navier–Stokes à surface libre. Ces équations peuvent être résolues au travers d'une approche monolithique, à l'aide de solveurs non-linéaires et itératifs, ou au travers d'une approche découplée. Cette dernière consiste à décomposer le problème en plusieurs sous problèmes linéaires, en appliquant les méthodes numériques les plus adaptées aux caractéristiques mathématiques de chacun d'entre eux. Par exemple, Maury [100] a étudié une approche éléments finis dans laquelle l'équation cinématique à la surface libre (1.3) est résolue en utilisant une méthode explicite, suivie d'une résolution mixte des équations de Navier–Stokes (1.1-1.2).
Casulli [27] a proposé une approche semi-implicite en différences finies pour la résolution des équations de Navier–Stokes à surface libre avec décomposition de pression. Comme énuméré dans la sous-section 1.2.3, la stratégie est basée sur la résolution d'une partie de prédiction hydrostatique et d'une partie de correction dynamique. Casulli et Cattani [29] ont démontré un résultat de stabilité conditionnelle sous CFL pour la partie hydrostatique. Vitousek et al. [134] ont étendu l'étude de stabilité à l'approche numérique complète. La décomposition en une partie hydrostatique et dynamique peut être vue comme une méthode des pas fractionnaires ou une méthode de projection, d'après Guermond et al. [67].

1.3.2 Prise en compte du domaine mobile

L'une des grandes difficultés de la représentation mathématique des écoulements à surface libre vient du mouvement de la surface libre, et donc par extension du domaine. Plusieurs approches existent pour le traitement des équations dans un domaine mobile telles que l'approche Lagrangienne, l'approche Eulérienne ou encore la formulation « Arbitrary Lagrangian-Eulerian » (ALE).

L'approche Lagrangienne [104] consiste à suivre les particules du fluide le long de leur trajectoire et permet de représenter de manière précise la surface libre. Elle se heurte toutefois à plusieurs difficultés, en particulier les temps de calcul élevés, la difficulté d'imposer les conditions aux limites ou la difficulté d'établir des preuves de convergence et de stabilité.
L'approche Eulérienne traite au contraire le problème dans un maillage fixe. Cette approche est plus simple puisqu'elle ne nécessite pas de remaillage. Cependant, avec ce type de maillage, il est plus difficile de suivre de façon précise la surface libre ou d'appliquer

des conditions aux limites naturelles. Cette approche est par exemple présente dans les travaux de Fontana [56], Casulli et al. [33], Nakayama et Mori [105]...
La formulation « Arbitrary Lagrangian-Eulerian » a été introduite par Hirt et al. [77] et consiste à déplacer le maillage à une vitesse arbitraire, différente de celle du fluide, ce qui permet un réarrangement continu des mailles. Par ailleurs, ce formalisme rend la mise à jour du maillage totalement implicite et permet de s'affranchir de l'interpolation des variables à chaque pas de temps sur le nouveau maillage. La formulation ALE permet également de discrétiser plus facilement les dérivées partielles en temps. Dans le cadre des écoulements à surface libre, cette méthode a été utilisée par de nombreux auteurs tels que Decoene [44], Decoene et Maury [46], Huerta [79] ou encore Hervouet [76].
Dans ce manuscrit, nous considérerons une méthode ALE particulière nommée la transformation ALE-Sigma [45]. Cette méthode consiste à déplacer le maillage uniquement selon la verticale, en suivant la forme et les mouvements du fond et de la surface libre du domaine. Ce type de méthode ALE permet une représentation continue de la surface libre et du fond. Elle simplifie l'imposition des conditions aux limites et permet d'incorporer facilement des couches limites. Initialement, la transformation était considérée comme une méthode à part entière et le lien avec la méthode ALE était peu connu. Decoene et Gerbeau [44, 45] ont démontré que la transformation Sigma était une formulation ALE spécifique. Différentes formes de la transformation ALE-Sigma existent. Une méthode classique consiste à adopter une transformation linéaire selon la verticale. Cependant, ce type de transformation peut entraîner des erreurs importantes en raison du fait que les mouvements sur la verticale se font toujours d'un bloc sur la colonne d'eau. Il n'est donc pas possible d'adapter la discrétisation verticale à l'écoulement considéré. Decoene et Gerbeau [45] ont introduit une transformation ALE-Sigma généralisée permettant une plus grande flexibilité de la discrétisation verticale. Le code Telemac-3D incorpore ces deux types de formulation ALE-Sigma.

Plusieurs techniques ont été développées afin de décrire le mouvement de la surface libre dans un contexte ALE. L'une d'elles se nomme le suivi de surface et consiste à résoudre de façon explicite la surface libre (ex : Maury [100], Decoene et Maury [46]), soit à travers une équation 2D obtenue par intégration sur la verticale de l'équation de continuité (ex : Casulli [28], Hervouet [76]), soit à travers la condition limite cinématique à la surface libre. Nous considérerons cette technique au sein de ce travail de thèse.

1.3.3 Propriétés numériques souhaitées

Dans le cadre des écoulements à surface libre, certaines propriétés numériques sont importantes à satisfaire afin de simuler au mieux ces écoulements. En fonction des méthodes numériques choisies, ces propriétés peuvent être plus ou moins difficiles à satisfaire simultanément. Au niveau discret, elles correspondent à :

- calculer une vitesse à divergence nulle, par exemple pour préserver la conservation de masse des traceurs ;
- calculer une surface libre qui satisfait l'équation cinématique à la surface libre, par

exemple pour s'assurer que la vitesse à divergence nulle satisfait les équations de quantité de mouvement et l'équation cinématique à la surface libre ;
- préserver la quantité de masse d'eau ;
- positivité de la hauteur d'eau.

1.4 Résolutions numériques des équations de Navier–Stokes à surface libre

Au sein des chapitres 2, 3 et 4, nous nous intéressons à la résolution numérique des équations de Navier–Stokes à surface libre (1.1-1.3) et (1.5-1.8) par la méthodes éléments finis. Le mouvement du domaine est pris en compte au travers de la méthode ALE particulière nommée la transformation ALE-Sigma [45].

1.4.1 Equations de Navier–Stokes à surface libre avec décomposition de pression

Les équations de Navier–Stokes à surface libre avec décomposition de pression (1.5-1.8) peuvent être résolues en découplant les équations afin de simplifier leur résolution [28, 76, 134]. La stratégie temporelle consiste à résoudre une étape de prédiction hydrostatique, suivie d'une étape de correction dynamique. La première étape de prédiction se compose des équations du moment sans le terme de pression dynamique et de l'équation verticalement moyennée sur la surface libre. Elle revient ainsi à résoudre les équations de Navier–Stokes hydrostatiques et une équation d'advection-diffusion sur la vitesse verticale. Cette étape permet de calculer la surface libre et une vitesse intermédiaire à divergence non-nulle. Le calcul de la surface libre permet de déterminer la pression hydrostatique (1.4), et permet d'obtenir une première approximation de la pression. La seconde étape de correction dynamique consiste à corriger la vitesse par la pression dynamique et permet d'assurer la divergence nulle de ces dernières. Elle correspond ainsi à résoudre un système de Darcy.
Dans le chapitre 2, nous étudions différentes stratégies de résolution éléments finis, préalablement proposées dans la littérature, des étapes de prédiction hydrostatique et de correction dynamique. Pour chacune des deux étapes, nous verrons des stratégies numériques visant à résoudre les équations de manière couplée ou de manière découplée.

Stratégies numériques couplées

Dans le cadre de stratégie couplée et pour l'étape de prédiction hydrostatique, nous discuterons de deux formulations dans lesquelles les conditions d'imperméabilité aux parois latérales du domaine

$$\mathbf{u} \cdot \mathbf{n} = 0$$

sont imposées essentiellement ou naturellement. Ces deux formulations ont été proposées et analysées par Decoene [44]. L'auteur a étudié l'existence et l'unicité de solution au niveau continu ou discret. Ces deux formulations admettent une solution unique lorsque

le coefficient de diffusion horizontale est non-nul. Dans le cas contraire, la vérification d'une condition inf-sup est nécessaire. Au niveau discret, les espaces éléments finis doivent satisfaire cette condition.

Les équations de Darcy de l'étape de correction dynamique peuvent être résolues directement. Au niveau discret, les espaces éléments finis doivent satisfaire une condition inf-sup afin d'assurer l'unicité et l'existence des solutions. Cette résolution permet de calculer une vitesse à divergence nulle au niveau discret.

Stratégies numériques découplées

Les étapes de prédiction hydrostatique et de correction dynamique peuvent être résolues en découplant les équations au niveau continu. L'étape de prédiction hydrostatique se ramène à un problème écrit sur la surface libre et se base ainsi sur la résolution d'une équation d'onde pour la surface libre. L'étape de correction dynamique se ramène quant à elle à un problème sur la pression dynamique et se base ainsi sur une équation de Poisson pour la pression dynamique. Par analogie avec les travaux de Guermond et Quartapelle [74], l'étape de correction dynamique peut être résolue avec des espaces éléments finis ne respectant pas la condition inf-sup. Cependant, une restriction sur le pas de temps existe :

$$\frac{1}{\|\mathbf{u}_{ref}\|}\max(\Delta x^2, \Delta y^2, \Delta z^2) \leq \Delta t, \tag{1.9}$$

où $\mathbf{u}_{ref}$ est une vitesse de référence et Δx, Δy (resp. Δz) sont les pas d'espaces horizontaux (resp. vertical). De plus, cette stratégie ne permet pas d'obtenir une vitesse à divergence nulle au niveau discret avec des espaces d'éléments finis classiques (de Lagrange par exemple).

Algorithme de Telemac-3D

Dans le chapitre 3, nous avons analysé l'algorithme de Telemac-3D. Les équations résolues sont les équations 3D de Navier–Stokes à surface libre avec décomposition de pression (1.5-1.8). Le mouvement vertical du domaine est pris en compte par la transformation ALE-Sigma. Une particularité du code réside dans la construction du maillage 3D. En effet, le domaine horizontal ω est d'abord triangulé et est ensuite successivement extrudé selon la verticale. Les éléments 3D du maillage du domaine Ω_t sont donc des prismes. La discrétisation spatiale se base sur la méthode des éléments finis. L'espace éléments finis adopté pour approximer la surface libre est l'espace de Lagrange $\mathbb{P}_1$. La vitesse et la pression du fluide sont approximées par des espaces de Lagrange "prismatique" $\mathbb{PR}_1$, voir Ern et Guermond [53].

Au cours de ce travail, nous avons relevé certaines limitations du code à l'aune des publications les plus récentes sur le sujet. Premièrement, l'étape de prédiction hydrostatique est résolue en considérant une équation d'onde sur la surface libre. Dans cette partie, les termes de diffusion horizontaux sont explicités impliquant une restriction parabolique

sur le pas de temps telle que :

$$\Delta t \leq \frac{1}{\nu} \min(\Delta x^2, \Delta y^2). \tag{1.10}$$

L'étape de correction dynamique est quant à elle résolue au travers d'une équation de Poisson sur la pression dynamique. Considérant des espaces éléments finis classiques, les vitesses corrigées ne sont donc pas à divergence nulle discrète. Une vitesse auxiliaire à divergence nulle discrète est alors ultérieurement calculée. Par ailleurs, les espaces éléments finis sur la vitesse et la pression ne respectant la condition inf-sup, nous avons ainsi relevé l'existence d'une condition sur le pas de temps du type (1.9). Notons que cette dernière condition associée avec (1.10) rend difficile le choix du pas de temps Δt.

1.4.2 Equations de Navier–Stokes à surface libre

Dans le chapitre 4, nous avons exploré des voies alternatives et ainsi proposé et analysé un algorithme basé sur la résolution des équations de Navier–Stokes (1.1-1.2) couplées à l'équation cinématique à la surface libre (1.3). Dans le contexte de la méthode des éléments finis, Maury [100] et Decoene et Maury [46] ont présenté et étudié une méthode des caractéristiques ALE pour ces équations. La méthode des caractéristiques présente l'avantage de ne pas introduire de restriction sur le pas de temps. Nonobstant, cette méthode n'assure pas la conservation de la masse d'eau. Cela peut impacter négativement la stabilité numérique du schéma appliqué aux équations de Navier–Stokes. Maury [100] montre que le schéma est stable si les vitesses sont à divergence nulle au niveau continu. Dans le chapitre 4, nous présentons et analysons une méthode numérique éléments finis pour les équations de Navier–Stokes à surface libre assurant la conservation de la masse d'eau. Nous montrons que cette dernière est conditionnellement stable indépendamment d'une vitesse à divergence nulle exacte.

Schéma explicite stabilisé pour l'équation de surface libre

Dans le chapitre 4, nous proposons de résoudre l'équation cinématique à la surface libre par un schéma en temps d'Euler explicite d'ordre 1 avec terme de stabilisation symétrique en éléments finis pour l'équation de surface libre tel que :

$$\begin{cases} \text{Trouver } \eta_h^{n+1} \in \mathcal{M}_h(\omega) \text{ tel que pour tout } \zeta_h \in \mathcal{M}_h(\omega) \\ \left(\dfrac{\eta_h^{n+1} - \eta_h^n}{\Delta t}, \zeta_h \right)_\omega + \left(\boldsymbol{u}^{n,hor}_{h|_{z=\eta_h^n}} \cdot \nabla \eta_h^n, \zeta_h \right)_\omega + s_h^n(\eta_h^n, \zeta_h) = \left(w^n_{h|_{z=\eta_h^n}}, \zeta_h \right)_\omega, \end{cases} \tag{1.11}$$

avec le terme de stabilization symétrique :

$$s_h^n(\eta_h^n, \zeta_h) = \frac{\mathrm{h}}{\| \boldsymbol{u}^{n,hor}_{h|_{z=\eta_h^n}} \|_\infty} (\boldsymbol{u}^{n,hor}_{h|_{z=\eta_h^n}} \cdot \nabla \eta_h^n, \boldsymbol{u}^{n,hor}_{h|_{z=\eta_h^n}} \cdot \nabla \zeta_h)_\omega,$$

et η_h^n est la surface libre discrète au temps $t = t^n$, $(\boldsymbol{u}^{n,hor}_{h|_{z=\eta_h^n}}, w^n_{h|_{z=\eta_h^n}})$ est la vitesse discrète à la surface libre au temps $t = t^n$. La notation h représente le pas d'espace horizontal

et Δt représente le pas de temps. L'espace fonctionnel discret $\mathcal{M}_h$ pour la surface libre est donné dans la Section 4.4. Nous utilisons un terme de stabilisation car l'équation cinématique de surface libre est une équation d'advection avec terme source. Or, il est connu que la combinaison d'un schéma explicite et d'une méthode spatiale centrée est inconditionnellement stable, voir Quarteroni et Valli [115]. Comme son nom l'indique, le terme de stabilisation permet de stabiliser conditionnellement le schéma. De nombreuses méthodes de stabilisations existent dans la littérature telles que les méthodes de Galerkin moindre carrés [81], de projection locale [18, 119], « interior penalty of gradient jumps » (CIP) [22, 26], « subgrid viscosity » [70, 72], « orthogonal subscale stabilization » [41, 42], SUPG [21, 23, 86]. Par analogie avec les travaux de Burman et al. [25], nous montrons que la stabilité de ce schéma est :

Proposition 1.1. *Nous supposons que η_h^{n+1} est une solution discrète de* (1.11) *et η_h^0 est une fonction qui approxime $\eta(x, y, 0)$. Nous considérons la condition CFL suivante :*

$$\Delta t \leq \frac{\mathrm{h}}{2\,\|\boldsymbol{u}_{h|_{z=\eta_h^n}}^{n,hor}\|_\infty\,(1+c_{inv}^2)},$$

avec c_{inv} une constante d'une inégalité inverse. Sous cette condition CFL, la solution discrète $\eta_h^{n+1} \in \mathcal{M}_h$ de (1.11) *satisfait le résultat de stabilité suivant :*

$$\|\eta_h^{N_T}\|_{0,\omega}^2 + \sum_{k=0}^{n-1} 2\,\beta^n\,\Delta t\,|\eta_h^k|_s^2 \leq \exp\left[\sum_{k=0}^{n-1}(1+\mu^k)(t^{k+1}-t^k)\right]\|\eta_h^0\|_{0,\omega}^2 + \sum_{k=0}^{n-1}\exp\left[\sum_{l=k}^{n-1}(1+\mu^l)(t^{l+1}-t^l)\right]\Delta t\big(1+2\,\Delta t\big)\|w_{h|_{z=\eta_h^k}}^k\|_{0,\omega}^2,$$

avec μ^n et β^n des constantes introduites en (4.107) *et* (4.108).

De plus, nous montrons que le schéma utilisé permet de conserver globalement la quantité d'eau telle que

Proposition 1.2. *Soit $\eta_h^{n+1} \in \mathcal{M}_h$ une solution discrète de (1.11), nous avons alors le résultat suivant de conservation globale de la quantité d'eau :*

$$\int_\omega \eta_h^{n+1} = \int_\omega \eta_h^0.$$

Schéma alternatif pour les équations de Navier–Stokes

Nous présentons un schéma éléments finis semi-implicite en temps pour les équations de Navier–Stokes sous formalisme « Arbitrary Lagrangian-Eulerian ». Boffi and Gastaldi [13], Formaggia et Nobile [57, 58], Ganessan et al. [61] et Bonito et al. [15] ont étudié la stabilité de schéma pour des problèmes ALE d'évolution en temps. Ils ont montré que la stabilité de schéma d'ordre 1 en temps ne dépend pas de la vitesse du maillage, qui est habituellement difficile à contrôler. Nonobstant, cette conclusion n'est pas valide

pour des schémas d'ordre 2. Par analogie avec leurs travaux, nous utilisons un schéma en temps d'ordre 1 pour les équations de Navier–Stokes et nous montrons que le schéma obtenu est stable indépendamment de la vitesse du maillage et d'une vitesse exactement à divergence nulle. Soient $\mathbf{u}_h^{n+1}$ and p_h^{n+1} les solutions discrètes de la vitesse et pression du fluide, le schéma proposé s'écrit :

$$\begin{cases} \text{Trouver } (\mathbf{u}_h^{n+1}, p_h^{n+1}) \in (\mathcal{V}_{h,0}^{n+1}(\Omega_h^{n+1}), \mathcal{Q}_h^{n+1}(\Omega_h^{n+1})) \\ \text{tel que pour tout } (\mathbf{v}_h^{n+1}, q_h^{n+1}) \in (\mathcal{V}_{h,0}^{n+1}(\Omega_h^{n+1}), \mathcal{Q}_h^{n+1}(\Omega_h^{n+1})) \\ (\mathbf{u}_h^{n+1}, \mathbf{v}_h^{n+1})_{h,n+1} - (\mathbf{u}_h^{n}, \mathbf{v}_{h,n}^{n+1})_{h,n} + \Delta t \Big[\overline{c}_{n+1}(\mathbf{u}_{h,n+1}^{n} - \mathbf{c}_{h,n+1}^{n}, \mathbf{u}_h^{n+1}, \mathbf{v}_h^{n+1}) \\ - \dfrac{1}{2}(\mathbf{u}_h^{n+1} \nabla \cdot \mathbf{c}_{h,n+1}^{n}, \mathbf{v}_h^{n+1})_{h,n+1} + a_{n+1}(\mathbf{u}_h^{n+1}, \mathbf{v}_h^{n+1}) \\ - b_{n+1}(\mathbf{v}_h^{n+1}, p_h^{n+1}) \Big] = (\mathbf{g}, \mathbf{v}_h^{n+1})_{h,n+1}, \qquad (1.12) \\ \\ - b_{n+1}(\mathbf{u}_h^{n+1}, q_h^{n+1}) = 0, \qquad (1.13) \end{cases}$$

où

$$\mathbf{u}_{h,n+1}^{n} = \mathbf{u}_h^{n} \circ \mathcal{A}_h^{n,n+1},$$

avec $\mathcal{A}_h^{n,n+1}$ le transformation discrète entre les domaines discrets Ω_h^n and Ω_h^{n+1}, introduite dans la sous-section 2.2.1 de ce manuscrit. Les formes bilinéaires $a_{n+1}(\cdot,\cdot)$, $b_{n+1}(\cdot,\cdot)$ et $\overline{c}_{n+1}(\cdot,\cdot,\cdot)$ sont définies dans la section 4.4. Nous démontrons le résultat de stabilité suivant :

Proposition 1.3. *Nous supposons que $\mathbf{u}_h^{n+1}$ est une solution discrète de (1.12-1.13) et $\mathbf{u}_h^0$ est la fonction discrète de $\mathbf{u}(\boldsymbol{x}, 0)$. Le résultat de stabilité sur la vitesse du fluide $\mathbf{u}_h^n$ est :*

$$\|\mathbf{u}_h^{N_T}\|_{0,N_T}^2 + \nu\, \Delta t \sum_{n=0}^{N_T-1} \|\nabla \mathbf{u}_h^{n+1}\|_{0,n+1}^2 \leq \|\mathbf{u}_h^0\|_{0,0}^2 + \frac{\Delta t}{\nu} g^2 \left|\omega^0\right| \sum_{n=0}^{N_T-1} c_p^2(\Omega_h^{n+1}),$$

où $c_p(\Omega_h^n)$ est la constante de Poincaré du domaine Ω_h^n.

1.5 Etude de l'équation de Berkhoff

Un des buts initiaux de la thèse était d'effectuer des comparaisons entre le logiciel Telemac-3D et le logiciel Artemis, nous nous sommes intéressés à l'équation de Berkhoff qui est résolue dans ce dernier code. Le logiciel Artemis [51] est aussi développé par EDF R&D et permet de simuler des vagues en zone portuaire et côtière. Cette étude nous a permis par ailleurs d'acquérir une vue d'ensemble du domaine des écoulements à surface libre. L'équation de Berkhoff permet ainsi de représenter les phénomènes physiques auxquels sont soumises les ondes de gravité : réfraction, réflexion, diffraction en zone

côtière ou portuaire. Ces phénomènes se produisent suite à la présence d'îles, de structures ou encore suite à la variation du gradient du fond. Cette équation a été dérivée par l'auteur du même nom [10, 11] à partir des équations de la houle linéaire et pour des ondes progressives. Par conséquent, nous nous sommes intéressés aux hypothèses de dérivation du modèle de Berkhoff et son domaine de validité a été revisité.

1.5.1 Modèle de la houle linéaire

Les équations de la houle linéaire ont été introduites par Airy [3] en 1841 et sont basées sur la théorie des écoulements potentiels. Elles permettent de décrire la propagation d'onde de gravité à la surface d'un fluide homogène (de densité ρ constante). De plus, ce même fluide est supposé parfait (viscosité nulle) et newtonien. Par ailleurs, l'écoulement est supposé incompressible ($\nabla \cdot \mathbf{u} = 0$) et irrotationnel ($\nabla \times \mathbf{u} = 0$). Ces équations sont dérivées à partir des équations d'Euler à surface libre, elles-même linéarisées. A noter que cette dérivation peut s'effectuer en adimensionalisant les équations et en supposant que le ratio de l'amplitude de la vague sur la hauteur moyenne est petite. Une dérivation peut être trouvée dans Lannes [90]. Considérant par ailleurs des ondes progressives, les équations de la houle linéaire s'écrivent sur $\Omega = \{(x, y, z \mid (x, y) \in \omega \text{ and } -h(x, y) < z < 0\}$:

$$\begin{cases} \Delta\phi(x,y,z) = 0, \quad \text{sur } \Omega, \\ \partial_z\phi(x,y,z) - \dfrac{\omega^2}{g}\,\phi(x,y,z) = 0, \quad \text{à } z = 0, \\ \partial_z\phi(x,y,z) + \nabla\phi(x,y,z)\ \nabla h(x,y) = 0, \quad \text{à } z = -h(x,y), \end{cases}$$

avec ϕ est le potentiel des vitesses tel que $\nabla\phi = \mathbf{u}$ et ω est la pulsation de l'onde et h la hauteur d'eau au repos.

1.5.2 Modèles asymptotiques horizontaux

Dans le chapitre 5, nous étudierons et comparerons des modèles asymptotiques horizontaux, dont l'équation de Berkhoff, dans différents régimes d'eau et sous l'hypothèse de faible pente du fond (i.e. $\nabla_{hor} h(x, y) \ll 1$). Considérant une solution approchée ϕ_{app} des équations de la houle linéaire telle que :

$$\phi_{app}(x,y,z) = \frac{\cosh[k(x,y)(z + h(x,y))]}{\cosh[k(x,y)\,h(x,y)]}\,\varphi(x,y),$$

où $k(x)$ est l'unique solution positive de

$$\omega^2 = g\ \ k(x,y)\ \tanh[k(x,y)\,h(x,y)],$$

et φ le potentiel horizontal. Les modèles asymptotiques sont dérivés à partir de l'équation de la houle linéaire en considérant ϕ_{app} et suite à des manipulations algébriques et des simplifications asymptotiques.

Equation de Berkhoff

L'équation de Berkhoff est une équation aux dérivées partielles permettant de représenter les effets de réfraction, diffraction et de réflexion auxquels les vagues sont sujettes. Elle a été introduite par Berkhoff [10, 11] en 1973 :

$$\nabla_{hor} \cdot \big(T(x,y)\,\nabla_{hor}\varphi(x,y)\big) + k(x,y)^2\,T(x,y)\,\varphi(x,y) = 0, \quad \text{sur }]0,L[,$$

avec

$$\begin{aligned} T(x,y) &= \int_{-h(x,y)}^{0} \frac{\cosh[k(x,y)(z+h(x,y))]^2}{\cosh[k(x,y)\,h(x,y)]^2}\,dz \\ &= \frac{1}{2\cosh[k(x,y)\,h(x,y)]^2}\left(h(x,y) + \frac{\sinh[2\,k(x,y)\,h(x,y)]}{2\,k(x,y)}\right). \end{aligned}$$

De nombreuses dérivations peuvent être trouvées dans la littérature. Par exemple, Mei et al. [101], Dingemans [47] ont proposé une dérivation en utilisant un principe variationel hamiltonien. Booij [16] a quant à lui proposé une dérivation basée sur le principe variationel de Luke. Par ailleurs, des études concernant la validité de l'équation de Berkhoff ont été menées. Nous pouvons par exemple citer les travaux de Tsay and Liu [128] qui ont montré que de bons résultats peuvent être obtenus pour des pentes allant jusqu'à 1:1, lorsque la propagation des vagues est « parallèle » à l'évolution de la pente du fond. Pour des vagues se propageant de manière aléatoire, Booij [17] a montré que des résultats acceptables peuvent être obtenus pour des pentes allant jusqu'à 1:3.

Equation de Saint Venant linéaire

En régime d'eau peu profonde et pour de faibles pentes de fond, l'équation asymptotique horizontale correspondante est l'équation de Saint Venant linéaire et s'écrit :

$$\nabla_{hor} \cdot \big(h(x,y)\,\nabla_{hor}\varphi(x,y)\big) + \frac{\omega^2}{g}\,\varphi(x,y) = 0.$$

De nombreuses dérivations de cette équation peuvent être trouvées dans la littérature, par exemple dans les ouvrages de Whitham [137] et Lannes [90], dans lesquelles l'équation de Saint Venant, introduite précédemment, est linéarisée. Berkhoff [10] a proposé une dérivation de l'équation de Saint Venant linéaire à partir des équations de la houle linéaire. De plus, une dérivation à partir de l'équation de Berkhoff peut être trouvée dans les travaux de Lozano et Meyer [96].

Equation de Helmholtz

Dans un régime d'eau profonde, le fond n'a pas d'influence sur le profil de la vague. Par conséquent, la pente du fond n'influence pas cette dernière. De plus, les ondes considérées sont progressives et se comportent comme des ondes se propageant sur un fond horizontal. Ainsi, en régime d'eau profonde ou encore pour des fonds horizontaux, l'équation asymptotique horizontale correspondante est l'équation de Helmholtz :

$$\Delta_{hor}\varphi(x,y) + k(x,y)^2\,\varphi(x,y) = 0.$$

où Δ_{hor} représente l'opérateur de Laplace horizontal. A noter que cette équation permet de représenter les effets de diffraction. Cependant, elle ne permet pas de représenter les effets de réfraction.

Au sein du chapitre 5, nous revisitons la dérivation asymptotique de l'équation de Berkhoff, l'équation de Saint Venant linéaire et l'équation de Helmholtz en fonction du paramètre de profondeur d'eau σ et de la pente du fond α. Avec l'appui d'une étude numérique, nous retrouvons le fait que l'équation de Berkhoff est la seule équation à fournir une solution proche de celle des équations de la houle linéaire en régime d'eau intermédiaire et sous l'hypothèse de pente faible. En régime d'eau peu profonde, nous retrouvons le fait qu'une solution de Berkhoff est proche de celle de l'équation de Saint Venant linéaire. En régime d'eau profond, nous retrouvons le fait qu'une solution de Berkhoff est proche de celle de l'équation de Helmholtz. En revanche, nous montrons numériquement que dans le cas d'un régime d'eau transitoire, passant d'un régime intermédiaire et à un régime peu profond, ou d'un régime profond à un régime intermédiaire, une solution de l'équation de Berkhoff est la seule proche de celle des équations de la houle linéaire. Nous observons par ailleurs que l'équation de Berkhoff est la seule équation horizontale à prendre en compte les effets de réfraction, diffraction et réflexion en régime intermédiaire.

1.5.3 Solution approchée analytique

Dans un second temps, nous dériverons une solution analytiquement approchée φ_{app} de l'équation de Berkhoff. Celle solution approchée sera déduite des méthodes de l'optique géométrique [117] et dépendra de deux paramètres : la pente du fond, ainsi que la profondeur moyenne. Nous étudierons ensuite les termes de reste de la solution approchée réintroduite dans les équations de la houle linéaire. Au travers d'une étude quantitative, le résultat principal est de retrouver des ordres de magnitude déduits de la littérature [10, 11] tels que:

$$\begin{aligned}
\|\mathsf{Be}(\varphi_{app})\|_\infty &\leq c_1 \|\nabla_{hor} h\|_\infty^2, \\
\|\mathsf{L}(\varphi_{app})\|_\infty &\leq c_2 \|\nabla_{hor} h\|_\infty, \\
\|\mathsf{Bo}(\varphi_{app})\|_\infty &\leq c_2 \|\nabla_{hor} h\|_\infty.
\end{aligned}$$

1.6 Conclusion et perspectives

Au cours de cette thèse, nous nous sommes intéressés à la résolution des équations ALE tridimensionnelles de Navier–Stokes à surface libre par la méthode des éléments finis.
Dans un premier temps, nous avons étudié les différentes méthodes éléments finis permettant de résoudre ces équations, ainsi que les limitations pouvant exister. Cela nous a permis d'appréhender la révision du cœur numérique du logiciel d'hydrodynamique Telemac-3D et de l'évaluer à l'aune des publications les plus récentes. Ainsi, nous avons mis en lumière les hypothèses et limitations existantes, et nous avons aussi proposé des perspectives d'améliorations. Nous avons par exemple soulevé une question concernant la résolution de l'étape de prédiction hydrostatique. Une première perspective serait

d'investiguer numériquement cette étape. Par ailleurs, nous avons aussi relevé que la vitesse du fluide calculée n'est pas à divergence nulle discrète, que la condition cinématique à la surface libre n'est pas satisfaite ou encore qu'une restriction sur le pas de temps est nécessaire. Le logiciel pourrait être amélioré en commençant par calculer une vitesse à divergence nulle au niveau discret dans l'étape de correction non-hydrostatique, par exemple en résolvant cette étape au travers d'une formulation mixte. Cela permettrait d'apporter de la flexibilité quant à la restriction sur le pas de temps. Cependant, la résolution des équations de Darcy nécessite des espaces éléments finis inf-sup stables, ce qui n'est pas le cas à l'heure actuelle dans Telemac-3D. Une solution consisterait à utiliser des méthodes de stabilisation qui permettent de se dispenser de la condition inf-sup (par exemple : méthode PSPG). Cette alternative nous paraît la plus simple à intégrer et elle n'impliquerait pas un changement fondamental de l'architecture du code. Concernant le respect de la condition à la surface libre, une possibilité serait de calculer l'équation cinématique correspondante à la fin de l'algorithme. Cependant, il faut être prudent concernant la méthode numérique utilisée afin de conserver la propriété de conservation globale de la masse.
Des voies alternatives ont été explorées. Nous avons ainsi proposé une méthode éléments finis pour les équations de Navier–Stokes à surface libre. En effet, nous avons étudié un schéma éléments finis explicite d'ordre 1 en temps avec un terme de stabilisation symétrique pour l'équation cinématique de surface libre. A noter qu'il pourrait être utilisé dans Telemac-3D dans le but de satisfaire la condition cinématique et la conservation globale de la masse. Nous avons montré que ce schéma est stable sous condition inf-sup et qu'il permet de conserver globalement la masse. De plus, nous avons proposé une nouvelle formulation variationnelle associée aux équations de Navier–Stokes. Nous avons montré que cette formulation permet d'aboutir à un schéma éléments finis semi-implicite en temps qui est stable indépendamment de la vitesse du domaine et d'une vitesse de convection à divergence nulle exacte. Bien que la conservation de la masse soit globalement assurée, le schéma devrait être amélioré afin d'assurer la positivité de l'eau, par exemple en se basant sur les travaux de Burman [24].

Suivant le but initial d'effectuer des comparaisons entre le logiciel Telemac-3D et le logiciel Artemis, nous nous sommes intéressés à l'équation de Berkhoff qui est résolu dans ce dernier code. Cela nous a permis par ailleurs d'acquérir une vue d'ensemble du domaine des écoulements à surface libre. A ce titre, nous avons revisité les hypothèses de dérivation et son domaine de validité. Nous avons ainsi discuté de la dérivation de l'équation de Berkhoff dans différents régimes. Nous avons vu qu'une solution de l'équation de Berkhoff est proche d'une solution de l'équation de Saint-Venant en régime d'eau peu profonde ou d'une solution de Helmholtz en régime d'eau profonde. Pour ces deux régimes, les solutions approximées des équations asymptotiques horizontales sont proches d'une solution de l'équation de la houle linéaire. En régime intermédiaire, nous avons vu que seule l'équation de Berkhoff permet d'obtenir une solution proche de celle de l'équation de la houle linéaire. Des cas tests numériques ont ensuite été effectués afin d'appuyer ces études asymptotiques. Nous avons ainsi pu notamment observer que lorsque le régime d'eau est transitoire (régime d'eau profonde vers régime d'eau intermédiaire ou régime d'eau inter-

médiaire vers régime d'eau peu profonde), seules les solutions numériques de l'équation de Berkhoff sont proches des solutions de l'équation de la houle linéaire. Une perspective à cette étude serait de développer un cadre de comparaisons entre les solutions temporelles d'Euler, définies dans un domaine où la surface libre est localisée à $z = \eta(x, y, t)$, et les solutions atemporelles de l'équation de Berkhoff, définies dans un domaine où la surface libre est localisée à $z = 0$. Ce cadre de comparaisons pourrait ainsi servir à des études entre Telemac-3D et Artemis.

Chapter 2

Finite Elements methods for the free surface Navier–Stokes equations

Contents

2.1 Introduction

2.1.1 Context

The study and simulation of free surface flows are major challenges in the environmental communities, comprising for example water and tidal waves, water quality, wave-structure interactions, etc. Such flows are very often found with in academic and industrial applications. Many computational tools devoted to oceans, coasts, estuaries and rivers have been developed. In the academic field, we can cite for example the following programs: Elcom [78], FVCOM [89], MITgcm [99], OpenFOAM [84], POM [12], POP [49, 98], ROMS [87, 121], Selfe [140], Suntans [60]. In the industry, we can find Adcirc [97], Delft3D [94], Flow-3D [120], Fluent [8], MIKE21 [135], Telemac-3D [76] and (Un)Trim [30, 33]. We are interested here in models able to easily handle large scale geophysical flows.

Geophysical flows can be modeled through the three-dimensional free surface Navier–Stokes equations from which simplified models can be derived. In particular, many tools for simulating environmental flows rely on the shallow water equation. Nevertheless, for some applications, the three dimensional effects cannot be neglected and 3D Navier–Stokes software have been developed. Several implementations were proposed relying on hydrostatic approximation [29, 30, 44, 103, 56, 76]. The latter consists in neglecting the vertical acceleration and diffusion terms in the vertical momentum equation of the Navier–Stokes model. Consequently, the pressure only depends on the weight of the fluid column. This assumption[1] is valid for shallow water flows where the wave length is greater than the depth. The hydrostatic model allows to represent 3D effects such as stratifications or vertical recirculations. Nonetheless, this model is restricted to geophysical flows with a vertical acceleration small with respect to the horizontal one. The Boussinesq approximation is a second assumption commonly used in environmental applications. It consists in assuming that the density is constant except in the computation of the hydrostatic pressure.

The free surface Navier–Stokes equations have been largely studied in order to avoid the restrictions on the hydrostatic equation and to extend the range of applications. Different formulations can be considered, and they lead to different numerical implementations. On one hand, the Navier–Stokes equations can be solved directly together with an advection equation for the free surface [46, 100]. On the other hand, it is possible to split the pressure into a hydrostatic part and a dynamic part [31, 102]. As a consequence, based on the hydrostatic model, a hydrostatic predictor step is solved giving an intermediate velocity, the free surface elevation and the hydrostatic pressure. Then, a non-hydrostatic corrector step is solved, providing a correction of the hydrostatic pressure by a dynamic one. Besides, this second step enables to ensure that the velocity field of the fluid is divergence-free. In most of environmental applications, the hydrostatic component dominates leading to a faster numerical computation. A comparison between

[1] It is exactly the same assumption as the one used to derive the shallow water equations, but the 3D system is kept instead of integrating over the vertical

these two approaches is performed in this work.

A major difficulty in simulating free surface flows is the approximation of the motion of the free surface, and by extension, of the domain. Several approaches have been developed to circumvent this difficulty. On the one hand, the Lagrangian approach consists in following the fluid particles along their trajectories (for example SPH method, see Monaghan [104]). Then, the discretization points move with the fluid velocity. This method allows to represent the free surface of the fluid with a good accuracy. Nevertheless, it is still faced with open questions regarding its convergence, and leads to high computational times. On the other hand, the Eulerian approach [105] treats the problem in a fixed domain. From the point of view of the spatial discretization, this method does not imply a re-meshing of the domain and prescribing the boundary conditions is natural. The Arbitrary Lagrangian-Eulerian (ALE) formulation [77] is a third approach. It consists in moving the domain at a velocity different from the velocity of the fluid. From the point of view of the spatial discretization, this method allows to re-organize the mesh avoiding a new interpolation of the variables at each time step. This third approach is adopted in this work.
A feature of the problem which leads to difficulties is that the free surface elevation is an unknown of the problem. To circumvent this problem, the surface tracking method can be adopted and consists in considering an equation on the free surface. It corresponds either to a depth-averaged continuity equation [30, 76] or to a kinematic equation which is the boundary condition at the free surface [100].

The Navier–Stokes equations with free surface can be spatially discretized by different methods such as the Finite Difference method, the Finite Elements method, the Finite Volume Method, the Smoothed Particle Hydrodynamics method. The Finite Difference method [59] is based on Taylor development formulations. It can be applied only on structured meshes and then complex geometries cannot be treated accurately. In terms of computational time, these schemes are inexpensive. Finite Difference method to solve free surface flows problems can be found in Casulli et al. [30, 32] and Vitousek et al. [134]. The Finite Elements method [20, 53] is based on the variational formulation of the partial differential equations and is supported by a rigorous mathematical framework. This method is applicable to unstructured meshes and the treatment of boundary conditions is more flexible. Thus, contrary to Finite Difference method, complex geometries are permitted. The Finite Elements method is the core feature to study free surface flows in the works of Decoene [44], Decoene and Maury [46], Fontana at al. [56], Maury [100], Hervouet [76] and Miglio et al. [102]. The Finite Volume Method is also applicable on unstructured meshes and presents the advantage to be mass conservative. However, the challenge is to ensure a high accuracy of the results. Casulli et al. [33, 34] studied free surface flows problems with the Finite Volume Method. The Smooth Particle Hydrodynamics Method, see Monaghan [104] or Violeau [133], is an alternative without the construction of meshes. It is a Lagrangian method in which the fluid is discretized through a set of particles that serve as interpolation points, move at the velocity of a fluid and carry the physical quantities of the fluid (pressure, density, velocity, etc). Fur-

thermore, it allows to treat the free surface as multi-valued function, enabling to treat breaking waves. It is one of the most established mesh-free methods in computational fluid dynamics.
There are many choices concerning time discretization of the Navier–Stokes equations. The equations can be treated directly using a non-linear solver, or through a decoupled approach. The decoupled approach consists in breaking the problem in two different sub-problems, by applying the projection method or the fractional steps method.

The present thesis aims at reviewing and studying some of the numerical formulations for simulating non-linear waves. For this purpose, we consider the Finite Elements method to solve the free surface Navier–Stokes equation in an ALE framework. Indeed, this approach presents a good tradeoff between accuracy and computational times. In this context, we aim at studying two different formulations, pointing out their advantages and limitations when it comes to industrial applications. Chapter 3 is dedicated to the analysis of an approach based on the pressure decomposition and Chapter 4 is devoted to the analysis of a mixed formulation of the Navier–Stokes equation together with an advection equation for the free surface. A third approach for simulating linear wave is studied in Chapter 5, based on the mild-slope equation.

In order to provide a basis for the Chapter 3 and 4, we review the Finite Elements method for the Navier–Stokes equations in an ALE framework. Firstly, the principle of the ALE method and its extension to the Finite Elements framework is introduced in Section 2.2. Secondly, the two abovementioned formulations of the ALE free surface Navier–Stokes equations are introduced in Sections 2.3 and 2.4. Since, the second formulation based on the pressure decomposition can be viewed as a projection-like method, Section 2.5 is devoted to a general discussion of these methods. Finally, Finite Elements method for the hydrostatic predictor and corrector steps of the formulation based on the pressure decomposition are discussed in Section 2.6.

2.1.2 Preliminaries and notations

We consider a fluid bounded from below by a topography $b(x, y)$ and from above by a free surface elevation $\eta(x, y, t)$. The free surface and bottom function are assumed to be single-valued. The three-dimensional variable is $\boldsymbol{x} = (x, y, z) \in \mathbb{R}^3$ such that $(x, y) \in \mathbb{R}^2$ is the field of horizontal coordinates and $z \in \mathbb{R}$ is the vertical variable. We define $h(x, y, t) = \eta(x, y, t) - b(x, y)$ the water depth. Let ω be a fixed and bounded two-dimensional polygonal domain. For any time $t \in]0, T[$ with $T \in \mathbb{R}_*^+$ a constant final time, we consider the three-dimensional fluid domain

$$\Omega_t = \{(x, y, z) \mid (x, y) \in \omega \text{ and } b(x, y) < z < \eta(x, y, t)\}. \tag{2.1}$$

The domain[2] Ω_t is bounded by the free surface boundary $\Gamma_{s,t}$ and by the solid boundaries $\Gamma_{l,t}$ and Γ_b which denote the bottom and vertical lateral boundaries, see Figure 2.1. The

[2]the subscript t represents the time dependency of Ω

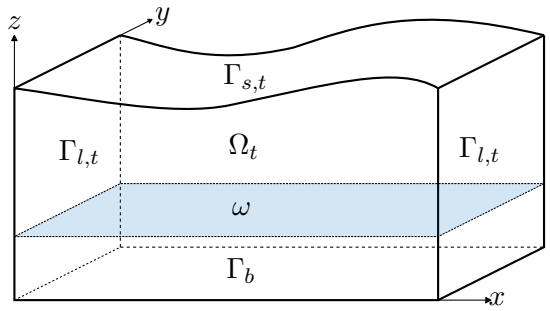

Figure 2.1: Representation of the 3D domain Ω_t

boundary of the domain is denoted by $\partial\Omega_t = \Gamma_{s,t} \cup \Gamma_{l,t} \cup \Gamma_b$ and it is assumed to be continuous Lipschitz. Besides, we denote by $\partial\omega$ the boundary of ω. For any time $t \in]0, T[$, the three-dimensional boundaries are defined such that:

$$\Gamma_{s,t} = \{(x, y, z) \mid (x, y) \in \omega, \;\; z = \eta(x, y, t)\}, \tag{2.2}$$

$$\Gamma_{l,t} = \{(x, y, z) \mid (x, y) \in \partial\omega, \;\; b(x, y) < z < \eta(x, y, t)\}, \tag{2.3}$$

$$\Gamma_b = \{(x, y, z) \mid (x, y) \in \omega, \;\; z = b(x, y)\}. \tag{2.4}$$

In this thesis, we consider the domain:

$$\mathcal{D}_T = \{(\boldsymbol{x}, t) \mid t \in]0, T[, \;\; \boldsymbol{x} \in \Omega_t\}. \tag{2.5}$$

Throughout this chapter, for a general domain Ω, $W^{s,p}(\Omega)$ denotes the Sobolev space of real-valued functions defined on the domain Ω with distributional derivatives of order up to $s \in \mathbb{N}$ in $L^p(\Omega)$. The associated norm is $\|\cdot\|_{W^{s,p}(\Omega)}$ and the seminorm is $|\cdot|_{W^{s,p}(\Omega)}$. In the case where $s = 0$, we obtain the Lebesgue spaces $W^{0,p}(\Omega) = L^p(\Omega)$. The case $p = 2$ will be distinguished by using the Hilbert space $W^{s,2}(\Omega) = H^s(\Omega)$. For simplicity, we denote respectively by $\|\cdot\|_{s,\Omega}$ and $|\cdot|_{s,\Omega}$ the norm and the seminorm in $H^s(\Omega)$. In the case, $s = 0, p = 2$, the inner product of $L^2(\Omega)$ is denoted by $(\cdot, \cdot)_\Omega$ and the corresponding norm by $\|\cdot\|_{0,\Omega}$. The norm of the space of essentially bounded functions $L^\infty(\Omega)$ is denoted by $\|\cdot\|_{\infty,\Omega}$. For the sake of simplicity and only for a moving domain Ω_t, we use the subscript t such that the inner product of $L^2(\Omega_t)$ is denoted by $(\cdot, \cdot)_t$ and the corresponding norm by $\|\cdot\|_{0,t}$. The norm of the space of essentially bounded functions $L^\infty(\Omega_t)$ is denoted by $\|\cdot\|_{\infty,t}$.

We denote by ∇ (resp. ∇_{hor}) the gradient operator on the domain Ω_t (resp. ω) such that for all $f : \mathbb{R}^3 \to \mathbb{R}$ and for all $g : \mathbb{R}^2 \to \mathbb{R}$:

$$\nabla f = \left(\frac{\partial f}{\partial x}, \frac{\partial f}{\partial y}, \frac{\partial f}{\partial z}\right), \qquad \nabla_{hor}\, g = \left(\frac{\partial g}{\partial x}, \frac{\partial g}{\partial y}\right). \tag{2.6}$$

Furthermore, we denote the divergence operator in Ω_t (resp. ω) by $\nabla\cdot$ (resp. $\nabla_{hor}\cdot$) such as for all $f = (f_1, f_2, f_3) : \mathbb{R}^3 \to \mathbb{R}^3$ and for all $g = (g_1, g_2) : \mathbb{R}^2 \to \mathbb{R}^2$:

$$\nabla \cdot f = \frac{\partial f_1}{\partial x} + \frac{\partial f_2}{\partial y} + \frac{\partial f_3}{\partial z}, \qquad \nabla_{hor} \cdot g = \frac{\partial g_1}{\partial x} + \frac{\partial g_2}{\partial y}. \tag{2.7}$$

2.2 Arbitrary Lagrangian-Eulerian framework

The Arbitrary Lagrangian-Eulerian formulation (ALE) has been introduced by Hirt et al. [77] with the aim of simplifying the numerical resolution of problems posed on moving domains. It consists in defining a reference configuration (generally fixed) and a mapping tracking the correspondence between the reference configuration and the real configuration (also called the current configuration). The mapping can be arbitrary but it has to be chosen conform to the evolution of the real domain boundaries. Moreover, it makes it possible to define the instantaneous velocity of the domain, which corresponds to the velocity of the mesh at the discrete level. Consequently, the approximation of a problem posed on a moving domain requires the construction of a mesh in the reference configuration. At any time $t \in \mathbb{R}^+$, the discretized ALE mapping provides the coordinates of each grid node in the real mesh. That enables to easily switch between the reference and real frames. Nonetheless, we cannot use the Finite Difference approach because a point belonging to a moving domain at time $t_1 \in \mathbb{R}^+$ might not belong to this domain at time $t_2 \in \mathbb{R}^+ \backslash \{t_1\}$. We can illustrate this by considering a moving domain Ω_t defined on a time interval $]0, T[\subset \mathbb{R}$ and a real-valued function $v(\boldsymbol{x}, t)$ defined on $\mathcal{D}_T$ (given in (2.33)). The Eulerian time derivative reads:

$$\frac{\partial v}{\partial t} = \frac{\partial v}{\partial t}(\boldsymbol{x}, t), \quad \forall (\boldsymbol{x}, t) \in \mathcal{D}_T. \tag{2.8}$$

Let us divide the time interval $]0, T[$ into $0 \leq n \leq N-1^*$ steps of equal duration $\Delta t \in \mathbb{R}_*^+$. At time $t^n = n\ \Delta t$ with $0 \leq n \leq N-1$, a first order discretization of the partial time derivative with the Finite Difference approach is:

$$\frac{\partial v}{\partial t}(\boldsymbol{x}, t^n) \approx \frac{v(\boldsymbol{x}, t^{n+1}) - v(\boldsymbol{x}, t^n)}{\Delta t}, \quad \forall \boldsymbol{x} \in \Omega_{t^n}. \tag{2.9}$$

If $\boldsymbol{x} \in \Omega_{t^n}$, the real-valued function $v(\boldsymbol{x}, t^n)$ is well defined but the function $v(\boldsymbol{x}, t^{n+1})$ may not be. This difficulty can be circumvented thanks to the ALE formulation. Indeed, the partial time derivatives can be transformed into the so-called ALE time derivatives. The latter are defined with respect to the time at a constant point in the reference configuration and take into account the movement of the domain. See below (2.15).

This section is devoted to a detailed description of the ALE formulation and its application in the Finite Elements framework. It is based on the Chapter 2 ("ALE formulation and Geometric Conservation Laws") of the thesis of Decoene [44]. We begin by introducing the ALE time derivative and some important results. Then, we present the ALE functional spaces and the notion of mapping regularity. Finally, we introduce the discretization of the ALE mapping in a Finite Elements framework.

2.2.1 ALE time derivative

Already introduced, let $\Omega_t \subset \mathbb{R}^3$ be a moving domain defined on a time interval $]0, T[\subset \mathbb{R}$ and $\widehat{\Omega} \subset \mathbb{R}^3$ a reference polygonal configuration. In order to define the ALE formulation

for a problem stated on this domain, we consider a mapping $\widehat{\mathcal{A}}_t$ which at time $t \in]0,T[$ associates to a point $\widehat{\boldsymbol{x}} \in \widehat{\Omega}$ a point $\boldsymbol{x} \in \Omega_t$ (Figure 2.2) such that:

$$\widehat{\mathcal{A}}_t : \widehat{\Omega} \to \Omega_t, \quad \widehat{\mathcal{A}}_t(\widehat{\boldsymbol{x}}) = \boldsymbol{x}(\widehat{\boldsymbol{x}}, t). \tag{2.10}$$

The ALE coordinates in $\widehat{\Omega}$ are defined by $\widehat{\boldsymbol{x}}$ and the Eulerian coordinates in Ω_t are defined by $\boldsymbol{x}$. Throughout this work, the mapping $\widehat{\mathcal{A}}_t$ is assumed to be an homeomorphism, i.e. $\widehat{\mathcal{A}}_t \in \mathcal{C}^0(\overline{\widehat{\Omega}})$ is invertible with continuous inverse $\widehat{\mathcal{A}}_t^{-1} \in \mathcal{C}^0(\overline{\Omega_t})$. The mapping needs only to satisfy for each $t \in]0,T[$: $\widehat{\mathcal{A}}_t(\partial\widehat{\Omega}) = \partial\Omega_t$. In addition, we assume that for each $\widehat{\boldsymbol{x}} \in \widehat{\Omega}$, the application $t \to \boldsymbol{x}(\widehat{\boldsymbol{x}}, t)$ is differentiable almost everywhere in $]0,T[$.

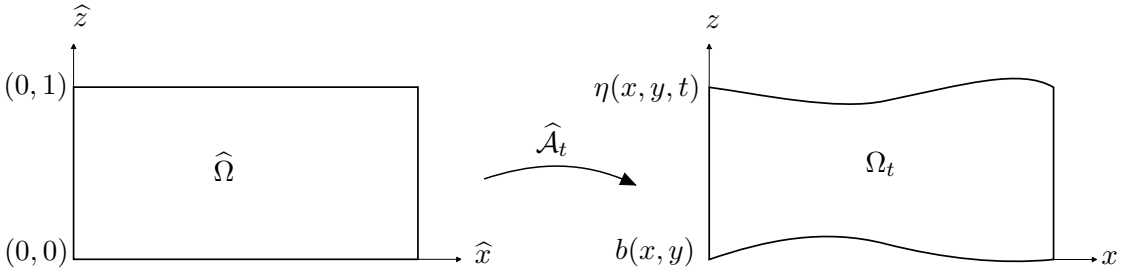

Figure 2.2: Mapping between the reference domain $\widehat{\Omega}$ and the current domain Ω_t

Let $v : \mathcal{D}_T \to \mathbb{R}$ be a function defined on the Eulerian frame and $\widehat{v} : \widehat{\Omega}\times]0,T[\to \mathbb{R}$ the associated function on the ALE frame, defined as:

$$\widehat{v}(\widehat{\boldsymbol{x}}, t) = v(\boldsymbol{x}, t), \quad \text{where} \quad \boldsymbol{x} = \widehat{\mathcal{A}}_t(\widehat{\boldsymbol{x}}). \tag{2.11}$$

The composition operator is applied to the spatial variables due to the fact that the time t is unchanged by the mapping. Let $\frac{\partial v}{\partial t}$ be the partial time derivative in the Eulerian framework and $\frac{\partial \widehat{v}}{\partial t}$ be the partial derivative in t of $\widehat{v}$. By analogy and a classical abuse of notations, we denote by $\frac{\partial v}{\partial t}\big|_{\widehat{\Omega}}$, the time derivative on the ALE framework such that:

$$\begin{aligned} &\left.\frac{\partial v}{\partial t}\right|_{\widehat{\Omega}} : \mathcal{D}_T \to \mathbb{R}, \\ &\qquad (\boldsymbol{x}, t) \mapsto \frac{\partial \widehat{v}}{\partial t}(\widehat{\boldsymbol{x}}, t) \quad \text{with} \quad \widehat{\boldsymbol{x}} = \widehat{\mathcal{A}}_t^{-1}(\boldsymbol{x}). \end{aligned} \tag{2.12}$$

The Jacobian matrix of $\widehat{\mathcal{A}}_t$ is denoted by $\widehat{\mathbf{J}}_t = \left[\frac{\partial \widehat{\mathcal{A}}_t}{\partial \widehat{\boldsymbol{x}}_j}\right]$ and $\widehat{J}_t$ its determinant. The instantaneous velocity of the domain $\boldsymbol{c}$ is defined such that:

$$\mathbf{c}(\boldsymbol{x}, t) = \frac{\partial \widehat{\mathcal{A}}_t}{\partial t}(\widehat{\boldsymbol{x}}) \quad \text{with} \quad \widehat{\boldsymbol{x}} = \widehat{\mathcal{A}}_t^{-1}(\boldsymbol{x}). \tag{2.13}$$

The ALE time derivative is appropriate for a problem raised on a moving domain, a first order discretization of the ALE time derivative (2.12) with Finite Difference approach is:

$$\left.\frac{\partial v}{\partial t}\right|_{\widehat{\Omega}} (\boldsymbol{x}, t^n) = \frac{\partial \widehat{v}}{\partial t}(\widehat{\boldsymbol{x}}, t^n) \approx \frac{\widehat{v}(\widehat{\boldsymbol{x}}, t^{n+1}) - \widehat{v}(\widehat{\boldsymbol{x}}, t^n)}{\Delta t}, \quad \forall\, \boldsymbol{x} \in \Omega_{t^n}, \tag{2.14}$$

with $\widehat{\boldsymbol{x}} = \widehat{\mathcal{A}}_t^{-1}(\boldsymbol{x})$. In the Eulerian framework, this approximation writes:

$$\left.\frac{\partial v}{\partial t}\right|_{\widehat{\Omega}}(\boldsymbol{x}, t^n) \approx \frac{v(\widehat{\mathcal{A}}_{t^{n+1}} \circ \widehat{\mathcal{A}}_{t^n}^{-1}(\boldsymbol{x}), t^{n+1}) - v(\boldsymbol{x}, t^n)}{\Delta t}, \quad \forall\, \boldsymbol{x} \in \Omega_{t^n}. \tag{2.15}$$

Since for $\boldsymbol{x} \in \Omega_{t^n}$, we have then $\widehat{\mathcal{A}}_{t^{n+1}} \circ \widehat{\mathcal{A}}_{t^n}^{-1}(\boldsymbol{x}) \in \Omega_{t^{n+1}}$ and all the terms are well-defined. Consequently, the difficulty encountered with the first order discretization of the Eulerian derivative (2.9) at time $t = t^n$ is circumvented.

Let us introduce the useful formula enabling to switch between the Eulerian and ALE frameworks. Let $v : \Omega_t \times]0, T[\to \mathbb{R}$ be regular enough, the chain rule applied to the time derivative gives:

$$\begin{aligned}\left.\frac{\partial v}{\partial t}\right|_{\widehat{\Omega}}(\boldsymbol{x}, t) &= \frac{\partial \widehat{v}}{\partial t}(\widehat{\boldsymbol{x}}, t) \\ &= \frac{\partial v}{\partial t}(\widehat{\mathcal{A}}_t^{-1}(\boldsymbol{x}), t) \\ &= \frac{\partial v}{\partial t}(\boldsymbol{x}, t) + \left(\mathbf{c} \cdot \nabla\right) v(\boldsymbol{x}, t).\end{aligned} \tag{2.16}$$

ALE mapping between current domains at different times

From $\widehat{\mathcal{A}}_t$, it is possible to define an ALE mapping between current domains Ω_t at different times $t = t_1 \in \mathbb{R}^+$ and $t = t_2 \in \mathbb{R}^+$:

$$\begin{aligned}\mathcal{A}(\cdot, t_1, t_2) :\ & \Omega_{t_1} \to \Omega_{t_2} \\ & \boldsymbol{x}_1 \mapsto \boldsymbol{x}_2 = \mathcal{A}(\boldsymbol{x}_1; t_1, t_2),\end{aligned} \tag{2.17}$$

where $\mathcal{A}(\boldsymbol{x}_1; t_1, t_2) = \widehat{\mathcal{A}}_{t_2} \circ \widehat{\mathcal{A}}_{t_1}^{-1}(\boldsymbol{x}_1)$.

Let $v : \mathcal{D}_T \to \mathbb{R}$ be a function defined on the Eulerian frame and for each time $\tau \in]0, T[$, $v_\tau : \Omega_\tau \times]0, T[\to \mathbb{R}$ the corresponding function on the ALE frame. For any time $t \in]0, T[$ and $\mathcal{A}(\boldsymbol{x}; t, \tau) = \widehat{\mathcal{A}}_\tau \circ \widehat{\mathcal{A}}_t^{-1}(\boldsymbol{x}) \in \Omega_\tau$ with $\boldsymbol{x} \in \Omega_t$, we can define the ALE function v_τ as:

$$v_\tau(\boldsymbol{x}_\tau, t) = v(\boldsymbol{x}, t), \quad \text{where } \boldsymbol{x}_\tau = \mathcal{A}(\boldsymbol{x}; t, \tau). \tag{2.18}$$

If $t = \tau$, the ALE time derivative is:

$$\frac{\partial v_\tau}{\partial t} = \frac{\partial v}{\partial t} + (\mathbf{c}_\tau \cdot \nabla)\, v, \tag{2.19}$$

where $\mathbf{c}_\tau$ is the velocity of the domain between Ω_t and Ω_τ, defined as follows:

$$\mathbf{c}_\tau(\mathcal{A}(\boldsymbol{x}; t, \tau), t) = \left.\frac{\partial \mathcal{A}(\boldsymbol{x}; t, \tau)}{\partial t}\right|_{t=\tau}. \tag{2.20}$$

2.2.2 Euler expansion and Reynolds transport theorem

We introduce the Euler expansion and the Reynolds transport theorem, which are two major results valid in the general framework. The Euler expansion formula expresses the evolution in time of the Jacobian determinant $\widehat{J}_t$ using the divergence of the velocity of the domain $\mathbf{c}$. This relation is defined in the following proposition, whose a proof can be found in [4].

Proposition 2.1. *Let Ω_t (resp. $\widehat{\Omega}$) be a real domain (resp. a reference domain) and consider a mapping $\widehat{\mathcal{A}}_t : \widehat{\Omega} \to \Omega_t$. Let $\widehat{J}_t$ be the determinant of the Jacobian matrix. We have the following relation, for all $(\widehat{\boldsymbol{x}}, t) \in \widehat{\Omega} \times]0, T[$:*

$$\frac{\partial \widehat{J}_t(\widehat{\boldsymbol{x}})}{\partial t} = \widehat{J}_t(\widehat{\boldsymbol{x}})\, \nabla \cdot \boldsymbol{c}(\widehat{\mathcal{A}}_t(\widehat{\boldsymbol{x}}), t), \tag{2.21}$$

where $\nabla\cdot$ is the spatial divergence operator with respect to $\boldsymbol{x}$.

The Reynolds transport theorem [118] is a generalization of the Leibniz integral rule [55].

Theorem 2.1. *Let Ω_t (resp. $\widehat{\Omega}$) be a real domain (resp. a reference domain) and a mapping $\widehat{\mathcal{A}}_t : \widehat{\Omega} \to \Omega_t$. Let $v : \mathcal{D}_T \to \mathbb{R}$ be a function defined on the Eulerian frame and $\widehat{v} : \widehat{\Omega} \times]0, T[\to \mathbb{R}$ the corresponding function on the ALE frame, defined as (2.11). We have the following result:*

$$\frac{d}{dt} \int_{\Omega_t} v(\boldsymbol{x}, t)\, d\boldsymbol{x} = \int_{\Omega_t} \left[\frac{\partial v}{\partial t}(\boldsymbol{x}, t) + \nabla \cdot (v(\boldsymbol{x}, t) \otimes \mathbf{c}(\boldsymbol{x}, t)) \right] d\boldsymbol{x}. \tag{2.22}$$

Proof. We integrate the function v on Ω_t and we proceed to change of variable, yielding:

$$\frac{d}{dt} \int_{\Omega_t} v(\boldsymbol{x}, t)\, d\boldsymbol{x} = \frac{d}{dt} \int_{\Omega_t} v(\widehat{\mathcal{A}}_t^{-1}(\widehat{\boldsymbol{x}}), t)\, |\widehat{J}_t(\widehat{\boldsymbol{x}})|\, d\widehat{\boldsymbol{x}}, \tag{2.23}$$

We derive in time and we obtain:

$$\begin{aligned}
\frac{d}{dt} \int_{\Omega_t} v(\boldsymbol{x}, t)\, d\boldsymbol{x} &= \int_{\widehat{\Omega}} \frac{\partial}{\partial t} \Big(\widehat{v}(\widehat{\boldsymbol{x}}, t)\, \widehat{J}_t(\widehat{\boldsymbol{x}}) \Big)\, d\widehat{\boldsymbol{x}}, \\
&= \int_{\widehat{\Omega}} \left[\widehat{J}_t(\widehat{\boldsymbol{x}})\, \frac{\partial \widehat{v}}{\partial t}(\widehat{\boldsymbol{x}}, t) + \widehat{v}(\boldsymbol{x}, t)\, \frac{\partial \widehat{J}_t(\widehat{\boldsymbol{x}})}{\partial t} \right] d\widehat{\boldsymbol{x}} \qquad (2.24) \\
&= \int_{\widehat{\Omega}} \left[\widehat{J}_t(\widehat{\boldsymbol{x}})\, \left. \frac{\partial v}{\partial t} \right|_{\widehat{\Omega}} (\widehat{\mathcal{A}}_t(\widehat{\boldsymbol{x}}), t) + \widehat{v}(\boldsymbol{x}, t)\, \frac{\partial \widehat{J}_t(\widehat{\boldsymbol{x}})}{\partial t} \right] d\widehat{\boldsymbol{x}}. \qquad (2.25)
\end{aligned}$$

Applying the Euler expansion formula (2.21), we obtain:

$$\frac{d}{dt} \int_{\Omega_t} v(\boldsymbol{x}, t)\, d\boldsymbol{x} = \int_{\widehat{\Omega}} \left[\left. \frac{\partial v}{\partial t} \right|_{\widehat{\Omega}} (\widehat{\mathcal{A}}_t(\widehat{\boldsymbol{x}}), t) + \widehat{v}(\widehat{\boldsymbol{x}}, t)\, \nabla \cdot \mathbf{c}(\widehat{\mathcal{A}}_t(\widehat{\boldsymbol{x}}), t) \right] \widehat{J}_t(\widehat{\boldsymbol{x}})\, d\widehat{\boldsymbol{x}},$$

and we get the result (2.22):

$$\begin{aligned}\frac{d}{dt}\int_{\Omega_t} v(\boldsymbol{x},t)\,d\boldsymbol{x} &= \int_{\Omega_t}\left[\left.\frac{\partial v}{\partial t}\right|_{\widehat{\Omega}}(\boldsymbol{x},t) + v(\boldsymbol{x},t)\,\nabla\cdot\mathbf{c}(\boldsymbol{x},t)\right]d\boldsymbol{x},\\ &= \int_{\Omega_t}\left[\left.\frac{\partial v}{\partial t}\right|_{\widehat{\Omega}}(\boldsymbol{x},t) + (\mathbf{c}(\boldsymbol{x},t)\cdot\nabla)v(\boldsymbol{x},t) + v(\boldsymbol{x},t)\,\nabla\cdot\mathbf{c}(\boldsymbol{x},t)\right]d\boldsymbol{x},\\ &= \int_{\Omega_t}\left[\left.\frac{\partial v}{\partial t}\right|_{\widehat{\Omega}}(\boldsymbol{x},t) + \nabla\cdot(v(\boldsymbol{x},t)\otimes\mathbf{c}(\boldsymbol{x},t))\right]d\boldsymbol{x}. \qquad (2.26)\end{aligned}$$

■

2.2.3 Functional spaces in the ALE framework

In this Subsection, we introduce a general type of functional spaces compatible with the ALE mapping. We consider a space of test functions $\widehat{\mathcal{X}}$ defined on the reference domain and containing all $\widehat{v}:\widehat{\Omega}\to\mathbb{R}$ that are smooth enough. The ALE mapping identifies a corresponding set $\mathcal{X}(\Omega_t)$ of test functions on the current domain, defined as follows:

$$\mathcal{X}(\Omega_t) = \{v : \mathcal{D}_T \to \mathbb{R} \mid v = \widehat{v}\circ\widehat{\mathcal{A}}_t^{-1},\ \widehat{v}\in\widehat{\mathcal{X}}\}. \qquad (2.27)$$

General types of functional spaces compatible with the ALE mapping allow to define functions involved in the variational formulations. These functions cannot be taken constant with respect to the time since they should vanish on the moving boundaries where the conditions are prescribed. Therefore, they depend on time and are defined on a moving domain.

Notice that the test functions in $\widehat{\mathcal{X}}$ do not depend on time. Therefore, the test functions of $\mathcal{X}(\Omega_t)$ depend on time only through the ALE mapping:

$$\forall v\in\mathcal{X}(\Omega_t),\quad 0 = \left.\frac{\partial v}{\partial t}\right|_{\widehat{\Omega}} = \frac{\partial v}{\partial t} + (\mathbf{c}\cdot\nabla)\,v. \qquad (2.28)$$

2.2.4 Construction of the ALE mapping and Finite Elements discretization

As mentioned previously, the ALE mapping can be chosen arbitrarily inside the domain but it needs only to satisfy for each $t\in]0,T[$: $\widehat{\mathcal{A}}_t(\partial\widehat{\Omega}) = \partial\Omega_t$. Consequently, the mapping must be chosen such as the instantaneous velocity of the domain $\mathbf{c}$ satisfies, for all $t\in]0,T[$:

$$\mathbf{c}\cdot\mathbf{n} = \mathbf{u}\cdot\mathbf{n}, \qquad (2.29)$$

on the physical boundaries, i.e. imperviousness solid boundaries and the free surface. We denote by $\mathbf{u}$ the velocity of the fluid and $\mathbf{n}$ is the outward normal to $\partial\Omega_t$ (which depends on time).

The fulfillment of the appropriate regularity condition imposes that $\mathbf{c}$ satisfies boundary conditions. For the test functions in $\mathcal{X}(\Omega_t)$, the regularity condition may impose some regularities on the ALE mapping. Let us now consider a problem which solution is defined on a current space belonging to $H^1(\Omega_t)$ at each time $t \in]0,T[$. A functional space $\widehat{\mathcal{X}}$ defined on the reference configuration $\widehat{\Omega}$ must be determined, such that the time-dependent test functions in the corresponding space $\mathcal{X}(\Omega_t)$ belong to $H^1(\Omega_t)$ at each time t. We assume that the mapping $\mathcal{A}_t$ verifies the following proposition proved in [57]:

Proposition 2.2. *Let $\widehat{\Omega}$ be a bounded domain with Lipschitz continuous boundary. Let $\mathcal{A}_t$ be invertible in $\overline{\widehat{\Omega}}$ and satisfying the following conditions, for each $t \in]0,T[$:*

i / $\Omega_t = \mathcal{A}_t(\widehat{\Omega})$ is bounded and Lipschitz continuous;

ii / we have:

$$\mathcal{A}_t \in W^{1,\infty}(\widehat{\Omega}), \quad \mathcal{A}_t^{-1} \in W^{1,\infty}(\Omega_t). \tag{2.30}$$

Then, for any function $v : \Omega_t \to \mathbb{R}$, $v \in H^1(\Omega_t)$ if and only if $\widehat{v}$, defined by (2.11) *belongs to $H^1(\widehat{\Omega})$. Moreover, $\|v\|_{1,\Omega_t}$ is equivalent to $\|\widehat{v}\|_{1,\widehat{\Omega}}$.*

In view of the study of a problem stated in the ALE framework by the Finite Elements method, we introduce some basics of this latter method. We consider $\widehat{\mathcal{T}}_h$ a triangulation of the reference domain $\widehat{\Omega}$. The discrete reference domain $\widehat{\Omega}_h$ is constituted of the union of all elements $\widehat{K}$ of the triangulation $\widehat{\mathcal{T}}_h$. It may differ from the reference domain $\widehat{\Omega}$ due to the approximation of the boundary geometry but we will assume that $\widehat{\Omega}_h = \widehat{\Omega}$. We introduce the general Finite Elements space $\mathcal{F}_{m,k}$ of degree m and a parametric mapping of degree k:

$$\mathcal{F}_{m,k}(\widehat{\mathcal{T}}_h) = \{\widehat{v}_h : \widehat{\Omega} \to \mathbb{R} \mid \widehat{v}_h \in C^0\big(\overline{\widehat{\Omega}}\big), \ \ \widehat{v}_h|_{\widehat{K}} \circ \mathcal{M}_k^{\widehat{K}} \ \in P_m(K_0), \ \ \forall \widehat{K} \in \widehat{\mathcal{T}}_h\}, \tag{2.31}$$

where $\widehat{v}_h|_{\widehat{K}}$ is the restriction of $\widehat{v}_h$ to the Finite Elements $\widehat{K}$, $P_m(K_0)$ is the space of polynomials of degree m defined on a reference element[3] K_0. The homeomorphic mapping $\mathcal{M}_k^{\widehat{K}} \in P_k(K_0)$ is polynomial from K_0 to $\widehat{K}$

$$\mathcal{M}_k^{\widehat{K}} : K_0 \to \widehat{K}, \ \widehat{\boldsymbol{x}}(\zeta) = M_k^{\widehat{K}}(\zeta) = \sum_{i \in \mathcal{N}^{\widehat{K}}} \widehat{\boldsymbol{x}}_i \, \phi_{0,i}(\zeta), \quad \zeta \in K_0, \ \phi_{0,i} \in P_k(K_0), \tag{2.32}$$

with $\phi_{0,i}(\zeta)$ is the basis function associated to the i-th vertex of the reference element. The coordinates of the corresponding vertex in $\widehat{\mathcal{T}}_h$ are denoted by $\widehat{\boldsymbol{x}}_i$ and $\mathcal{N}^{\widehat{K}}$ corresponds to the set of nodes that composes the reference element K_0. It can be shown that $\mathcal{F}_{m,k}(\widehat{\mathcal{T}}_h) \subset H^1(\widehat{\Omega})$. In general $k \leq n$ and in particular, k is either equal to 1 (in the case of affine mapping) or to m (in the case of isoparametric mapping). Throughout this thesis, we consider $k = 1$.

[3]Note that the reference element K_0 is different from $\widehat{K} \in \widehat{T}_h$

The ALE mapping has to be discretized in order to approximate a problem stated in the ALE framework by a Finite Element method. Note that the choice of the Finite Elements spaces for the unknows of the problem affect the type of discretization used for the ALE mapping. In particular, the discrete ALE mapping should be chosen such that the triangulation is maintained with respect to the chosen Finite Elements space, when the mesh moves. Throughout this thesis, we will only consider Lagrangian Finite Elements. The ALE mapping is denoted by $\widehat{\mathcal{A}}_{h,t}$ and it is discretized by means of functions in the isoparametric space $\mathcal{F}_{k,k}(\widehat{\mathcal{T}}_h)$ for some specific values of k. Let $\Omega_{h,t}$ be the discrete domain of Ω_t and $\mathcal{T}_{h,t}$ its triangulation. The discrete domain $\Omega_{h,t}$ is formed by the union of the elements $K_t \in \mathcal{T}_{h,t}$ and it may differ from Ω_t due to the approximation of the boundary geometry. In the sequel, we consider:

$$\mathcal{D}_{h,T} = \{(\boldsymbol{x}, t) \mid t \in]0, T[,\ \boldsymbol{x} \in \Omega_{h,t}\}. \tag{2.33}$$

At each time t, the position $\boldsymbol{x}_i$ of the i-th node in the triangulation $\mathcal{T}_{h,t}$ is defined by:

$$\boldsymbol{x}_i(t) = \widehat{\mathcal{A}}_{h,t}(\widehat{\boldsymbol{x}}_i), \quad \text{for } i = 1, ..., N^{\widehat{K}}. \tag{2.34}$$

The discrete velocity of the domain $\mathbf{c}_h$ is defined by

$$\mathbf{c}_h(\boldsymbol{x}_i, t) = \frac{\partial \widehat{\mathcal{A}}_{h,t}}{\partial t}(\widehat{\boldsymbol{x}}_i), \quad \text{where } \ \widehat{\boldsymbol{x}}_i = \widehat{\mathcal{A}}_{h,t}^{-1}(\boldsymbol{x}_i),\ \forall i = 1, ..., N^{\widehat{K}}, \tag{2.35}$$

For all $t \in]0, T[$, the triangulation $\mathcal{T}_{h,t}$ is the image of $\widehat{\mathcal{T}_h}$ by $\widehat{\mathcal{A}}_{h,t}$ such that:

$$\mathcal{T}_{h,t} = \{K_t = \widehat{\mathcal{A}}_{h,t}(\widehat{K}), \quad \widehat{K} \in \widehat{\mathcal{T}}_h\}, \tag{2.36}$$

with

$$\widehat{\mathcal{A}}_{h,t} : \widehat{\Omega} \to \Omega_{h,t}. \tag{2.37}$$

Note that the connectivity of the mesh remains the same during the time evolution and only the coordinates of the mesh nodes and the edges change. Consequently, no interpolation is required between each time step. This constitutes a major advantage of the ALE formulation for problems posed on moving domains. Throughout this thesis, we will consider that the edges do not change since we will use Lagrangian Finite Elements spaces.

2.2.5 Finite Elements spaces in the ALE framework

We now introduce a general type of Finite Elements space used to discretize the ALE formulation of a problem stated on a moving domain Ω_t.

Semi-discretization (continuous in time) of the current domain

We consider a finite dimension space $\widehat{\mathcal{X}}_h(\widehat{\Omega}) \subset \widehat{\mathcal{X}}(\widehat{\Omega})$ defined on $\widehat{\Omega}$. The corresponding discrete space $\mathcal{X}_h(\Omega_{h,t})$ on $\Omega_{h,t}$ is:

$$\mathcal{X}_h(\Omega_t) = \{v_h : \mathcal{D}_{h,T} \to \mathbb{R},\ v_h = \widehat{v}_h \circ \widehat{\mathcal{A}}_{h,t}^{-1},\ \widehat{v}_h \in \widehat{\mathcal{X}}(\widehat{\Omega})\}, \tag{2.38}$$

The discrete functional space $\widehat{\mathcal{X}}_h(\widehat{\Omega})$ coincides with $\mathcal{F}_{m,k}(\widehat{\mathcal{T}}_h)$ defined by (2.31), for some arbitrary values of n and for a value $k \leq n$ used for all discrete spaces. In the previous Subsection, we mention that the Finite Elements space for the discrete ALE mapping is chosen for regularity reasons. Formaggia and Nobile [57] demonstrated that this choice guarantees that:

$$\mathcal{X}_h(\Omega_t) = \mathcal{F}_{m,k}(\mathcal{T}_{h,t}), \tag{2.39}$$

where $\mathcal{F}_{m,k}(\mathcal{T}_{h,t})$ is the general Finite Elements space defined on the triangulation $\mathcal{T}_{h,t}$ of the current domain defined as follows:

$$\mathcal{F}_{m,k}(\mathcal{T}_{h,t}) = \{v_h : \mathcal{D}_T \to \mathbb{R} \mid v_h \in C^0\big(\overline{\Omega_t}\big),\ \ v_h|_{K_t} \circ \mathcal{M}_k^{K_t}\ \in P_n(K_0),\ \ \forall K_t \in \mathcal{T}_{h,t}\} \tag{2.40}$$

with $v_h|_{K_t}$ is the restriction of v_h to the Finite Element K_t. The homeomorphic mapping $\mathcal{M}_k^{K_t} \in P_k(K_0)$ is polynomial from K_0 to K_t such that

$$\mathcal{M}_k^{K_t} : K_0 \to K_t,\ \boldsymbol{x}(\zeta) = M_k^{K_t}(\zeta) = \sum_{i \in \mathcal{N}^K} \boldsymbol{x}_i\, \phi_{0,i}(\zeta),\ \zeta \in K_0,\ \phi_{0,i} \in P_k(K_0). \tag{2.41}$$

We now introduce the decomposition of $\widehat{v}_h \in \widehat{\mathcal{X}}_h(\widehat{\Omega})$ and $v_h \in \mathcal{X}_h(\Omega_{h,t})$ according to Finite Elements basis functions. For this purpose, we consider the following set of Finite Elements nodal basis functions on $\widehat{\mathcal{X}}_h(\widehat{\Omega})$:

$$\{\widehat{\varphi}_i,\ \widehat{\varphi}_i \in \widehat{\mathcal{X}}_h(\widehat{\Omega}),\ i \in [\![1, N_h]\!]\ \}, \tag{2.42}$$

where N_h is the dimension of $\widehat{\mathcal{X}}_h$ and $\widehat{\varphi}_i$ is the Finite Elements function associated to the i-th node in $\widehat{\mathcal{T}}_h$. The dimension of $\mathcal{X}_h(\Omega_{h,t})$ is also N_h and the set of Finite Elements nodal basis functions of $\mathcal{X}_h(\Omega_{h,t})$ is:

$$\{\varphi_i = \widehat{\varphi}_i \circ \widehat{\mathcal{A}}_{h,t}^{-1},\ \widehat{\varphi}_i \in \widehat{\mathcal{X}}_h,\ i \in [\![1, N_h]\!]\ \}. \tag{2.43}$$

where φ_i is the Finite Elements function associated to the i-th node in $\mathcal{T}_h$.
Any function $\widehat{v}_h \in \widehat{\mathcal{X}}_h(\widehat{\Omega})$ can then be decomposed as follows:

$$\widehat{v}_h(\widehat{\boldsymbol{x}}) = \sum_{i=1}^{N_h} v_i(t)\, \widehat{\varphi}_i(\widehat{\boldsymbol{x}}), \quad \widehat{\boldsymbol{x}}\ \in \widehat{\Omega},\ t \in]0, T[, \tag{2.44}$$

where v_i is the coefficient of $\widehat{v}_h$ associated to the i-th degree of freedom. The corresponding decomposition for any function $v_h \in \mathcal{X}_h(\Omega_{h,t})$ is:

$$v_h(\boldsymbol{x}, t) = \sum_{i=1}^{N_h} v_i(t)\, \varphi_i(\boldsymbol{x}, t), \quad \forall (\boldsymbol{x}, t) \in \mathcal{D}_{h,T}. \tag{2.45}$$

Apply the relation (2.28) to φ_i, we may write:

$$\left.\frac{\partial v_h}{\partial t}\right|_{\widehat{\Omega}} (\boldsymbol{x}, t) = \sum_{i=1}^{N_h} \frac{dv_i}{dt}(t)\, \varphi_i(\boldsymbol{x}, t), \quad \forall (\boldsymbol{x}, t) \in \mathcal{D}_{h,T}. \tag{2.46}$$

We can point out that these coefficients are the same regardless of the domain on which the function is defined. Indeed, the corresponding function of $v_h(\boldsymbol{x}, t)$ on the ALE frame can be decomposed on the basis functions of its definition space $\widehat{\mathcal{X}}_h$ as (2.44).

Full discretization of the current domain

We introduce a general type of Finite Elements space for a problem raised on a moving domain approximated in space and time. Let Ω_h^n be the discrete domain and $\mathcal{T}_h^n$ its triangulation. The discrete domain Ω_h^n is formed by the union of the elements $K^n \in \mathcal{T}_h^n$ and it may differ from Ω_n due to the approximation of the boundary geometry. We denote by $\mathcal{A}_{h,n}$ the discrete mapping between $\widehat{\mathcal{T}}_h$ and $K^n \in \mathcal{T}_h^n$. We use the following general Finite Elements space defined on the triangulation $\mathcal{T}_h^n$:

$$\mathcal{F}_{m,k}(\mathcal{T}_h^n) = \{v_h : \Omega_h^n \to \mathbb{R} \mid v_h \in C^0\big(\overline{\Omega^n}\big), \;\; v_h|_{K^n} \circ \mathcal{M}_k^{K^n} \;\; \in P_m(K_0), \;\; \forall K^n \in \mathcal{T}_h^n\}, \tag{2.47}$$

and the discrete functional space reads:

$$\mathcal{X}_h(\Omega_h^n) = \{v_h : \Omega_h^n \to \mathbb{R}, \; v_h = \widehat{v}_h \circ \widehat{\mathcal{A}}_{h,n}^{-1}, \; \widehat{v}_h \in \widehat{\mathcal{X}}_h(\widehat{\Omega})\}. \tag{2.48}$$

The set of Finite Elements nodal basis functions of $\mathcal{V}_h^n(\Omega_h^n)$ is:

$$\{\varphi_i^n = \widehat{\varphi}_i \circ \widehat{\mathcal{A}}_{h,n}^{-1}, \; \widehat{\varphi}_i \in \widehat{\mathcal{X}}_h(\widehat{\Omega}), \; i \in [\![1, N_h]\!] \}, \tag{2.49}$$

where φ_i^n is the Finite Elements function associated to the i-th node in $\mathcal{T}_h^n$. Any function $v_h^n \in \mathcal{X}_h(\Omega_h^n)$ can be written as:

$$v_h^n = \sum_{i=1}^{N_h} v_i^n \, \varphi_i^n, \tag{2.50}$$

where v_i^n is the coefficient at time $t = t^n$ of $\widehat{v}_h$ associated to the i-th degree of freedom.

2.3 Free surface Navier–Stokes equations

In this section, we introduce the three-dimensional free surface problem posed on moving domains. Throughout this chapter, we consider only solid and vertical lateral boundaries, i.e. imperviousness boundaries with no-slip boundary conditions. We begin by describing the three-dimensional Navier–Stokes equations governing the motion of a fluid. Then, we present the boundary conditions at the free surface and solid boundaries in order to close the system. The entire problem is then formulated in the ALE framework as well as its variational formulation.

2.3.1 Three-dimensional Navier–Stokes equations

We consider an inviscid, homogeneous (constant density ρ) and Newtonian fluid bounded from below by a topography $b(x, y)$ and from above by a free surface $\eta(x, y, t)$. The fluid

is subjected to external forces $\mathbf{f} = (\boldsymbol{f}_{xy},\, f_z)$ and to the gravity force $\mathbf{g} = -g\,\mathbf{e}_z$. The flow is assumed to be incompressible. The velocity field of the fluid is given by $\mathbf{u} = \mathbf{u}(\boldsymbol{x}, t)$ and its pressure is denoted by $p = p(\boldsymbol{x}, t)$. The horizontal velocity of $\mathbf{u}$ is denoted by $\boldsymbol{u}^{hor}$ and the vertical velocity is w. At the free surface $\Gamma_{s,t}$, the horizontal and vertical velocities are respectively represented by $\boldsymbol{u}^{hor}_{|_{z=\eta}}$ and $w_{|_{z=\eta}}$. The geophysical flows are governed by the Navier–Stokes equations. These equations are a specific case of the Cauchy equations [66] of the representation of a continuous media. They express the mass conservation of the fluid as well as the conservation of the momemtum. The non-conservative form of the Navier–Stokes equations reads:

$$\begin{cases} \dfrac{\partial \mathbf{u}}{\partial t} + \big(\mathbf{u}\cdot\nabla\big)\mathbf{u} - \dfrac{1}{\rho}\nabla\cdot\sigma = \mathbf{f} + \mathbf{g}, & \text{on } \mathcal{D}_T, \quad (2.51) \\ \nabla\cdot\mathbf{u} = 0, & \text{on } \mathcal{D}_T, \quad (2.52) \end{cases}$$

where σ is the Cauchy stress tensor:

$$\sigma = 2\,\mu\,\mathbf{D}(\mathbf{u}) - p\,\mathbf{I}, \tag{2.53}$$

with μ the dynamic viscosity and $\mathbf{I}$ the identity matrix. In this thesis, we consider a constant dynamic viscosity. Furthermore, $\mathbf{D}(\mathbf{u})$ is the strain rate tensor such that:

$$\mathbf{D}(\mathbf{u}) = \frac{1}{2}\big(\nabla\mathbf{u} + (\nabla\mathbf{u})^T\big). \tag{2.54}$$

Since the fluid is Newtonian and the flow is incompressible, the divergence of the strain rate tensor can be expressed with the following behavior law:

$$\nabla\cdot\sigma = \mu\,\Delta\mathbf{u} - \nabla p. \tag{2.55}$$

The Navier–Stokes equations in non-conservative form are:

$$\begin{cases} \dfrac{\partial \mathbf{u}}{\partial t} + \big(\mathbf{u}\cdot\nabla\big)\mathbf{u} - \nu\Delta\mathbf{u} + \dfrac{1}{\rho}\nabla p = \mathbf{f} + \mathbf{g}, & \text{on } \mathcal{D}_T, \quad (2.56) \\ \nabla\cdot\mathbf{u} = 0, & \text{on } \mathcal{D}_T, \quad (2.57) \end{cases}$$

where $\nu = \dfrac{\mu}{\rho}$ represents the kinematic viscosity of the fluid.

In this thesis, we consider the system (2.56-2.57). The rewriting (2.55) modifies the expression of the energy balance, the weak formulation of the problem and the boundary conditions. In general, it is more convenient to keep the form (2.51,2.52) in order to prescribe the physical boundary conditions of the problem and to obtain the correct expression of the energy.

2.3.2 Boundary conditions

Let $\mathbf{n} = (\mathbf{n}_{xy}, n_z)$ be the three-dimensional outward normal unit vector to $\partial\Omega_t$ where $\mathbf{n}_{xy} = (n_x, n_y)$ is the horizontal component part and n_z is the vertical one. At the free surface boundary $\Gamma_{s,t}$, we denote specifically by $\mathbf{n}_{s,t}$ the outward normal unit vector which reads

$$\mathbf{n}_{s,t} = \frac{(-\nabla_{hor}\eta, 1)}{\sqrt{1 + |\nabla\eta|^2}}. \tag{2.58}$$

At the vertical lateral boundaries $\Gamma_{l,t}$, we have that $\mathbf{n}_{xy} = \mathbf{n}_\omega$ and $n_z = 0$, where $\mathbf{n}_\omega$ is the two-dimensional outward normal unit vector to $\partial\omega$. In this section, we begin by introducing the boundary conditions at the free surface $\Gamma_{s,t}$ and the ones at the solid boundaries $\Gamma_{l,t}$ and Γ_b.

Boundary condition at the free surface

Kinematic condition:
The kinematic condition at the free surface expresses the fact that a particle at the free surface moves tangentially to the free surface for any time $t \in]0, T[$. If we denote the trajectory of a particle at the free surface by $\boldsymbol{x}(t) = (x(t), y(t), z(t))$ for any time $t \in]0, T[$, the kinematic condition reads:

$$z(t) = \eta(x(t), y(t), t), \tag{2.59}$$

and then, by applying the operator $\dfrac{d}{dt}$:

$$\frac{d}{dt}\big(\eta(x(t), y(t), t) - z(t)\big) = 0. \tag{2.60}$$

Consequently, the advection equation with source term at the free surface reads:

$$\frac{\partial\eta}{\partial t} + (\boldsymbol{u}^{hor}_{|_{z=\eta}} \cdot \nabla_{hor})\,\eta = w_{|_{z=\eta}}, \quad \text{on } \omega\times]0, T[. \tag{2.61}$$

By considering the outward normal unit vector at the free surface $\mathbf{n}_{s,t}$ (see (2.58)), the kinematic condition is written as an equality between the velocity of the fluid at the free surface and the free surface elevation itself:

$$\frac{\partial\eta}{\partial t} - \sqrt{1 + |\nabla\eta|^2}\,\mathbf{u}_{|_{z=\eta}} \cdot \mathbf{n}_{s,t} = 0 \quad \text{on} \quad \Gamma_{s,t}. \tag{2.62}$$

Since the free surface elevation η of the current domain Ω_t is an unknown of the problem, the kinematic free surface condition is an additional equation of the free surface Navier–Stokes equations.

Dynamic condition
We consider that the fluid is in contact with an external perfect fluid, typically the air.

For any time $t \in]0,T[$, the physical dynamic condition expresses the continuity of forces at the free surface:

$$(\sigma \cdot \mathbf{n}_{s,t})_{fluid} = (\sigma \cdot \mathbf{n}_{s,t})_{air}, \quad \text{on} \quad \Gamma_{s,t}. \tag{2.63}$$

We assume that the pressure of the external fluid is equal to the atmospheric pressure p_{atm} and that the viscous air stress is negligible, we then have for any $t \in]0,T[$:

$$\sigma \cdot \mathbf{n}_{s,t} = -p_{atm} \cdot \mathbf{n}_{s,t}, \quad \text{on} \quad \Gamma_{s,t}. \tag{2.64}$$

In the case where the influence of wind is taken into account, wind forcing appears in the equations through the physical dynamic condition at the free surface. For each tangential unit vector $\mathbf{t}_{s,t}$ to $\Gamma_{s,t}$, the condition writes, for any $t \in]0,T[$:

$$(\sigma \cdot \mathbf{n}_{s,t}) \cdot \mathbf{t}_{s,t} = \gamma_{wind} \, (\mathbf{u}_{air} - \mathbf{u}) \cdot \mathbf{t}_{s,t}, \quad \text{on} \quad \Gamma_{s,t}, \tag{2.65}$$

$$(\sigma \cdot \mathbf{n}_{s,t}) \cdot \mathbf{n}_{s,t} = -p_{atm}, \quad \text{on} \quad \Gamma_{s,t}, \tag{2.66}$$

where $\mathbf{u}_{air}$ is the wind velocity, γ_{wind} a non-negative wind stress coefficient.

Recall that throughout this thesis, we consider a Newtonian fluid and an incompressible flow. As a consequence, using the simplification (2.55), we consider the following dynamic condition at the free surface, for any $t \in]0,T[$:

$$(\mu \nabla \mathbf{u} \cdot \mathbf{n}_{s,t}) \cdot \mathbf{t}_{s,t} = \gamma_{wind} \, (\mathbf{u}_{air} - \mathbf{u}) \cdot \mathbf{t}_{s,t}, \quad \text{on} \quad \Gamma_{s,t}, \tag{2.67}$$

$$\big((\mu \nabla \mathbf{u} - p) \cdot \mathbf{n}_{s,t}\big) \cdot \mathbf{n}_{s,t} = -p_{atm}, \quad \text{on} \quad \Gamma_{s,t}. \tag{2.68}$$

Throughout this thesis, we assume that the atmospherical pressure is zero, i.e $p_{atm} = 0$.

Boundary condition at solid lateral and bottom boundaries

At the solid lateral and bottom boundaries, an adherence condition applies:

$$\mathbf{u} = 0, \quad \text{on} \quad \Gamma_b \cup \Gamma_{l,t}. \tag{2.69}$$

However, this condition is not always prescribed as such in the model. Indeed, in the case of turbulent flows, boundary layers appear in the neighborhood of the solid boundaries. Inside these layers, the velocity field of the fluid strongly increases[4]. Thus, the boundary layers are usually modeled and the first discretization point close to the solid boundary is placed at a distance equivalent to the thickness of the boundary layer. In view of the spatial discretization, the velocity field in the first mesh element is not taken equal to zero. Two weak conditions expressing the kinematic and dynamic condition are used instead of the adherence condition (2.69).

[4]To accurately represent the boundary layer effects in the model requires to fully discretize it, which is overwhelmingly expensive when considering high Reynolds numbers. It is always the case in environmental applications

Kinematic condition
The kinematic condition expresses the imperviousness of the wall:

$$\mathbf{u} \cdot \mathbf{n} = 0, \quad \text{on} \quad \Gamma_b \cup \Gamma_{l,t}. \tag{2.70}$$

Dynamic condition
The dynamic boundary condition at the solid boundaries is usually used in order to take into account the shear stress τ acting on the fluid. This stress is opposed to the velocity of the fluid and acts as a brake. Therefore, the dynamic condition translates the collinearity of the tangential shear stress and the tangential velocity of the fluid at walls. For each tangential unit vector $\mathbf{t}$ to $\Gamma_b \cup \Gamma_{l,t}$, the condition reads for any $t \in]0, T[$:

$$\boldsymbol{\tau} \cdot \mathbf{t} = -(\sigma \cdot \mathbf{n}) \cdot \mathbf{t}, \quad \text{on } \Gamma_b \cup \Gamma_{l,t}. \tag{2.71}$$

where $\boldsymbol{\tau}$ is the shear stress. Since the shear stress $\boldsymbol{\tau}$ depends on the flow, it must be modeled in terms of the unknowns. Dimensional analysis shows that, assuming $\mathbf{u}$ sufficiently far from the solid boundaries, $\boldsymbol{\tau}$ has the form:

$$\boldsymbol{\tau} \cdot \mathbf{t} = \frac{1}{2} \rho C_f |\mathbf{u} \cdot \mathbf{t}| \, \mathbf{u} \cdot \mathbf{t}, \quad \text{on } \Gamma_b \cup \Gamma_{l,t}, \tag{2.72}$$

where C_f is a dimensionless positive friction coefficient. It can be determined using a turbulence model or an empirical formula. For instance, we can use the Strickler formula where C_f depends on the water depth and the bottom roughness. For the sake of simplicity, we denote by $\kappa_f : \mathbb{R}^3 \to \mathbb{R}$ a function such as

$$\kappa_f(|\mathbf{u} \cdot \mathbf{t}|) = \frac{1}{2} \rho C_f |\mathbf{u} \cdot \mathbf{t}|. \tag{2.73}$$

Therefore, we consider the following dynamic condition at the solid boundaries in the form, for any $t \in]0, T[$:

$$(\sigma \cdot \mathbf{n}) \cdot \mathbf{t} = -\kappa_f(|\mathbf{u} \cdot \mathbf{t}|) \, \mathbf{u} \cdot \mathbf{t} \quad \text{on} \quad \Gamma_b \cup \Gamma_{l,t}. \tag{2.74}$$

Since we consider an incompressible flow and Newtonian fluid, by using the simplification (2.55), the dynamic condition (2.74) becomes, for any $t \in]0, T[$:

$$\mu \, (\nabla \mathbf{u} \cdot \mathbf{n}) \cdot \mathbf{t} = -\kappa_f(|\mathbf{u} \cdot \mathbf{t}|) \, \mathbf{u} \cdot \mathbf{t}, \quad \text{on} \quad \Gamma_b \cup \Gamma_{l,t}. \tag{2.75}$$

2.3.3 Free surface Navier–Stokes equations with ALE formulation

Throughout this thesis, we consider that the solutions verify the equations in a L^2 framework. According to the definition of the ALE time derivative (2.16), the free surface Navier–Stokes equations with ALE formulation reads:

$$\begin{cases} \left.\dfrac{\partial \mathbf{u}}{\partial t}\right|_{\widehat{\Omega}} + \big((\mathbf{u} - \mathbf{c}) \cdot \nabla\big)\mathbf{u} - \nu \Delta \mathbf{u} + \dfrac{1}{\rho} \nabla p = \mathbf{f} + \mathbf{g}, & \text{on } \mathcal{D}_T, \quad (2.76) \\ \nabla \cdot \mathbf{u} = 0, & \text{on } \mathcal{D}_T, \quad (2.77) \\ \dfrac{\partial \eta}{\partial t} + \boldsymbol{u}^{hor}_{|z=\eta} \cdot \nabla_{hor} \eta = w_{|z=\eta}, & \text{on } \omega \times]0, T[, \quad (2.78) \end{cases}$$

with the boundary conditions (introduced in Subsection 2.3.2), for any $t \in]0,T[$:

$$\big((\mu\nabla\mathbf{u})\cdot\mathbf{n}_{s,t}\big)\cdot\mathbf{t}_{s,t} = \gamma_{wind}\,(\mathbf{u}_{air}-\mathbf{u})\cdot\mathbf{t}_{s,t}, \quad \text{on} \quad \Gamma_{s,t}, \tag{2.79}$$

$$\big((\mu\nabla\mathbf{u}-p)\cdot\mathbf{n}_{s,t}\big)\cdot\mathbf{n}_{s,t} = 0, \quad \text{on} \quad \Gamma_{s,t}, \tag{2.80}$$

$$\mu(\nabla\mathbf{u}\cdot\mathbf{n})\cdot\mathbf{t} = -\kappa_f(|\mathbf{u}\cdot\mathbf{t}|)\,\mathbf{u}\cdot\mathbf{t}, \quad \text{on} \quad \Gamma_b\cup\Gamma_{l,t}, \tag{2.81}$$

$$\mathbf{u}\cdot\mathbf{n} = 0, \quad \text{on} \quad \Gamma_b\cup\Gamma_{l,t}. \tag{2.82}$$

2.3.4 Time discretization

Let us recall that we consider a time interval $]0,T[$ divided into N time steps of equal length $\Delta t \in \mathbb{R}_*^+$. For $n \in [\![0, N-1]\!]$, we denote by Ω^n the approximation of the domain occupied by the fluid at time $t^n = n\Delta t$. The time approximation of the boundaries dependent on time are denoted by Γ_s^n and Γ_l^n. The time approximation of the outward normal and tangential vectors (of the tangential domain) at the free surface are respectively denoted by $\mathbf{n}_s^n$ and $\mathbf{t}_s^n$. The time-discrete solutions are $\mathbf{u}^n$, p^n and η^n. At the free surface, we denote by $(\boldsymbol{u}^{hor,n}_{|_{z=\eta^n}}, w^n_{|_{z=\eta^n}})$ the time-discrete velocity. The time-discrete velocity of the domain between Ω^n and Ω^{n+1} is $\mathbf{c}^n$ and it is defined in Ω^n. For the sake of simplicity, we denote by $\mathbf{u}_{n+1}^n$ and $\mathbf{c}_{n+1}^n$ in Ω^{n+1} the velocities defined as follows:

$$\mathbf{u}_{n+1}^n = \mathbf{u}^n \circ \mathcal{A}_{n,n+1}, \quad \text{in } \Omega^{n+1}, \tag{2.83}$$

$$\mathbf{c}_{n+1}^n = \mathbf{c}^n \circ \mathcal{A}_{n,n+1}, \quad \text{in } \Omega^{n+1}, \tag{2.84}$$

where $\mathcal{A}_{n,n+1}$ is the given mapping between Ω^n and Ω^{n+1} (see (2.17)) written as follows:

$$\mathcal{A}_{n,n+1}(\boldsymbol{x}) = \widehat{\mathcal{A}}^{n+1} \circ \big(\widehat{\mathcal{A}}^n\big)^{-1}(\boldsymbol{x}), \tag{2.85}$$

with $\widehat{\mathcal{A}}^n$ the time-discrete mapping between the reference domain $\widehat{\Omega}$ and the current domain Ω^n (defined in (2.10)).

The free surface Navier–Stokes equations (2.76-2.78) can be solved numerically by advecting the free surface elevation and by solving the Navier–Stokes equations. We present a time discretization with a first order Euler scheme (other time schemes can be considered [115]).

i/ Time-discrete kinematic free surface equation:
We consider an explicit Euler scheme in time, the time-discrete kinematic free surface equation on ω writes:

$$\frac{\eta^{n+1}-\eta^n}{\Delta t} - \boldsymbol{u}^{hor,n}_{|_{z=\eta^n}}\cdot\nabla\eta^n = w^n_{|_{z=\eta^n}}, \quad \text{on } \omega. \tag{2.86}$$

At the boundaries, we have that $\boldsymbol{u}^{hor,n}_{|_{z=\eta^n}}\cdot\mathbf{n}_\omega = 0$ since the fluid velocity satisfies the impermeability condition (2.70) and $\mathbf{n} = (\mathbf{n}_\omega, 0)$ on Γ_l^n. We notice that the kinematic

free surface equation is an advection equation with a source term. When explicit time schemes are used, the hyperbolic nature of the advection equation implies that the space derivatives must be upwinded. In the Finite Elements framework, this equation can be numerically solved by the method of characteristics [113], the MURD method [108, 111] or stabilized methods [126]. The Chapter 4 is devoted to a stability analysis of a first-order explicit scheme in time and Finite Elements with symmetric stabilization term for the kinematic free surface equation.

ii/ Time-discrete Navier–Stokes equations:
We consider a first order semi-implicit Euler scheme in time, the time-discrete Navier–Stokes equations on Ω^{n+1} read:

$$\begin{cases} \dfrac{\mathbf{u}^{n+1}-\mathbf{u}^{n}_{n+1}}{\Delta t} + \big((\mathbf{u}^{n}_{n+1}-\mathbf{c}^{n}_{n+1})\cdot\nabla\big)\mathbf{u}^{n+1} - \nu\Delta\mathbf{u}^{n+1} + \dfrac{1}{\rho}\nabla p^{n+1} = \mathbf{f}^{n+1}+\mathbf{g}, & (2.87) \\ \nabla\cdot\mathbf{u}^{n+1} = 0, & (2.88) \end{cases}$$

with the boundary conditions:

$$\big(\mu\nabla\mathbf{u}^{n+1}\cdot\mathbf{n}^{n+1}_{s}\big)\cdot\mathbf{t}^{n+1}_{s} = \gamma_{wind}\,(\mathbf{u}^{n+1}_{air}-\mathbf{u}^{n+1})\cdot\mathbf{t}^{n+1}_{s}, \quad \text{on } \Gamma^{n+1}_{s}, \tag{2.89}$$

$$\big((\mu\nabla\mathbf{u}^{n+1}-p^{n+1})\cdot\mathbf{n}^{n+1}_{s}\big)\cdot\mathbf{n}^{n+1}_{s} = 0, \quad \text{on } \Gamma^{n+1}_{s}, \tag{2.90}$$

$$(\mu\nabla\mathbf{u}^{n+1}\cdot\mathbf{n})\cdot\mathbf{t} = -\kappa_f(|\mathbf{u}^{n+1}\cdot\mathbf{t}|)\,\mathbf{u}^{n+1}\cdot\mathbf{t}, \quad \text{on } \Gamma_b\cup\Gamma^{n+1}_{l}, \tag{2.91}$$

$$\mathbf{u}^{n+1}\cdot\mathbf{n} = 0, \quad \text{on } \Gamma_b\cup\Gamma^{n+1}_{l}. \tag{2.92}$$

This strategy in time has been adopted in Maury [100]. The author proposed and showed the unconditional stability of characteristic ALE scheme in the Finite Elements context. Afterwards, this method has been used by Decoene and Maury [46] with a particular ALE method that is commonly used in the hydrodynamic communities: the ALE-Sigma method [45].

2.3.5 Semi-discrete in time variational formulations

Throughout this thesis, $\widehat{\mathcal{V}}(\widehat{\Omega})$, $\widehat{\mathcal{Q}}(\widehat{\Omega})$ and $\mathcal{M}(\omega)$ are respectively general functional spaces for the velocity, the pressure and the free surface. The functional spaces $\widehat{\mathcal{V}}(\widehat{\Omega})$, $\widehat{\mathcal{Q}}(\widehat{\Omega})$ are defined on the reference domain $\widehat{\Omega}$ and $\mathcal{M}(\omega)$ is defined on ω. The regularity will be adapted and specified according to the studied variational formulations. In this subsection, we consider:

$$\widehat{\mathcal{V}}(\widehat{\Omega}) = H^1(\widehat{\Omega}), \tag{2.93}$$

$$\widehat{\mathcal{Q}}(\widehat{\Omega}) = L^2(\widehat{\Omega}), \tag{2.94}$$

$$\mathcal{M}(\omega) = H^1(\omega). \tag{2.95}$$

The corresponding ALE functional spaces $\mathcal{V}^{n+1}(\Omega^{n+1})$ and $\mathcal{Q}^{n+1}(\Omega^{n+1})$ determined by the time-discrete ALE mapping $\widehat{\mathcal{A}}^{n+1}$ (see Subsection 2.2.5) are:

$$\mathcal{V}(\Omega^{n+1}) = \{v^{n+1} : \Omega^{n+1} \to \mathbb{R} \mid v^{n+1} = \widehat{v} \circ (\widehat{\mathcal{A}}^{n+1})^{-1},\ \widehat{v} \in \widehat{\mathcal{V}}(\widehat{\Omega})\}. \tag{2.96}$$

$$\mathcal{Q}(\Omega^{n+1}) = \{q^{n+1} : \Omega^{n+1} \to \mathbb{R} \mid q^{n+1} = \widehat{q} \circ (\widehat{\mathcal{A}}^{n+1})^{-1},\ \widehat{q} \in \widehat{\mathcal{Q}}(\widehat{\Omega})\}. \tag{2.97}$$

These spaces are defined on the current domain Ω^{n+1}. In addition, we define:

$$\mathcal{V}_0(\Omega^{n+1}) = \{\mathbf{v}^{n+1} \in \left(\mathcal{V}^{n+1}(\Omega^{n+1})\right)^3 \ \mid \ \mathbf{v}^{n+1} \cdot \mathbf{n} = 0 \text{ on } \Gamma_b \cup \Gamma_l^{n+1}\}. \tag{2.98}$$

i/ Semi-discrete in time variational formulation of the kinematic free surface equation:
A well-posed semi-discrete in time variational formulation of the kinematic free surface equation (2.86), see [115], is:

$$\begin{cases} \text{Find } \eta^{n+1} \in \mathcal{M}(\omega) \text{ such that for all } \psi \in \mathcal{M}(\omega) \\ \left(\dfrac{\eta^{n+1} - \eta^n}{\Delta t}, \psi\right)_\omega + \left(\boldsymbol{u}^{hor,n}_{|_{z=\eta^n}} \cdot \nabla_{hor}\eta^n, \psi\right)_\omega = \left(w^n_{|_{z=\eta^n}}, \psi\right)_\omega, \end{cases} \tag{2.99}$$

ii/ Semi-discrete in time variational formulation of the Navier–Stokes equations:
The time-discrete Navier–Stokes equations (2.87-2.88) can be solved through a coupled method or a projection method (Guermond et al. [67]). A semi-discrete in time mixed variational formulation is:

$$\begin{cases} \text{Find } (\mathbf{u}^{n+1}, p^{n+1}) \in \mathcal{V}_0(\Omega^{n+1}) \times \mathcal{Q}(\Omega^{n+1}) \\ \text{such that for all } (\mathbf{v}^{n+1}, q^{n+1}) \in \mathcal{V}_0(\Omega^{n+1}) \times \mathcal{Q}(\Omega^{n+1}) \\ \displaystyle\int_{\Omega^{n+1}} \frac{\mathbf{u}^{n+1} - \mathbf{u}^n_{n+1}}{\Delta t} \cdot \mathbf{v}^{n+1} + c_{n+1}(\mathbf{u}^n_{n+1} - \mathbf{c}^n_{n+1}, \mathbf{u}^{n+1}, \mathbf{v}^{n+1}) \\ + a_{n+1}(\mathbf{u}^{n+1}, \mathbf{v}^{n+1}) - \dfrac{1}{\rho} b_{n+1}(\mathbf{v}^{n+1}, p^{n+1}) = (\mathbf{f}^{n+1}, \mathbf{v}^{n+1})_{n+1} + (\mathbf{g}, \mathbf{v}^{n+1})_{n+1}, \quad (2.100) \\ - b_{n+1}(\mathbf{u}^{n+1}, q^{n+1}) = 0, \quad (2.101) \end{cases}$$

where

$$a_{n+1}(\mathbf{u}^{n+1}, \mathbf{v}^{n+1}) = \nu \left(\nabla \mathbf{u}^{n+1}, \nabla \mathbf{v}^{n+1}\right)_{n+1}, \tag{2.102}$$

$$c_{n+1}(\mathbf{u}^n_{n+1} - \mathbf{c}^n_{n+1}, \mathbf{u}^{n+1}, \mathbf{v}^{n+1}) = \left(\left((\mathbf{u}^n_{n+1} - \mathbf{c}^n_{n+1}) \cdot \nabla\right)\mathbf{u}^{n+1}, \mathbf{v}^{n+1}\right)_{n+1}, \tag{2.103}$$

$$b_{n+1}(\mathbf{v}^{n+1}, p^{n+1}) = \left(\nabla \cdot \mathbf{v}^{n+1}, p^{n+1}\right)_{n+1}, \tag{2.104}$$

with $(\cdot,\cdot)_{n+1}$ the time-discrete inner product in $L^2(\Omega^{n+1})$. The formulation (2.100,2.101) is well posed since it exists $\beta > 0$ such that:

$$\inf_{q^{n+1} \in \mathcal{Q}(\Omega^{n+1})} \sup_{\mathbf{v}^{n+1} \in \mathcal{V}_0(\Omega^{n+1})} \frac{b_{n+1}(\mathbf{v}^{n+1}, q^{n+1})}{\|\mathbf{v}^{n+1}\|_{1,n+1} \|q\|_{0,n+1}} \geq \beta. \tag{2.105}$$

where $\|\cdot\|_{1,n+1}$ is the H^1-norm and $\|\cdot\|_{0,n+1}$ is the L^2-norm in Ω^{n+1}. An interested reader can refer to Brezzi [19] or Ern and Guermond [53]. This condition is called the Ladyzhenskaya–Babuška–Brezzi condition or simply the inf-sup condition.

2.3.6 Fully discrete variational formulations

We consider the discrete domain Ω_h^n, that is deduced from $\widehat{\Omega}$ through the discrete ALE mapping $\mathcal{A}_h^n$ (see Subsection 2.2.4). Notice that since the discrete ALE mapping is defined from the free surface, the domain Ω_h^n is different from Ω_{h,t^n}, i.e. $\Omega_h^n \neq \Omega_{h,t^n}$. The approximation of the free surface boundary is denoted by $\Gamma_{h,s}^n$. Since ω is a polygonal domain, it is equal to the two-dimensional horizontal discrete domain. In the sequel, we denote the discrete solutions by $\mathbf{u}_h^n$, p_h^n and η_h^n. At the free surface, we denote the discrete fluid velocities by $\boldsymbol{u}_{h,|_{z=\eta_h^n}}^{hor,n}$ and $w_{h,|_{z=\eta^n}}^n$. The mesh velocity between Ω_h^n and Ω_h^{n+1} is denoted by $\mathbf{c}_h^n$ and it is defined in Ω_h^n. We denote by $\mathbf{u}_{h,n+1}^n$ and $\mathbf{c}_{h,n+1}^n$ the discrete velocity fields in Ω_h^{n+1} defined as follows:

$$\mathbf{u}_{h,n+1}^n = \mathbf{u}_h^n \circ \mathcal{A}_{h,n,n+1} \quad \text{in } \Omega_h^{n+1}, \tag{2.106}$$

$$\mathbf{c}_{h,n+1}^n = \mathbf{c}_h^n \circ \mathcal{A}_{h,n,n+1} \quad \text{in } \Omega_h^{n+1}, \tag{2.107}$$

where $\mathcal{A}_{h,n,n+1}$ is the given arbitrary discrete mapping between Ω_h^{n+1} and Ω_h^n.

The discrete functional spaces for the velocity and the pressure are respectively $\widehat{\mathcal{V}}_h(\widehat{\Omega}) \subset \widehat{\mathcal{V}}(\widehat{\Omega})$ and $\widehat{\mathcal{Q}}_h(\widehat{\Omega}) \subset \widehat{\mathcal{Q}}(\widehat{\Omega})$. They are defined on $\widehat{\Omega}$. The discrete functional space for the free surface is $\mathcal{M}_h(\omega) \subset \mathcal{M}(\omega)$. It is defined on ω. The discrete ALE mapping $\widehat{\mathcal{A}}_h^{n+1}$ identifies the corresponding discrete functional spaces defined on the current domain Ω_h^{n+1} such that:

$$\mathcal{V}_h(\Omega_h^{n+1}) = \{v_h^{n+1} : \Omega_h^{n+1} \to \mathbb{R} \mid v_h^{n+1} = \widehat{v}_h \circ (\widehat{\mathcal{A}}_h^{n+1})^{-1},\ \widehat{v}_h \in \widehat{\mathcal{V}}_h(\widehat{\Omega})\}, \tag{2.108}$$

$$\mathcal{Q}_h(\Omega_h^{n+1}) = \{q_h^{n+1} : \Omega_h^{n+1} \to \mathbb{R} \mid q_h^{n+1} = \widehat{q}_h \circ (\widehat{\mathcal{A}}_h^{n+1})^{-1},\ \widehat{q}_h \in \widehat{\mathcal{Q}}_h(\widehat{\Omega})\}. \tag{2.109}$$

Notice that since $\Omega_h^{n+1} \neq \Omega^{n+1}$, we have that $\mathcal{V}_h(\Omega_h^{n+1}) \not\subset \mathcal{V}(\Omega^{n+1})$ and $\mathcal{Q}_h(\Omega_h^{n+1}) \not\subset \mathcal{Q}(\Omega^{n+1})$. However, since $\widehat{\mathcal{V}}_h(\widehat{\Omega}) \subset \widehat{\mathcal{V}}(\widehat{\Omega})$ and $\widehat{\mathcal{Q}}_h(\widehat{\Omega}) \subset \widehat{\mathcal{Q}}(\widehat{\Omega})$, we have that $\mathcal{V}_h(\Omega_h^{n+1}) \subset \widehat{\mathcal{V}}(\Omega_h^{n+1})$ and $\mathcal{Q}_h(\Omega_h^{n+1}) \subset \widehat{\mathcal{Q}}(\Omega_h^{n+1})$. In addition, we define:

$$\mathcal{V}_{0,h}(\Omega_h^{n+1}) = \{\mathbf{v}_h \in \left(\mathcal{V}_h(\Omega_h^{n+1})\right)^3 \ \mid \ \mathbf{v}_h \cdot \mathbf{n} = 0 \text{ on } \Gamma_b \cup \Gamma_l^{n+1}\}. \tag{2.110}$$

i/ Fully discrete variational formulation of the kinematic free surface equation:
The combination of an explicit scheme in time combined to a centered strategy in space is unconditionally unstable for hyperbolic problem (see [115]). To circumvent this problem, we consider a stabilization term $s(\eta_h, \psi_h)$ (not specified here, see [126] for more details) in the fully discrete scheme. The fully discrete variational formulation of (2.99) is:

$$\begin{cases} \text{Find } \eta_h^{n+1} \in \mathcal{M}_h(\omega) \text{ such that for all } \psi_h \in \mathcal{M}_h(\omega) \\ \left(\dfrac{\eta_h^{n+1} - \eta_h^n}{\Delta t}, \psi_h\right)_\omega + \left(\boldsymbol{u}_{h,|_{z=\eta_h^n}}^{hor,n} \cdot \nabla_{hor}\eta_h^n, \psi_h\right)_\omega + s(\eta_h^{n+1}, \psi_h) = \left(w_{h,|_{z=\eta^n}}^n, \psi_h\right)_\omega. \end{cases} \tag{2.111}$$

ii/ Fully discrete variational formulation of the Navier–Stokes equations:
The fully discrete mixed variational formulation of (2.100-2.101) is:

$$\begin{cases} \text{Find } (\mathbf{u}_h^{n+1}, p_h^{n+1}) \in \mathcal{V}_{0,h}(\Omega_h^{n+1}) \times \mathcal{Q}_h(\Omega_h^{n+1}) \\ \text{such that for all } (\mathbf{v}_h^{n+1}, q_h^{n+1}) \in \mathcal{V}_{0,h}(\Omega_h^{n+1}) \times \mathcal{Q}_h(\Omega_h^{n+1}) \\ \displaystyle\int_{\Omega_h^{n+1}} \frac{\mathbf{u}_h^{n+1} - \mathbf{u}_{h,n+1}^{n}}{\Delta t} \cdot \mathbf{v}_h^{n+1} + c_{h,n+1}(\mathbf{u}_{h,n+1}^{n} - \mathbf{c}_{h,n+1}^{n}, \mathbf{u}_h^{n+1}, \mathbf{v}_h^{n+1}) \\ + a_{h,n+1}(\mathbf{u}_h^{n+1}, \mathbf{v}_h^{n+1}) - \frac{1}{\rho} b_{h,n+1}(\mathbf{v}_h^{n+1}, p_h^{n+1}) = (\mathbf{f}_h^{n+1}, \mathbf{v}_h^{n+1})_{h,n+1} \\ \qquad\qquad + (\mathbf{g}, \mathbf{v}_h^{n+1})_{h,n+1}, \qquad (2.112) \\ \qquad\qquad - b_{h,n+1}(\mathbf{u}_h^{n+1}, q_h^{n+1}) = 0, \qquad (2.113) \end{cases}$$

where

$$\begin{aligned} a_{h,n+1}(\mathbf{u}_h^{n+1}, \mathbf{v}_h^{n+1}) &= \nu \left(\nabla \mathbf{u}_h^{n+1}, \nabla \mathbf{v}_h^{n+1}\right)_{h,n+1}, \\ c_{h,n+1}(\mathbf{u}_{h,n+1}^{n} - \mathbf{c}_{h,n+1}^{n}, \mathbf{u}_h^{n+1}, \mathbf{v}_h^{n+1}) &= \left(\left((\mathbf{u}_{h,n+1}^{n} - \mathbf{c}_{h,n+1}^{n}) \cdot \nabla\right)\mathbf{u}_h^{n+1}, \mathbf{v}_h^{n+1}\right)_{h,n+1}, \\ b_{h,n+1}(\mathbf{v}_h^{n+1}, p_h^{n+1}) &= \left(\nabla \cdot \mathbf{v}_h^{n+1}, p_h^{n+1}\right)_{h,n+1}, \end{aligned}$$

with $(\cdot,\cdot)_{h,n+1}$ denotes the discrete inner product on $L^2(\Omega_h^{n+1})$. Notice that $a_{h,n+1}(\cdot,\cdot)$ (resp. $c_{h,n+1}(\cdot,\cdot,\cdot)$ and $b_{h,n+1}(\cdot,\cdot)$) is different from $a_{n+1}(\cdot,\cdot)$ (resp. $c_{n+1}(\cdot,\cdot,\cdot)$ and $b_{n+1}(\cdot,\cdot)$) since they are not defined on the same vectorial space. In the Finite Elements context, the problem is well-posed if the spaces chosen to approximate the velocity and the pressure satisfy a discrete version of the inf-sup condition (2.105): there exists $\beta > 0$ a constant independent on the mesh size such that:

$$\inf_{q_h^{n+1} \in \mathcal{Q}_h(\Omega_h^{n+1})} \sup_{\mathbf{v}_h^{n+1} \in \mathcal{V}_{0,h}(\Omega_h^{n+1})} \frac{b_{h,n+1}(\mathbf{v}_h^{n+1}, q_h^{n+1})}{\|\mathbf{v}_h^{n+1}\|_{1,h,n+1} \|q_h\|_{0,h,n+1}} \geq \beta, \qquad (2.114)$$

where $\|\cdot\|_{1,h,n+1}$ is the H^1-norm and $\|\cdot\|_{0,h,n+1}$ is the L^2-norm in Ω_h^{n+1}. For example, the classical Lagrangian Finite Elements spaces $\mathbb{P}_1$-bubble$\times\mathbb{P}_1$ or $\mathbb{P}_2 \times \mathbb{P}_1$ satisfy this condition. As previously mentioned, an interested reader can refer to Ern and Guermond [53].

2.3.7 Properties of numerical schemes

Some numerical properties need to be satisfied in order to simulate hydrodynamics flows with the best accuracy. Depending to the numerical methods, these properties can be more or less difficult to satisfy simultaneously. They correspond at the discrete level to:

i/ ensure the free divergence condition of the fluid velocity: it is depend on the numerical scheme used, this requirement is necessary to advect the fluid velocity or scalar quantities in order to preserve the mass conservation,

ii/ compute a free surface that satisfies the kinematic free surface equation (2.78): this requirement ensures that the free divergence velocity is compatible with the momentum equations and the free surface boundary condition. Since the ALE discrete mapping is defined from the free surface, the kinematic free surface equation can be written as (2.62) and we have that

$$\mathbf{u}_h^n \cdot \mathbf{n}_{h,s}^n = \mathbf{c}_h^n \cdot \mathbf{n}_{h,s}^n, \quad \text{on } \Gamma_{h,s}^n. \tag{2.115}$$

that ensures the mass conservation of scalar quantities,

iii/ preserve the mass conservation of the water quantity and the positivity of the water height: the mass conservation of the water quantity allows to obtain stability results independent of the movement of the domain. Numerical schemes should be chosen carefully in order to ensure these requirements since the kinematic free surface equation is a non-conservative equation. In Chapter 4, we study a numerical scheme able to ensure the mass conservation of the water.

2.4 Free surface Navier–Stokes equations with pressure decomposition

In this section, we introduce a formulation of the Navier–Stokes equations which is based on the decomposition of the pressure into a hydrostatic and a dynamic part. We begin by introducing the hydrostatic assumption that allows to obtain an expression of the pressure, assumed to be hydrostatic in this case. Then, we focus on the depth-averaged free surface equation which is a conservative equation equivalent to the kinematic free surface equation (2.78). After, we introduce the hydrostatic Navier–Stokes equations with free surface. These equations are used to represent geophysical flows in shallow water and with weak vertical accelerations. Finally, in the case where the flow cannot be considered as hydrostatic, we present a formulation equivalent to (2.76,2.77), which is based on the decomposition of the pressure into a hydrostatic and a dynamic part.

2.4.1 Hydrostatic assumption

The hydrostatic assumption consists in neglecting the vertical acceleration, the diffusion and source terms[5] in the vertical momentum equation of the Navier–Stokes equations. Thus, it is reduced to:

$$\frac{\partial p}{\partial z} = -\rho\, g. \tag{2.116}$$

The equation (2.116) is obtained by neglecting the vertical momentum equation and the continuity equation. If the horizontal scale of the motion dominates the vertical one and if the Reynolds number is large, the vertical acceleration and viscous terms can thereby be neglected. These conditions are verified in shallow water, for long waves or for turbulent

[5]Other than the gravity

flows with dominating horizontal motions. Integrating (2.116) over the depth, we deduce an approximation of the pressure:

$$p(\boldsymbol{x},t) = \rho\, g\ \ (\eta(x,y,t) - z) + p_{atm}, \tag{2.117}$$

using the condition $p(x,y,\eta(x,y,t),t) = p_{atm}$. Applying the horizontal gradient operator on (2.117), we obtain:

$$\nabla_{hor}\, p(\boldsymbol{x},t) = \rho\, g\, \nabla_{hor}\eta(x,y,t). \tag{2.118}$$

2.4.2 Depth-averaged free surface equation

Let us now introduce the depth-averaged free surface equation, which is equivalent to the kinematic equation (2.61). It corresponds to a conservative formulation of the free surface equation. At the discrete level, this formulation enables to enforce the conservation of the water quantity. Nevertheless, this formulation does not enable to ensure (2.115). The depth-averaged free surface equation is often used in hydrodynamics models [30, 31, 76] and it corresponds to:

Proposition 2.3. *If the continuity equation (2.57) as well as the kinematic boundary condition at the bottom (2.70) are satisfied, then we have the following equivalence between the kinematic condition at the free surface*

$$\frac{\partial \eta}{\partial t} + (\boldsymbol{u}^{hor}_{|_{z=\eta}} \cdot \nabla_{hor})\, \eta = w_{|_{z=\eta}}, \qquad on\ \omega\times]0,T[,$$

and the free surface equation which is under conservative form:

$$\frac{\partial \eta}{\partial t} + \nabla_{hor} \cdot \int_b^\eta \boldsymbol{u}^{hor}\, dz = 0, \qquad on\ \omega\times]0,T[. \tag{2.119}$$

A demonstration of this Proposition can be found in the PhD thesis of Decoene [44] in Subsection 5.5.

2.4.3 Hydrostatic equations

Based on the hydrostatic assumption (2.116) and on Proposition 2.3, the free surface Navier–Stokes equations (2.76-2.78) can be reduced to the so-called hydrostatic Navier–Stokes equations. They are composed of the horizontal momentum equations and the free surface equation such that:

$$\begin{cases} \left.\dfrac{\partial \boldsymbol{u}^{hor}}{\partial t}\right|_{\widehat{\Omega}} + ((\mathbf{u}-\mathbf{c})\cdot\nabla)\,\boldsymbol{u}^{hor} - \nu\Delta\boldsymbol{u}^{hor} + g\,\nabla_{hor}\eta = \boldsymbol{f}_{xy}, & \text{on } \mathcal{D}_T, \quad (2.120) \\ \dfrac{\partial \eta}{\partial t} + \nabla_{hor}\cdot\left(\displaystyle\int_b^\eta \boldsymbol{u}^{hor}\, dz\right) = 0, & \text{on } \omega\times]0,T[, \quad (2.121) \\ \nabla_{hor}\cdot\boldsymbol{u}^{hor} + \dfrac{\partial w}{\partial z} = 0, & \text{on } \mathcal{D}_T. \quad (2.122) \end{cases}$$

The boundary conditions associated to the hydrostatic equations are adapted to the problem. We denote by $\mathbf{t}_{xy}$ the horizontal vector of each tangential unit vector $\mathbf{t}$. The boundary conditions reads:

$$\mu \nabla \boldsymbol{u}^{hor} \cdot \mathbf{n}_{s,t} = \gamma_{wind} \left(\boldsymbol{u}^{hor}_{air} - \boldsymbol{u}^{hor}\right), \qquad \text{on } \Gamma_{s,t}, \tag{2.123}$$

$$(\mu \nabla_{hor} \boldsymbol{u}^{hor} \cdot \mathbf{n}_{xy}) \cdot \mathbf{t}_{xy} = -\kappa_f(|\boldsymbol{u}^{hor} \cdot \mathbf{t}_{xy}|)\, \boldsymbol{u}^{hor} \cdot \mathbf{t}_{xy}, \qquad \text{on } \Gamma_{l,t}, \tag{2.124}$$

$$\boldsymbol{u}^{hor} \cdot \mathbf{n}_{xy} = 0, \qquad \text{on } \Gamma_{l,t}, \tag{2.125}$$

$$\mu \nabla \boldsymbol{u}^{hor} \cdot \mathbf{n} = -\kappa_f(|\boldsymbol{u}^{hor}|)\, \boldsymbol{u}^{hor}, \qquad \text{on } \Gamma_b. \tag{2.126}$$

Notice that the hydrostatic equations do not involve the time-derivative of the vertical velocity w. As a consequence, no initial condition on w is required. In the literature, these equations are also called the three-dimensional shallow water equations [30]. Several software have been originally developed to solve the hydrostatic equations such as (Un)Trim-3D [30, 33], Telemac-3D [76], Delft3D [94], etc. In the Finite Difference framework, Casulli and Cattani [29] studied the stability of a semi-implicit discretization in time of the hydrostatic equations. The authors show that unconditional stability is ensured in the case where the diffusion and free surface terms are treated in an implicit way. An advantage of this problem is its lower computational cost compared to the free surface Navier–Stokes equations (2.76-2.82). However, the three-dimensional hydrostatic model is known to be ill-posed when open boundaries are considered [107, 98].

2.4.4 Non-hydrostatic correction

The hydrostatic assumption is not valid in many cases, in particular, when a steep bottom causes significant changes in the vertical velocity, for flows around structures, for flows influenced by density changes, internal waves, etc. When the pressure cannot be assumed hydrostatic and when the vertical accelerations are important compared to the horizontal acceleration, the free surface Navier–Stokes equations (2.76-2.77) must be used. These equations can be reformulated using the following pressure splitting:

$$p(\boldsymbol{x}, t) = p_h(\boldsymbol{x}, t) + p_d(\boldsymbol{x}, t), \tag{2.127}$$

where p_h is the hydrostatic pressure, i.e. given by (2.116), and p_d is the dynamic pressure. The non-conservative free surface Navier–Stokes equations based on the pressure decomposition are, for all $t \in]0, T[$:

$$\begin{cases} \left.\dfrac{\partial \boldsymbol{u}^{hor}}{\partial t}\right|_{\widehat{\Omega}} + \big((\mathbf{u} - \mathbf{c}) \cdot \nabla\big)\boldsymbol{u}^{hor} - \nu\, \Delta \boldsymbol{u}^{hor} + g\, \nabla_{hor}\eta + \dfrac{1}{\rho}\nabla_{hor} p_d = \mathbf{f}_{xy}, & \text{on } \Omega_t, \quad (2.128) \\ \left.\dfrac{\partial w}{\partial t}\right|_{\widehat{\Omega}} + ((\mathbf{u} - \mathbf{c}) \cdot \nabla) w - \nu\, \Delta w + \dfrac{1}{\rho}\dfrac{\partial p_d}{\partial z} = \mathbf{f}_z, & \text{on } \Omega_t, \quad (2.129) \\ \nabla \cdot \mathbf{u} = 0, & \text{on } \Omega_t, \quad (2.130) \\ \dfrac{\partial \eta}{\partial t} + \nabla_{hor} \cdot \displaystyle\int_b^{\eta} \boldsymbol{u}^{hor}\, dz = 0, & \text{on } \omega, \quad (2.131) \end{cases}$$

with the boundary conditions:

$$\left(\mu\nabla\mathbf{u}\cdot\mathbf{n}_{s,t}\right)\cdot\mathbf{t}_{s,t}=\gamma_{wind}\left(\mathbf{u}_{air}-\mathbf{u}\right)\cdot\mathbf{t}_{s,t},\qquad\text{on}\quad\Gamma_{s,t},\tag{2.132}$$

$$\left(\left(\mu\nabla\mathbf{u}-p_d\right)\cdot\mathbf{n}_{s,t}\right)\cdot\mathbf{n}_{s,t}=0,\qquad\text{on}\quad\Gamma_{s,t},\tag{2.133}$$

$$\mu(\nabla\mathbf{u}\cdot\mathbf{n})\cdot\mathbf{t}=-\kappa_f(|\mathbf{u}\cdot\mathbf{t}|)\,\mathbf{u}\cdot\mathbf{t},\qquad\text{on}\quad\Gamma_b\cup\Gamma_{l,t},\tag{2.134}$$

$$\mathbf{u}\cdot\mathbf{n}=0,\qquad\text{on}\quad\Gamma_b\cup\Gamma_{l,t}.\tag{2.135}$$

In the sequel of this Chapter, we present numerical strategies and variational formulations to solve numerically these equations. Chapter 3 is devoted to the numerical study of an industrial software based on the free surface Navier–Stokes equations with pressure decomposition.

2.4.5 Numerical strategy in time

A numerical strategy in time for the free surface Navier–Stokes equations consists in solving a hydrostatic predictor part and a non-hydrostatic corrector part. This strategy presents the advantage to speed up the convergence compared to solving (2.76-2.77). In particular, in the case where the fluid is hydrostatic, the dynamic pressure p_d is close to zero. On the one hand, the hydrostatic predictor step is composed of the hydrostatic equations (2.120,2.121) and the vertical momentum equation (2.129) without the dynamic pressure term. It consists in computing a free surface η^{n+1} and an intermediate velocity $\tilde{\mathbf{u}}^{n+1}=(\tilde{\boldsymbol{u}}^{hor,n+1},\tilde{w}^{n+1})$ which do not satisfy the free divergence condition. The hydrostatic pressure is computed by using (2.117) and yields a first approximation of the pressure. On the other hand, the non-hydrostatic corrector consists in correcting the free divergence velocity $\mathbf{u}^{n+1}$ by the dynamic pressure p_d^{n+1}. For this purpose, the velocity $\tilde{\mathbf{u}}^{n+1}$ is broken down into a free divergence final velocity $\mathbf{u}^{n+1}$ and the gradient of the dynamic pressure p_d^{n+1}. These numerical strategies are commonly used in the literature such as in Casulli [34], Vitousek and Fringer [134] and in Telemac-3D [76], that will be detailed in the next Chapter.

In this Subsection, we introduce numerical strategies in time for both parts. On the one hand, we present numerical strategies that imply to solve coupled problems with mixed formulations, i.e $(\boldsymbol{u}^{hor},\eta)$-problem and/or $(\mathbf{u},p_d)$-problem. On the other hand, we present strategies that implies decoupled formulations. These strategies will be studied in the Finite Elements framework in Section 2.6. We choose a first order implicit Euler scheme in time (other time schemes could have been chosen [115]). The notations used in the Subsection 2.3.4 are considered here.

Coupled numerical strategy in time

Coupled numerical strategies consist in solving a $(\boldsymbol{u}^{hor},\eta)$ problem in the hydrostatic predictor part and a $(\mathbf{u},p_d)$ problem in the non-hydrostatic corrector part. For the hydrostatic predictor part, a first sub-step can be applied in order to isolate the advection terms from the rest of the equations. This idea corresponds in applying a time fractional

step method. If we choose a first order time fractional step, we consider the advection equation on a sub-intermediate velocity field $\tilde{\mathbf{u}}^{n+\frac{1}{2}} = (\tilde{\boldsymbol{u}}^{hor,n+\frac{1}{2}}, \tilde{w}^{n+\frac{1}{2}})$:

$$\frac{\tilde{\mathbf{u}}^{n+\frac{1}{2}} - \mathbf{u}^n}{\Delta t} + \big((\mathbf{u}^n - \mathbf{c}^n)\cdot\big)\nabla \mathbf{u}^{n+\frac{1}{2}} = 0, \quad \text{on } \Omega^n. \tag{2.136}$$

As previously mentioned, the advection term implies to upwind the space derivative in the Finite Elements context. This term can be treated by using the method of characteristics [113], the MURD method [108, 111] or stabilization methods [126].

Then, the hydrostatic Navier–Stokes equations (2.120,2.121) and the vertical momentum equation (2.129) without the advection terms are solved in order to compute the intermediate velocity field $\tilde{\mathbf{u}}^{n+1} = (\tilde{\boldsymbol{u}}^{n+1}, \tilde{w}^{n+1})$. The hydrostatic equations write in this case:

$$\begin{cases} \dfrac{\tilde{\boldsymbol{u}}^{hor,n+1} - \tilde{\boldsymbol{u}}^{hor,n+\frac{1}{2}}}{\Delta t} - \nu\,\Delta\tilde{\boldsymbol{u}}^{hor,n+1} + g\,\nabla_{hor}\eta^{n+1} = \boldsymbol{f}_{xy}^{n+1}, & \text{on } \Omega^n, \quad (2.137) \\ \dfrac{\eta^{n+1} - \eta^n}{\Delta t} + \nabla_{hor}\cdot\displaystyle\int_{b^n}^{\eta^n} \tilde{\boldsymbol{u}}^{hor,n+1}\,dz = 0, & \text{on } \omega, \quad (2.138) \end{cases}$$

with the boundary conditions:

$$\mu\,\nabla\tilde{\boldsymbol{u}}^{hor,n+1}\cdot\mathbf{n}_s^{n+1} = \gamma_{wind}\,(\boldsymbol{u}_{air}^{hor} - \tilde{\boldsymbol{u}}^{hor,n+1}), \qquad \text{on } \Gamma_s^n, \tag{2.139}$$

$$(\mu\,\nabla_{hor}\tilde{\boldsymbol{u}}^{hor,n+1}\cdot\mathbf{n}_{xy})\cdot\mathbf{t}_{xy} = -\kappa_f(|\tilde{\boldsymbol{u}}^{hor,n+1}\cdot\mathbf{t}_{xy}|)\,\tilde{\boldsymbol{u}}^{hor,n+1}\cdot\mathbf{t}_{xy}, \qquad \text{on } \Gamma_l^n, \tag{2.140}$$

$$\tilde{\boldsymbol{u}}^{hor,n+1}\cdot\mathbf{n}_{xy} = 0, \qquad \text{on } \Gamma_l^n, \tag{2.141}$$

$$\mu\,\nabla\tilde{\boldsymbol{u}}^{hor,n+1}\cdot\mathbf{n} = -\kappa_f(|\tilde{\boldsymbol{u}}^{hor,n+1}|)\,\tilde{\boldsymbol{u}}^{hor,n+1}, \qquad \text{on } \Gamma_b. \tag{2.142}$$

Since the vertical momentum equation does not depend on the free surface, its solution can be computed separately from the hydrostatic equations by:

$$\begin{cases} \dfrac{\tilde{w}^{n+1} - \tilde{w}^{n+\frac{1}{2}}}{\Delta t} - \nu\,\Delta\tilde{w}^{n+1} = f_z^{n+1} - g, & \text{on } \Omega^n, \quad (2.143) \\ \mu\,\nabla\tilde{w}^{n+1}\cdot\mathbf{n}_s^n = \gamma_{wind}\,(w_{air}^{hor} - \tilde{w}^{n+1}), & \text{on } \Gamma_s^n, \quad (2.144) \\ \mu\,\nabla\tilde{w}^{n+1}\cdot\mathbf{n} = -\kappa_f(|\tilde{w}^{n+1}|)\,\tilde{w}^{n+1}, & \text{on } \Gamma_l^n \cup \Gamma_b, \quad (2.145) \end{cases}$$

Once the hydrostatic predictor step is performed, the non-hydrostatic corrector step can be solved through the Darcy-type equations:

$$\begin{cases} \dfrac{\mathbf{u}^{n+1} - \tilde{\mathbf{u}}_n^{n+1}}{\Delta t} + \dfrac{1}{\rho}\nabla p_d^{n+1} = 0, & \text{on } \Omega^{n+1}, \quad (2.146) \\ \nabla\cdot\mathbf{u}^{n+1} = 0, & \text{on } \Omega^{n+1}, \quad (2.147) \\ p_d^{n+1} = 0, & \text{on } \Gamma_s^{n+1}, \quad (2.148) \\ \mathbf{u}^{n+1}\cdot\mathbf{n} = 0, & \text{on } \Gamma_b \cup \Gamma_l^{n+1}. \quad (2.149) \end{cases}$$

Decoupled numerical strategy in time

The predictor and corrector parts can be solved by decoupling the hydrostatic Navier–Stokes equations and/or the Darcy equations. On the one hand, the $(\boldsymbol{u}^{hor}, \eta)$ problem consists in computing the free surface and then the velocity. On other hand, the $(\mathbf{u}, p_d)$ problem consists in computing the pressure and the velocity. For the hydrostatic predictor part, a first sub-step can be applied in order to isolate the advection, diffusion and source terms. As previously mentioned, we consider a first order time fractional step and the advection-diffusion equation with source term on a sub-intermediate horizontal velocity field $\tilde{\mathbf{u}}^{n+\frac{1}{2}}$ is for all $\boldsymbol{x} \in \Omega^n$:

$$\begin{cases} \dfrac{\tilde{\boldsymbol{u}}^{hor,n+\frac{1}{2}} - \boldsymbol{u}^{hor,n}}{\Delta t} + \big((\mathbf{u}^n - \mathbf{c}^n)\cdot\big)\nabla \boldsymbol{u}^{hor,n+\frac{1}{2}} - \nu\,\Delta \tilde{\boldsymbol{u}}^{hor,n+\frac{1}{2}} = \mathbf{f}_{xy}^{n+1}, & (2.150) \\ \dfrac{\tilde{w}^{n+\frac{1}{2}} - w^n}{\Delta t} + \big((\mathbf{u}^n - \mathbf{c}^n)\cdot\big)\nabla w^{n+\frac{1}{2}} - \nu\,\Delta \tilde{w}^{n+\frac{1}{2}} = f_z^{n+1} - g, & (2.151) \end{cases}$$

with the boundary conditions

$$\begin{aligned} \big(\mu \nabla \tilde{\mathbf{u}}^{n+\frac{1}{2}} \cdot \mathbf{n}_s^n\big)\cdot \mathbf{t}_s^n &= \gamma_{wind}\,(\mathbf{u}_{air}^{n+1} - \tilde{\mathbf{u}}^{n+\frac{1}{2}})\cdot \mathbf{t}_s^n, && \text{on } \Gamma_s^n, && (2.152)\\ (\mu \nabla \tilde{\mathbf{u}}^{n+\frac{1}{2}} \cdot \mathbf{n}_s^n)\cdot \mathbf{n}_s^n &= 0, && \text{on } \Gamma_s^n, && (2.153)\\ \mu(\nabla \tilde{\mathbf{u}}^{n+\frac{1}{2}} \cdot \mathbf{n})\cdot \mathbf{t} &= -\kappa_f(|\tilde{\mathbf{u}}^{n+\frac{1}{2}}\cdot \mathbf{t}|)\,\tilde{\mathbf{u}}^{n+\frac{1}{2}}\cdot \mathbf{t}, && \text{on } \Gamma_b \cup \Gamma_l^n, && (2.154)\\ \tilde{\mathbf{u}}^{n+\frac{1}{2}}\cdot \mathbf{n} &= 0, && \text{on } \Gamma_b \cup \Gamma_l^n. && (2.155) \end{aligned}$$

We have that $\tilde{w}^{n+1} = \tilde{w}^{n+\frac{1}{2}}$ since the vertical momentum equation is not dependent on the free surface.

The hydrostatic Navier–Stokes equations (2.120,2.121) (without the advection, diffusion and source terms) are then solved in order to compute the intermediate horizontal velocity field $\tilde{\boldsymbol{u}}^{n+1}$. They write in this case:

$$\begin{cases} \dfrac{\tilde{\boldsymbol{u}}^{hor,n+1} - \tilde{\boldsymbol{u}}^{hor,n+\frac{1}{2}}}{\Delta t} + g\,\nabla_{hor}\eta^{n+1} = 0, \quad \text{on } \Omega^n & (2.156) \\ \dfrac{\eta^{n+1} - \eta^n}{\Delta t} + \nabla_{hor}\cdot \displaystyle\int_{b^n}^{\eta^n} \tilde{\boldsymbol{u}}^{hor,n+1}\,dz = 0, \quad \text{on } \omega, & (2.157) \\ \tilde{\boldsymbol{u}}^{hor,n+1}\cdot \mathbf{n}_\omega = 0, \quad \text{on } \Gamma_l^n. & (2.158) \end{cases}$$

These equations can be manipulated in order to obtain a wave equation on the free surface. The idea consists in isolating the horizontal velocity filed $\tilde{\boldsymbol{u}}^{hor,n+1}$ in (2.156) and in replacing its expression in (2.157). A wave equation on the free surface η^{n+1} is then obtained:

$$\begin{cases} \eta^{n+1} - g\,h^n\,\Delta t^2\,\Delta_{hor}\eta^{n+1} = \eta^n - \Delta t\,\nabla_{hor}\cdot\left(\displaystyle\int_{b^n}^{\eta^n} \boldsymbol{u}^{hor,n} dz\right), \quad \text{on } \omega, & (2.159) \\ \nabla_{hor}\eta^{n+1}\cdot \mathbf{n}_\omega = 0, \quad \text{on } \partial\omega. & (2.160) \end{cases}$$

with $h^n = \eta^n - b$ the approximation in time of the water height. Notice that the boundary conditions are obtained by applying the normal outward unit vector[6] $\mathbf{n} = (\mathbf{n}_\omega, 0)$ to Γ_l on the horizontal momentum equation (2.156). Once the free surface is known, the intermediate velocity $\tilde{\boldsymbol{u}}^{hor,n+1}$ is computed as the solution of (2.156) that allows to deduce $\tilde{\mathbf{u}}^{n+1} = (\tilde{\boldsymbol{u}}^{hor,n+1}, \tilde{w}^{n+1})$.

Once the hydrostatic predictor step is performed, the non-hydrostatic corrector step can be considered. The Darcy equations (2.146-2.147) can be manipulated in order to obtain a pressure Poisson equation on the dynamic pressure which reads:

$$\begin{cases} \Delta p_d^{n+1} = \dfrac{\rho}{\Delta t} \nabla \cdot \tilde{\mathbf{u}}_n^{n+1}, & \text{on } \Omega^{n+1}, \quad (2.161) \\ p_d^{n+1} = 0 & \text{on } \Gamma_s^{n+1}, \quad (2.162) \\ \nabla p_d^{n+1} \cdot \mathbf{n} = 0 & \text{on } \Gamma_l^{n+1} \cup \Gamma_b. \quad (2.163) \end{cases}$$

Note that it induces a homogeneous Neumann condition on the dynamic pressure at the solid boundaries which is non-physical. The final velocity $\mathbf{u}^{n+1}$ is then updated through

$$\mathbf{u}^{n+1} = \tilde{\mathbf{u}}_n^{n+1} - \frac{\Delta t}{\rho} \nabla p_d^{n+1}, \quad \text{on } \Omega^{n+1}. \quad (2.164)$$

This manipulation is usual [34, 76] and can be viewed as projection methods [67] since the dynamic pressure term is isolated from the momentum equations. The next Section 2.5 is devoted to a brief review of the projection methods.

2.5 Projection methods for the Navier–Stokes equations

The time discretization methods for the resolution of the incompressible Navier–Stokes equations can be classified as fully coupled or splitting techniques. A classical splitting method initially introduced by Chorin [38] and Temam [124, 125], consists in separating the pressure term from the advection, diffusion and source terms. As a consequence, at each time step, a succession of decoupled elliptic equations for the velocity and the pressure are solved. This constitutes a very attractive feature of the projection methods, making them quite efficient for large scale numerical simulations. Moreover, this technique is easy to implement. A large body of literature has been devoted to the construction, analysis, implementation and the improvement of the projection methods. An interested reader may look at the overview of Guermond, Minev and Shen [67]. In view of the spatial discretization, the projection methods can be combined with any kind of spatial discretization techniques, Finite Difference (Bell et al. [9]), Finite Elements (Donea et al. [48], Gresho and Chan [63]), spectral approximation (Ku et al. [88]), SPH method (Leroy [92]).

[6] Keep in mind that at the lateral boundaries $\mathbf{n}_{xy} = \mathbf{n}_\omega$ and $n_z = 0$

In this section, we aim to give a brief literature review on the projection techniques classified as pressure-correction methods. First, we introduce the classical Chorin–Temam method [38, 124, 125], also named non-incremental pressure-correction method. This method consists in solving an intermediate velocity field $\tilde{\mathbf{u}}^{n+1}$ solution of the momentum equations without the pressure gradient term, not satisfying the incompressibility condition. This first part is called the prediction step. Then, this intermediate solution is decomposed into the sum of a final velocity field with free-divergence $\mathbf{u}^{n+1}$ and the gradient of the pressure p^{n+1}. This second part is called the correction step. Afterwards, we introduce alternative methods: the incremental pressure-correction method or the rotational incremental pressure-correction method. Finally, based on the work of Guermond and Quartapelle [74], we discuss on the resolution of the projection scheme by the Finite Elements method.

In order to simplify the introduction of the projection methods, we consider the time-dependent Navier–Stokes equations defined on a finite time interval $]0,T[$ and in an open fixed, connected, bounded domain $\Omega \subset \mathbb{R}^3$ with a boundary $\partial\Omega$ sufficiently smooth. We assume that the following non trivial partition holds: $\partial\Omega = \Gamma_1 \cup \Gamma_2$, $\Gamma_1 \cap \Gamma_2 = \emptyset$. We impose homogeneous Dirichlet boundary conditions on Γ_1 and a particular dynamic condition on Γ_2. Therefore, the Navier–Stokes problem reads:

$$\begin{cases} \dfrac{\partial \mathbf{u}}{\partial t} + (\mathbf{u}\cdot\nabla)\mathbf{u} - \nu\,\Delta\mathbf{u} + \dfrac{1}{\rho}\nabla p = \mathbf{f}, & (2.165) \\ \nabla\cdot\mathbf{u} = 0, & (2.166) \\ \mathbf{u}|_{\Gamma_1} = 0, & (2.167) \\ [(\mu\,\nabla\mathbf{u} - p\mathbf{I})\cdot\mathbf{n}]|_{\Gamma_2} = 0. & (2.168) \end{cases}$$

In order to introduce the projection method, let us divide the time interval $]0,T[$ into $0 \leq n \leq N-1$ steps of equal duration $\Delta t \in \mathbb{R}_*^+$ such as $t^n = n\ \Delta t$.

2.5.1 Non-incremental pressure-correction method

The pressure-correction scheme in its non-incremental version is the classical method proposed by Chorin [38] and Temam [124, 125]. First, an intermediate velocity field $\tilde{\mathbf{u}}^{n+1}$, that does not satisfy the free divergence condition, is calculated as a solution of a discretized version of the momentum equation without the pressure gradient term ∇p^{n+1}. This first part is called the prediction step. If we consider a first order semi-implicit scheme in time, for all $\boldsymbol{x} \in \Omega$, the prediction step reads:

$$\begin{cases} \dfrac{\tilde{\mathbf{u}}^{n+1} - \mathbf{u}^n}{\Delta t} + \big(\mathbf{u}^n\cdot\nabla\big)\tilde{\mathbf{u}}^{n+1} - \nu\,\Delta\tilde{\mathbf{u}}^{n+1} = \mathbf{f}^{n+1}, & (2.169) \\ \tilde{\mathbf{u}}^{n+1}\big|_{\Gamma_1} = 0, & (2.170) \\ [\mu\,\nabla\tilde{\mathbf{u}}^{n+1}\cdot\mathbf{n}]\big|_{\Gamma_2} = 0. & (2.171) \end{cases}$$

Then, the intermediate velocity field $\tilde{\mathbf{u}}^{n+1}$ is decomposed into the sum of a final velocity field which is divergence-free and the gradient of a scalar function proportional to

the unknown pressure field ∇p^{n+1}. For all $\boldsymbol{x} \in \Omega$, we obtain the following Darcy-type equation:

$$\begin{cases} \dfrac{\mathbf{u}^{n+1} - \tilde{\mathbf{u}}^{n+1}}{\Delta t} + \dfrac{1}{\rho}\nabla p^{n+1} = 0, & (2.172) \\ \nabla \cdot \mathbf{u}^{n+1} = 0, & (2.173) \\ [\mathbf{u}^{n+1} \cdot \mathbf{n}]\big|_{\Gamma_1} = 0, & (2.174) \\ p^{n+1}\big|_{\Gamma_2} = 0. & (2.175) \end{cases}$$

As done in Chorin [38] and Temam [124, 125], the second step can be reformulated and solved differently in order to reduce the computational time. Indeed, applying the divergence to (2.172) and using (2.173), we obtain a Poisson equation on the pressure p^{n+1}. Therefore, we have the following pressure Poisson equation:

$$\begin{cases} \Delta p^{n+1} = \dfrac{\rho}{\Delta t}\nabla \cdot \tilde{\mathbf{u}}^{n+1}, & (2.176) \\ \nabla p^{n+1} \cdot \mathbf{n}\big|_{\Gamma_1} = 0, & (2.177) \\ p^{n+1}\big|_{\Gamma_2} = 0. & (2.178) \end{cases}$$

Notice that the boundary condition on Γ_1 is obtained by multiplying (2.172) by the normal vector $\mathbf{n}$. Using the boundary conditions imposed by the first step (2.170) and by the second step (2.174), we obtain a homogenous Neumann boundary condition for p^{n+1} on Γ_1.

Once the pressure field p^{n+1} has been determined, the final velocity field $\mathbf{u}^{n+1}$, satisfying the incompressibility condition, is obtained from the equality:

$$\mathbf{u}^{n+1} = \tilde{\mathbf{u}}^{n+1} - \frac{\Delta t}{\rho}\nabla p^{n+1}, \quad \text{in } \Omega. \tag{2.179}$$

In the purely Dirichlet case, i.e $\Gamma_2 = \emptyset$, the accuracy of this method has been studied by Prohl [114], Rannacher [116] and Shen [122] leading to:

Theorem 2.2. *Assuming that $(\mathbf{u}, p)$, solving the Navier–Stokes equations (2.165-2.166) is sufficiently smooth, the solution of (2.169-2.175), satisfies the following error estimates:*

$$\|\mathbf{u}(t^n) - \mathbf{u}^n\|_{l^\infty[L^2(\Omega)]^2} + \|\mathbf{u}(t^n) - \tilde{\mathbf{u}}^n\|_{l^\infty[L^2(\Omega)]^2} \leq c\,\Delta t \tag{2.180}$$

$$\|\mathbf{u}(t^n) - \mathbf{u}^n\|_{l^\infty[H^1(\Omega)]^2} + \|p(t^n) - p^n\|_{l^\infty[L^2(\Omega)]^2} \leq c\,\Delta t^{\frac{1}{2}} \tag{2.181}$$

where c is a constant independent of the time step.

Rannacher [116] observed that the artificial Neumann condition (2.177) induces a numerical boundary layer on (2.172-2.175) that prevents the scheme from being fully first-order on the velocity in the H^1-norm and on the pressure in the L^2-norm. Furthermore, we note that this scheme has an irreducible splitting error of order $\mathcal{O}(\Delta t)$ that prevents improving the overall accuracy with a higher-order scheme in time.

2.5.2 Alternative pressure-correction methods

In order to increase the accuracy of the non-incremental projection method, Goda [65] proposed to add the gradient of the pressure p^n in (2.169). This method is known as the incremental pressure-correction scheme. This idea was made popular by Van Kan [130], who proposed a second-order incremental pressure-correction scheme.

In the purely Dirichlet case, i.e. $\Gamma_2 = \emptyset$, the errors on the velocity in the H^1-norm and on the pressure in the L^2-norm are of order $\mathcal{O}(\Delta t)$, see [67, 71, 122, 136]. Compared to the non-incremental pressure-correction method, the errors are then improved by a factor $\mathcal{O}(\Delta t^{\frac{1}{2}})$. The splitting error is improved by a factor $\mathcal{O}(\Delta t)$ leading to a splitting error of order $\mathcal{O}(\Delta t^2)$. However, this method changes the boundary condition (2.177) into the non-physical Neumann boundary $\nabla(p^{n+1} - p^n) \cdot \mathbf{n}_{|\Gamma_1} = 0$. This condition implies that

$$\nabla p^{n+1} \cdot \mathbf{n}_{|\Gamma_1} = \nabla p^n \cdot \mathbf{n}_{|\Gamma_1} = \cdots = \nabla p^0 \cdot \mathbf{n}_{|\Gamma_1}. \tag{2.182}$$

introducing a numerical boundary layer that prevents the scheme to be fully second-order on the velocity in the H^1-norm and on the pressure in the L^2-norm. In the general case, i.e. $\Gamma_2 \neq \emptyset$, the accuracy of the approximation on the pressure in L^2-norm and on the velocity in H^1-norm is degraded. The errors of the non-incremental pressure-correction scheme are retrieved. In order to recover optimal error estimates, Bonito et al. [14] modified the incremental pressure-correction scheme by adding a consistent grad-div term in the prediction momentum equation. The authors recovered an optimal error estimate for a first order time scheme.

In order to circumvent the difficulty caused by the non-physical pressure Neumann boundary condition, Timmermans et al. [127] add a grad-div term on the intermediate velocity $\tilde{\mathbf{u}}^{n+\frac{1}{2}}$ in the correction step. This modification changes the Neumann condition leading to the following consistent pressure boundary condition:

$$\nabla p^{n+1} \cdot \mathbf{n}\big|_{\Gamma_1} = [\rho\, \mathbf{f}^{n+1} - \mu \nabla \times \nabla \times \mathbf{u}^{n+1}]\big|_{\Gamma_1}. \tag{2.183}$$

In the purely Dirichlet case, i.e. $\Gamma_2 = \emptyset$, Guermond and Shen [69] studied the accuracy for a second-order scheme in time. The authors showed that the errors on the velocity in the H^1-norm and on the pressure in the L^2-norm are of order $\mathcal{O}(\Delta t^{\frac{3}{2}})$. Moreover, the splitting error is of order $\mathcal{O}(\Delta t^2)$. In the general case, i.e. $\Gamma_2 \neq \emptyset$, Guermond, Minev and Shen [68] performed the same study also with a second-order scheme in time. The authors showed that the errors on the velocity in the H^1-norm and on the pressure in the L^2-norm are of order $\mathcal{O}(\Delta t)$. The errors estimates are improved by a factor $\mathcal{O}(\Delta t^{\frac{1}{2}})$. The splitting error is of order $\mathcal{O}(\Delta t^{\frac{3}{2}})$. The approximation stays emphasis sub-optimal. In order to recover optimal error estimates, Lee and Salgado [91] provided a stability analysis for the rotational version of the grad-div stabilized scheme based on [14].

2.5.3 On the resolution by the Finite Elements method

For this Subsection, we consider $\mathbf{u}_h^{n+1}$ (resp. p_h^{n+1}) the velocity and pressure that belong respectively to the Finite Elements spaces $\mathcal{V}_h$ and $\mathcal{Q}_h$.

Role of the inf-sup condition

We consider the correction step (2.172-2.175) solved in the framework of the Finite Elements method. The problem is well-posed if the Finite Element spaces chosen for the velocity and the pressure satisfy the inf-sup condition. The numerical consequences often appear as severe node-to-node spatial oscillations on the pressure field because of the non-unicity of the pressure. However, the idea emerged that solving a Poisson equation (2.176,2.178) on the pressure, as introduced by Chorin [38] and Temam [124, 125], makes it possible to use spatial interpolations which do not satisfy the inf-sup condition. Indeed, the Poisson equation on the pressure is well-posed for any Finite Element spaces. Guermond and Quartapelle [74] investigated the effect on the stability of using Finite Elements spaces that do not satisfy the inf-sup condition for purely Dirichlet case. In the case of the non-incremental pressure-correction scheme, the authors proved that:

$$\|p_h^{n+1}\|_1 \leq \Delta t^{-1} \|\mathbf{u}_h^{n+1} - \mathbf{u}(t^{n+1})\|_0 \leq \sigma \left(1 + \frac{h^{l+1}}{\Delta t}\right). \tag{2.184}$$

From this, the pressure satisfies the stability estimate $\|p_h^{n+1}\|_{l^\infty(H^1)} \leq \sigma$ if and only if

$$\Delta t \geq \sigma\, h^{l+1}, \tag{2.185}$$

where σ is a reference velocity, h the space step and l the polynomial order of interpolation for the velocity. In the case of the incremental pressure-correction scheme, the authors demonstrated that the stability of numerical scheme is ensured only if the inf-sup condition is satisfied.

Divergence-free constraint

For the formulation based on the pressure Poisson equation, the velocity field may not be divergence-free at the discrete level. Indeed, as we could see in the sequel (in Subsection 2.6.2), the velocity field is not divergence-free with classical Lagrange Finite Elements spaces since the algebraic formulations between the Darcy problem and the decoupled problem are not equivalent at the discrete level. Notice that the Raviart-Thomas Finite Elements spaces allow to ensure the free divergence condition on the velocity.

2.6 Finite Elements methods for the free surface Navier–Stokes equations with pressure decomposition

This section is devoted to Finite Elements methods for the coupled or decoupled numerical strategies on the free surface Navier–Stokes equations with pressure decomposition

(introduced in Subsection 2.4.5). In particular, we focus on the Finite Elements method for the hydrostatic equation (2.137-2.138) or the Darcy equations (2.146-2.147). An interested reader can find details about the Finite Elements method for the advection equations (2.136), the advection-diffusion equations with source term (2.150) in Ern and Guermond [53] or in Quarteroni and Valli [115].

We give the semi-discrete in time variational and algebraic formulations[7]. Since the decoupled strategy are based on a wave equation on the free surface and a pressure Poisson equation, the satisfying of inf-sup condition is not required in order to ensure the existence and the unicity of the solutions. This condition is required to the coupled $(\boldsymbol{u}^{hor}, \eta)$ and $(\mathbf{u}, p_d)$ problems. If we consider an internal approximation method[8], the continuous functional space includes the finite dimensional space. Then, the discrete problem allows to obtain a solution computable in finite number of operations. For this purpose, the discrete solution are then decomposed in a Finite Elements space, see Subsection 2.2.5. For more details, see Ern and Guermond [53].

Throughout this Section, we consider the notations introduced in Subsection 2.3.5 and 2.4.5. The regularity on the reference functional spaces will be specified. For the sake of simplicity, we assume that $\kappa_f(|\mathbf{u}\cdot\mathbf{t}|) = 0$ and $\gamma_{air} = 0$.

2.6.1 Coupled numerical strategies

In this Subsection, we consider the coupled numerical strategy in time for the hydrostatic predictor and non-hydrostatic corrector steps.

Hydrostatic predictor step

Let us consider the hydrostatic Navier–Stokes equations (2.137-2.138) and the following reference functional spaces for each component of the velocity and the free surface:

$$\widehat{\mathcal{V}}(\widehat{\Omega}) = H^1(\widehat{\Omega}) \quad \text{and} \quad \mathcal{M}(\omega) = L^2(\omega). \tag{2.186}$$

In addition, let us define:

$$\mathcal{V}_{0,l}(\Omega^n) = \{\mathbf{v} \in \left(\mathcal{V}(\Omega^n)\right)^2 \ \mid \mathbf{v}\cdot\mathbf{n}_\omega = 0 \text{ on } \Gamma_l^n\}, \tag{2.187}$$

with $\mathcal{V}(\Omega^n)$ the corresponding ALE functional space given in (2.108). In $\mathcal{V}_{0,l}(\Omega^n)$, the imperviousness conditions at the lateral boundaries Γ_l^n are essential. A classical time-

[7]The discrete variational formulation that leads to the algebraic formulation is not written

[8]We just briefly recall that an internal approximation method of continuous in space variational formulation consists in finding a discrete solution in a finite dimensional space.

discrete mixed variational formulation of the hydrostatic equations (2.137-2.138) is:

$$\begin{cases} \text{Find } (\tilde{\boldsymbol{u}}^{hor,n+1}, \eta^{n+1}) \in \mathcal{V}_{0,l}(\Omega^n) \times \mathcal{M}(\omega) \\ \text{such that for all } (\boldsymbol{v}^n, \psi) \in \mathcal{V}_{0,l}(\Omega^n) \times \mathcal{M}(\omega) \\ \left(\dfrac{\tilde{\boldsymbol{u}}^{hor,n+1} - \tilde{\boldsymbol{u}}^{hor,n+\frac{1}{2}}}{\Delta t}, \boldsymbol{v}^n \right)_n + a_n(\tilde{\boldsymbol{u}}^{hor,n+1}, \boldsymbol{v}^n) \\ \qquad - d(\boldsymbol{v}^n, \eta^{n+1}) = (\boldsymbol{f}_{xy}^{n+1}, \boldsymbol{v}^n)_n, \qquad (2.188) \\ \left(\dfrac{\eta^{n+1} - \eta^n}{\Delta t}, \psi \right)_\omega + d(\tilde{\boldsymbol{u}}^{hor,n+1}, \psi) = 0, \qquad (2.189) \end{cases}$$

with the bilinear forms:

$$d(\boldsymbol{v}, \psi) = \int_\omega \psi \, \nabla_{hor} \cdot \left(\int_{b^n}^{\eta^n} \boldsymbol{v} \, dz \right) dy \, dx. \qquad (2.190)$$

The bilinear form $d(\cdot, \cdot)$ is defined on $\mathcal{V}_{0,l}(\Omega^n) \times \mathcal{M}(\omega)$ and it defines the linear operator $D : \mathcal{V}_{0,l}(\Omega^n) \to \mathcal{M}'(\omega)$ and its transpose $D^T : \mathcal{M}(\omega) \to \mathcal{V}'_{0,l}(\Omega^n)$ such that:

$$d(\boldsymbol{v}, \psi) = < D\boldsymbol{v}, \psi >_{\mathcal{M}(\omega) \times \mathcal{M}(\omega)} = < \boldsymbol{v}, D^T \psi >_{\mathcal{V}_{0,l}(\Omega^n) \times \mathcal{V}'_{0,l}(\Omega^n)} . \qquad (2.191)$$

This mixed variational formulation was studied by Decoene [44]. The author demonstrated the existence and the unicity of solutions since it exists $\beta > 0$ satisfying an inf-sup condition (2.105). Additionally, the author showed that the order in time of this formulation is in $\mathcal{O}(\Delta t)$.

Algebraic formulations:

After performing an internal approximation for the mixed variational formulation (2.188-2.189) that it is not detailed here, the algebraic formulation is, for $n = 0, ..., N-1$:

$$\begin{pmatrix} A_u^n & -\Delta t \, D^n \\ \Delta t \, (D^n)^T & M_\eta \end{pmatrix} \begin{pmatrix} \tilde{U}_{hor}^{n+1} \\ E^{n+1} \end{pmatrix} = \begin{pmatrix} M_u^n \, \tilde{U}_{hor}^{n+\frac{1}{2}} + \Delta t \, F_{xy}^{n+1} \\ M_\eta \, E^n \end{pmatrix}, \qquad (2.192)$$

where

$$A_u^n = M_u^n + \nu \Delta t R_u^n. \qquad (2.193)$$

The unknown vectors $\tilde{U}_{hor}^{n+1}$ and E^{n+1} contain respectively the discrete values of the intermediate horizontal velocity and of the free surface. On the one hand, the three-dimensional mass matrix of the velocity is defined in the domain Ω_h^n and is denoted by M_u^n. On the other hand, the three-dimensional rigidity matrix of the velocity is defined in the domain Ω_h^n and is denoted by R_u^n. Both matrices are defined as follows:

$$M_{u,ij}^n = \int_{\Omega_h^n} \varphi_i^n \, \varphi_j^n \, d\boldsymbol{x}, \qquad (2.194)$$

$$R_{u,ij}^n = \int_{\Omega_h^n} \nabla \varphi_i^n : \nabla \varphi_j^n \, d\boldsymbol{x}, \qquad (2.195)$$

where φ_i^n denotes the three-dimensional basis function in Ω_h^n corresponding to the $i-$th degree of freedom for the velocity. It depends on the components x, y and z. The mass matrix of the free surface variable is denoted by M_η, such that:

$$M_{\eta,ij} = \int_\omega \zeta_i \, \zeta_j \, dy \, dx. \tag{2.196}$$

where ζ_i denotes the two-dimensional basis function corresponding to the i-th degree of freedom for the free surface. It depends on x and y. The matrix D^n is defined as an interaction between the two-dimensional and three-dimensional basis functions. It represents the algebraic counterpart of the divergence operator such as:

$$D_{ij}^n = \int_\omega \zeta_i \, \nabla_{hor} \cdot \left(\int_{b_h^n}^{\eta_h^n} \varphi_j^n \, dz \right) \, dy \, dx. \tag{2.197}$$

In the algebraic formulation (2.192), the Finite Element basis functions (chosen to approximate the free surface and the velocity) need to satisfies the associated inf-sup condition. This property allows to ensure that the block matrix is inversible. For this purpose, Decoene [44] studied a coupled of inf-sup stable pair of Finite Elements spaces.

The algebraic problem (2.192) can be solved using a Schur complement [139]. This method allows to consider two sub-problems of dimension $N_\mathbf{u} \times N_\mathbf{u}$ and $N_\eta \times N_\eta$ instead of a problem of dimension $(N_\eta + N_\mathbf{u})(N_\eta + N_\mathbf{u})$, where N_η and $N_\mathbf{u}$ are the number of nodes corresponding to the chosen basis function for the free surface and the velocity. The strategy consists in computing an algebraic equation on the free surface vector η^{n+1} such that:

$$\begin{aligned}(M_\eta + \Delta t^2 \, (D^n)^T (A^n)^{-1} D^n) \eta^{n+1} = M_\eta \eta^n - \, & \Delta t^2 \, (D^n)^T (A^n)^{-1} F^{n+1} \\ & - \Delta t (D^n)^T (A^n)^{-1} M_u^n \, \tilde{U}_{hor}^{n+\frac{1}{2}},\end{aligned} \tag{2.198}$$

and then a correction of the velocity vector $\tilde{U}_{hor}^{n+1}$ such that:

$$A_u^n \tilde{U}_{hor}^{n+1} = M_u^n \, \tilde{U}_{hor}^{n+\frac{1}{2}} + \Delta t F_{xy}^{n+1} + \Delta t \, D^n \, \eta^{n+1}. \tag{2.199}$$

Notice that (2.198) needs to know explicitly the inverse of the matrix A_u^n which is not easy to compute and costly. In Chapter 3, we will discuss about the computation of $\left(A_u^n\right)^{-1}$ in the industrial code Telemac-3D. Furthermore, we can remark that the (2.199) can be computed node by node since A_u^n has been already inversed.

Treatment of the imperviousness condition at the lateral boundaries

The essential treatment of imperviousness condition at the lateral boundaries is a drawback of this formulation because they are difficult to implement. In fact, the construction of a Finite Elements space of functions with zero normal component is delicate, especially if the domain is polyhedral and the degrees of freedom on the boundary are located at

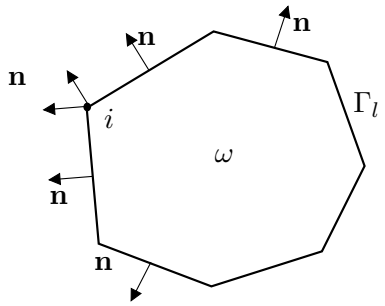

Figure 2.3: Polyhedral domain whose normal vector is undefined at the boundary nodes

the vertices. This requires the construction of the outgoing normal vectors $\mathbf{n}_h$ at the vertices of the solid boundaries which are not univoqualy defined on the polyhedral domain, see Figure 2.3. A method to overcome this problem is to use the normal vector to the regular domain. This particular approximation of the imperviousness condition has been studied by Verfürth [132] in the framework of the Stokes problem. He showed that the resulting scheme is still convergent - provided compatible Finite Elements spaces are used - but the error is in $\mathcal{O}(h^{\frac{1}{2}})$ independently of the Finite Elements spaces chosen. Note that such a scheme is costly because the imperviousness condition couples the components of the fluid velocity. One way to overcome these difficulties is to prescribe naturally the imperviousness condition. This way allows to circumvent the difficulty of the strong treatment of the lateral imperviousness conditions. The idea was introduced in the framework of compressible flows [52] and was applied in several other contexts. Decoene [44] studied this strategy applied to the hydrostatic Navier–Stokes equations. The reference functional spaces are now:

$$\widehat{\mathcal{V}}(\widehat{\Omega}) = H^1(\widehat{\Omega}) \text{ and } \mathcal{M}(\omega) = H^1(\omega). \tag{2.200}$$

As previously, we consider the corresponding ALE functional space $\mathcal{V}^n$, given in (2.108). Integrating by parts the divergence term in the depth-averaged free surface equation (2.138) instead of the gradient term of the free surface in the horizontal momentum equation (2.137) leads to a time-discrete mixed variational formulation with natural imperviousness conditions at the lateral boundaries. It writes:

$$\begin{cases} \text{Find } (\tilde{\boldsymbol{u}}^{hor,n+1}, \eta^{n+1}) \in \mathcal{V}(\Omega^n) \times \mathcal{M}(\omega) \\ \text{such that for all} (\boldsymbol{v}^n, \psi) \in \mathcal{V}(\Omega^n) \times \mathcal{M}(\omega) \\ \left(\dfrac{\tilde{\boldsymbol{u}}^{hor,n+1} - \tilde{\boldsymbol{u}}^{hor,n+\frac{1}{2}}}{\Delta t}, \boldsymbol{v}^n \right)_n + a_n(\tilde{\boldsymbol{u}}^{n+1}, \boldsymbol{v}^n) \\ \qquad\qquad + \tilde{d}(\boldsymbol{v}^n, \eta^{n+1}) = (\boldsymbol{f}_{xy}^{n+1}, \boldsymbol{v}^n)_n, \qquad (2.201) \\ \left(\dfrac{\eta^{n+1} - \eta^n}{\Delta t}, \psi \right)_\omega - \tilde{d}(\tilde{\boldsymbol{u}}^{hor,n+1}, \psi) = 0, \qquad (2.202) \end{cases}$$

with the bilinear form:

$$\tilde{d}(\boldsymbol{v},\psi)=\int_{\Omega^n}\boldsymbol{v}\cdot\nabla_{hor}\,\psi\,d\boldsymbol{x}. \tag{2.203}$$

Contrary to $d(\cdot,\cdot)$ given in (2.190), the bilinear form $\tilde{d}(\cdot,\cdot)$ is defined on $\mathcal{V}_0(\Omega^n)\times\mathcal{M}(\omega)$ and it defines the linear operator $\tilde{D}:\mathcal{V}(\Omega^n)\rightarrow\mathcal{M}'(\omega)$ and its transpose $\tilde{D}^T:\mathcal{M}(\omega)\rightarrow\mathcal{V}'(\Omega^n)$ such as:

$$\tilde{d}(\boldsymbol{v},\psi)=<\tilde{D}\boldsymbol{v},\psi>_{\mathcal{M}(\omega)\times\mathcal{M}(\omega)}=<\boldsymbol{v},\tilde{D}^T\psi>_{\mathcal{V}(\Omega^n)\times\mathcal{V}'(\Omega^n)}. \tag{2.204}$$

Decoene [44] demonstrated that this formulation is ill-posed and cannot be analyzed in the Lax-Milgram and mixed formulation frameworks at the time-discrete level. Indeed, the corresponding bilinear form

$$\begin{aligned}L_\omega((\boldsymbol{u}^{hor,n},\eta^n),(\boldsymbol{v}^n,\psi^n))=&(\boldsymbol{u}^{hor,n},\boldsymbol{v}^n)_n+a_n(\boldsymbol{u}^{hor,n},\boldsymbol{v}^n)\\&+\tilde{d}(\boldsymbol{u}^{hor,n},\eta^n)-\tilde{d}(\boldsymbol{u}^n,\psi)+(\eta^n,\psi)_\omega,\end{aligned}$$

is symmetric and continuous, but is not coercive in $(\mathcal{V}(\Omega^n)\times\mathcal{M}(\omega))^2$. The analysis of the existence and unicity of a couple of solution can be performed only at the discrete level, as done in [44]. The author showed that the discrete problem is well-posed if the associated inf-sup condition (2.105) is satisfied. As a consequence, as previously, the pair of Finite Elements spaces for the free surface and the velocity has to satisfy an inf-sup condition. It is worthwhile to note that this is not an internal approximation of the continuous variational hydrostatic equations. Indeed, the bilinear form $\tilde{d}(\cdot,\cdot)$ is different from $d(\cdot,\cdot)$. Therefore, we cannot use the standard techniques as the Céa Lemma (see Ern and Guermond [53]) in order to estimate the error between a solution of the discrete problem and a solution of the continuous problem. In fact, a more complex analysis would be needed to estimate this error. Note that in [110], Parés analyzed an approximation of the Stokes problem with a natural treatment of the imperviousness condition. Using non standard techniques, the author established an error estimate of the solution of the discrete problem for the case where the velocity and the pressure are approximated in Finite Elements spaces satisfying an inf-sup condition. This error is in $\mathcal{O}(h^{\frac{1}{2}})$.

The algebraic formulation is the same structure as (2.192) where the matrix D^n is replaced by $\tilde{D}^n$, representing the algebraic counterpart of the divergence operator such as:

$$\tilde{D}^n_{ij}=\int_\omega\varphi^n_i\,\nabla_{hor}\zeta_j\,dy\,dx. \tag{2.205}$$

As previously introduced, a Schur complement can be used in order to solve two successive sub-problems, see formulations (2.198-2.199).

Non-hydrostatic corrector step

Let us consider the Darcy equations (2.147-2.146) and the following reference functional spaces (introduced in Subsection 2.3.4) recalled here for convenience:

$$\mathcal{V}(\widehat{\Omega})=H^1(\widehat{\Omega})\text{ and }\mathcal{Q}(\widehat{\Omega})=L^2(\widehat{\Omega}).$$

In addition, we also consider the functional space (2.98) with essential imperviousness conditions on the solid boundaries recalled here:

$$\mathcal{V}_0(\Omega^{n+1}) = \{\mathbf{v}^{n+1} \in \left(\mathcal{V}(\Omega^{n+1})\right)^3 \ \mid \ \mathbf{v}^{n+1} \cdot \mathbf{n} = 0 \text{ on } \Gamma_b \cup \Gamma_l^{n+1}\}.$$

A classical time-discrete mixed variational formulation of the Darcy equations (2.146-2.147) is:

$$\begin{cases} \text{Find } (\mathbf{u}^{n+1}, p_d^{n+1}) \in (\mathcal{V}_0(\Omega^{n+1}), \mathcal{Q}(\Omega^{n+1})) \\ \text{such that for all} (\mathbf{v}^{n+1}, q^{n+1}) \in (\mathcal{V}_0(\Omega^{n+1}), \mathcal{Q}(\Omega^{n+1})) : \\ \left(\dfrac{\mathbf{u}^{n+1} - \tilde{\mathbf{u}}_n^{n+1}}{\Delta t}, \mathbf{v}^{n+1}\right)_{n+1} - \dfrac{1}{\rho}\, b(\mathbf{v}^{n+1}, p_d^{n+1}) = 0, & (2.206) \\ b(\mathbf{u}^{n+1}, q^{n+1}) = 0, & (2.207) \end{cases}$$

where $b(\cdot,\cdot)$ has been given in (2.104). This variational formulation is well-posed since the associated inf-sup condition (2.105) is satisfied, see Ern and Guermond [53]. Hence, at the discrete level, a pair of Finite Elements spaces satisfying an inf-sup condition is necessary to ensure the existence and unicity of a discrete solution such as the Taylor-Young Finite Elements.

Algebraic formulations:
After performing an internal approximation for the mixed variational formulation (2.206-2.207) that it is not detailed here and after decomposing the discrete solutions in Finite Elements basis, the algebraic formulation is, for $n = 0, ..., N-1$:

$$\begin{pmatrix} M_u^{n+1} & -\dfrac{\Delta t}{\rho}(B^{n+1})^T \\ B^{n+1} & 0 \end{pmatrix} \begin{pmatrix} U^{n+1} \\ P_d^{n+1} \end{pmatrix} = \begin{pmatrix} M_u^{n+1}\tilde{U}^{n+1} \\ 0 \end{pmatrix} \tag{2.208}$$

where U^{n+1} and P_d^{n+1} are the unknown vectors containing the discrete values of the velocity field and of the non-hydrostatic pressure. The mass matrix M_u^{n+1} corresponds to (2.194) at t^{n+1}. The matrix B^{n+1} defined in Ω_h^{n+1} represents the interaction between the three-dimensional basis functions of the pressure and of the velocity. It represents the algebraic counterpart of the divergence operator such as:

$$B_{ij}^{n+1} = \int_{\Omega_h^{n+1}} \varphi_i^{n+1}\, \nabla \cdot \alpha_j^{n+1}\, d\boldsymbol{x}, \tag{2.209}$$

where φ_i denotes the basis function corresponding to the $i-$th degree of freedom for the unknown $\mathbf{u}$ and α_i denotes the three-dimensional basis function corresponding to the $i-$th degree of freedom for the unknown p_d. These basis functions depend on the components x, y and z.

As previously mentioned, this algebraic formulation can also be computed by using a Schur complement [139]. Therefore, two sub-problems of dimension $N_{\mathbf{u}} \times N_{\mathbf{u}}$ and $N_p \times N_p$

are considered instead of a problem of dimension $(N_p + N_{\mathbf{u}})(N_p + N_{\mathbf{u}})$. After algebraic manipulations, the matrix equation on dynamic pressure is:

$$(B^{n+1}(M_u^{n+1})^{-1}(B^{n+1})^T)\, P_d^{n+1} = -\frac{\rho}{\Delta t} B^{n+1}\, \tilde{U}^{n+1}. \tag{2.210}$$

Then, the velocity vector U^{n+1} is corrected through:

$$U^{n+1} = \tilde{U}^{n+1} + \frac{\Delta t}{\rho}(M_u^{n+1})^{-1}(B^{n+1})^T \tilde{U}^{n+1}. \tag{2.211}$$

The algebraic formulation (2.210) requires to compute explicitly the inverse of the mass matrix M_u^{n+1}. However, this computation for a sparse matrix is very expensive. Therefore, the mass matrix is generally mass lumped [85] leading to a diagonal matrix, which enables to easily compute the inverse of the mass matrix. An alternative formulation could be used in order to impose the imperviousness conditions naturally but we do not formulate this one here.

Free divergence condition at the discrete level:
Let us verify that the final velocity field satisfies the incompressibility condition at the discrete level. By applying the matrix associated to the divergence operator B^{n+1}:

$$\begin{aligned} B^{n+1}U^{n+1} &= B^{n+1}\tilde{U}^{n+1} + \frac{\Delta t}{\rho} B^{n+1}(M_u^{n+1})^{-1}(B^{n+1})^T P_d^{n+1}, \\ &= B^{n+1}\tilde{U}^{n+1} - B^{n+1}\, \tilde{U}^{n+1}, \\ &= 0. \end{aligned} \tag{2.212}$$

The free divergence condition of the velocity is verified at the discrete level.

2.6.2 Decoupled numerical strategies

In this Subsection, we consider the decoupled numerical approach in time for the hydrostatic predictor and non-hydrostatic corrector steps.

Hydrostatic predictor step

Let us consider the wave equation on the free surface (2.159) and the horizontal momentum equation (2.156). Furthermore, we consider the following reference functional spaces for the velocity and the free surface:

$$\widehat{\mathcal{V}}(\widehat{\Omega}) = L^2(\widehat{\Omega}) \text{ and } \mathcal{M}(\omega) = H^1(\omega) \tag{2.213}$$

We also consider the corresponding ALE functional space for the velocity $\mathcal{V}(\Omega^{n)}$, given in (2.108). Multiplying 2.159 by test function $\psi \in \mathcal{M}$, integrating on ω and applying

integration by parts leads to the following semi-discrete variational formulation of the wave equation on the free surface (2.159):

$$\left\{\begin{array}{l} \text{Find } \eta^{n+1} \in \mathcal{M}(\omega) \text{ such that for all } \psi \in \mathcal{M}(\omega) \\ \displaystyle\int_\omega \eta^{n+1}\,\psi\,dy\,dx + g\,\Delta t^2 \int_\omega h^n\,\nabla_{hor}\eta^{n+1}\,\nabla_{hor}\psi\,dy\,dx \\ \qquad\qquad = \displaystyle\int_\omega \eta^n\,\psi\,dy\,dx + \Delta t \int_\omega \left(\int_{b^n}^{\eta^n} \tilde{\boldsymbol{u}}^{hor,n+\frac{1}{2}}\,dz\right)\nabla_{hor}\psi\,dy\,dx. \end{array}\right. \quad (2.214)$$

Then, the intermediate horizontal velocities are computed through the following time-discrete variational formulation of (2.137):

$$\left\{\begin{array}{l} \text{Find } \tilde{\boldsymbol{u}}^{hor,n+1} \in \left(\mathcal{V}(\Omega^n)\right)^2 \text{ such that for all } v^n \in \left(\mathcal{V}(\Omega^n)\right)^2 \\ \left(\dfrac{\tilde{\boldsymbol{u}}^{hor,n+1} - \tilde{\boldsymbol{u}}^{hor,n+\frac{1}{2}}}{\Delta t}, \boldsymbol{v}^n\right)_n + \displaystyle\int_{\Omega^n} \nabla_{hor}\eta^{n+1}\,\boldsymbol{v}^n d\boldsymbol{x} = 0. \end{array}\right. \quad (2.215)$$

Due to the nature of these equations, the variational formulations (2.214) and (2.215) are well-posed without the requirement to satisfy the inf-sup condition, see Ern and Guermond [53].

Algebraic formulations:

After performing an internal approximation for the mixed variational formulation (2.214-2.215) and after decomposing the discrete solutions in the Finite Elements basis, the algebraic formulation of (2.214) is, for $n = 0, ..., N-1$:

$$(M_\eta + g\,h^n\,\Delta t^2\,R_\eta)\,E^{n+1} = M_\eta\,E^n + \Delta t\,(\tilde{D}^n)\,\tilde{U}_{hor}^{n+\frac{1}{2}}. \quad (2.216)$$

The mass matrix M_η and the matrix of the gradient operator $\tilde{D}^n$ are respectively equal to (2.196) and (2.205). The two-dimensional rigidity matrix R_η in ω_h of the free surface term is equal to :

$$R_{\eta,ij} = \int_\omega \nabla_{hor}\zeta_i : \nabla_{hor}\zeta_j\,dy\,dx. \quad (2.217)$$

The algebraic formulation of (2.215) is, for $n = 0, ..., N-1$:

$$M_u^n\,\tilde{U}_{hor}^{n+1} = M_u^n\,\tilde{U}_{hor}^{n+\frac{1}{2}} + \Delta t\,\tilde{D}^n\,E^{n+1}. \quad (2.218)$$

Recall that $\tilde{U}_{hor}^{n+1}$ is the vector of unknowns containing the discrete values of the intermediate horizontal velocities and M_u^n the three-dimensional mass matrix given by (2.194). Notice that (2.216) does no require to inverse explicitly a matrix. The discrete problem is well-posed without inf-sup pair of Finite Elements spaces. However, by analogy with the study of Guermond and Quartapelle [74] (discussed in Subsection 2.5.3), the stability could be ensured only if the Finite Elements spaces are inf-sup stable or if Δt satisfies a particular condition. This constitues an open question.

Non-hydrostatic corrector step

Let us consider the pressure Poisson equation on the dynamic pressure (2.161) and the correction of the velocity (2.164) of the non-hydrostatic corrector step. In addition, we consider the following reference functional spaces for the velocity and the free surface:

$$\widehat{\mathcal{V}}(\widehat{\Omega}) = L^2(\widehat{\Omega}) \text{ and } \mathcal{Q}(\omega) = H^1(\omega) \tag{2.219}$$

We also consider the corresponding ALE functional space for the velocity $\mathcal{V}^n$ given in (2.108). A time-discrete variational formulation of the pressure Poisson equation (2.161) is:

$$\begin{cases} \text{Find } p_d^{n+1} \in \mathcal{Q}(\Omega^{n+1}) \text{ such that for all } q \in \mathcal{Q}(\Omega^{n+1}). \\ (\nabla p_d^{n+1}, \nabla q^{n+1})_{n+1} = -\dfrac{\rho}{\Delta t}(\nabla \cdot \tilde{\mathbf{u}}_n^{n+1}, q^{n+1})_{n+1}. \end{cases} \tag{2.220}$$

Then, the time-discrete variational formulation of (2.164) for the correction of the velocity is:

$$\begin{cases} \text{Find } \mathbf{u}^{n+1} \in \left(\mathcal{V}(\Omega^{n+1})\right)^3 \text{ such that for all } \mathbf{v}^{n+1} \in \left(\mathcal{V}(\Omega^{n+1})\right)^3 \\ (\mathbf{u}^{n+1}, \mathbf{v}^{n+1})_{n+1} = (\tilde{\mathbf{u}}_n^{n+1}, \mathbf{v}^{n+1})_{n+1} - \dfrac{\Delta t}{\rho}(\nabla p_d^{n+1}, \mathbf{v}^{n+1})_{n+1}. \end{cases} \tag{2.221}$$

Due to the nature of these equations, the variational formulations (2.220) and (2.221) are well-posed without the requirement to satisfy the inf-sup condition, see Ern and Guermond [53].

Algebraic formulations:
After performing an internal approximation for the mixed variational formulation (2.220) and (2.221) and after decomposing the discrete solutions in Finite Elements basis, the algebraic formulation of (2.214) is, for $n = 0, ..., N-1$:

$$B^{n+1}(B^{n+1})^T P_d^{n+1} = -\frac{\rho}{\Delta t} B^{n+1} \tilde{U}^{n+1}, \tag{2.222}$$

where P_d^{n+1} is the unknown vector containing the discrete values of the non-hydrostatic pressure. The matrix B^{n+1} is the algebraic counterpart of the divergence operator defined in (2.209). The algebraic formulation corresponding to (2.220) is given in (2.211).

We recalled that Guermond and Quartapelle [74] showed that the stability is ensured only either if the Finite Elements spaces are inf-sup stable or if Δt satisfies an inverse CFL (2.185), see Subsection 2.5.3.

Free divergence condition at the discrete level:
Let us discuss about the free divergence condition at the discrete level. For any Lagrangian Finite Elements functions, the final velocity field $\mathbf{u}^{n+1}$ is not divergence-free at the discrete level. Indeed, by applying the matrix B^{n+1} associated to the divergence

operator, we have:

$$\begin{aligned} B^{n+1}U^{n+1} &= B^{n+1}\tilde{U}^{n+1} - \frac{\Delta t}{\rho}B^{n+1}(M_u^{n+1})^{-1}(B^{n+1})^T P_d^{n+1}, \\ &= \frac{\Delta t}{\rho}B^{n+1}(B^{n+1})^T P_d^{n+1} - \frac{\Delta t}{\rho}B^{n+1}(M_u^{n+1})^{-1}(B^{n+1})^T P_d^{n+1}, \\ &\neq 0. \end{aligned} \tag{2.223}$$

Since M_u^{n+1} is not equal to the identity matrix, the discrete divergence of the final velocity cannot be equal to zero. The free divergence condition can be obtained if an appropriate pair of Finite Elements spaces is used on the velocity such as the Raviart–Thomas Finite Elements. Otherwise, with classical Finite Elements spaces, the way to solve the non-hydrostatic corrector step as a decoupled algebraic problem is to consider (2.210) and (2.211), which require to satisfy a discrete inf-sup condition.

Chapter 3

Telemac-3D algorithm

Contents

This Chapter is the result of a collaboration with Emmanuel Audusse, Astrid Decoene, Agnès Leroy and Chi-Tuân Pham.

3.1 Introduction

Telemac-3D is an open source software initially developed by the Laboratoire National d'Hydraulique et Environnement (LNHE - EDF R&D). It is dedicated to solve large scale 3D flows using the Finite Elements method, such as free surface flows in oceans, coasts, estuaries and rivers. For this purpose, Telemac-3D solves the free surface Navier–Stokes equations based on the pressure decomposition (2.128-2.130). To take into account the vertical movement of the domain, a particular ALE formulation called the sigma transformation is used in Telemac-3D. As introduced in Subsection 2.4.5, the numerical strategy consists in splitting the equations into a hydrostatic predictor step and a non-hydrostatic corrector step. The hydrostatic predictor part is composed of the hydrostatic equation (2.120,2.121) and the vertical momentum equation (2.129) omitting the dynamic pressure term. This step allows to compute the free surface elevation and intermediate velocities that do not satisfy the incompressibility condition. From the free surface elevation, a first approximation of the pressure is deduced with the hydrostatic pressure. The non-hydrostatic corrector step is Darcy-like equation. It enables to correct the free divergence velocity by the dynamic pressure.

For more convenience, we recall here the fluid domain previously defined in Subsection 2.1.2. We consider homogeneous (constant density ρ)[1] and Newtonian fluid under the influence of the gravity $\mathbf{g} = -g\,\mathbf{e}_z$ and bounded from below by a topography[2] $b(x, y)$ and from above by a free surface $\eta(x, y, t)$. The atmospheric pressure is assumed to be zero. The flow is supposed to be incompressible. We assume that the bottom and the free surface functions are single-valued functions. The three-dimensional variable is denoted $\boldsymbol{x} = (x, y, z) \in \mathbb{R}^3$ such that $(x, y) \in \mathbb{R}^2$ is the field of horizontal coordinates and $z \in \mathbb{R}$ is the vertical variable. The water depth is denoted by $h(x, y, t) = \eta(x, y, t) - b(x, y)$. We denote by ω a fixed and two-dimensional polygonal domain. For any time $t \in]0, T[$ with $T \in \mathbb{R}_*^+$ a constant final time, we assume that the domain Ω_t defined as:

$$\Omega_t = \{(x, y, z) \mid (x, y) \in \omega \ \text{ and } b(x, y) < z < \eta(x, y, t)\}.$$

The domain Ω_t is bounded by the free surface boundary $\Gamma_{s,t}$ and by the solid boundaries Γ_b and $\Gamma_{l,t}$ which denote respectively the bottom and vertical lateral boundaries (see Figure 2.1). The boundary of the domain is denoted $\partial\Omega_t = \Gamma_{s,t} \cup \Gamma_{l,t} \cup \Gamma_b$. Moreover, we denote by $\partial\omega$ the boundary of the domain ω. The normal outward vector at $\partial\Omega$ is denoted by $\mathbf{n}$. In particular, the normal vector at the free surface boundary is $\mathbf{n}_{s,t}$.

This chapter is devoted to the investigation of the Telemac-3D algorithm, in view of pointing out its limitations, especially when it comes to simulating non-linear waves. The

[1] Notice that it is possible to consider variable density in Telemac-3D

[2] In Telemac-3D, topography that depends on time can be considered for sediment study

main purpose is to provide clues for possible improvements. We begin by introducing the particular ALE method used in this algorithm called the ALE-Sigma transformation, see Section 3.2. We give the different approaches available in the software. Afterwards, we detail the Finite Elements spaces defined on the two-dimensional and three-dimensional domain in Section 3.3. In Section 3.4, we examine the numerical strategy to solve the free surface Navier–Stokes equations performed in Telemac-3D. Finally, Section 3.5 is devoted to a discussion about the limits and the hypotheses of the Telemac-3D algorithm. We highlight possible improvements and their consequences regarding properties of the software.

3.2 The ALE-Sigma transform approach

Widely used in the atmospheric and oceanographic communities [12, 121], the ALE-Sigma transformation approach is a technique allowing to take into account the vertical movement of the domain. It consists in performing a transformation of the vertical coordinate z. This transformation leads to a vertical discretization of the domain which follows the topography and the free surface at each time step. Based on the choice of the discrete transformation function, different systems have been developed on this approach. Originally, the sigma transformation was not considered as an ALE approach. In [44], Decoene demonstrated the equivalence between the Sigma transformation and the ALE approach.

3.2.1 The ALE-Sigma mapping

The σ-transform approach can only be applied to three-dimensional domains in which the lateral boundaries are perfectly vertical. In this case, only the free surface and the bottom functions defined on the two-dimensional domain ω may move. The idea of the ALE-Sigma transformation approach is to transform, by a variable change, the vertical coordinate z of Ω_t into reference vertical coordinate $\widehat{z}$ contained in a fixed interval $]0,1[$. The transformation depends on time and on the position of this point in the two-dimensional domain.

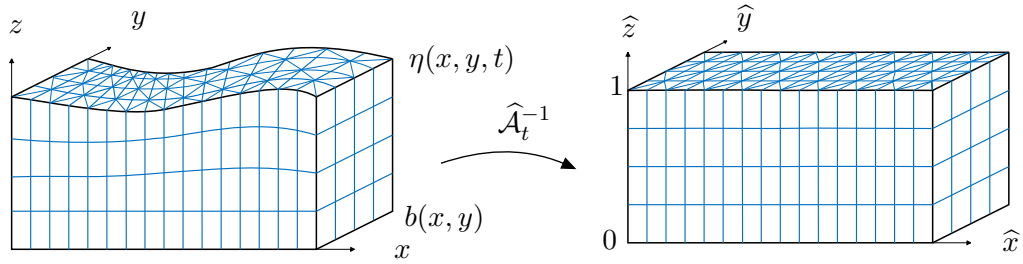

Figure 3.1: ALE mapping between the current domain Ω_t (on the left) and the reference domain $\widehat{\Omega}$ (on the right)

The ALE-Sigma transformation approach consists in transforming the Cartesian coordinate system (x, y, z, t) into a topography-following coordinate system $(\widehat{x}, \widehat{y}, \widehat{z}, \widehat{t})$, called σ-coordinate system and defined by

$$\widehat{\boldsymbol{x}}_{hor} = (x, y), \quad \widehat{z} = \widehat{Z}(x, y, z, t) \quad \text{and} \quad \widehat{t} = t, \tag{3.1}$$

where the function $\widehat{Z}(x, y, z, t)$ is arbitrary continuous and monotonic satisfying, for all $(x, y, t) \in \omega \times]0, T[$:

$$\begin{cases} \widehat{Z}(x, y, \eta(x, y, t), t) = 1, & (3.2) \\ \widehat{Z}(x, y, b(x, y), t) = 0. & (3.3) \end{cases}$$

As a consequence, the reference configuration is:

$$\widehat{\Omega} = \{\widehat{\boldsymbol{x}} = (\widehat{\boldsymbol{x}}_{hor}, \widehat{z}) = (\widehat{x}, \widehat{y}, \widehat{z}) \mid \widehat{\boldsymbol{x}}_{hor} \in \omega \quad \text{and } 0 < \widehat{z} < 1\}. \tag{3.4}$$

The ALE mapping between the reference domain $\widehat{\Omega}$ and the real one Ω_t is:

$$\widehat{\mathcal{A}}_t : \widehat{\Omega} \to \Omega_t, \quad \widehat{\mathcal{A}}_t(\widehat{\boldsymbol{x}}) = \boldsymbol{x}(\widehat{\boldsymbol{x}}, t). \tag{3.5}$$

Note that the real domain Ω_t is defined at each time step through the transformation $\widehat{Z}((x, y, \widehat{z}), t)$. Thus, Ω_t moves only in the vertical direction. As a consequence, the domain velocity $\mathbf{c}$ has only a vertical non zero component, i.e. $\mathbf{c} = (0, 0, c)$.

In Telemac-3D [76], some equations are written in the reference domain; more precisely the derivatives are transformed into derivatives with respect to the σ-coordinates $(x, y, \widehat{z})$. The σ-transformation method allows an accurate and smooth definition of the bed and surface boundaries at any time. One can easily incorporate bottom and surface boundary layers, and increase their resolution without having to increase the global number of layers. Another essential advantage of the ALE-Sigma transformation is the fact that it simplifies the kinematic boundary condition considerably both at the bottom and the free surface. However, it prevents from the representation of non single-valued defined free surface and in particular wave breaking.

3.2.2 Sigma transform approaches

In this Subsection, we describe the sigma coordinate systems used in Telemac-3D to simulate three-dimensional free surface flows. It is currently possible to choose between the classical sigma transformation, the generalized sigma transformation, or a hybrid method.

The classical sigma transformation

The classical sigma transformation proposed by Phillips [112] is the first and the most common approach based on the σ-coordinate system. It consists in adopting the following vertical transformation function leading to a linear transformation of the vertical

coordinate:

$$\widehat{Z}(x,y,z,t) = \frac{z - b(x,y)}{h(x,y,t)}. \tag{3.6}$$

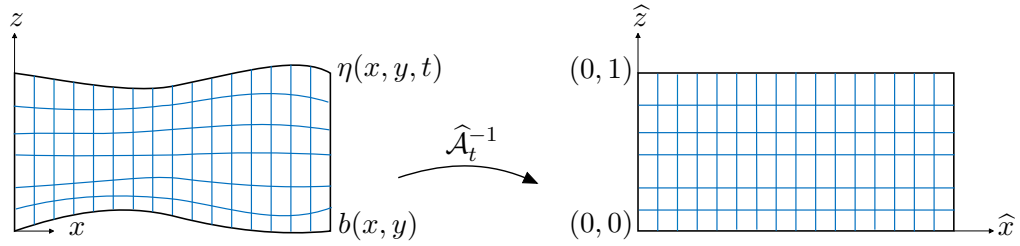

Figure 3.2: Reference domain

A clear advantage of this coordinate system is its simplicity. Indeed, the implementation is easy as well as the formulae for the variable change between the real and the reference framework. In particular, the determinant of the transformation is equal to the water depth function:

$$\frac{\partial z}{\partial \widehat{z}} = h(x,y,t). \tag{3.7}$$

Nevertheless, the classical sigma transformation also presents major drawbacks due to the restriction it imposes on the vertical discretization. Indeed, this transformation implies that all the levels necessarily follow the bottom and the free surface functions, and that the relative width of each layer is constant. As a consequence, it cannot maintain equally high resolution in specific zones (for instance near the surface and the bottom layers) independently of local water depth. With a constant number of horizontal levels, deeper and shallower zones of the domain can be respectively under-discretized and over-discretized. This may cause severe CFL restrictions. Many applications need a high resolution of the surface layer everywhere, for instance to accurately represent a surface mixing process arising from wind, thermal forcing and turbulence. In addition, the classical sigma transformation prevents from fixing the mesh in a particular zone of the domain which must be solved more accurately on the vertical. The movement of the mesh generates an amplification of the numerical diffusion. Finally, such a coordinate system can yield important errors, especially in the case of stratified flows over steep topographies. This problem is known as the sigma-coordinate pressure gradient error [62, 83] and is due the fact that the topography follows the shape of the mesh.

The generalized sigma transformation

Decoene and Gerbeau [45] proposed a general z-coordinate transformation in the ALE sigma approach. It allows a great adaptability of the vertical discretization and therefore overcomes the drawbacks of the classical sigma transformation. In Telemac-3D, a hybrid method can be chosen in which only parts of the $\widehat{z}_k$ are fixed in space and time, and a classical transformation is used.

The reference configuration $\widehat{\Omega}$ is first discretized by N_z horizontal levels, distributed along the vertical and following an arbitrary partition of the interval $]0,1[$:

$$0 = \widehat{z}_1 < \cdots \leq \widehat{z}_k \leq \cdots < \widehat{z}_{N_z} = 1. \tag{3.8}$$

We consider $\widehat{\mathcal{T}}_h$ the prismatic discretization of $\widehat{\Omega}$. The height of the grid nodes located on the k-th level of $\widehat{\mathcal{T}}_h$ is therefore $\widehat{z}_k$, which is constant in space and time. We denote by $\widehat{l}_{k+\frac{1}{2}}$ the layer delimited by levels k and $k+1$, for $k = 1, \ldots, (N_z - 1)$, in the reference mesh $\widehat{\mathcal{T}}_h$ and by $\Delta\widehat{z}_{k+\frac{1}{2}} = \widehat{z}_{k+1} - \widehat{z}_k$, its width.

The transformation function $Z(x, y, \widehat{z}, t)$ is then discretized by means of piecewise linear functions in the vertical direction. Inside each layer, this transformation can be expressed as a classical sigma transformation, characterized by the heights in the real domain of the levels delimiting the layer. Indeed, the restriction of the discrete transformation on each layer $\widehat{l}_{k+\frac{1}{2}}$ can be defined as follows on $\omega\times]\widehat{z}_k, \widehat{z}_{k+1}[\times]0, T[$:

$$\widehat{Z}_{k+\frac{1}{2}}(x, y, z, t) = \frac{z_k(x, y, t)}{\widehat{z} - \widehat{z}_k} \frac{\Delta\widehat{z}_{k+\frac{1}{2}}}{\Delta z_{k+\frac{1}{2}}(x, y, t)}, \tag{3.9}$$

where z_k is an arbitrary discrete function of (x, y, t) describing the current height of the grid k at each two-dimensional node and at each time step. Then, $\Delta z_{k+\frac{1}{2}}(x, y, t) = z_{k+1}(x, y, t) - z_k(x, y, t)$ denotes the width of the layer $l_{k+\frac{1}{2}}$, which corresponds to $\widehat{l}_{k+\frac{1}{2}}$ in the current mesh $\mathcal{T}_t^{3D}$ of Ω_t.

Obviously, it is the choice of the set of discrete functions $\{z_k(x, y, t) \mid k = 1, \ldots, N_z\}$ which determines the discrete mapping to be used for a particular simulation. We point out that they are defined by their value at each node on the two-dimensional mesh and at each time step. Moreover, they must satisfy the following conditions for all $(x, y, t) \in \omega \times]0, T[$:

$$z_1(x, y, t) = b_h(x, y), \tag{3.10}$$

$$z_{N_z}(x, y, t) = h_h(x, y, t), \tag{3.11}$$

$$z_{k+1}(x, y, t) - z_k(x, y, t) \geq \Delta z_{min} > 0, \quad \forall k \in [\![1, N_z - 1]\!], \tag{3.12}$$

where Δz_{min} is a constant minimal width chosen arbitrarily.

The discrete current domain $\Omega_{h,t}$ and its triangulation $\mathcal{T}_{h,t}^{3D}$ are then defined as in Section 2.2. The discrete ALE mapping is defined as follows:

$$\widehat{\mathcal{A}}_{h,t} : \widehat{\Omega} \to \Omega_{h,t}, \quad x = \widehat{x},\ y = \widehat{y},\ z = \widehat{Z}_h^{-1}(x, y, \widehat{z}, t), \tag{3.13}$$

with $\widehat{Z}_h(x, y, z, t)$ defined by (3.9). It is a continuous function and linear on each layer $l_{k+\frac{1}{2}}$. Notice that compared to the Jacobian determinant of the classical transformation,

the Jacobian determinant $\widehat{J}_{h,t}$ of a discrete particular mapping $\widehat{\mathcal{J}}_{h,t}$ varies along the vertical direction but it remains constant on each grid layer. Its expression on each layer $l_{k+\frac{1}{2}}$, for $k = 1, \ldots, (N_z - 1)$ is:

$$\widehat{J}_{h,t}(x, y) = \frac{\Delta z_{k+\frac{1}{2}}(x, y, t)}{\Delta \widehat{z}_{k+\frac{1}{2}}}, \quad \text{in } \omega \times]0, T[. \tag{3.14}$$

The value of this discrete Jacobian determinant characterizes the particular transformation defined in each grid element and at each time step.

3.3 Finite Elements spaces

Let $\mathcal{T}_h^{2D}$ be a triangulation of the two-dimensional domain ω. The three-dimensional mesh $\widehat{\mathcal{T}}_h^{3D}$ of the reference domain $\widehat{\Omega}$ is built by piling up the two-dimensional mesh on the vertical. As a consequence, the elements of $\widehat{\mathcal{T}}_h^{3D}$ are prismatic at any time t with vertical lateral side and horizontal plane at the top and bottom of the prism. The three-dimensional mesh $\mathcal{T}_{h,t}^{3D}$ of $\Omega_{h,t}$, the space-discrete domain of Ω_t, is built using a discrete ALE mapping as defined in Subsection 2.2.4.

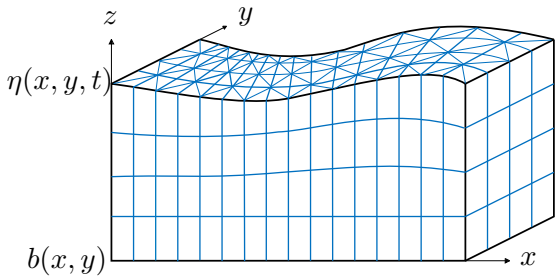

Figure 3.3: Prismatic and triangular discretizations of $\Omega_{h,t}$ and ω

3.3.1 Two-dimensional Finite Elements space

In this Subsection, we describe the two-dimensional Finite Elements used to approximate the free surface elevation η. This function is approximated by $\mathbb{P}_1$-Lagrangian Finite Elements basis functions. We define $K_{0,T}$ a reference triangle element such as each triangle element $K_T \in \mathcal{T}_h^{2D}$ is given by:

$$K_T = \mathcal{M}_1^T(K_{0,T}), \tag{3.15}$$

where $\mathcal{M}_1^{K_T}$ is an homeomorphic mapping of degree 1 from $K_{0,T}$ to K_T, see Figure 3.4. The reference $\mathbb{P}_1$-Lagrangian Finite Elements basis functions are denoted by $\{\zeta_{0,i}\}_{i=1,\cdots,3} \in \mathbb{P}_1(K_{0,T})$ such that:

$$\zeta_{0,1}(x_0, y_0) = 1 - x_0 - y_0, \quad \zeta_{0,2}(x_0, y_0) = x_0, \quad \zeta_{0,3}(x_0, y_0) = y_0,$$

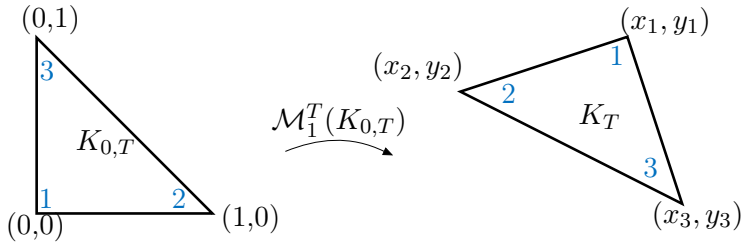

Figure 3.4: Reference element (on the left) and current element (on the right)

where $(x_0, y_0) \in \mathbb{R}^2$ are the vertex coordinates of the reference triangular element $K_{0,T}$. The free surface function defined in ω is approximated by $\mathbb{P}_1$ Lagrangian Finite Elements in $\mathcal{T}_h^{2D}$. We consider the set of Lagrange basis functions on the two-dimensional mesh $\mathcal{T}_h^{2D}$:

$$\{\zeta_i,\ \zeta_i \in \mathcal{F}_{1,1}(\mathcal{T}_h^{2D}),\ 0 \leq i \leq N_{2D}\}, \tag{3.16}$$

where N_{2D} is the set of nodes of the two-dimensional mesh. The Finite Elements space $\mathcal{F}_{1,1}(\mathcal{T}_h^{2D})$ on $\mathcal{T}_h^{2D}$ is defined as follows:

$$\mathcal{F}_{1,1}(\mathcal{T}_h^{2D}) = \{\zeta_h : \omega \to \mathbb{R} \mid \quad \zeta_h \in C^0(\overline{\omega}),\ \ \zeta_h|_{K_T} \circ \mathcal{M}_1^{K_T} \in \mathbb{P}_1(K_{0,T})\}. \tag{3.17}$$

3.3.2 Three-dimensional Finite Elements space

We now describe the three-dimensional Finite Elements space used to approximate the velocity field and the pressure. Let $\mathcal{M}_1^{K_{0,P}}$ be an homeomorphic mapping from a reference prismatic linear element $K_{0,P}$ to a current prismatic linear element $K_P \in \mathcal{T}_{h,t}^{3D}$ as represented on Figure 3.5. Each prismatic linear element K_P is given by:

$$K_P = \mathcal{M}_1^P(K_{0,P}). \tag{3.18}$$

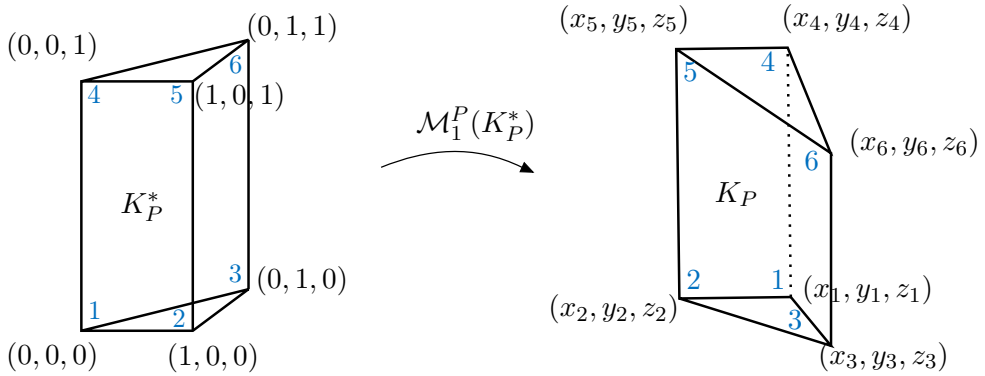

Figure 3.5: Reference prismatic element (on the left) and current prismatic element (on the right)

The coordinates in $K_{0,P}$ are denoted $(x_0, y_0, z_0) \in \mathbb{R}^3$. We consider $\mathbb{P}_{1,xy}$ (resp $\mathbb{P}_{1,z}$) the set of piecewise linear functions in x and y (resp. z). The prismatic Lagrange Finite Elements space is $\mathbb{PR}_1 = \mathbb{P}_{1,xy} \times \mathbb{P}_{1,z}$ such as:

$$\mathbb{PR}_1(K_{0,P}) = \{\varphi_0(x_0, y_0, z_0) = \varphi_0^h(x, y)\ \ \varphi_0^v(z),\ \ \ \varphi_0^h \in \mathbb{P}_{1,xy},\ \ \ \varphi_0^v \in \mathbb{P}_{1,z}\}. \tag{3.19}$$

The velocity field and the pressure functions are approximated by $\mathbb{PR}_1$-Lagrangian Finite Elements basis functions. Let us denote by $\{\varphi_{0,i}\}_{i=1,\cdots,6} \in \mathbb{P}_1(K_{0,P})$ the set of reference Finite Elements basis functions in $K_{0,P}$. These functions are defined on a reference prismatic element $K_{0,P}$ by:

$$\begin{aligned}
&\varphi_{0,1}(x_0, y_0, z_0) = (1 - x_0 - y_0)\,(1 - z_0), && \varphi_{0,4}(x_0, y_0, z_0) = (1 - x_0 - y_0)\,z_0,\\
&\varphi_{0,2}(x_0, y_0, z_0) = x_0\,(1 - z_0), && \varphi_{0,5}(x_0, y_0, z_0) = x_0\,z_0,\\
&\varphi_{0,3}(x_0, y_0, z_0) = y_0\,(1 - z_0), && \varphi_{0,6}(x_0, y_0, z_0) = y_0\,z_0.
\end{aligned}$$

Let N_{3D} be the number of nodes of the Finite Elements mesh $\mathcal{T}_{h,t}^{3D}$. We consider the set of prismatic Lagrange basis functions on the three-dimensional mesh $\mathcal{T}_{h,t}^{3D}$:

$$\{\varphi_i,\ \varphi_i \in \mathbb{PR}_1(\mathcal{T}_h),\ 0 \leq i \leq N_{3D}\}, \tag{3.20}$$

where the first order prismatic Finite Elements space $\mathbb{PR}_1(\mathcal{T}_h)$ on $\mathcal{T}_{h,t}^{3D}$ is defined as follows:

$$\mathbb{PR}_1(\mathcal{T}_h) = \{\varphi_i : \Omega_t \to \mathbb{R}\ \ |\ \ \ \varphi_i \in C^0(\overline{\Omega}_t),\ \ \varphi_i|_P \circ \mathcal{M}^{K_P} \in \mathbb{PR}_1(K_{0,P}),\ \forall K_P \in \mathcal{T}_{h,t}^{3D}\}. \tag{3.21}$$

The construction of the three-dimensional mesh in Telemac-3D implies that the column of prismatic elements are perfectly vertical, as represented in Figure 3.6. Therefore, the horizontal coordinates of nodes of a same column are equal. This property implies that the Jacobian determinant (of the transformation between the reference and a real prismatic element) does not depend on the vertical component z. From (3.19), we can remark that the Finite Elements basis functions of the triangular basis of a prismatic element coincide with the reference triangular element ($\varphi^h(x, y) = \zeta(x, y)$). We consider prismatic elements $\widehat{K}_P \in \widehat{\mathcal{T}}_h^{3D}$. The prismatic elements are a linear transformation of $K_{0,P}$. Any function $\widehat{\varphi} \in \mathbb{PR}_1(\widehat{K}_P)$ can be written as the product of a function $\widehat{\zeta} \in \mathbb{P}_1(K_T)$ and a function $\widehat{\varphi}_{i_v}^v$ defined on the vertical edge of $K_P \in \mathbb{P}_{1,z}(K_P)$ such that:

$$\widehat{\varphi}_i(x, y, \widehat{z}) = \widehat{\zeta}_{0,i_h}(x, y)\,\widehat{\varphi}_{i_v}^v(\widehat{z}),\ \ \text{in}\ \ \widehat{K}_P, \tag{3.22}$$

where i_h denotes the associated node in K_T and i_v the level on which node i is located, as illustrated by Figure 3.6.

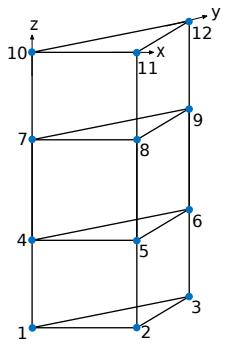

Figure 3.6: A prism column in the reference mesh $\widehat{\mathcal{T}_h}$

3.4 Telemac-3D algorithm

Now, we present the numerical strategies used to solve the Navier–Stokes equations with pressure decomposition (2.128-2.130) in Telemac-3D, recalled here for convenience:

$$\begin{cases} \left.\dfrac{\partial \boldsymbol{u}^{hor}}{\partial t}\right|_{\widehat{\Omega}} + \big((\mathbf{u}-\mathbf{c})\cdot\nabla\big)\boldsymbol{u}^{hor} - \nu\,\Delta\boldsymbol{u}^{hor} + g\,\nabla_{hor}\eta + \dfrac{1}{\rho}\nabla_{hor}p_d = \mathbf{f}_{xy}, & \text{on } \Omega_t, \\ \left.\dfrac{\partial w}{\partial t}\right|_{\widehat{\Omega}} + ((\mathbf{u}-\mathbf{c})\cdot\nabla)w - \nu\,\Delta w + \dfrac{1}{\rho}\dfrac{\partial p_d}{\partial z} = \mathbf{f}_z + g, & \text{on } \Omega_t, \\ \nabla\cdot\mathbf{u} = 0, & \text{on } \Omega_t, \\ \dfrac{\partial \eta}{\partial t} + \nabla_{hor}\cdot\displaystyle\int_b^\eta \boldsymbol{u}^{hor}\,dz = 0, & \text{on } \omega, \end{cases}$$

with the boundary conditions (2.132-2.135). As explained in the previous Chapter, the time discretization consists in splitting the equations into hydrostatic predictor and non-hydrostatic corrector steps. However, an additional step is performed at the end of the algorithm since the final velocity field is not divergence-free due to numerical choice. As a consequence, a continuity equation is solved in order to compute a velocity field $\mathbf{u}^c$ which is divergence-free. In the next iterative step, this velocity is used to advection term of the Navier–Stokes equations or in transport equations for scalar quantities.

Many options leading to different numerical strategies are available in Telemac-3D. In this thesis, we focus on the default algorithm. We will describe and discuss the algebraic formulations (compared with the previous Chapter). For this purpose, we consider that a time interval $]0,T[$ is divided into $N_T \in \mathbb{N}^*$ time steps of equal length $\Delta T \in \mathbb{R}_*^+$. The time step Δt is fixed in Telemac-3D and chosen by the user. On the one hand, the discrete solutions $\mathbf{u}_h^n$ and $p_{h,d}^n$ are approximated by $\varphi^n \in \mathbb{PR}_1(\mathcal{T}_h^{n,3D})$ prismatic linear Lagrange Finite Elements functions. On the other hand, the discrete solution η_h^n is approximated by $\zeta \in \mathbb{P}_1(\mathcal{T}_h^{2D})$ triangular Lagrange Finite Elements functions. The free surface Navier–Stokes equations are discretized in time by a first order Euler scheme in which all the terms are implicit, except the diffusion terms. Indeed, on the one hand, the

vertical component of the diffusion term and the friction condition (2.126) at the solid boundaries are implicit. On the other hand, the horizontal diffusion terms and the wind condition (2.123) at the free surface are treated explicitly. Notice that the hydrostatic step can be discretized in time[3] with θ-scheme in order to increase the order in time ($\mathcal{O}(\delta t) \leq 2$).

3.4.1 Hydrostatic predictor step

As introduced in the previous Chapter, the hydrostatic predictor step consists in solving the hydrostatic equations (2.120,2.121) and the vertical momentum equation (2.129) without the dynamic pressure. As a consequence, the discrete free surface η_h^{n+1} and the intermediate velocity field $\tilde{\mathbf{u}}_h^{n+1}$ which does not satisfy the free divergence condition are computed. As mentioned previously, a first particularity in Telemac-3D is that the equations are advected by $\mathbf{u}_h^{c,n}$, which is a free divergence velocity additionally computed at the end of the algorithm (see Subsection 3.4.3). A second particularity is that the horizontal diffusion terms and the wind condition are treated explicitly (discussed in Section 3.5). Notice that Casulli and Cheng [30] performed the same strategy in their Finite Differences approach of the hydrostatic Navier–Stokes equations.

The hydrostatic predictor step can be treated following two strategies: either a coupled numerical strategy of the hydrostatic Navier–Stokes equations or a decoupled numerical one. The way how these strategies are taken into account in Telemac-3D is presented below.

Coupled numerical approach

The Navier–Stokes equations of hydrostatic predictor step are split by a first order in time fractional step method (see Section 2.4.5). Therefore, an advection equation is considered in first, the hydrostatic Navier–Stokes equations and the vertical momentum equation are then solved.

Advection equation:
In Telemac-3D, advection equations are solved by the characteristics method [113] or the MURD method [108, 111]. It writes at the time-discrete level:

$$\begin{cases} \dfrac{\tilde{\boldsymbol{u}}^{hor,n+\frac{1}{2}} - \boldsymbol{u}^{hor,n}}{\Delta t} + \big((\mathbf{u}^{c,n} - \mathbf{c}^n) \cdot \nabla\big)\tilde{\boldsymbol{u}}^{hor,n+\frac{1}{2}} = 0, \quad \text{on } \Omega^n, & (3.23) \\ \dfrac{\tilde{w}^{n+\frac{1}{2}} - w^n}{\Delta t} + \big((\mathbf{u}^{c,n} - \mathbf{c}^n) \cdot \big)\nabla\tilde{w}^{n+\frac{1}{2}} = 0, \quad \text{on } \Omega^n. & (3.24) \end{cases}$$

Diffusion equation on the vertical velocity:
The vertical intermediate velocity $\tilde{w}_h^{n+\frac{1}{2}}$ is then computed separately from the hydrostatic

[3] With an appropriate option

equations, since it does not depend on the free surface. In Telemac-3D, the time-discrete equation is:

$$\begin{cases} \dfrac{\tilde{w}^{n+1} - \tilde{w}^{n+\frac{1}{2}}}{\Delta t} - \nu(\Delta_{hor}\tilde{w}^{n+\frac{1}{2}} - \partial_{zz}\tilde{w}^{n+1}) = f_z^{n+1} - g, & \text{on } \Omega^n, \\ \mu\,(\nabla_{hor}\tilde{w}^{n+\frac{1}{2}} \cdot \mathbf{n}_{s,xy}^n + \partial_z\tilde{w}^{n+1} \cdot n_{s,z}^n) = \gamma_{wind}\,(w_{air}^{n+\frac{1}{2}} - \tilde{w}^{n+\frac{1}{2}}), & \text{on } \Gamma_s^n, \\ \mu\,(\nabla_{hor}\tilde{w}^{n+\frac{1}{2}} \cdot \mathbf{n}_{xy} + \partial_z\tilde{w}^{n+1} \cdot n_z) = -\kappa_f(|\tilde{w}^{n+1}|)\,\tilde{w}^{n+1}, & \text{on } \Gamma_l^n \cup \Gamma_b, \end{cases}$$

As mentioned previously, the vertical component of the diffusion term and the friction condition (2.126) at the solid boundaries are implicit. The horizontal diffusion terms and the wind condition (2.123) at the free surface are treated explicitly.

The algebraic formulation is then, for $n = 0, \cdots, N_T - 1$:

$$A_{1,u}^n\,\tilde{W}^{n+1} = A_{2,u}^n\,\tilde{W}^{n+\frac{1}{2}} + \Delta t\,F_z^n, \tag{3.25}$$

where the vector $\tilde{W}^n$ contains the discrete values of $\tilde{w}_h^n$. The vector of the vertical source term and of the gravity term is denoted by F_z^{n+1}. The matrix $A_{1,u}^{n+1}$ and $A_{2,u}^n$ are respectively equal to:

$$A_{1,u}^n = M_u^n + \nu\,\Delta t\,(R_u^{z,n} - Bc_u^{n,fric}), \tag{3.26}$$

$$A_{2,u}^n = M_u^n + \nu\,\Delta t\,(-R_u^{hor,n} + Bc_u^{n,wind}). \tag{3.27}$$

We recall that M_u^n is the three-dimensional mass matrix of the velocity defined on Ω_h^n given by (2.194). It is recalled here for convenience:

$$M_{u,ij}^n = \int_{\Omega_h^n} \varphi_i^n\,\varphi_j^n\,d\boldsymbol{x}.$$

In addition, the matrices $R_u^{hor,n}$ and $R_u^{z,n}$ represent respectively the three-dimensional horizontal and vertical rigidity matrices of the velocity, which are defined on Ω_h^n such that:

$$R_{u,ij}^{hor,n} = \int_{\Omega_h^n} \nabla_{hor}\varphi_i^n : \nabla_{hor}\varphi_j^n\,d\boldsymbol{x}, \tag{3.28}$$

$$R_{u,ij}^{z,n} = \int_{\Omega_h^n} \frac{\varphi_i^n}{\partial z} : \frac{\varphi_j^n}{\partial z}\,d\boldsymbol{x}. \tag{3.29}$$

The three-dimensional matrices $Bc_{u,ij}^{n,fric}$ and $Bc_{u,ij}^{n,wind}$ are respectively the boundary matrices on the friction and wind conditions. They are defined according to the right-hand side terms of the boundary conditions. Since these terms are different according the considered numerical strategies in time, we do not detail these matrices.

Hydrostatic equations:
At the time-discrete level, the hydrostatic equations are given by (2.137-2.138) with a different time discretization of the diffusion terms such that:

$$\begin{cases} \dfrac{\tilde{\boldsymbol{u}}^{hor,n+1} - \tilde{\boldsymbol{u}}^{hor,n+\frac{1}{2}}}{\Delta t} - \nu(\Delta_{hor}\tilde{\boldsymbol{u}}^{hor,n+\frac{1}{2}} - \partial_{zz}\tilde{\boldsymbol{u}}^{hor,n+1}) + g\,\nabla_{hor}\eta^{n+1} = \boldsymbol{f}_{xy}^{n+1}, & \text{on } \Omega^n \\ \dfrac{\eta^{n+1} - \eta^n}{\Delta t} + \nabla_{hor} \cdot \displaystyle\int_{b^n}^{\eta^n} \tilde{\boldsymbol{u}}^{hor,n+1}\, dz = 0, & \text{on } \omega, \end{cases}$$

with at the boundary conditions

$$\begin{aligned} \mu\,(\nabla_{hor}\tilde{\boldsymbol{u}}^{hor,n+\frac{1}{2}} \cdot \mathbf{n}_{s,xy}^n + \partial_z\tilde{\boldsymbol{u}}^{hor,n+1} \cdot n_{s,z}^n) &= \gamma_{wind}\,(\boldsymbol{u}_{air}^{hor} - \tilde{\boldsymbol{u}}^{hor,n+\frac{1}{2}}), && \text{on } \Gamma_s^n, \\ (\mu\,\nabla_{hor}\tilde{\boldsymbol{u}}^{hor,n+\frac{1}{2}} \cdot \mathbf{n}_{xy}) \cdot \mathbf{t}_{xy} &= -\kappa_f(|\tilde{\boldsymbol{u}}^{hor,n+\frac{1}{2}} \cdot \mathbf{t}_{xy}|)\,\tilde{\boldsymbol{u}}^{hor,n+\frac{1}{2}} \cdot \mathbf{t}_{xy}, && \text{on } \Gamma_l^n, \\ \tilde{\boldsymbol{u}}^{hor,n+\frac{1}{2}} \cdot \mathbf{n}_{xy} &= 0, && \text{on } \Gamma_l^n, \\ \mu\,(\nabla_{hor}\tilde{\boldsymbol{u}}^{hor,n+\frac{1}{2}} \cdot \mathbf{n}_{xy} + \partial_z\tilde{\boldsymbol{u}}^{hor,n+1} \cdot n_z) &= -\kappa_f(|\tilde{\boldsymbol{u}}^{hor,n+1}|)\,\tilde{\boldsymbol{u}}^{hor,n+1}, && \text{on } \Gamma_b. \end{aligned}$$

As presented in Subsection 2.6.1, the imperviousness conditions at the lateral boundaries are treated naturally in the Finite Elements approach adopted in the software. These equations are solved in Telemac-3D by using a Schur complement [139] at the algebraic level. The free surface is then computed in first through the following algebraic formulation,

$$A_\eta E^{n+1} = M_\eta\, E^n + \Delta t^2 (\tilde{D}^n)(A_{1,u}^n)^{-1} F_{xy}^n + \Delta t\,(\tilde{D}^n)\,(A_{1,u}^n)^{-1}\,C_u^n\,\tilde{U}_{hor}^{n+\frac{1}{2}}, \tag{3.30}$$

where E^{n+1} is the unknown vector containing the discrete values of the free surface. The matrix M_η is the two-dimensional mass matrix of the free surface, already given in (2.196). The vector of horizontal source terms is denoted F_{xy}^n. In addition, the matrix $\tilde{D}^n$ is the algebraic counterpart of the gradient operator already given in (2.205). Furthermore, the matrix A_η is such that:

$$A_\eta = M_\eta + g\,\Delta t^2\,(\tilde{D}^n)\left((A_{1,u}^n)^{-1}\,M_u^n\right)\tilde{D}^n. \tag{3.31}$$

As mentioned in the previous Chapter, this expression requires to invert explicitly the matrix $A_{1,u}^n$ given in (3.26), that is very costly. In Telemac-3D, the mass matrix $M_{\mathbf{u}}^n$ is mass lumped [35] leading to diagonal matrix (the notion of mass lumping is briefly introduced in Appendix 3.7.1). In addition, a particularity in Telemac-3D is that the vertical rigidity matrix $R_u^{z,n}$ is rewritten by taking into account the choice of the prismatic elements and the variable decomposition of the three-dimensional Finite Elements basis functions ϕ.

Proposition 3.1. *Let ζ and ϕ^n be Finite Elements basis functions in $\mathbb{P}_1(\mathcal{T}_h^{2D})$ and $\mathbb{PR}_1(\mathcal{T}_h^{3D,n})$ then the vertical rigidity matrix $R_u^{z,n}$ can be written as follows:*

$$R_{u,ij}^{n,z} = \left(\int_\omega \frac{\partial\varphi_{i_v}}{\partial z} : \frac{\partial\varphi_{j_v}}{\partial z}\,dy\,dx\right)\left(\int_{b_h}^{\eta_h^n} \zeta_{i_h}\zeta_{j_h}\,dz\right). \tag{3.32}$$

Proof. We use the fact that the basis functions ϕ can be written as the product of a function $\zeta \in \mathbb{P}_1(\mathcal{T}_h^{2D})$ and a function $\widehat{\varphi}_{i_v}^v$ in $\mathbb{P}_{1,z}(\mathcal{T}_h^{3D,n})$ through the reference basis functions $\widehat{\varphi}$ and the relation (3.22). Consequently, we have:

$$R_{u,ij}^{n,z} = \int_{\Omega_h^n} \frac{\partial \varphi_i^n}{\partial z} : \frac{\partial \varphi_j^n}{\partial z} d\boldsymbol{x} = \int_{\Omega_h^n} \zeta_{i_h} \frac{\partial \varphi_{i_v}}{\partial z} : \zeta_{j_h} \frac{\partial \varphi_{j_v}}{\partial z} d\boldsymbol{x} = \int_{\omega} \frac{\partial \varphi_{i_v}}{\partial z} : \frac{\partial \varphi_{j_v}}{\partial z} dy\, dx \int_b^{\eta_h^n} \zeta_{i_h} \zeta_{j_h}\, dz.$$

■

As a consequence, the matrix $R_u^{z,n}$ expresses only the interactions between the nodes of the vertical edge of the prismatic elements. This matrix and $A_{1,u}^n$ are then composed of the diagonal and two extra-diagonals. In Telemac-3D, the numbering of the nodes in the three-dimensional mesh is adopted in order to write $A_{1,u}^n$ as a tridiagonal matrix. Consequently, the matrix can be inverted by using a technique such as Usmani [129].

Once the free surface vector E^{n+1} is known, the horizontal intermediate velocity vector $\tilde{U}_{hor}^{n+1}$ containing the discrete values of $\tilde{\boldsymbol{u}}_h^{n+1,hor}$ is computed through, for $n = 0, \cdots, N_T - 1$:

$$A_{1,u}^n \tilde{U}_{hor}^{n+1} = A_{2,u}^n \tilde{U}_{hor}^{n+\frac{1}{2}} + \Delta t \left(F_{xy}^n + \tilde{D}^n \eta^{n+1} \right). \tag{3.33}$$

We can remark that the algebraic formulations described above cannot be assimilated to the coupled numerical strategy given in Subsection 2.6.1. Indeed, the formulation on the free surface (3.30) cannot be compared to (2.198) with $D^n = \tilde{D}^n$, since an additional three-dimensional mass matrix M_u^n appears in (3.31). Moreover, before applying a Schur complement method, the block matrix allowing to retrieve (3.30) is, for $n = 0, ..., N_T - 1$:

$$\begin{pmatrix} A_{1,u}^n & -\Delta t\, M_u^n\, \tilde{D}^n \\ \Delta t\, (\tilde{D}^n) & M_\eta \end{pmatrix} \begin{pmatrix} \tilde{U}_{hor}^{n+1} \\ E^{n+1} \end{pmatrix} = \begin{pmatrix} A_{1,u}^n\, \tilde{U}_{hor}^{n+\frac{1}{2}} + \Delta t\, F_{xy}^n \\ M_\eta\, E^n \end{pmatrix}. \tag{3.34}$$

From (3.34), we can deduce that the algebraic formulation on $\tilde{U}_{hor}^{n+1}$ leading to (3.30) is:

$$A_{1,u}^n \tilde{U}_{hor}^{n+1} = A_{1,u}^n \tilde{U}_{hor}^{n+\frac{1}{2}} + \Delta t\, F_{xy}^n + \Delta t\, M_u^n\, \tilde{D}^n\, E^{n+1}, \tag{3.35}$$

which is different from (3.33). The coupled numerical strategy used to solve the hydrostatic equations in Telemac-3D cannot be linked to a rigorous mathematical explanation. Indeed, we cannot write this algebraic formulation to a discrete variational formulation.

Decoupled numerical approach

The hydrostatic predictor step can also be solved in Telemac-3D by using a decoupled numerical strategy. In this case, an advection-diffusion equation with source terms is first solved as introduced in Section 2.4.5. Then, the free surface equation is computed through a wave equation and the intermediate horizontal velocity is finally corrected by the free surface.

Advection-diffusion equation with source terms:
At the time-discrete level, we consider in Telemac-3D the advection-diffusion equation with source terms given in (2.150) with a different time discretization of the diffusion terms such that for all $\boldsymbol{x} \in \Omega^n$:

$$\begin{cases} \dfrac{\tilde{\boldsymbol{u}}^{hor,n+\frac{1}{2}} - \boldsymbol{u}^{hor,n}}{\Delta t} + \big((\mathbf{u}^{c,n} - \mathbf{c}^n) \cdot \nabla\big)\tilde{\boldsymbol{u}}^{hor,n+\frac{1}{2}} - \nu(\Delta_{hor}\boldsymbol{u}^{hor,n} - \partial_{zz}\tilde{\boldsymbol{u}}^{hor,n+\frac{1}{2}}) = \boldsymbol{f}_{xy}^{n+1}, \\ \dfrac{\tilde{w}^{n+1} - w^n}{\Delta t} + \big((\mathbf{u}^{c,n} - \mathbf{c}^n) \cdot \nabla\big)\tilde{w}^{n+1} - \nu(\Delta_{hor} w^n - \partial_{zz}\tilde{w}^{n+1}) = f_z^{n+1} - g, \end{cases}$$

with the boundary conditions:

$$\begin{aligned} \mu\big(\nabla_{xy}\mathbf{u}^n \cdot \mathbf{n}_{s,xy}^n + \partial_z\tilde{\mathbf{u}}^{n+\frac{1}{2}} \cdot n_{s,z}^n\big) \cdot \mathbf{t}_s^n &= \gamma_{wind}\,(\mathbf{u}_{air}^{n+1} - \mathbf{u}^n) \cdot \mathbf{t}_s^n, && \text{on } \Gamma_s^n, \\ \mu\,(\nabla_{xy}\mathbf{u}^n \cdot \mathbf{n}_{s,xy}^n + \partial_z\tilde{\mathbf{u}}^{n+\frac{1}{2}} \cdot n_{s,z}^n) \cdot \mathbf{n}_s^n &= 0, && \text{on } \Gamma_s^n, \\ \mu(\nabla_{xy}\mathbf{u}^n \cdot \mathbf{n}_{xy} + \partial_z\tilde{\mathbf{u}}^{n+\frac{1}{2}} \cdot n_z) \cdot \mathbf{t} &= -\kappa_f(|\tilde{\mathbf{u}}^{n+\frac{1}{2}} \cdot \mathbf{t}|)\,\tilde{\mathbf{u}}^{n+\frac{1}{2}} \cdot \mathbf{t}, && \text{on } \Gamma_b \cup \Gamma_l^n, \\ \tilde{\mathbf{u}}^{n+\frac{1}{2}} \cdot \mathbf{n} &= 0, && \text{on } \Gamma_b \cup \Gamma_l^n. \end{aligned}$$

These equations are solved by the SUPG method [21]. A particularity of this software is that the stabilized test functions of the SUPG method replace only the test functions which are multiplied to the advection term. The algebraic formulation is then, for $n = 0, \cdots, N_T - 1$:

$$\begin{cases} \big[A_{1,u}^n + \dfrac{\Delta t^2}{2}\,(R_u^n + K_u^n)\big]\tilde{U}_{hor}^{n+\frac{1}{2}} = A_{2,u}^n\,U^n + \Delta t\,F_{xy}^n, & (3.36) \\ \big[A_{1,u}^n + \dfrac{\Delta t^2}{2}\,(R_u^n + K_u^n)\big]\tilde{W}^{n+1} = A_{2,u}^n\,W^n + \Delta t\,F_z^n, & (3.37) \end{cases}$$

where $R_u^n = R_u^{hor,n} + R_u^{z,n}$ is the three-dimensional rigidity matrix of the velocity and $F^n = F_{xy}^n + F_z^n$ is the vector of source terms. Recall that the matrices $A_{1,u}^{n+1}$ and $A_{2,u}^n$ are given in (3.26) and (3.27). Furthermore, K_u^n is a matrix induced by the SUPG method and defined as follows:

$$K_{u,ij}^n = \int_{\Omega_h^n} |\mathbf{u}_h^{c,n} - \mathbf{c}_h^n|^2\,\varphi_i^n \cdot \nabla\varphi_j^n\,d\boldsymbol{x}. \tag{3.38}$$

Since the vertical momentum equation is not dependent on the free surface elevation, we have that the vector of intermediate vertical velocity is $\tilde{W}^{n+1} = \tilde{W}^{n+\frac{1}{2}}$.

Hydrostatic equations
The decoupled numerical strategy in time for the hydrostatic equations consists in solving a wave equation on the free surface (2.159) and to correct the intermediate horizontal velocity through (2.156) (see Section 2.4.5 and Subsection 2.6.2). The time-discrete equation is (2.159), recalled here for convenience:

$$\begin{aligned} \eta^{n+1} - g\,h^n\,\Delta t^2\,\Delta_{hor}\eta^{n+1} &= \eta^n - \Delta t\,\nabla_{hor} \cdot \left(\int_{b^n}^{\eta^n} \boldsymbol{u}^{hor,n} dz\right), && \text{on } \omega, \\ \nabla_{hor}\eta^{n+1} \cdot \mathbf{n}_\omega &= 0, && \text{on } \partial\omega. \end{aligned}$$

The associate algebraic formulation is (2.216), recalled here for convenience:

$$(M_\eta + g\,h^n\,\Delta t^2\,R_\eta)\,E^{n+1} = M_\eta\,E^n + \Delta t\,(\tilde{D}^n)\,\tilde{U}_{hor}^{n+\frac{1}{2}}.$$

where R_η is the two-dimensional rigidity matrix of the free surface, already given in (2.217). The velocity is then corrected through the time-discrete equation (2.156) recalled below:

$$\begin{aligned}\frac{\tilde{\boldsymbol{u}}^{hor,n+1} - \tilde{\boldsymbol{u}}^{hor,n+\frac{1}{2}}}{\Delta t} + g\,\nabla_{hor}\eta^{n+1} = 0, &\text{ on } \Omega^n,\\ \tilde{\boldsymbol{u}}^{hor,n+1}\cdot\mathbf{n}_\omega = 0, &\text{ on } \Gamma_l^n.\end{aligned}$$

The associate algebraic formulation is (2.218), which is also recalled here for convenience:

$$M_u^n\,\tilde{U}_{hor}^{n+1} = M_u^n\,\tilde{U}_{hor}^{n+\frac{1}{2}} + \Delta t\,\tilde{D}^n\,E^{n+1}.$$

For both numerical strategies, once the hydrostatic predictor step is performed, the new mesh is updated such that $\mathcal{T}_h^{3D,n+1} = \widehat{\mathcal{A}}_h^{n+1}(\widehat{\mathcal{T}}_h^{3D})$ where $\widehat{\mathcal{A}}_h^{n+1}$ is the discrete ALE-Sigma mapping of (3.5).

3.4.2 Non-hydrostatic corrector step

As introduced in the previous Chapter, the non-hydrostatic corrector step consists in computing a free divergence velocity field $\mathbf{u}_h^{n+1}$ through the Darcy equations (2.146,2.147). In Telemac-3D, this system is solved by adopting a decoupled numerical strategy presented in Sections 2.4.5 and 2.6.2. This approach consists in solving a pressure Poisson equation (2.161) on the dynamic pressure $p_{d,h}^{n+1}$ and in correcting the final velocity $\mathbf{u}_h^{n+1}$ through (2.164). The algebraic formulations corresponding to these equations have been introduced in Subsection 2.6.2.

The time-discrete equation on the dynamic pressure is (2.161) recalled here:

$$\begin{cases}\Delta p^{n+1} = \dfrac{\rho}{\Delta t}\,\nabla\cdot\tilde{\mathbf{u}}_n^{n+1}, & \text{on } \Omega^{n+1}\\ p^{n+1} = 0, & \text{on } \Gamma_s^{n+1},\\ \nabla p^{n+1}\cdot\mathbf{n} = 0, & \text{on } \Gamma_b\cup\Gamma_l^{n+1}.\end{cases}$$

In Telemac-3D, the algebraic equation corresponding to these equation is given by (2.222) and it is recalled here for convenience:

$$B^{n+1}(B^{n+1})P_d^{n+1} = -\frac{\rho}{\Delta t}B^{n+1}\tilde{U}^{n+1}.$$

Then, the velocity is corrected through the time-discrete equation (2.164), recalled here:

$$\mathbf{u}^{n+1} = \tilde{\mathbf{u}}_n^{n+1} - \frac{\Delta t}{\rho}\nabla p_d^{n+1}, \text{ on } \Omega^{n+1}.$$

where $\tilde{\mathbf{u}}_n^{n+1}$ is the velocity in Ω^{n+1} through the relation (2.83). In Telemac-3D, the algebraic equation corresponding to these equation given by (2.211) and it is also recalled here for convenience:

$$U^{n+1} = \tilde{U}^{n+1} + \frac{\Delta t}{\rho}(M_u^{n+1})^{-1}(B^{n+1})\tilde{U}^{n+1}.$$

The free divergence of the velocity $\mathbf{u}_h^{n+1}$ is not satisfied at the discrete level (see Subsection 2.6.2). We recall that this property is required to advect the fluid velocity or scalar quantities. Consequently, a continuity equation is additionally solved in order to compute a velocity field $\mathbf{u}_h^c$ which is divergence-free.

3.4.3 Continuity equation

As mentioned previously, a free divergence velocity field $\mathbf{u}_h^c$ is computed as the solution of the continuity equation. Actually, the idea is based on the computation of a free divergence velocity for the hydrostatic Navier–Stokes equations (2.120-2.122). As a consequence, the horizontal velocity field of $\mathbf{u}_h^c$ is equal to the intermediate horizontal velocity field $\tilde{\mathbf{u}}_h^{hor,n+1}$ resulting from the hydrostatic predictor step. Then, a vertical velocity $w^{c,n+1}$ making $\mathbf{u}^{c,n+1} = (\tilde{\boldsymbol{u}}^{hor,n+1}, w^{c,n+1})$ divergence-free is computed from the continuity equation such that:

$$\frac{\partial \tilde{w}^{c,n+1}}{\partial z} = \nabla_{hor} \cdot \tilde{\boldsymbol{u}}^{n+1,hor}. \tag{3.39}$$

The variational formulation associated to (3.39) in Telemac-3D is introduced in Decoene [44] and it corresponds to:

$$\begin{cases} \text{Find } w^{c,n+1} \in \mathcal{W}_{1,t}(\Omega_t) \text{ such that for all } \mathbf{v} \in \mathcal{W}_{2,t}(\Omega_t) \\ \displaystyle\int_{\Omega_t} (w^{c,n+1} - c^n)\partial_z \mathbf{v}\, d\boldsymbol{x} - \int_{\Omega_t} (\tilde{\boldsymbol{u}}^{hor,n+1})\nabla_{hor}\,\mathbf{v}\, d\boldsymbol{x} = \frac{d}{dt}\int_{\Omega_t} \mathbf{v}\, d\boldsymbol{x} \end{cases} \tag{3.40}$$

where

$$\mathcal{W}_{1,t}(\Omega_t) = \{\mathbf{v} : \Omega_t \to \mathbb{R} \mid \mathbf{v}_t = \widehat{\mathbf{v}} \circ \widehat{\mathcal{A}}_t^{-1},\ \widehat{\mathbf{v}} \in \widehat{\mathcal{W}}_1(\widehat{\Omega})\} \text{ with } \widehat{\mathcal{W}}_1(\widehat{\Omega}) = L^2(\Omega_t), \tag{3.41}$$

$$\mathcal{W}_{2,t}(\Omega_t) = \{\mathbf{v} : \Omega_t \to \mathbb{R} \mid \mathbf{v}_t = \widehat{\mathbf{v}} \circ \widehat{\mathcal{A}}_t^{-1},\ \widehat{\mathbf{v}} \in \widehat{\mathcal{W}}_2(\widehat{\Omega})\} \text{ with } \widehat{\mathcal{W}}_2(\widehat{\Omega}) = H^1(\Omega_t). \tag{3.42}$$

Using a first order Euler scheme in time and performing an internal approximation which are not detailed here, the algebraic formulation used in Telemac-3D is:

$$C_{u,1}^{n+1} W^{c,n+1} = \frac{1}{\Delta t}(M_u^{n+1} - M_u^n) - C_{u,2}^{n+1}\, \tilde{U}_{hor}^{n+1}, \tag{3.43}$$

where $W^{c,n+1}$ is the unknown vector containing the discrete values of $w_h^{c,n+1}$ and $C_{u,1}^{n+1}$ and $C_{u,2}^{n+1}$ are the three-dimensional matrices defined on Ω_h^{n+1} such that:

$$C_{u,1}^{n+1} = \int_{\Omega_h^{n+1}} \varphi_i^{n+1} \cdot \frac{\partial \varphi_i^{n+1}}{\partial z}\, d\boldsymbol{x}, \tag{3.44}$$

$$C_{u,2}^{n+1} = \int_{\Omega_h^{n+1}} \varphi_i^{n+1} \cdot \nabla_{hor}\varphi_i^{n+1}\, d\boldsymbol{x}. \tag{3.45}$$

3.5 Limits and possible improvements

In this Section, we discuss about the limitations of the numerical strategy performed in Telemac-3D. Afterwards, we provide clues for possible improvements regarding to the existing hypotheses of the algorithm.

3.5.1 θ-scheme

In Telemac-3D, a θ-scheme in time is available with the aim of increasing the order in time. In this software, the θ implicitation is only applied on the free surface gradient term in the momentum equation (2.128) and on the horizontal velocity term in the depth-averaged free surface equation (2.131). By analogy with the Subsection 3.4.1, we briefly give the algebraic formulations induced with θ-scheme in time for the hydrostatic equations.

Coupled numerical approach:
In the case where a coupled numerical strategy is adopted to solve the hydrostatic predictor step, the algebraic formulation of the wave equation on the free surface equation is, for $n = 0, \cdots, N_T - 1$:

$$\begin{aligned} A_{1,\eta,\theta}\, E^{n+1} =& A_{2,\eta,\theta}\, E^n + \Delta t\, \tilde{D}^T \left[\theta_u (A_u^n)^{-1}\, C_u^n \tilde{U}_{hor}^{n+\frac{1}{2}} + (1-\theta_u)\, U_{hor}^n\right] \\ &+ \theta_u\, \Delta t^2\, (\tilde{D})(A_u^n)^{-1} F_{xy}^n, \end{aligned} \tag{3.46}$$

where the implicitation parameters on the free surface and the velocity are respectively denoted by θ_η and θ_u. The two-dimensional matrix $A_{1,\eta,\theta}$ and $A_{2,\eta,\theta}$ are respectively:

$$A_{1,\eta,\theta} = M_\eta + g\, \theta_u\, \theta_\eta\, \Delta t^2 (\tilde{D}^n)\, ((A_{1,u}^n)^{-1}\, M_u^n)\, \tilde{D}^n, \tag{3.47}$$

$$A_{2,\eta,\theta} = M_\eta - g\, (1-\theta_\eta)\, \theta_u\, \Delta t^2\, (\tilde{D}^n)(A_u^n)^{-1} \tilde{D}^n. \tag{3.48}$$

As previously mentioned in Subsection (2.128), we observe the presence of the additional matrix M_u^n in (3.47). The velocity is then corrected through, for $n = 0, \cdots, N_T - 1$:

$$A_{1,u}^n\, \tilde{U}_{hor}^{n+1} = A_{2,u}^n\, \tilde{U}_{hor}^{n+\frac{1}{2}} + \Delta t\, \tilde{D}^n\, (\theta_\eta\, E^{n+1} + (1-\theta_\eta)\, E^n) + \Delta t\, F_{xy}^n. \tag{3.49}$$

Decoupled numerical approach:
In the case where a decoupled numerical strategy is adopted to solve the hydrostatic predictor step, the algebraic formulation of the wave equation on the free surface equation is, for $n = 0, \cdots, N_T - 1$:

$$\begin{aligned} (M_\eta + g\, h^n\, \theta_\eta\, \theta_u\, \Delta t^2\, R_\eta)\, E^{n+1} =& (M_\eta - g\, h^n\, (1-\theta_\eta)\, \theta_u\, \Delta^2\, R_\eta)\, E^n \\ &+ \Delta t\, (\tilde{D}^n)\, (\theta_u\, \tilde{U}_{hor}^{n+\frac{1}{2}} + (1-\theta_u)\, U_{hor}^n), \end{aligned} \tag{3.50}$$

The velocity is then corrected through, for $n = 0, \cdots, N_T - 1$:

$$M_u^n\, \tilde{U}_{hor}^{n+1} = M_u^n\, \tilde{U}_{hor}^{n+\frac{1}{2}} + \Delta t\, \tilde{D}^n\, (\theta_\eta\, E^{n+1} + (1-\theta_\eta)\, E^n). \tag{3.51}$$

Casulli and Cheng [30] analyzed the stability of a semi-implicit Finite Difference method applied on the three-dimensional hydrostatic problem. The authors point out that the time-scheme is stable for $\frac{1}{2} \leq \theta \leq 1$. The highest accuracy and efficiency is achieved for $\theta = \frac{1}{2}$, leading to a second order in time scheme. Vitousek and Fringer [134] extended this analysis to the free surface Navier–Stokes equations with pressure decomposition providing the same conclusion.

The θ-scheme allows to increase the order in time when it comes to solve the hydrostatic equations in Telemac-3D. Thus, this numerical strategy implies to improve only the accuracy of the free surface elevation. It should be convenient to improve the projection method by an incremental or rotational projection methods (see Subection 2.5.2) in order to increase the overall accuracy (on the velocity and on the pressure). However, the pair of Lagrangian Finite Elements space for the velocity and the pressure has to be inf-sup stable in order to ensure the stability of schemes. Stabilization techniques [85] can also be used in order to avoid the inf-sup condition (described briefly in Subsection 3.5.5).

3.5.2 Kinematic condition at the free surface

The fulfillment of the kinematic condition at the free surface (2.61) is important when it comes to simulate non-linear water waves (see 2.3.7). Indeed, it is a requirement to ensure that $\mathbf{c}\cdot\mathbf{n} = \mathbf{u}\cdot\mathbf{n}$ (at the discrete level) and to preserve the global mass conservation of scalar quantities. Consequently, it allows to ensure that the free divergence velocity is compatible with the momentum equations and the free surface boundary condition. In Telemac-3D, the mass conservation of the water quantity is preserved since the free surface elevation is computed through the depth-averaged free surface equation (2.119). However, the kinematic condition at the free surface is not fulfilled.

A perspective of improvement could be to update the free surface through the kinematic equation (2.61) at the end of the Telemac-3D algorithm. Nevertheless, we recall that this equation is an advection equation with source term. Therefore, the numerical scheme must be chosen carefully in order to ensure the mass conservation and positivity of the water quantity, see Subsection 2.3.7. In the next Chapter 4, we study a numerical scheme for the kinematic equation allowing to ensure the mass conservation of the water quantity. The scheme could be used in Telemac-3D. Otherwise, Pavan [111] developed MURD schemes in Telemac-2D, a Finite Elements software solving the shallow water equations [76]. The libraries of this method could be adopted directly in Telemac-3D.

3.5.3 Discrete free divergence

As seen in Subsection 3.4.3, a continuity equation is solved additionally in order to compute a discrete free divergence velocity $\mathbf{u}_h^{c,n+1}$ since the discrete velocity $\mathbf{u}_h^{n+1}$ is not divergence-free. However, the conservative velocity $\mathbf{u}^c$ is no longer compatible with the momentum equations and the boundary conditions.

Several numerical strategies can be considered in order to compute a free divergence final velocity field at the discrete level, consistent with the momentum equations and boundary conditions. First, the Darcy equations (2.146-2.147) can be solved directly. Nonetheless, this numerical strategy requires that the pair of Finite Elements spaces of the velocity and the pressure is inf-sup stable or to use stabilization techniques [85] avoiding the inf-sup condition (described briefly in Subsection 3.5.5). Otherwise, particular Finite Elements functions which allow to ensure the free divergence can be used, such as the Raviart-Thomas Finite Elements function [53].

3.5.4 Time-discretization of the diffusion term

We discuss now the time discretization of the diffusion terms in the momentum Navier–Stokes equations. Originally proposed by Casulli and Cheng [30] in a Finite Difference scheme for the hydrostatic equations, the authors showed that the explicit treatment of the horizontal diffusion term induced a parabolic CFL condition which reads:

$$\Delta t \leq \frac{1}{\nu} \min\left((\Delta x)^2, (\Delta y)^2\right), \tag{3.52}$$

where Δx and Δy are the space step in the horizontal directions x and y, respectively.

In the Finite Elements framework, an advantage of this writing concerns the structure of the rigidity matrix $R_u^{z,n}$. As we can see in Subsection 3.4.1, $R_u^{z,n}$ expresses only the interaction between the vertical nodes and it rewrites as a tridiagonal matrix in Telemac-3D. Consequently, the matrix $A_{1,u}^n$ given in (3.26) presents the same structure since the mass matrix is mass lumped. This is a benefit in terms of implementation and in computational time since the inverse of the matrix is easier to compute. An easy way to circumvent the time restriction (3.52) is to fully implicit the diffusion term. However, a more complex matrix $R_u^{hor,n}$ should be taken into account in the definition of A_u^n, increasing the computational time.

3.5.5 On the inf-sup condition

The pair of Finite Elements spaces $\mathbb{PR}_1 \times \mathbb{PR}_1$ for the velocity and the pressure is not inf-sup stable. Indeed, it is easier to see the prismatic elements as square in a 2D vertical domain (x, z). The Finite Elements spaces correspond then to $\mathbb{Q}_1 \times \mathbb{Q}_1$ and it is known that this pair of Finite Elements is not inf-sup stable, see Ern and Guermond [53].

As mentioned in Section 3.4.2, the non-hydrostatic predictor step is based on a pressure Poisson equation, in Telemac-3D. Furthermore, we recall that the pair of Finite Elements spaces $\mathbb{PR}_1 \times \mathbb{PR}_1$ used in this software is not inf-sup stable. As a consequence and by analogy with the study of Guermond and Quartapelle [74] discussed in Subsection 2.5.3, inverse CFL condition is induced in Telemac-3D such that:

$$\frac{1}{\|\mathbf{u}_{ref}\|} \max(\Delta x^2, \Delta y^2, \Delta z^2) \leq \Delta t, \tag{3.53}$$

where Δx, Δy (resp Δz) are the reference mesh sizes in the horizontal directions (resp. in the vertical direction) and $\mathbf{u}_{ref}$ a reference velocity (typically the celerity of water waves). A similar condition could exist also for the hydrostatic problem $(\boldsymbol{u}^{hor}, \eta)$ based on a wave equation on the free surface. This condition can be circumvent by adopting a pair of Finite Elements space inf-sup stable. It could be possible that the stabilization techniques avoiding the inf-sup condition (described briefly below) can avoid this difficulty. This is an open question.

According to the time step restrictions (3.52) and (3.53), the main restriction on the time step in Telemac-3D is:

$$\frac{1}{\|\mathbf{u}_{ref}\|}\max(\Delta x^2, \Delta y^2, \Delta z^2) \leq \Delta t \leq \frac{1}{\nu}\min(\Delta x^2, \Delta y^2). \tag{3.54}$$

In the previous Subsection, we mentioned many times the change of the pair of Finite Element spaces on the velocity and the pressure in Telemac-3D in order to adopt inf-sup stable pair of Finite Elements. However, this change cannot be in agreement with the construction of the three-dimensional matrices in Telemac-3D. Indeed, most of three-dimensional matrices are built using the variable decomposition (3.22) such as (3.32). The chosen three-dimensional Finite Elements basis functions should be then chosen carefully in order to hold (3.22).
An alternative to circumvent the inf-sup condition consists in using stabilization techniques [85]. Indeed, some stabilization techniques allow to solve saddle-point problems without a pair of Finite Elements spaces inf-sup stable. In particular, the Pressure Stabilized Petrov-Galerkin (PSPG) method, see Hugues et al. [80]. This method seems to be the easiest method to implement in order to improve Telemac-3D. Indeed, this technique enables to keep the pair Lagrange Finite Elements $\mathbb{PR}_1 \times \mathbb{PR}_1$, ensuring the correct construction of the three-dimensional matrices.

3.6 Conclusion

In this chapter, we investigated the numerical strategies performed in the Telemac-3D algorithm, that is an industrial software dedicated to solve large scale 3D flows by using the Finite Elements method.
We pointed out the limitations of the algorithm and we provided clues for possible improvements regarding the simulation of non-linear waves. The coupled approach adopted in Telemac-3D to solve the hydrostatic predictor step cannot be linked to a discrete variational formulation. A perspective is to investigate numerically the reason of the additional presence of the mass matrix in this formulation. We exhibit also a restriction on the time step (3.54) and that the final velocity field is not divergence-free at the discrete level. As a consequence, a computed conservative velocity is additionally computed but it is no longer compatible with the momentum equations and boundary conditions. This is an important drawback when it comes to simulating non-linear waves. This drawback could be circumvented by adopting a coupled strategy for the non-hydrostatic corrector step,

i.e. to solve directly the Darcy equations. Indeed, in this way, a free divergence velocity field at the discrete level can be computed and the restriction on the time step can be relieved. However, this numerical approach involves that the Finite Elements space satisfies the inf-sup condition. In order to avoid this latter, a stabilization technique can be used such as the PSPG method [80]. This method would be easy to implement in Telemac-3D without implying to change fundamentally the structure of the code. Since the free surface elevation is computed through the depth-averaged free surface equation, the kinematic condition at the free surface is not fulfilled. It is a requirement to ensure that $\mathbf{c} \cdot \mathbf{n} = \mathbf{u} \cdot \mathbf{n}$ (at the discrete level) and to preserve the global mass conservation of scalar quantities. An idea is to compute a new free surface from the kinematic free surface condition at the end of the algorithm. The numerical scheme could be chosen carefully in order to preserve the global mass conservation of the water quantity. In the next Chapter, we analyse a numerical scheme for the kinematic equation at the free surface that allows to preserve this property.

3.7 Appendix

3.7.1 Mass lumping approximation

In this section, we present the notion of mass lumping. Currently, in Telemac-3D, all the mass matrices applied to the velocity are mass lumped. Furthermore, an option is available to lump the mass matrix on the free surface in (3.30) or (2.216). The mass lumping technique is widely used in the Finite Elements community. It consists in replacing the consistent mass matrix by a diagonal matrix usually referred to as the lumped mass matrix. This process makes it possible to avoid invoking costly linear algebra solvers to invert the consistent mass matrix at each time step. A simple way to obtain the lumped matrix consists in replacing each line of the consistent mass matrix by their sum, such that $\overline{a}_{jj} = \sum_{i=1}^{N} a_{j\,i}$. This procedure may also be interpreted as being the application of a quadrature formula on the consistent mass matrix, instead of an exact integration [35]. About the overall accuracy of the Galerkin method, it is known, for instance, that using quadrature formulae that are exact for $\mathbb{P}_{2k-2}$ polynomials is sufficient to preserve the overall accuracy of the Galerkin method [73]. Nonetheless, it is well-known that lumping the mass matrix induces dispersion errors that have negative effects when solving transport-like equations [73].

Chapter 4

An alternative Finite Elements method for the free surface Navier–Stokes equations

Contents

This Chapter is the result of a collaboration with Emmanuel Audusse, Gabriel Barranechea and Astrid Decoene.

4.1 Introduction

4.1.1 Presentation of the problem

We consider an homogeneous (of constant density ρ) and Newtonian fluid under the influence of the gravity $\mathbf{g} = -g\,\mathbf{e}_z$ and bounded from below by a topography $b(x,y)$ and from above by a free surface $\eta(x,y,t)$. We neglect the surface tension and the atmospheric pressure is assumed to be constant. The flow is supposed to be incompressible. We assume that the bottom and the free surface are single-valued functions. Moreover, we suppose that the bottom is polyhedral. The three-dimensional variable is $\boldsymbol{x} = (x,y,z) \in \mathbb{R}^3$ such that $(x,y) \in \mathbb{R}^2$ is the field of horizontal coordinates and $z \in \mathbb{R}$ is the vertical variable. The water depth at rest is denoted by $h(x,y,t) = \eta(x,y,t) - b(x,y)$. For any time $t \in [0,T]$ with $T \in \mathbb{R}_*^+$ a constant final time, we assume that the fluid domain Ω_t moves only in the vertical direction. The three-dimensional moving bounded domain Ω_t is:

$$\Omega_t = \{(x,y,z) \mid (x,y) \in \omega \ \text{ and } b(x,y) < z < \eta(x,y,t)\}, \tag{4.1}$$

where ω is a bounded and horizontal and polygonal domain, see Figure 2.1. The domain Ω_t is bounded by the free surface boundary $\Gamma_{s,t}$ and by the solid boundaries Γ_b and $\Gamma_{l,t}$, which denote the bottom and vertical lateral boundaries, respectively. The boundary of Ω_t (resp ω) is denoted by $\partial\Omega_t = \Gamma_{s,t} \cup \Gamma_{l,t} \cup \Gamma_b$ (resp. $\partial\omega$). We denote by $\mathbf{n}$ the outward normal vector on $\partial\Omega_t$ and more particularly, $\mathbf{n}_{s,t}$ the outward normal vector on $\Gamma_{s,t}$.

The velocity field of the fluid is represented by $\mathbf{u} = \mathbf{u}(\boldsymbol{x},t)$ and its pressure is denoted $p = p(\boldsymbol{x},t)$. The horizontal velocity of $\mathbf{u}$ is denoted by $\boldsymbol{u}^{hor} = (u,v)$ and the vertical velocity is w. At the free surface $\Gamma_{s,t}$, these velocities are respectively denoted by $\boldsymbol{u}^{hor}_{|z=\eta}$ and $w_{|z=\eta}$. The movement of the fluid domain is taken into account in the model by considering the classical ALE-Sigma transformation, see Subsection 3.2.2. The velocity of the domain $\mathbf{c}$ is then defined as follows:

$$\mathbf{c} = \left(0, 0, \frac{\partial\eta}{\partial t}\frac{z-b}{h}\right). \tag{4.2}$$

The free surface Navier–Stokes equations in the ALE framework studied in this Chapter are:

$$\begin{cases} \left.\dfrac{\partial \mathbf{u}}{\partial t}\right|_{\widehat{\Omega}} + \big((\mathbf{u}-\mathbf{c})\cdot\nabla\big)\mathbf{u} - \nu\,\Delta\mathbf{u} + \dfrac{1}{\rho}\,\nabla p = \mathbf{g}, & \text{on } \Omega_t\times]0,T[, \quad (4.3) \\ \nabla\cdot\mathbf{u} = 0, & \text{on } \Omega_t\times]0,T[, \quad (4.4) \\ \dfrac{\partial\eta}{\partial t} + \boldsymbol{u}^{hor}_{|z=\eta}\cdot\nabla_{hor}\,\eta = w_{|z=\eta}, & \text{on } \omega\times]0,T[, \quad (4.5) \end{cases}$$

with the boundary conditions:

$$\begin{cases} (\mu\,\nabla\mathbf{u} - p\,\mathbf{I})\cdot\mathbf{n}_{s,t} = 0, & \text{on } \Gamma_{s,t}, \quad (4.6)\\ \mathbf{u}\cdot\mathbf{n} = 0, & \text{on } \Gamma_b \cup \Gamma_{l,t}, \quad (4.7)\\ \mu(\nabla\mathbf{u}\cdot\mathbf{n})\cdot\mathbf{t} = 0, & \text{on } \Gamma_b \cup \Gamma_{l,t}, \quad (4.8) \end{cases}$$

where ν is the constant kinematic viscosity and $\mu = \rho\,\nu$ is the dynamic viscosity. Notice that in this case we choose $p_{atm} = 0$. We recall that (4.6) and (4.8) are the dynamic conditions at the free surface and solid boundaries, respectively. The relation (4.7) is the kinematic condition at the solid boundaries.

The free surface Navier–Stokes equations can be solved in the Finite Elements framework by considering: at first the free surface equation and then the Navier–Stokes equations in the ALE framework. As introduced in Chapter 2, the mass conservation of the water quantity is an important property which should be satisfied. Maury [100] proposed a characteristics ALE method for the free surface Navier–Stokes equations in the Finite Elements framework. This work has been extended by Decoene and Maury [46] using a classical ALE-Sigma transformation. The characteristics method presents the advantage to not require a Courant-Friedrichs–Lewy (CFL) condition for the stability leading to an unconditionally stable scheme. Nevertheless, the method proposed in [100] does not ensure the global mass conservation of the water quantity, which can affect negatively the stability of the numerical scheme on the Navier–Stokes equations. In addition, Maury [100] shown that the characteristics ALE method for the free surface Navier–Stokes equations is stable independently of the mesh velocity if the discrete fluid velocity is exactly divergence-free.
On the one hand, we study a first-order in time Euler scheme for the free surface equation (4.5) in view of satisfying the mass conservation property. The free surface equation corresponds to an advection equation with source terms. It is known that an explicit scheme in time combined to a centered strategy in space is unconditionally unstable, see [115]. In the Finite Element framework, stabilization techniques have been developed to circumvent this problem. Popular stabilization methods are Galerkin least-square [81], local projection [18, 119], interior penalty of gradient jumps (CIP) [22, 26], subgrid viscosity [70, 72], orthogonal subscale stabilization [41, 42], SUPG [21, 23, 86]. As a consequence, we study a first order forward Euler scheme in time with a Finite Element symmetric stabilization term in space [25] for the free surface equation. This scheme is conditionally stable and enables to preserve the global mass conservation of the water quantity at the discrete level.
On the other hand, we study an alternative Finite Elements ALE formulation of the Navier–Stokes equations, in view of obtaining a stability result in which the fluid velocity field has not to be exactly divergence-free. Many authors studied the stability of ALE time-dependent problems, such as Boffi and Gastaldi [13], Formaggia and Nobile [57, 58], Ganessan et al. [61] and Bonito et al. [15]. The authors shown that the time advancing scheme may be affected by the mesh velocity, which is usually difficult to control. In

particular, the stability results do not depend on the mesh velocity with a first order backward or forward Euler scheme. Nevertheless, the stability results can depend on the mesh velocity with a second order scheme in time. As a consequence, we discretize in time the Finite Elements ALE formulation of the Navier–Stokes equations by a first order scheme [61] and we prove the unconditionally stability which is independent of the mesh velocity. The stability results presented involve hypothesis of the regularity that we do not demonstrate. We consider that the free surface is Lipschitz continuous and that the velocity field belongs to $W^{1,\infty}(]0,T[;\Omega_t)$ (Girault et al. [64]). According to us, these results have not been demonstrated for the free surface Navier–Stokes equations.

This Chapter is organized as follows: in Sections 4.2, 4.3 and 4.4, we study the variational formulation of the equations from the continuous level to the fully discrete level. The energy and stability estimates are studied in each Section as well as the property of the mass conservation of the water. The regularity assumption used in energy and stability results are introduced in 4.2. In Section 4.5, we perform numerical comparisons with other numerical strategies.

4.1.2 Preliminaries and notations

For more convenience, we recall the notations previously introduced. Throughout this Chapter, for a general domain Ω, $W^{s,p}(\Omega)$ denotes the Sobolev space of real-valued functions defined on the domain Ω with distributional derivatives of order up to $s \in \mathbb{N}$ are in $L^p(\Omega)$. The associated norm is $\|\cdot\|_{W^{s,p}(\Omega)}$ and the seminorm is $|\cdot|_{W^{s,p}(\Omega)}$. In the case where $s = 0$, we obtain the Lebesgue space $W^{0,p}(\Omega) = L^p(\Omega)$. The case $p = 2$ will be distinguished by using the Hilbert space $W^{s,2}(\Omega) = H^s(\Omega)$. For simplicity, we denote respectively by $\|\cdot\|_{s,\Omega}$ and $|\cdot|_{s,\Omega}$ the norm and the seminorm in $H^s(\Omega)$. In the case, $s = 0, p = 2$, the inner product of $L^2(\Omega)$ is denoted by $(\cdot,\cdot)_\Omega$ and the corresponding norm by $\|\cdot\|_{0,\Omega}$. The norm of the space of essentially bounded functions $L^\infty(\Omega)$ is denoted by $\|\cdot\|_{\infty,\Omega}$. For the sake of simplicity, for a moving domain Ω_t, we use the following notation: $(\cdot,\cdot)_t = (\cdot,\cdot)_{\Omega_t}$ and the corresponding norm is: $\|\cdot\|_{0,t} = \|\cdot\|_{0,\Omega_t}$. The norm of the space of essentially bounded functions $L^\infty(\Omega_t)$ is denoted by $\|\cdot\|_{\infty,t}$.

We denote by ∇ the three-dimensional gradient operator and by ∇_{hor} the two-dimensional gradient operator such that for all $f : \mathbb{R}^3 \to \mathbb{R}$ and for all $g : \mathbb{R}^2 \to \mathbb{R}$:

$$\nabla f = \left(\frac{\partial f}{\partial x}, \frac{\partial f}{\partial y}, \frac{\partial f}{\partial z}\right), \qquad \nabla_{hor}\, g = \left(\frac{\partial g}{\partial x}, \frac{\partial g}{\partial y}\right). \tag{4.9}$$

Furthermore, we denote the three-dimensional divergence operator by $\nabla\cdot$ and the two-dimensional divergence operator by $\nabla_{hor}\cdot$ such that for all $\mathbf{f} = (f_1, f_2, f_3) : \mathbb{R}^3 \to \mathbb{R}^3$ and for all $\mathbf{g} = (g_1, g_2) : \mathbb{R}^2 \to \mathbb{R}^2$:

$$\nabla \cdot \mathbf{f} = \frac{\partial f_1}{\partial x} + \frac{\partial f_2}{\partial y} + \frac{\partial f_3}{\partial z}, \qquad \nabla_{hor} \cdot \mathbf{g} = \frac{\partial g_1}{\partial x} + \frac{\partial g_2}{\partial y}. \tag{4.10}$$

Let us recall three classical results used in this Chapter:

Theorem 4.1. *Gauss's theorem*
Let assume $\Omega \in \mathbb{R}^d$ ($d \in \mathbb{N}^*$) which is a compact with a piecewise smooth boundary $\partial\Omega$. If $\mathbf{f}$ is a continuous differentiable vector field defined on a neighborhood of Ω, we have then:

$$\int_\Omega \nabla \cdot \mathbf{f}\, d\boldsymbol{x} = \int_{\partial\Omega} \mathbf{f} \cdot n\, d\boldsymbol{x}. \tag{4.11}$$

Lemma 4.1. *Gronwall's lemma*
Let $\beta \in \mathbb{R}$, $\varphi \in \mathcal{C}^1([0,T];\mathbb{R})$ and $f \in \mathcal{C}^0([0,T];\mathbb{R})$ such that, for all $t \in \mathbb{R}$:

$$\frac{d}{dt}\varphi(t) \leq \beta\, \varphi(t) + f, \tag{4.12}$$

then, for all $t \in [0,T]$:

$$\varphi(t) \leq \exp[\beta\, t]\, \varphi(0) + \int_0^t \exp[\beta(t-\tau)]\, f(\tau)\, d\tau. \tag{4.13}$$

Lemma 4.2. *Discrete Gronwall's lemma*
Let us consider $\lambda \in \mathbb{R}^+$ and two sequences of real $(a^n)_{n\geq 0}$ and $(f^n)_{n\geq 0}$. If we have $\forall n \in \mathbb{N}^*,\ \ a^{n+1} \leq (1+\lambda\Delta t)\, a^n + f^n$, we get then:

$$a^n \leq e^{\lambda\,(t^n - t^0)} a^0 + \sum_{i=0}^{n-1} e^{\lambda\,(t^n - t^{i+1})} f^i. \tag{4.14}$$

4.2 Continuous problem

In this Section, we introduce the continuous variational formulations of the free surface Navier–Stokes equations (4.3-4.5). As introduced in Section 2.2, we consider $\widehat{\Omega}$ the reference polygonal domain and $\mathcal{A}_t$ which at time $t \in]0;T[$ associates a point $x \in \Omega_t$, given in (2.10), to a point $\widehat{x} \in \widehat{\Omega}$. Recall that the ALE mapping is conforming to the motion of the domain at the boundaries such that:

$$\mathbf{c} \cdot \mathbf{n} = \mathbf{u} \cdot \mathbf{n}, \tag{4.15}$$

with $\mathbf{c}$ the domain velocity given by (4.2).

The functional spaces for the velocity and the pressure are respectively $\widehat{\mathcal{V}}(\widehat{\Omega}) = H^1(\widehat{\Omega})$ and $\widehat{\mathcal{Q}}(\widehat{\Omega}) = L^2(\widehat{\Omega})$. They are defined on the reference domain $\widehat{\Omega}$. The ALE mapping identifies corresponding functional spaces defined on the current domain Ω_t such that:

$$\mathcal{V}(\Omega_t) = \{v :]0,T[\times\Omega_t \to \mathbb{R},\ v = \widehat{v} \circ \widehat{\mathcal{A}}_t^{-1},\ \widehat{v} \in \widehat{\mathcal{V}}(\widehat{\Omega})\}, \tag{4.16}$$

$$\mathcal{Q}(\Omega_t) = \{q :]0,T[\times\Omega_t \to \mathbb{R},\ q = \widehat{q} \circ \widehat{\mathcal{A}}_t^{-1},\ \widehat{q} \in \widehat{\mathcal{Q}}(\widehat{\Omega})\}. \tag{4.17}$$

We recall that the reference test function $\widehat{\mathbf{v}} \in \widehat{\mathcal{V}}$ does not depend on time, i.e. $\partial_t \widehat{\mathbf{v}} = 0$, see Subsection 2.2.3. In addition, we define:

$$\mathcal{V}_0(\Omega_t) = \{\mathbf{v} \in \big(\mathcal{V}(\Omega_t)\big)^3 \;\mid\; \mathbf{v}\cdot\mathbf{n} = 0 \text{ on } \Gamma_b \cup \Gamma_{l,t}\}. \tag{4.18}$$

The functional spaces for the time-dependent velocity and pressure are denoted $\mathcal{V}(\Omega_t, t)$ and $\mathcal{Q}(\Omega_t, t)$. They are defined on the current domain Ω_t and identified by the ALE mapping such that:

$$\mathcal{V}(\Omega_t, t) = \{v :]0,T[\times\Omega_t \to \mathbb{R},\ v(\boldsymbol{x},t) = \widehat{v}\circ\widehat{\mathcal{A}}_t^{-1}(\boldsymbol{x}),\ \widehat{v}(\cdot,t) \in \widehat{\mathcal{V}}(\widehat{\Omega})\}, \tag{4.19}$$

$$\mathcal{Q}(\Omega_t, t) = \{q :]0,T[\times\Omega_t \to \mathbb{R},\ q(\boldsymbol{x},t) = \widehat{q}\circ\widehat{\mathcal{A}}_t^{-1}(\boldsymbol{x}),\ \widehat{q}(\cdot,t) \in \widehat{\mathcal{Q}}(\widehat{\Omega})\}. \tag{4.20}$$

In addition, we define:

$$\mathcal{V}_0(\Omega_t, t) = \{\mathbf{v} \in \big(\mathcal{V}(\Omega_t, t)\big)^3 \;\mid\; \mathbf{v}\cdot\mathbf{n} = 0 \text{ on } \Gamma_b \cup \Gamma_{l,t}\}. \tag{4.21}$$

The functional space for the free surface is defined on ω and is denoted by $\mathcal{N}(\omega)$ such that:

$$\mathcal{N}(\omega) = L^\infty(]0,T[, L^2(\omega)) \cap L^2(]0,T[, H^1(\omega)). \tag{4.22}$$

A variational formulation of the free surface Navier–Stokes equations (4.3-4.5) is:

$$\begin{cases} \text{Find } (\mathbf{u}, p) \in \mathcal{V}_0(\Omega_t, t) \times \mathcal{Q}(\Omega_t, t) \text{ and } \eta \in \mathcal{N}(\omega) \\ \text{such that for all} (\mathbf{v}, q) \in \mathcal{V}_0(\Omega_t) \times \mathcal{Q}(\Omega_t),\ \psi \in \mathcal{N}(\omega) \text{ and for any } t \in]0,T[\\ \displaystyle\int_{\widehat{\Omega}} \left.\frac{\partial \mathbf{u}}{\partial t}\right|_{\widehat{\Omega}} \cdot \mathbf{v} + c(\mathbf{u}-\mathbf{c}, \mathbf{u}, \mathbf{v}) + a(\mathbf{u}, \mathbf{v}) - \frac{1}{\rho} b(\mathbf{v}, p) = (\mathbf{g}, \mathbf{v})_t, & (4.23) \\ \qquad\qquad - b(\mathbf{u}, q) = 0, & (4.24) \\ \displaystyle\Big(\frac{\partial \eta}{\partial t}, \psi\Big)_\omega + (\boldsymbol{u}^{hor}_{|_{z=\eta}} \cdot \nabla\eta, \psi)_\omega = (w_{|_{z=\eta}}, \psi)_\omega, \end{cases}$$

with the following bilinear forms

$$c(\mathbf{u}-\mathbf{c}, \mathbf{u}, \mathbf{v}) = \Big(\big((\mathbf{u}-\mathbf{c})\cdot\nabla\big)\mathbf{u}, \mathbf{v}\Big)_t, \tag{4.25}$$

$$a(\mathbf{u}, \mathbf{v}) = \nu\,(\nabla\mathbf{u}, \nabla\mathbf{v})_t, \tag{4.26}$$

$$b(\mathbf{v}, p) = (\nabla\cdot\mathbf{v}, p)_t. \tag{4.27}$$

Thanks to the theorem of Sobolev injection [2], the functional space $\mathcal{N}(\omega)$ ensures that the inner product $(\boldsymbol{u}^{hor}_{|_{z=\eta}} \cdot \nabla\eta, \psi)_\omega$ is well-posed since $\nabla\eta \in L^2(\omega)$, $\psi \in H^1(\omega)$ and $\boldsymbol{u}^{hor}_{|_{z=\eta}} \in \mathcal{N}_u$ where $\mathcal{N}_u = \{t \in]0,T[,\ \boldsymbol{u}^{hor}_{|_{z=\eta}} \in H^{\frac{1}{2}}(\omega)\}$.

In stability analysis, the convective term c reveals a term that complicates the study. In [100], Maury needs to consider a velocity field which is exactly divergence-free to obtain a stability result. In order to circumvent this difficulty, we aim at replacing the convective term $c(\cdot,\cdot,\cdot)$ by a skew-symmetric term $\overline{c}(\cdot,\cdot,\cdot)$ such that:

$$\overline{c}(\mathbf{u}-\mathbf{c},\mathbf{u},\mathbf{v}) = \frac{1}{2}\Big[\Big(\big((\mathbf{u}-\mathbf{c})\cdot\nabla\big)\mathbf{u},\mathbf{v}\Big)_t - \Big(\big((\mathbf{u}-\mathbf{c})\cdot\nabla\big)\mathbf{v},\mathbf{u}\Big)_t\Big]. \tag{4.28}$$

Then, we have $\overline{c}(\mathbf{u}-\mathbf{c},\mathbf{u},\mathbf{v}) = -\overline{c}(\mathbf{u}-\mathbf{c},\mathbf{v},\mathbf{u})$ that enables to make to zero the convective term in stability analysis. As a consequence, we consider the following alternative variational formulation for the Navier–Stokes equations.

Proposition 4.1. *Let* $\mathbf{u}$ *be a solution of (4.23-4.24). An equivalent variational formulation including the skew-symmetric term is:*

$$\begin{cases} \textit{Find } (\mathbf{u},p,\eta)\in\mathcal{V}_0(\Omega_t)\times\mathcal{Q}(\Omega_t)\times\mathcal{N}(\omega) \\ \textit{such that for all}(\mathbf{v},q,\psi)\in\mathcal{V}_0(\Omega_t)\times\mathcal{Q}(\Omega_t)\times\mathcal{N}(\omega) \\ \dfrac{d}{dt}(\mathbf{u},\mathbf{v})_t + \overline{c}(\mathbf{u}-\mathbf{c},\mathbf{u},\mathbf{v}) - \dfrac{1}{2}(\mathbf{u}\nabla\cdot\mathbf{c},\mathbf{v})_t + a(\mathbf{u},\mathbf{v}) - \dfrac{1}{\rho}\,b(\mathbf{v},p) = (\mathbf{g},\mathbf{v})_t, & (4.29) \\ \qquad\qquad - b(\mathbf{u},q) = 0, & (4.30) \\ \Big(\dfrac{\partial\eta}{\partial t},\psi\Big)_\omega + (\boldsymbol{u}^{hor}_{|_{z=\eta}}\cdot\nabla\eta,\psi)_\omega = (w_{|_{z=\eta}},\psi)_\omega, & (4.31) \end{cases}$$

Proof. Let us consider (4.23-4.24). By using the Reynolds transport theorem and the no dependency on time of the reference test function $\widehat{\mathbf{v}}$, the time-derivative term can be rewritten as follows:

$$\frac{d}{dt}\int_{\Omega_t}\mathbf{u}\cdot\mathbf{v} = \int_{\widehat{\Omega}}\left.\frac{\partial\mathbf{u}}{\partial t}\right|_{\widehat{\Omega}}\cdot\mathbf{v} + \int_{\Omega_t}(\mathbf{u}\cdot\mathbf{v})\,\nabla\cdot\mathbf{c}. \tag{4.32}$$

We replace the ALE-time derivative term in (4.23) by (4.32), yielding:

$$\frac{d}{dt}(\mathbf{u},\mathbf{v})_t + c(\mathbf{u}-\mathbf{c},\mathbf{u},\mathbf{v}) - (\mathbf{u}\nabla\cdot\mathbf{c},\mathbf{v})_t + a(\mathbf{u},\mathbf{v}) - \frac{1}{\rho}\,b(\mathbf{v},p) = (\mathbf{g},\mathbf{v})_t. \tag{4.33}$$

The convective term $c(\cdot,\cdot,\cdot)$ can be rewritten as follows:

$$c(\mathbf{u}-\mathbf{c},\mathbf{u},\mathbf{v}) = \frac{1}{2}\Big[\Big(\big((\mathbf{u}-\mathbf{c})\cdot\nabla\big)\mathbf{u},\mathbf{v}\Big)_t + \Big(\big((\mathbf{u}-\mathbf{c})\cdot\nabla\big)\mathbf{u},\mathbf{v}\Big)_t\Big]. \tag{4.34}$$

An integration by parts on the second term leads to:

$$c(\mathbf{u}-\mathbf{c},\mathbf{u},\mathbf{v}) = \overline{c}(\mathbf{u}-\mathbf{c},\mathbf{u},\mathbf{v}) + \frac{1}{2}\big((\mathbf{u}-\mathbf{c})\cdot\mathbf{n},\mathbf{u}\cdot\mathbf{v}\big)_{\partial\Omega_t} - \frac{1}{2}\Big(\mathbf{u}\,\nabla\cdot(\mathbf{u}-\mathbf{c}),\mathbf{v}\Big)_t. \tag{4.35}$$

Using the relation (4.15) and the free divergence of the velocity (4.24), the convective term finally reads:

$$c(\mathbf{u}-\mathbf{c},\mathbf{u},\mathbf{v}) = \overline{c}(\mathbf{u}-\mathbf{c},\mathbf{u},\mathbf{v}) + \frac{1}{2}\Big(\mathbf{u}\,\nabla\cdot\mathbf{c},\mathbf{v}\Big)_t. \tag{4.36}$$

Replace (4.36) in (4.33) yields the variational formulation of the momentum equation (4.29). That concludes the proof. ■

At the continuous level, Girault et al. [64] derived a sufficient condition for the regularity $\nabla \mathbf{u} \in L^1(]0,T[;L^\infty(\Omega_t))$ for the steady incompressible Navier–Stokes equations. For a fixed domain and Dirichlet boundary conditions, the authors demonstrated that a condition on the source term of the form $\mathbf{f} \in L^{3+\epsilon}(\Omega)$ with $0 < \epsilon \leq 3/2$ is sufficient. In our case, the only source term is the gravity field $\mathbf{g}$ which is constant and this condition is then valid. According to us, no similar result exists for the free surface Navier–Stokes equations. In this Chapter, we consider that $\mathbf{u} \in W^{1,\infty}(]0,T[;\Omega_t)$ and that the free surface elevation η is Lipschitz continuous.

4.3 Semi-discretized (or continuous in time) problem in space

We now introduce the semi-discrete variational formulations in space of (4.29,4.30,4.31). In view of an energy estimate, we use a stabilization term in the formulation of the free surface. Moreover, we study the global mass conservation property of the water quantity and the energy estimates on the free surface and on the velocity, under regularity assumptions.

For this purpose, we consider $\mathcal{T}_h^{2D}$ the quasiuniform triangulation of the horizontal domain ω. The discrete domain is $\omega_h = \omega$. We denote by $\widehat{\mathcal{T}}_h^{3D}$ the triangulation of the reference domain $\widehat{\Omega}$. The current triangulation $\mathcal{T}_{h,t}^{3D}$ of the domain Ω_t is built from $\widehat{\mathcal{T}}_h^{3D}$ through the semi-discrete ALE mapping $\mathcal{A}_{h,t}$ as introduced in Subsection 2.2.4. The semi-discrete in space domain is denoted $\Omega_{h,t}$. Notice that the approximation of the free surface allows to define the semi-discrete in space ALE mapping, and then the domain $\Omega_{h,t}$ that is different from Ω_t, i.e. $\Omega_{h,t} \neq \Omega_t$. The semi-discrete boundary of the domain is denoted $\partial\Omega_{h,t}$ and the semi-discrete free surface boundary is $\Gamma_{h,s,t}$. In the sequel, we denote by $(\mathbf{u}_h, p_h, \eta_h)$ the semi-discrete in space solution. The mesh velocity of the domain $\Omega_{h,t}$ is denoted by $\mathbf{c}_h$.

The functional space for the free surface is $\mathcal{N}_h(\omega) \subset \mathcal{N}(\omega)$. Besides, we consider the discrete functional spaces $\widehat{\mathcal{V}}_h(\widehat{\Omega}) \subset \widehat{\mathcal{V}}(\widehat{\Omega})$ and $\widehat{\mathcal{Q}}_h(\widehat{\Omega}) \subset \widehat{\mathcal{Q}}(\widehat{\Omega})$ defined on the discrete reference domain $\widehat{\Omega}$. The semi-discrete in space ALE mapping identifies the corresponding discrete functional spaces defined on the current domain $\Omega_{h,t}$, of the velocity and the pressure, such that:

$$\mathcal{V}_h(\Omega_{h,t}) = \{v_h :]0,T[\times\Omega_{h,t} \to \mathbb{R},\ v_h = \widehat{v}_h \circ \widehat{\mathcal{A}}_{h,t}^{-1},\ \widehat{v}_h \in \widehat{\mathcal{V}}_h(\widehat{\Omega})\}, \tag{4.37}$$

$$\mathcal{Q}_h(\Omega_{h,t}) = \{q_h :]0,T[\times\Omega_{h,t} \to \mathbb{R},\ q_h = \widehat{q}_h \circ \widehat{\mathcal{A}}_{h,t}^{-1},\ \widehat{q}_h \in \widehat{\mathcal{Q}}_h(\widehat{\Omega})\}. \tag{4.38}$$

In addition, we define:

$$\mathcal{V}_{0,h}(\Omega_{h,t}) = \{\mathbf{v}_h \in \left(\mathcal{V}_h(\Omega_{h,t})\right)^3 \ \mid\ \mathbf{v}_h \cdot \mathbf{n} = 0 \text{ on } \Gamma_b \cup \Gamma_{l,t}\}. \tag{4.39}$$

The discrete functional spaces for the time-dependent velocity and pressure are denoted $\mathcal{V}_h(\Omega_t,t)$ and $\mathcal{Q}_h(\Omega_t,t)$. They are defined on the current domain Ω_t and identified by the ALE mapping such that:

$$\mathcal{V}_h(\Omega_{h,t},t)=\{v_h:]0,T[\times\Omega_{h,t}\to\mathbb{R},\ v_h(\boldsymbol{x},t)=\widehat{v}_h\circ\widehat{\mathcal{A}}_{h,t}^{-1}(\boldsymbol{x}),\ \widehat{v}_h(\cdot,t)\in\widehat{\mathcal{V}}_h(\widehat{\Omega})\},\quad(4.40)$$

$$\mathcal{Q}_h(\Omega_{h,t},t)=\{q_h:]0,T[\times\Omega_{h,t}\to\mathbb{R},\ q_h(\boldsymbol{x},t)=\widehat{q}_h\circ\widehat{\mathcal{A}}_{h,t}^{-1}(\boldsymbol{x}),\ \widehat{q}_h(\cdot,t)\in\widehat{\mathcal{Q}}_h(\widehat{\Omega})\}.\quad(4.41)$$

In addition, we define:

$$\mathcal{V}_{0,h}(\Omega_{h,t},t)=\{\mathbf{v}\in\big(\mathcal{V}_h(\Omega_{h,t},t)\big)^3\ \mid\ \mathbf{v}_h\cdot\mathbf{n}=0\text{ on }\Gamma_b\cup\Gamma_{l,t}\}.\quad(4.42)$$

In view of the Finite Element discretization, we only consider pairs of Finite Elements spaces $(\mathcal{V}_h(\Omega_{h,t})\times\mathcal{Q}_h(\Omega_{h,t}))$ satisfying the discrete inf-sup condition [19]:

$$\inf_{q_h\in\mathcal{Q}_{h,t}(\Omega_{h,t})}\sup_{v_h\in\mathcal{V}_{h,t}(\Omega_{h,t})}\frac{(\nabla\cdot v_h,q_h)}{\|v_h\|_{1,t}\|q_h\|_{0,t}}\geq\beta_0,\quad(4.43)$$

with $\beta_0>0$, a constant independent of the mesh size. This condition ensures that the Navier–Stokes equations are well-posed. In this Chapter, we consider classical Lagrange Finite Elements spaces. For the three-dimensional unknowns, we use $\mathbb{P}_1$-bubble for the velocity and $\mathbb{P}_1$ for the pressure. Notice that these spaces satisfy the discrete inf-sup condition (4.43). For the two-dimensional unknown, we use $\mathbb{P}_1$ elements for the free surface.

The semi-discretized (or continuous in time) variational formulation in space that we consider is:

$$\begin{cases}\text{Find }(\mathbf{u}_h,p_h)\in\mathcal{V}_{0,h}(\Omega_{h,t},t)\times\mathcal{Q}_h(\Omega_{h,t},t)\text{ and }\eta_h\in\mathcal{N}_h(\omega)\text{ such that}\\ \text{for all }(\mathbf{v}_h,q_h)\in\mathcal{V}_{0,h}(\Omega_{h,t})\times\mathcal{Q}_h(\Omega_{h,t}),\ \zeta_h\in\mathcal{N}_h(\omega)\text{ and for any }t\in]0,T[\\ \dfrac{d}{dt}(\mathbf{u}_h,\mathbf{v}_h)_t+\overline{c}_h(\mathbf{u}_h-\mathbf{c}_h,\mathbf{u}_h,\mathbf{v}_h)-\dfrac{1}{2}(\mathbf{u}_h\nabla\cdot\mathbf{c}_h,\mathbf{v}_h)_t\\ \qquad\qquad+a(\mathbf{u}_h,\mathbf{v}_h)-\dfrac{1}{\rho}b(\mathbf{v}_h,p_h)=(\mathbf{g},\mathbf{v}_h)_t,\quad(4.44)\\ \qquad\qquad-b(\mathbf{u}_h,q_h)=0,\quad(4.45)\\ \left(\dfrac{\partial\eta_h}{\partial t},\zeta_h\right)_\omega+\left(\boldsymbol{u}^{hor}_{h|_{z=\eta_h}}\cdot\nabla\eta_h,\zeta_h\right)_\omega+s_h(\eta_h,\zeta_h)=\left(w_{h|_{z=\eta_h}},\zeta_h\right)_\omega,\quad(4.46)\end{cases}$$

where the stabilization bilinear form $s_h(\cdot,\cdot)$ is, for all $(\eta_h,\zeta_h)\in(\mathcal{N}_h(\omega),\mathcal{N}_h(\omega))$:

$$s_h(\eta_h,\zeta_h)=\frac{\mathrm{h}}{\|\boldsymbol{u}^{hor}_{h|_{z=\eta_h}}\|_\infty}(\boldsymbol{u}^{hor}_{h|_{z=\eta_h}}\cdot\nabla\eta_h,\boldsymbol{u}^{hor}_{h|_{z=\eta_h}}\cdot\nabla\zeta_h)_\omega,\quad(4.47)$$

with h is the minimal diameter of an element $K_T^{2D}\in\mathcal{T}_h^{2D}$. The stabilization term s_h is symmetric and non-negative. Therefore, we can define on $\mathcal{N}_h(\omega)$ the semi-norm:

$$|\cdot|_s=s_h(\cdot,\cdot)^{\frac{1}{2}}.\quad(4.48)$$

4.3.1 Mass conservation of the water quantity

Since ρ is assumed constant, the global mass conservation of the water quantity implies that the volume of the time-dependent domain is constant in time. This property allows to obtain an energy estimate of the semi-discretized variational formulation in space (4.44-4.45) independent of the movement of the domain. In this Subsection, we demonstrate that the semi-discrete variational formulation in space on the free surface (4.46) preserves the global mass conservation of the water quantity. For this purpose, we consider $\mathbf{n}_h$ the semi-discrete in space non unit normal vector to $\Omega_{h,t}$. Besides, $\mathbf{n}_{h,t,s}$ is a semi-discrete in space non unit outward vector at the free surface, given by $\mathbf{n}_{h,t,s} = (-\nabla_{hor}\,\eta_h, 1)$.

Proposition 4.2. *Let $\eta_h \in \mathcal{N}_h(\omega)$ be a solution of (4.46). For all $t \in [0,T]$, we have that:*

$$\frac{d}{dt}\int_{\omega}(\eta_h)\,dy\,dx = 0. \tag{4.49}$$

Proof. We consider (4.46) with $\zeta_h \in \mathcal{N}_h$ equal to 1, we obtain:

$$\left(\frac{\partial \eta_h}{\partial t}, 1\right)_{\omega} + \left(\boldsymbol{u}^{hor}_{h|_{z=\eta_h}} \cdot \nabla \eta_h, 1\right)_{\omega} = \left(w_{h|_{z=\eta_h}}, 1\right)_{\omega}. \tag{4.50}$$

We define the change of variable between ω and $\Gamma_{s,t}$ such that:

$$d\Gamma_{h,s,t} = \|\mathbf{n}_{h,s,t}\|\,d\omega = \sqrt{1 + \left(\frac{\partial \eta_h}{\partial x}\right)^2 + \left(\frac{\partial \eta_h}{\partial y}\right)^2}\,d\omega. \tag{4.51}$$

Using the change of variable (4.51), the equation (4.50) can be rewritten as follows:

$$\frac{d}{dt}\int_{\omega}\eta_h - \int_{\Gamma_{h,s,t}} \boldsymbol{u}_{h|_{z=\eta_h}} \cdot \frac{\mathbf{n}_{h,s,t}}{\|\mathbf{n}_{h,s,t}\|} = 0. \tag{4.52}$$

The essential imperviousness condition (4.7) leads to:

$$\frac{d}{dt}\int_{\omega}\eta_h - \int_{\partial\Omega_{h,t}} \mathbf{u}_h \cdot \frac{\mathbf{n}_h}{\|\mathbf{n}_h\|} = 0. \tag{4.53}$$

The Gauss theorem (4.1) yields:

$$\frac{d}{dt}\int_{\omega}\eta_h = -\int_{\Omega_{h,t}} \nabla \cdot \mathbf{u}_h = -b(\mathbf{u}_h, 1) = 0. \tag{4.54}$$

Since $q_h = 1$ is included in $\mathcal{Q}_{h,t}(\Omega_{h,t})$. That concludes the proof. ■

4.3.2 Energy estimate on the free surface

In this Subsection, we introduce the energy estimate of the semi-discrete variational formulation in space (4.46) on the free surface. We do not have an uniform infimum and supremum and we assume that $\mathbf{u}_h \in W^{1,\infty}(]0,T[;\Omega_{h,t})$.

Proposition 4.3. *Let $\eta_h \in \mathcal{N}_h(\omega)$ be a solution of (4.46). For all $t \in [0,T]$, we have the following energy estimate:*

$$\|\eta_h\|^2_{0,\omega} + 2\int_0^t |\eta_h|^2_s \leq \exp\left[\int_0^t (1+\mu_h(s))\,ds\right] \|\eta_h(0)\|^2_{0,\omega} + \int_0^t \exp\left[\int_\tau^t (1+\mu_h(s))\,ds\right] \|w_{h|_{z=\eta_h}}\|^2_{0,\omega}\,d\tau, \tag{4.55}$$

where $\mu_h(t) = \|\nabla_{hor}\cdot \boldsymbol{u}^{hor}_{h|_{z=\eta_h}}(t)\|_{\infty,\omega}$.

Proof. We consider (4.46) with $\zeta_h = \eta_h$ leading to:

$$\big(\frac{\partial \eta_h}{\partial t}, \eta_h\big)_\omega + \big(\boldsymbol{u}^{hor}_{h|_{z=\eta_h}} \cdot \nabla_{hor}\,\eta_h, \eta_h\big)_\omega + |\eta_h|^2_s = \big(w_{h|_{z=\eta_h}}, \eta_h\big)_\omega, \tag{4.56}$$

and then:

$$\frac{1}{2}\frac{d}{dt}\|\eta_h\|^2_{0,\omega} + \big(\boldsymbol{u}^{hor}_{h|_{z=\eta_h}} \cdot \nabla_{hor}\,\eta_h, \eta_h\big)_\omega + |\eta_h|^2_s = \big(w_{h|_{z=\eta_h}}, \eta_h\big)_\omega. \tag{4.57}$$

We integrate by parts the convective part, yielding:

$$\big(\boldsymbol{u}^{hor}_{h|_{z=\eta_h}} \cdot \nabla_{hor}\,\eta_h, \eta_h\big)_\omega = -\frac{1}{2}\big(\nabla_{hor}\cdot \boldsymbol{u}^{hor}_{h|_{z=\eta_h}}, \eta_h^2\big)_\omega. \tag{4.58}$$

We substitute (4.58) in (4.57) leading to:

$$\frac{1}{2}\frac{d}{dt}\|\eta_h\|^2_{0,\omega} - \frac{1}{2}\big(\nabla_{hor}\cdot \boldsymbol{u}^{hor}_{h|_{z=\eta_h}}, \eta_h^2\big)_\omega + |\eta_h|^2_s = \big(w_{h|_{z=\eta_h}}, \eta_h\big)_\omega. \tag{4.59}$$

We apply Cauchy–Schwarz and Young inequalities on (4.59) yielding:

$$\begin{aligned}\frac{1}{2}\frac{d}{dt}\|\eta_h\|^2_{0,\omega} - \frac{1}{2}\,\mu_h(t)\,\|\eta_h\|^2_{0,\omega} + |\eta_h|^2_s &\leq \|w_{h|_{z=\eta_h}}\|_{0,\omega}\ \|\eta_h\|_{0,\omega} \\ &\leq \frac{1}{2}\|w_{h|_{z=\eta_h}}\|^2_{0,\omega} + \frac{1}{2}\,\|\eta_h\|^2_{0,\omega},\end{aligned} \tag{4.60}$$

where $\mu_h(t) = \|\nabla_{hor}\cdot \boldsymbol{u}^{hor}_{h|_{z=\eta_h}}\|_{\infty,\omega}$. Consequently, we have:

$$\frac{d}{dt}\|\eta_h\|^2_{0,\omega} + 2\,|\eta_h|^2_s \leq \|w_{h|_{z=\eta_h}}\|^2_{0,\omega} + (1+\mu_h(t))\,\|\eta_h\|^2_{0,\omega}. \tag{4.61}$$

Applying the Gronwall's Lemma 4.1, we obtain the energy estimate result (4.55). That concludes the proof. ■

4.3.3 Energy estimate on the velocity

In this Subsection, we derive the energy estimate of the semi-discrete variational formulations in space (4.44-4.45) on the velocity field. The semi-discrete variational formulations (4.44-4.45) constitute an ALE time-dependent problem. In the Finite Elements framework, the stability of ALE time-dependent problem was studied by Boffi and Gastaldi [13], Formaggia and Nobile [57, 58], Ganessan et al. [61]. At the semi-discrete level in space, the authors established energy estimates not depending on the mesh velocity $\mathbf{c}_h$.

For the energy estimate, we consider that the boundary of the domain is Lipschitz continuous. The Lipschitz continuous regularity of the free surface boundary $\Gamma_{s,t}$ is equivalent to a Lipschitz continuous regularity of the free surface η_h.

Proposition 4.4. *Let $\mathbf{u}_h$ be a semi-discrete solution of (4.44-4.45). For all $t \in [0,T]$, we have the following energy estimate result independent of the mesh velocity $\mathbf{c}_h$:*

$$\|\mathbf{u}_h\|^2_{0,t} + \nu \int_0^t \|\nabla \mathbf{u}_h\|^2_{0,t} \leq \|\mathbf{u}_{h,0}\|^2_{0,0} + \frac{\int_0^t c_p(\Omega_{h,\tau})^2 \, d\tau}{\nu} \, g^2 \, |\Omega_{h,0}| \, t, \tag{4.62}$$

where $c_p(\Omega_{h,t})$ is the Poincaré's constant of the domain $\Omega_{h,t}$, $\mathbf{u}_{h,0}$ is the initial semi-discrete in space velocity field and $\Omega_{h,0}$ is the initial discrete domain.

Proof. Since (4.29) is derived using $\frac{\partial \widehat{\mathbf{v}}}{\partial t} = 0$, we cannot take $\mathbf{v}_h = \mathbf{u}_h$ to derive the energy estimate in (4.44). Nevertheless, each component of $\mathbf{u}_h \in \mathcal{V}_{0,h,t}$ can be defined as a linear combination of basis functions $\varphi_i \in \mathcal{V}_{h,t}$ with time-dependent coefficients:

$$\mathbf{u}_h(\boldsymbol{x}, t) = \sum_{i \in \mathcal{N}_u} \mathbf{u}_i(t) \, \varphi_i(\boldsymbol{x}). \tag{4.63}$$

We recall that the basis functions φ_i do not depend on time in the reference domain, and thus

$$\left.\frac{\partial \mathbf{u}_h}{\partial t}\right|_{\widehat{\Omega}} (\boldsymbol{x}, t) = \sum_{i \in \mathcal{N}_u} \frac{d\mathbf{u}_i(t)}{dt} \varphi_i(\boldsymbol{x}). \tag{4.64}$$

Taking $q_h = p_h$ in (4.45) leads to:

$$b(\mathbf{u}_h, p_h) = 0. \tag{4.65}$$

We proceed now component by component on the velocity field $\mathbf{u}_h$. First of all, we start on the velocity component u_h. We take $\mathbf{v}_h = (\varphi_i, 0, 0)$ in (4.44). Then, we multiply the equation by $u_i(t) \in \mathbb{R}$ and we use the expressions of bilinear forms to get:

$$\begin{aligned}
&u_i(t) \, \frac{d}{dt} \int_{\Omega_{h,t}} u_h \varphi_i + \frac{1}{2} \, u_i(t) \int_{\Omega_{h,t}} ((\mathbf{u}_h - \mathbf{c}_h) \cdot \nabla) u_h \, \varphi_i \\
&- \frac{1}{2} \, u_i(t) \int_{\Omega_{h,t}} ((\mathbf{u}_h - \mathbf{c}_h) \cdot \nabla) u_h \, \varphi_i - \frac{1}{2} \, u_i(t) \int_{\Omega_{h,t}} (u_h \, \varphi_i) \, \nabla \cdot \mathbf{c}_h \\
&+ u_i(t) \, \nu \int_{\Omega_{h,t}} \nabla u_h : \nabla \varphi_i + u_i(t) \, \frac{1}{\rho} \int_{\Omega_{h,t}} \partial_x \varphi_i \, p_h = 0.
\end{aligned} \tag{4.66}$$

Since $u_i(t)$ depends only on time, the first term can be rewritten as follows:

$$u_i(t)\,\frac{d}{dt}\int_{\Omega_{h,t}} u_h\,\varphi_i = \frac{d}{dt}\int_{\Omega_{h,t}} u_h\,u_i(t)\,\varphi_i - \int_{\Omega_{h,t}} u_h\,\left.\frac{\partial u_i(t)\varphi_i}{\partial t}\right|_{\widehat{\Omega}}. \tag{4.67}$$

We add (4.66) over $i = 1, \cdots, N_u$:

$$\begin{aligned}\frac{d}{dt}\|u_h\|_{0,t}^2 - \int_{\Omega_{h,t}} u_h \cdot \left.\frac{\partial u_h}{\partial t}\right|_{\widehat{\Omega}} - \frac{1}{2}\int_{\Omega_{h,t}} u_h^2\,\nabla\cdot\mathbf{c}_h \\ + \nu\|\nabla u_h\|_{0,t}^2 + \frac{1}{\rho}\int_{\Omega_{h,t}} \partial_x u_h\,p_h = 0.\end{aligned} \tag{4.68}$$

We perform the same operation on the horizontal velocity component v_h with $\mathbf{v}_h = (0, \varphi_i, 0)$ and on the vertical velocity component w_h with $\mathbf{v}_h = (0, 0, \varphi_i)$, yielding:

$$\begin{aligned}\frac{d}{dt}\|v_h\|_{0,t}^2 - \int_{\Omega_{h,t}} v_h \cdot \left.\frac{\partial v_h}{\partial t}\right|_{\widehat{\Omega}} - \frac{1}{2}\int_{\Omega_{h,t}} v_h^2\,\nabla\cdot\mathbf{c}_h \\ + \nu\|\nabla v_h\|_{0,t}^2 + \frac{1}{\rho}\int_{\Omega_{h,t}} \partial_y v_h\,p_h = 0,\end{aligned} \tag{4.69}$$

and

$$\begin{aligned}\frac{d}{dt}\|w_h\|_{0,t}^2 - \int_{\Omega_{h,t}} w_h \cdot \left.\frac{\partial w_h}{\partial t}\right|_{\widehat{\Omega}} - \frac{1}{2}\int_{\Omega_{h,t}} w_h^2\,\nabla\cdot\mathbf{c}_h \\ + \nu\|\nabla w_h\|_{0,t}^2 + \frac{1}{\rho}\int_{\Omega_{h,t}} \partial_z w_h\,p_h = -\int_{\Omega_{h,t}} g\,w_h.\end{aligned} \tag{4.70}$$

Adding (4.68), (4.69) and (4.70) and using (4.65) leads to:

$$\frac{d}{dt}\|\mathbf{u}_h\|_{0,t}^2 - \int_{\Omega_{h,t}} \mathbf{u}_h \cdot \left.\frac{\partial \mathbf{u}_h}{\partial t}\right|_{\widehat{\Omega}} - \frac{1}{2}\int_{\Omega_{h,t}} |\mathbf{u}_h|^2\,\nabla\cdot\mathbf{c}_h + \nu\|\nabla\mathbf{u}_h\|_{0,t}^2 = \int_{\Omega_{h,t}} \mathbf{g}\cdot\mathbf{u}_h. \tag{4.71}$$

Using the Reynolds transport theorem, we have:

$$\int_{\Omega_{h,t}} \mathbf{u}_h \cdot \left.\frac{\partial \mathbf{u}_h}{\partial t}\right|_{\widehat{\Omega}} = \frac{1}{2}\int_{\Omega_{h,t}} \left.\frac{\partial |\mathbf{u}_h|^2}{\partial t}\right|_{\widehat{\Omega}} = \frac{1}{2}\frac{d}{dt}\|\mathbf{u}_h\|_{0,\Omega_{h,t}}^2 - \frac{1}{2}\int_{\Omega_{h,t}} |\mathbf{u}_h|^2\,\nabla\cdot\mathbf{c}_h. \tag{4.72}$$

Substitute (4.72) in (4.71) yields:

$$\frac{1}{2}\frac{d}{dt}\|\mathbf{u}_h\|_{0,t}^2 + \nu\|\nabla\mathbf{u}_h\|_{0,t}^2 = \int_{\Omega_{h,t}} \mathbf{g}\cdot\mathbf{u}_h. \tag{4.73}$$

Apply the Cauchy-Schwarz's inequality on the right-hand side:

$$\frac{d}{dt}\|\mathbf{u}_h\|_{0,t}^2 + 2\,\nu\,\|\nabla\mathbf{u}_h\|_{0,t}^2 \leq 2\,\|\mathbf{g}\|_{0,t}\,\|\mathbf{u}_h\|_{0,t}. \tag{4.74}$$

The imperviousness condition (4.7) at the solid boundaries allows to control all the components of $\mathbf{u}_h$. The Poincaré's inequality can be applied since there is a Dirichlet boundary condition on at least a non zero-measure part of the domain boundaries. We get then:

$$\frac{d}{dt}\|\mathbf{u}_h\|_{0,t}^2 + 2\,\nu\,\|\nabla\mathbf{u}_h\|_{0,t}^2 \leq 2\,c_p(\Omega_{h,t})\,\|\mathbf{g}\|_{0,t}\,\|\nabla\mathbf{u}_h\|_{0,t}. \tag{4.75}$$

We now use Young's inequality and we have:

$$\frac{d}{dt}\|\mathbf{u}_h\|_{0,t}^2 + 2\,\nu\,\|\nabla\mathbf{u}_h\|_{0,t}^2 \leq \frac{c_p(\Omega_{h,t})^2}{\nu}\|\mathbf{g}\|_{0,t}^2 + \nu\,\|\nabla\mathbf{u}_h\|_{0,t}^2. \tag{4.76}$$

Using Proposition (4.2), the norm of the gravity term can be rewritten as follows:

$$\|\mathbf{g}\|_{0,t}^2 = g^2|\Omega_{h,t}| = g^2|\Omega_{h,0}|, \tag{4.77}$$

and then:

$$\frac{d}{dt}\|\mathbf{u}_h\|_{0,t}^2 + \nu\|\nabla\mathbf{u}_h\|_{0,t}^2 \leq \frac{c_p(\Omega_{h,t})^2}{\nu}\,g^2\,|\Omega_{h,0}|. \tag{4.78}$$

Integrating on time the inequality (4.78) leads to the result (4.62). That concludes the proof. ■

4.4 A fully discrete method

In this section, we present the fully discrete variational formulations of (4.29-4.30) and (4.31). Besides, we study the global mass conservation property of the water quantity. The stability of these schemes on the free surface and on the velocity is then studied.

Let us consider a time interval $]0,T[$ divided into N time steps of equal length $\Delta t \in \mathbb{R}_*^+$. For $n \in [\![0, N-1]\!]$, we denote by $\mathcal{T}_h^{n,3D}$ the triangulation of the semi-discrete domain Ω^n at time t^n. This triangulation is built from $\widehat{\mathcal{T}}_h^{3D}$ through the discrete ALE mapping $\mathcal{A}_{h,n}$ as introduced in Subsection 2.2.4. The discrete domain is denoted Ω_h^n. Notice that the approximation of the free surface allows to define the discrete ALE mapping, and then the domain Ω_h^n different from Ω_{h,t^n}, i.e. $\Omega_h^n \neq \Omega_{t^n}$. The discrete boundary of the domain Ω_h^n is denoted $\partial\Omega_h^n$ and the discrete free surface part is $\Gamma_{h,s}^n$, then $\partial\Omega_h^n = \Gamma_{h,s}^n \cup \Gamma_{h,l}^n \cup \Gamma_b$. In the sequel, we denote by $(\mathbf{u}_h^n, p_h^n, \eta_h^n)$ the discrete solution. The mesh velocity between Ω_h^n and Ω_h^{n+1} is represented by $\mathbf{c}_h^n$. The discrete inner product on the discrete domain Ω_h^n at time $t = t^n$ is denoted by $(\cdot,\cdot)_{h,n}$ and the corresponding norm is, by an abuse of notation, $\|\cdot\|_{0,n}$.

We denote by $\mathcal{M}_h(\omega) \subset H^1(\omega)$ the discrete functional space, defined on ω, of the free surface. From the discrete reference functional spaces $\widehat{\mathcal{V}}_h(\widehat{\Omega})$ and $\widehat{\mathcal{Q}}_h(\widehat{\Omega})$ defined in the previous Section, the discrete ALE mapping $\mathcal{A}_{h,n}$ identifies the corresponding discrete

functional spaces defined on the current domain Ω_h^n, of the velocity and the pressure, such that:

$$\mathcal{V}_h(\Omega_h^n) = \{v_h^n :]0,T[\times\Omega_h^n \to \mathbb{R},\ v_h^n = \widehat{v}_h \circ \widehat{\mathcal{A}}_{h,n}^{-1},\ \widehat{v}_h \in \widehat{\mathcal{V}}_h(\widehat{\Omega})\}, \tag{4.79}$$

$$\mathcal{Q}_h(\Omega_h^n) = \{q_h^n :]0,T[\times\Omega_h^n \to \mathbb{R},\ q_h^n = \widehat{q}_h \circ \widehat{\mathcal{A}}_{h,n}^{-1},\ \widehat{q}_h \in \widehat{\mathcal{Q}}_h(\widehat{\Omega})\}. \tag{4.80}$$

In addition, we define:

$$\mathcal{V}_{0,h}(\Omega_h^n) = \{\mathbf{v}_h^n \in \left(\mathcal{V}_h(\Omega_h^n)\right)^3 \ \mid\ \mathbf{v}_h^n \cdot \mathbf{n} = 0 \text{ on } \Gamma_b \cup \Gamma_l^n\}. \tag{4.81}$$

In view of the Finite Elements approximation, we consider the Finite Elements spaces $\mathcal{F}_{m,k}^{\mathcal{V}}(\mathcal{T}_h^{n,3D}) = \mathcal{V}_h(\Omega_h^n)$ and $\mathcal{F}_{m',k'}^{\mathcal{Q}}(\mathcal{T}_{h,t}^{n,3D}) = \mathcal{Q}_h(\Omega_h^n)$, as introduced in Subsection 2.2.5. Recall that we only consider pairs of Finite Element spaces which satisfy the discrete inf-sup condition [19] given by (2.114) and recalled here for convenience:

$$\inf_{q_h^n \in \mathcal{Q}_h(\Omega_h^n)} \sup_{v_h^n \in \mathcal{V}_h(\Omega_h^n)} \frac{(\nabla \cdot v_h^n, q_h^n)}{\|v_h^n\|_{1,n}\|q_h^n\|_{0,n}} \geq \beta_0,$$

with $\beta_0 > 0$, a constant independent of the mesh size. This property ensures that the system (4.84-4.85), introduced below, is well-posed.

As mentioned in Subsection 2.3.4, the numerical strategy consists successively in:

i/ advecting the free surface in order to compute η_h^{n+1},
ii/ updating the discrete domain to Ω_h^{n+1} through the ALE mapping (2.17),
iii/ solving the Navier–Stokes equations in order to determinate $(\mathbf{u}_h^{n+1}, p_h^{n+1})$.

For the first step, we discretize in time the semi-discrete variational formulation in space on the free surface (4.46) by a first order forward Euler scheme. As a consequence, we consider the following fully explicit discrete method on the free surface:

$$\begin{cases} \text{Find } \eta_h^{n+1} \in \mathcal{M}_h(\omega) \text{ such that for all } \zeta_h \in \mathcal{M}_h(\omega) \\ \left(\dfrac{\eta_h^{n+1} - \eta_h^n}{\Delta t}, \zeta_h\right)_\omega + \left(\boldsymbol{u}_{h|_{z=\eta_h^n}}^{n,hor} \cdot \nabla \eta_h^n, \zeta_h\right)_\omega + s_h^n(\eta_h^n, \zeta_h) = \left(w_{h|_{z=\eta_h^n}}^n, \zeta_h\right)_\omega, \end{cases} \tag{4.82}$$

where the stabilization term is:

$$s_h^n(\eta_h^n, \zeta_h) = \frac{\mathrm{h}}{\|\boldsymbol{u}_{h|_{z=\eta_h^n}}^{n,hor}\|_\infty} (\boldsymbol{u}_{h|_{z=\eta_h^n}}^{n,hor} \cdot \nabla \eta_h^n, \boldsymbol{u}_{h|_{z=\eta_h^n}}^{n,hor} \cdot \nabla \zeta_h)_\omega. \tag{4.83}$$

For the third step, we integrate over the time Navier–Stokes equations (4.44,4.45) and

we consider then the following discrete method on the velocity and the pressure:

$$\begin{cases} \text{Find } (\mathbf{u}_h^{n+1}, p_h^{n+1}) \in (\mathcal{V}_{h,0}^{n+1}(\Omega_h^{n+1}), \mathcal{Q}_h^{n+1}(\Omega_h^{n+1})) \\ \text{such that for all } (\mathbf{v}_h^{n+1}, q_h^{n+1}) \in (\mathcal{V}_{h,0}^{n+1}(\Omega_h^{n+1}), \mathcal{Q}_h^{n+1}(\Omega_h^{n+1})) \\ (\mathbf{u}_h^{n+1}, \mathbf{v}_h^{n+1})_{h,n+1} - (\mathbf{u}_h^n, \mathbf{v}_{h,n}^{n+1})_{h,n} + \Delta t \left[\overline{c}_{n+1}(\mathbf{u}_{h,n+1}^n - \mathbf{c}_{h,n+1}^n, \mathbf{u}_h^{n+1}, \mathbf{v}_h^{n+1}) \right. \\ - \dfrac{1}{2}(\mathbf{u}_h^{n+1} \nabla \cdot \mathbf{c}_{h,n+1}^n, \mathbf{v}_h^{n+1})_{h,n+1} + a_{n+1}(\mathbf{u}_h^{n+1}, \mathbf{v}_h^{n+1}) \\ \left. - b_{n+1}(\mathbf{v}_h^{n+1}, p_h^{n+1}) \right] = (\mathbf{g}, \mathbf{v}_h^{n+1})_{h,n+1}, \qquad (4.84) \\ \\ - b_{n+1}(\mathbf{u}_h^{n+1}, q_h^{n+1}) = 0, \qquad (4.85) \end{cases}$$

where $\mathbf{u}_{h,n+1}^n$ and $\mathbf{c}_{h,n+1}^n$, defined in Ω^{n+1}, represent the discrete velocities $\mathbf{u}_h^n$ and $\mathbf{c}_h^n$, defined in Ω^n, such that for all $n \in [\![0, N]\!]$:

$$\mathbf{u}_{h,n+1}^n = \mathbf{u}_h^n \circ \mathcal{A}_h^{n,n+1} = \mathbf{u}_h^n \circ \widehat{\mathcal{A}}_{h,n+1} \circ \widehat{\mathcal{A}}_{h,n}^{-1}, \qquad (4.86)$$

$$\mathbf{c}_{h,n+1}^n = \mathbf{c}_h^n \circ \mathcal{A}_h^{n,n+1} = \mathbf{c}_h^n \circ \widehat{\mathcal{A}}_{h,n+1} \circ \widehat{\mathcal{A}}_{h,n}^{-1}. \qquad (4.87)$$

Recall that $\mathcal{A}_h^{n,n+1}$ is the discrete ALE mapping between Ω_h^n and Ω_h^{n+1}, as introduced in Subsection 2.2.1. The multilinear forms are $a_n(\cdot,\cdot)$, $b_n(\cdot,\cdot)$ and $\overline{c}_n$ are the corresponding multilinear forms of (4.26), (4.27) and (4.28) on Ω_h^n, respectively.

Proposition 4.5. *The discrete variational form (4.84,4.85) is well-posed*

Proof. Let us demonstrate that the bilinear form

$$\begin{aligned} A(\mathbf{u}, \mathbf{v}) = (\mathbf{u}_h^{n+1}, \mathbf{v}_h^{n+1})_{h,n+1} + \Delta t \left[\overline{c}_{n+1}(\mathbf{u}_{h,n+1}^n - \mathbf{c}_{h,n+1}^n, \mathbf{u}_h^{n+1}, \mathbf{v}_h^{n+1}) \right. \\ \left. - \frac{1}{2}(\mathbf{u}_h^{n+1} \nabla \cdot \mathbf{c}_{h,n+1}^n, \mathbf{v}_h^{n+1})_{h,n+1} + a_{n+1}(\mathbf{u}_h^{n+1}, \mathbf{v}_h^{n+1}) \right], \end{aligned}$$

is coercive. Under the inf-sup condition (2.114), it exists a constant β_0 independent of the mesh size that allows to ensure the coercivity of $b_{n+1}(\cdot,\cdot)$. The coercivity of $a_{n+1}(\cdot,\cdot)$ is ensured classically by using the Poincaré's inequality, see Ern and Guermond [53]. Afterwards, $\overline{c}_h^{n+1}(\mathbf{u}, \mathbf{v}, \mathbf{v})$ is equal to zero by anti-symmetry.
We show now that

$$(\mathbf{u}_h^{n+1}, \mathbf{v}_h^{n+1})_{n+1} - \frac{1}{2}(\mathbf{u}_h^{n+1} \nabla \cdot \mathbf{c}_{h,n+1}^n, \mathbf{v}_h)_{n+1}, \qquad (4.88)$$

is coercive, independently of the space and the time steps. For this purpose, it is sufficient to prove that:

$$1 - \frac{\Delta t}{2} \nabla \cdot \mathbf{c}_{h,n+1}^n \geq 0. \qquad (4.89)$$

The mesh velocity $c^n_{h,n+1}$ is defined in Ω^{n+1}_h, i.e. the horizontal coordinates $(x,y) \in \omega$ and the vertical one $z \in [b^{n+1}, \eta^{n+1}_h]$. Using (4.2), this velocity corresponds to:

$$\begin{aligned} c^n_{h,n+1}(x,y,z) &= c^n_h \circ \mathcal{A}^{n,n+1}_h(x,y,z) \\ &= c^n_h \circ \widehat{\mathcal{A}}_{h,n+1} \circ \widehat{\mathcal{A}}^{-1}_{h,n}(x,y,z) \\ &= \left(0, 0, \frac{\eta^{n+1}_h - \eta^n_h}{\Delta t} \frac{\mathcal{A}^{n,n+1}_h(0,0,z) - b}{\eta^n_h - b}\right). \end{aligned} \tag{4.90}$$

However, the coordinates in Ω^{n+1}_h through the ALE mapping read; $\forall z \in [b^{n+1}, \eta^{n+1}_h]$:

$$\mathcal{A}^{n,n+1}_h(x,y,z) = (\eta^n_h - b)\frac{z-b}{\eta^{n+1}_h} + b. \tag{4.91}$$

Replace (4.91) in (4.90) yields:

$$\mathbf{c}^n_{h,n+1} = \left(0, 0, \frac{\eta^{n+1}_h - \eta^n_h}{\Delta t} \frac{z-b}{\eta^{n+1}_h}\right). \tag{4.92}$$

As a consequence, the divergence of the mesh velocity $\mathbf{c}^n_{h,n+1}$ is:

$$\nabla \cdot \mathbf{c}^n_{h,n+1} = \left(0, 0, \frac{\eta^{n+1}_h - \eta^n_h}{\Delta t} \frac{1}{\eta^{n+1}_h}\right). \tag{4.93}$$

Thus, we obtain:

$$1 - \frac{\Delta t}{2} \frac{\eta^{n+1}_h - \eta^n_h}{\Delta t} \frac{1}{\eta^{n+1}_h} = \frac{\eta^{n+1}_h + \eta^n_h}{2\eta^{n+1}_h} \geq 0. \tag{4.94}$$

As a consequence, $A(\mathbf{u}, \mathbf{v})$ is coercive and the problem is well-posed. That concludes the proof. ■

4.4.1 Mass conservation of the water quantity

In this Subsection, we demonstrate that the fully discrete variational formulation in space on the free surface (4.82) preserves the global mass conservation, is equivalent here to the fact that the volume of the discrete domain is constant, i.e. $|\Omega^n_h| = |\Omega^{n-1}_h| = \cdots = |\Omega^0_h|$.

Proposition 4.6. *Let $\eta^{n+1}_h \in \mathcal{M}_h(\omega)$ be a discrete solution of (4.82). For all $n \in \mathbb{N}$, we have the following global mass conservation result:*

$$\int_\omega \eta^{n+1}_h = \int_\omega \eta^0_h. \tag{4.95}$$

Proof. The proof is the same as the one of Proposition 4.2 in Subsection 4.3.1. In order to ensure the global mass conservation at the discrete level, the key idea is to approximate the fluid velocity $\mathbf{u}_h$ and the free surface η_h at the same time $t^\theta = \theta\, t^{n+1} + (1-\theta)\, t^n$ with $\theta \in \{0, 1\}$. Here we choose $\theta = 0$. ■

The choice to discretize in time (4.82) by a first-order forward Euler scheme in time is motivated by the fact that the free surface and Navier-Stokes equations can be solved separately. Consequently, we compute the free surface η_h^{n+1}. After updating the fluid domain at Ω_h^{n+1} from η_h^{n+1}, the velocity of the fluid $\mathbf{u}_h^{n+1}$ and the pressure p_h^{n+1} are computed. It could be possible to discretize in time (4.46) by a first order backward Euler scheme. The preservation of the mass of the water quantity would continue to be held. This strategy does not involve a CFL restriction [115] but the resolution is coster since the fully implicit method leads to a Finite Elements monolithic method.

4.4.2 Stability estimate on the free surface

In this Subsection, we introduce the stability result of the fully discrete variational formulation (4.82) on the free surface. For this purpose, we assume that $\mathbf{u}_h^n \in W^{1,\infty}(\Omega_h^n)$. Before presenting the stability result, let us introduce an intermediate result on $\|\eta_h^{n+1} - \eta_h^n\|_{0,\omega}$.

Proposition 4.7. *Let $\eta_h^n \in \mathcal{M}_h(\omega)$ be a discrete solution of (4.82). We have the following result:*

$$\|\eta_h^{n+1} - \eta_h^n\|_{0,\omega}^2 \leq \; 2\,\Delta t \left[\Delta t \, \|w^n_{h|_{z=\eta_h^n}}\|_{0,\omega}^2 + 2\,\frac{\Delta t}{\mathrm{h}}\,|\eta_h^n|_s^2\,\|\boldsymbol{u}^{n,hor}_{h|_{z=\eta_h^n}}\|_{\infty,\omega}\left(1 + c_{inv}^2\right)\right], \tag{4.96}$$

where h *is the minimal diameter of elements $K_T^{2D} \in \mathcal{T}_h^{2D}$ and c_{inv} a constant of an inverse inequality.*

Proof. We consider the discrete variational formulation of the free surface equation (4.82) with $\zeta_h = \eta_h^{n+1} - \eta_h^n$:

$$\begin{aligned}\|\eta_h^{n+1} - \eta_h^n\|_{0,\omega}^2 = \Delta t \left[\left(w^n_{h|_{z=\eta_h^n}}, \eta_h^{n+1} - \eta_h^n\right)_\omega - \left(\boldsymbol{u}^{n,hor}_{h|_{z=\eta_h^n}} \cdot \nabla \eta_h^n, \eta_h^{n+1} - \eta_h^n\right)_\omega\right] \\ -\Delta t\, s_h^n(\eta_h^n, \eta_h^{n+1} - \eta_h^n).\end{aligned} \tag{4.97}$$

Applying absolute value to (4.97) and use Cauchy–Schwarz's inequality, we obtain:

$$\begin{aligned}\|\eta_h^{n+1} - \eta_h^n\|_{0,\omega}^2 \leq & \Delta t\, \|\eta_h^{n+1} - \eta_h^n\|_{0,\omega} \left[\|w^n_{h|_{z=\eta_h^n}}\|_{0,\omega} + \|\boldsymbol{u}^{n,hor}_{h|_{z=\eta_h^n}} \cdot \nabla \eta_h^n\|_{0,\omega}\right] \\ & + \Delta t \, \left| s_h^n(\eta_h^n, \eta_h^{n+1} - \eta_h^n)\right|.\end{aligned} \tag{4.98}$$

At this stage, the aim is to bound the terms on the right-hand side of (4.98). The term $\|\boldsymbol{u}^{n,hor}_{h|_{z=\eta_h^n}} \cdot \nabla \eta_h^n\|_{0,\omega}$ can be rewritten as follows:

$$\begin{aligned}\|\boldsymbol{u}^{n,hor}_{h|_{z=\eta_h^n}} \cdot \nabla \eta_h^n\|_{0,\omega}^2 &= \frac{\|\boldsymbol{u}^{n,hor}_{h|_{z=\eta_h^n}}\|_\infty}{\mathrm{h}} \frac{\mathrm{h}}{\|\boldsymbol{u}^{n,hor}_{h|_{z=\eta_h^n}}\|_\infty} (\boldsymbol{u}^{n,hor}_{h|_{z=\eta_h^n}} \cdot \nabla \eta_h^n, \boldsymbol{u}^{n,hor}_{h|_{z=\eta_h^n}} \cdot \nabla \eta_h^n)_\omega \\ &= \frac{\|\boldsymbol{u}^{n,hor}_{h|_{z=\eta_h^n}}\|_\infty}{\mathrm{h}}\,|\eta_h^n|_s^2.\end{aligned} \tag{4.99}$$

Therefore, we replace (4.99) in (4.98) and we get:

$$\|\eta_h^{n+1}-\eta_h^n\|_{0,\omega}^2 \leq \Delta t\,\|\eta_h^{n+1}-\eta_h^n\|_{0,\omega}\left[\|w^n_{h|_{z=\eta_h^n}}\|_{0,\omega}+\frac{\left\|\boldsymbol{u}^{n,hor}_{h|_{z=\eta_h^n}}\right\|_\infty^{\frac{1}{2}}}{\mathrm{h}^{\frac{1}{2}}}\,|\eta_h^n|_s\right] + \Delta t\,\left|s_h^n(\eta_h^n,\eta_h^{n+1}-\eta_h^n)\right|. \tag{4.100}$$

We seek now to bound the stabilization term $s_h^n(\eta_h^n,\eta_h^{n+1}-\eta_h^n)$. For that, we use the symmetry property on the stabilization term and Cauchy–Schwarz inequality leading to:

$$\begin{aligned} s_h^n(\eta_h^n,\eta_h^{n+1}-\eta_h^n) &\leq s_h^n(\eta_h^n,\eta_h^n)^{\frac{1}{2}}\; s_h(\eta_h^{n+1}-\eta_h^n,\eta_h^{n+1}-\eta_h^n)^{\frac{1}{2}} \\ &\leq \frac{\mathrm{h}^{\frac{1}{2}}}{\left\|\boldsymbol{u}^{n,hor}_{h|_{z=\eta_h^n}}\right\|_\infty^{\frac{1}{2}}}\,|\eta_h^n|_s\,\|\boldsymbol{u}^{n,hor}_{h|_{z=\eta_h^n}}\cdot\nabla(\eta_h^{n+1}-\eta_h^n)\|_{0,\omega}, \end{aligned} \tag{4.101}$$

and then:

$$s_h^n(\eta_h^n,\eta_h^{n+1}-\eta_h^n) \leq \mathrm{h}^{\frac{1}{2}}\,|\eta_h^n|_s\,\|\boldsymbol{u}^{n,hor}_{h|_{z=\eta_h^n}}\|_{\infty,\omega}^{-\frac{1}{2}}\,\|\nabla(\eta_h^{n+1}-\eta_h^n)\|_{0,\omega}. \tag{4.102}$$

Using an inverse inequality on (4.102) yields:

$$s_h^n(\eta_h^n,\eta_h^{n+1}-\eta_h^n) \leq c_{inv}\,\mathrm{h}^{-\frac{1}{2}}\,|\eta_h^n|_s\left\|\boldsymbol{u}^{n,hor}_{h|_{z=\eta_h^n}}\right\|_{\infty,\omega}^{-\frac{1}{2}}\|\eta_h^{n+1}-\eta_h^n\|_{0,\omega}. \tag{4.103}$$

We insert (4.103) in (4.100) and we have:

$$\begin{aligned} \|\eta_h^{n+1}-\eta_h^n\|_{0,\omega}^2 \leq \Delta t\,\|\eta_h^{n+1}-\eta_h^n\|_{0,\omega}\Big[&\|w^n_{h|_{z=\eta_h^n}}\|_{0,\omega} \\ &+\mathrm{h}^{-\frac{1}{2}}\,|\eta_h^n|_s\left[\|\boldsymbol{u}^{n,hor}_{h|_{z=\eta_h^n}}\|_\infty^{\frac{1}{2}}+c_{inv}\,\|\boldsymbol{u}^{n,hor}_{h|_{z=\eta_h^n}}\|_{\infty,\omega}^{\frac{1}{2}}\right]\Big]. \end{aligned} \tag{4.104}$$

We divide by $\|\eta_h^{n+1}-\eta_h^n\|_{0,\omega}$ and we put to the square giving:

$$\begin{aligned} \|\eta_h^{n+1}-\eta_h^n\|_{0,\omega}^2 &\leq \Delta t^2\left[\mathrm{h}^{-\frac{1}{2}}\,|\eta_h^n|_s\,\|\boldsymbol{u}^{n,hor}_{h|_{z=\eta_h^n}}\|_\infty^{\frac{1}{2}}\left[1+c_{inv}\right]+\|w^n_{h|_{z=\eta_h^n}}\|_{0,\omega}\right]^2 \\ &\leq \Delta t^2\left[2\,\mathrm{h}^{-1}\,|\eta_h^n|_s^2\,\|\boldsymbol{u}^{n,hor}_{h|_{z=\eta_h^n}}\|_\infty\left[1+c_{inv}\right]^2+2\,\|w^n_{h|_{z=\eta_h^n}}\|_{0,\omega}^2\right] \\ &\leq 2\,\Delta t\left[2\,\frac{\Delta t}{\mathrm{h}}\,|\eta_h^n|_s^2\,\|\boldsymbol{u}^{n,hor}_{h|_{z=\eta_h^n}}\|_\infty\left[1+c_{inv}^2\right]+\Delta t\|w^n_{h|_{z=\eta_h^n}}\|_{0,\omega}^2\right]. \end{aligned}$$

That concludes the proof. ■

The Proposition 4.7 is used to demonstrate the stability result of the fully discrete variational formulation (4.82) on the free surface, which reads:

Proposition 4.8. *Let $\eta_h^n \in \mathcal{M}_h(\omega)$ be a discrete solution of (4.82). The function η_h^0 is the interpolated function of $\eta(x,y,0)$. We consider the following CFL condition:*

$$\Delta t \leq \frac{\mathrm{h}}{2\,\|\boldsymbol{u}^{n,hor}_{h|_{z=\eta_h^n}}\|_\infty\,(1+c_{inv}^2)}. \tag{4.105}$$

Under this CFL condition, the numerical solution $\eta_h^{n+1} \in \mathcal{M}_h(\omega)$ of (4.82) satisfies the stability result:

$$\begin{aligned}\|\eta_h^T\|_{0,\omega}^2 + \sum_{k=0}^{n-1} 2\,\beta_h^n\,\Delta t\,|\eta_h^k|_s^2 \leq\ & \exp\left[\sum_{k=0}^{n-1}(1+\mu_h^k)(t^{k+1}-t^k)\right]\|\eta_h^0\|_{0,\omega}^2 \\ &+ \sum_{k=0}^{n-1}\exp\left[\sum_{l=k}^{n-1}(1+\mu_h^l)(t^{l+1}-t^l)\right]\Delta t\big(1+2\,\Delta t\big)\|w^k_{h|_{z=\eta_h^k}}\|_{0,\omega}^2,\end{aligned} \tag{4.106}$$

with the following constant:

$$\mu_h^n = \big\|\nabla\cdot\boldsymbol{u}^{n,hor}_{h|_{z=\eta_h^n}}\big\|_{\infty,\omega}, \tag{4.107}$$

$$\beta_h^n = 1 - 2\,\frac{\Delta t}{\mathrm{h}}\,\|\boldsymbol{u}^{n,hor}_{h|_{z=\eta_h^n}}\|_\infty\,(1+c_{inv}^2). \tag{4.108}$$

Proof. We consider the discrete variational formulation of the free surface equation (4.82) with $\zeta_h = \eta_h^n$:

$$\begin{aligned}\|\eta_h^{n+1}\|_{0,\omega}^2 - \|\eta_h^n\|_{0,\omega}^2 + 2\,\Delta t\,|\eta_h^n|_s^2 =\ & 2\,\Delta t\,\big(w^n_{h|_{z=\eta_h^n}},\eta_h^n\big)_\omega \\ & - 2\,\Delta t\,\big(\boldsymbol{u}^{n,hor}_{h|_{z=\eta_h^n}}\cdot\nabla\eta_h^n,\eta_h^n\big)_\omega + \|\eta_h^{n+1}-\eta_h^n\|_{0,\omega}^2.\end{aligned} \tag{4.109}$$

By analogy with the proof of Proposition 4.3, the terms on the right-hand side (4.109) including $\boldsymbol{u}^{n,hor}_{h|_{z=\eta_h^n}}$ and $w^n_{h|_{z=\eta_h^n}}$ are treated on the same way, leading to the following inequalities:

$$2\,\Delta t\,\big(w^n_{h|_{z=\eta_h^n}},\eta_h^n\big)_\omega \leq \Delta t\big(\|w^n_{h|_{z=\eta_h^n}}\|_{0,\omega}^2 + \|\eta_h^n\|_{0,\omega}^2\big), \tag{4.110}$$

and

$$-\big(\boldsymbol{u}^{n,hor}_{h|_{z=\eta_h^n}}\cdot\nabla\eta_h^n,\eta_h^n\big)_\omega \leq \frac{1}{2}\big\|\nabla\cdot\boldsymbol{u}^{n,hor}_{h|_{z=\eta_h^n}}\big\|_{\infty,\omega}\,\|\eta_h^n\|_{0,\omega}^2. \tag{4.111}$$

Substituting (4.110) and (4.111) in (4.109), we get:

$$\begin{aligned}\|\eta_h^{n+1}\|_{0,\omega}^2 - \|\eta_h^n\|_{0,\omega}^2 + 2\,\Delta t\,|\eta_h^n|_s^2 & \\ \leq \Delta t\|w^n_{h|_{z=\eta_h^n}}\|_{0,\omega}^2 + \big(1+\mu_h^n\big)\,\Delta t\,\|\eta_h^n\|_{0,\omega}^2 + \|\eta_h^{n+1}-\eta_h^n\|_{0,\omega}^2,\end{aligned} \tag{4.112}$$

with $\mu_h^n = \big\| \nabla \cdot \boldsymbol{u}^{n,hor}_{h|_{z=\eta_h^n}} \big\|_{\infty,\omega}$.

Using Proposition 4.7 to bound $\|\eta_h^{n+1} - \eta_h^n\|^2_{0,\omega}$, we obtain:

$$\begin{aligned}
&\|\eta_h^{n+1}\|^2_{0,\omega} - \|\eta_h^n\|^2_{0,\omega} + 2\,\Delta t\,|\eta_h^n|^2_s \\
&\quad \leq \Delta t \|w^n_{h|_{z=\eta_h^n}}\|^2_{0,\omega} + \big(1+\mu_h^n\big)\,\Delta t\,\|\eta_h^n\|^2_{0,\omega} \\
&\qquad + 2\,\Delta t\,\Big[\,\Delta t\,\|w^n_{h|_{z=\eta_h^n}}\|^2_{0,\omega} + 2\,\frac{\Delta t}{\mathrm{h}}\,|\eta_h^n|^2_s\,\|\boldsymbol{u}^{n,hor}_{h|_{z=\eta_h^n}}\|_\infty\,(1+c^2_{inv})\Big]. \qquad (4.113)
\end{aligned}$$

Easy computations lead to:

$$\|\eta_h^{n+1}\|^2_{0,\omega} + 2\,\beta_h^n\,\Delta t\,|\eta_h^n|^2_s \;\; \leq \Big(1 + \big(1+\mu_h^n\big)\,\Delta t\Big)\|\eta_h^n\|^2_{0,\omega} + \big(\Delta t + 2\,\Delta t^2\big)\,\|w^n_{h|_{z=\eta_h^n}}\|^2_{0,\omega}. \qquad (4.114)$$

with $\beta_h^n = 1 - 2\,\dfrac{\Delta t}{\mathrm{h}}\|\boldsymbol{u}^{n,hor}_{h|_{z=\eta_h^n}}\|_\infty\,(1+c^2_{inv}) \geq 0$ under the CFL condition (4.105).

We add (4.114) over $k = 0, \cdots, T-1$ and we apply the Gronwall's lemma (4.2). As a consequence, we obtain the stability result (4.106) under the CFL condition (4.105). That concludes the proof. ■

4.4.3 Stability estimate on the velocity field

In this Subsection, we derive the stability estimate of the fully discrete variational formulation in space (4.84-4.85) on the velocity field. For this purpose, we assume that the fully discrete function η_h^n is Lipschitz continuous at time t^n. Before performing this analysis, we briefly introduce the concept of the geometric conservation laws (GCL). This concept is used in the stability analysis of (4.84,4.85) in order to have a stability result not depending on the mesh velocity $\mathbf{c}_h^n$, as for the semi-discrete case.

Brief introduction to the geometric conservation laws

The GCL condition governs the geometric parameters of a given numerical scheme. On the one hand, this condition allows to a numerical scheme to preserve some constant states of a conservative equation. On the other hand, this condition also enables that a numerical scheme preserves the global conservation properties when it is applied to equation in non-conservative form. For the Finite Element ALE formulation, the geometric conservation law has been introduced in Formaggia and Nobile [57] and Lesoinne and Farhat [93] such that:

$$\int_{\Omega_h^{n+1}} \mathbf{v}_h^{n+1}\,d\boldsymbol{x} - \int_{\Omega_h^n} \mathbf{v}_h^n\,d\boldsymbol{x} = \int_{t^n}^{t^{n+1}} \int_{\Omega_{h,t}} \mathbf{v}_h(t)\,\nabla\cdot\mathbf{c}_h(t)\,d\boldsymbol{x}\,dt. \qquad (4.115)$$

Remark that (4.115) is a particular discretization of the Euler's expansion formula (2.21). We apply the same quadrature rule as (4.84,4.85) leading to:

$$\int_{\Omega_h^{n+1}} \mathbf{v}_h^{n+1}\, d\boldsymbol{x} - \int_{\Omega_h^n} \mathbf{v}_{h,n}^{n+1}\, d\boldsymbol{x} = \Delta t \int_{\Omega_h^{n+1}} \mathbf{v}_h^{n+1}\, \nabla\cdot \mathbf{c}_{h,n+1}^n\, d\boldsymbol{x}\, dt. \tag{4.116}$$

In our case the mesh velocity is purely vertical, in this case the GCL condition (4.116) is automatically satisfied as shown in Decoene [44].

The stability result of the fully discrete variational formulations (4.84-4.85) on the velocity reads:

Proposition 4.9. *Let $\mathbf{u}_h^n$ be a discrete solution of (4.84-4.85). We consider $\mathbf{u}_h^0$ the interpolated function of $\mathbf{u}(\boldsymbol{x},0)$. The stability result on the velocity $\mathbf{u}_h^n$ reads:*

$$\|\mathbf{u}_h^T\|_{0,T}^2 + \nu\,\Delta t \sum_{n=0}^{T-1} \|\nabla \mathbf{u}_h^{n+1}\|_{0,n+1}^2 \leq \|\mathbf{u}_h^0\|_{0,0}^2 + \frac{\Delta t}{\nu} g^2\, |\Omega_h^0| \sum_{n=0}^{T-1} c_p^2(\Omega_h^{n+1}), \tag{4.117}$$

where $c_p(\Omega_h^n)$ is the Poincaré's constant of the domain Ω_h^n

Proof. We consider the discrete variational formulation (4.84) with $\mathbf{v}_h^{n+1} = \mathbf{u}_h^{n+1}$ leading to:

$$\begin{aligned}&(\mathbf{u}_h^{n+1}, \mathbf{u}_h^{n+1})_{h,n+1} - (\mathbf{u}_h^n, \mathbf{u}_{h,n}^{n+1})_{h,n} - \frac{\Delta t}{2}(\mathbf{u}_h^{n+1}\nabla\cdot \mathbf{c}_{h,n+1}^n, \mathbf{u}_h^{n+1})_{h,n+1} \\ &+ \Delta t\, a_{n+1}(\mathbf{u}_h^{n+1}, \mathbf{u}_h^{n+1}) = \Delta t\, (\mathbf{g}, \mathbf{u}_h^{n+1})_{h,n+1}.\end{aligned} \tag{4.118}$$

Applying the Cauchy–Schwarz's inequality, we get:

$$\begin{aligned}&\|\mathbf{u}_h^{n+1}\|_{0,n+1}^2 - \|\mathbf{u}_h^n\|_{0,n}\|\mathbf{u}_{h,n}^{n+1}\|_{0,n} - \frac{\Delta t}{2}(\mathbf{u}_h^{n+1}\nabla\cdot \mathbf{c}_{h,n+1}^n, \mathbf{u}_h^{n+1})_{h,n+1} \\ &+ \nu\,\Delta t\, \|\nabla \mathbf{u}_h^{n+1}\|_{0,n+1}^2 \leq \Delta t\, \|\mathbf{g}\|_{0,n+1}\, \|\mathbf{u}_h^{n+1}\|_{0,n+1}.\end{aligned} \tag{4.119}$$

Denoting by $c_p(\Omega_h^{n+1})$ the Poincaré's constant on the domain Ω_h^{n+1}, we use the Poincaré's inequality on the term on the right-hand side to obtain:

$$\begin{aligned}&\|\mathbf{u}_h^{n+1}\|_{0,n+1}^2 - \|\mathbf{u}_h^n\|_{0,n}\|\mathbf{u}_{h,n}^{n+1}\|_{0,n} - \frac{\Delta t}{2}(\mathbf{u}_h^{n+1}\nabla\cdot \mathbf{c}_{h,n+1}^n, \mathbf{u}_h^{n+1})_{h,n+1} \\ &+ \nu\,\Delta t\, \|\nabla \mathbf{u}_h^{n+1}\|_{0,n+1}^2 \leq \Delta t\, c_p(\Omega_h^{n+1})\, \|\mathbf{g}\|_{0,n+1}\, \|\nabla\mathbf{u}_h^{n+1}\|_{0,n+1}.\end{aligned} \tag{4.120}$$

Applying the Young's inequality, we get:

$$\begin{aligned}&\|\mathbf{u}_h^{n+1}\|_{0,n+1}^2 - \frac{1}{2}\|\mathbf{u}_h^n\|_{0,n}^2 - \frac{1}{2}\|\mathbf{u}_{h,n}^{n+1}\|_{0,n}^2 - \frac{\Delta t}{2}(\mathbf{u}_h^{n+1}\nabla\cdot \mathbf{c}_{h,n+1}^n, \mathbf{u}_h^{n+1})_{h,n+1} \\ &+ \nu\,\Delta t\, \|\nabla \mathbf{u}_h^{n+1}\|_{0,n+1}^2 \leq \frac{\Delta t}{2\,\nu}\, c_p^2(\Omega_h^{n+1})\, \|\mathbf{g}\|_{0,n+1}^2 + \frac{\Delta t}{2}\,\nu\, \|\nabla\mathbf{u}_h^{n+1}\|_{0,n+1}^2.\end{aligned} \tag{4.121}$$

The GCL condition (4.116) with $\mathbf{v}_h^{n+1} = |\mathbf{u}_h^{n+1}|^2$ allows to obtain the following relation:

$$-\frac{\Delta t}{2}(\mathbf{u}_h^{n+1}\nabla\cdot\mathbf{c}_{h,n+1}^n, \mathbf{u}_h^{n+1})_{h,n+1} = -\frac{1}{2}\|\mathbf{u}_h^{n+1}\|_{0,n+1}^2 + \frac{1}{2}\|\mathbf{u}_{h,n}^{n+1}\|_{0,n}^2. \tag{4.122}$$

Inserting (4.122) in (4.121) leads to:

$$\frac{1}{2}\|\mathbf{u}_h^{n+1}\|_{0,n+1}^2 - \frac{1}{2}\|\mathbf{u}_h^{n}\|_{0,n}^2 + \nu\,\frac{\Delta t}{2}\,\|\nabla\mathbf{u}_h^{n+1}\|_{0,n+1}^2 \leq \frac{\Delta t}{2\,\nu}\,c_p^2(\Omega_h^{n+1})\,\|\mathbf{g}\|_{0,n+1}^2. \tag{4.123}$$

Using the discrete mass conservation (4.95), we rewrite the term on the right-hand side such that:

$$\|\mathbf{g}\|_{0,n+1}^2 = \int_{\Omega_h^{n+1}} |\mathbf{g}|^2\,d\boldsymbol{x} = g^2\,|\Omega_h^{n+1}| = g^2\,|\Omega_h^0|. \tag{4.124}$$

Thus, (4.123) writes:

$$\|\mathbf{u}_h^{n+1}\|_{0,n+1}^2 - \|\mathbf{u}_h^{n}\|_{0,n}^2 + \nu\,\Delta t\,\|\nabla\mathbf{u}_h^{n+1}\|_{0,n+1}^2 \leq \Delta t\frac{c_p^2(\Omega_h^{n+1})}{\nu}\,g^2\,|\Omega_h^0|$$

Finally, we add over all the time steps to find the unconditional stability result (4.117). That concludes the proof. ■

4.5 Numerical results

In this Section, we now present numerical test cases with the current method introduced in this work. Additionally, we compare the numerical results with three other ones obtained by using different numerical methods. Note that we caption the alternative method presented in this Chapter in the figures by "current".
Firstly, we consider the characteristics ALE method proposed by Maury [100]. In this method, the numerical strategy is closed to our current method. It consists in convecting the free surface by using the method of characteristics. Then, the Navier–Stokes equations are solved by a first semi-implicit Euler scheme in time, and the convective part is computed by using the method of characteristics. The numerical approach is described in Appendix 4.7.2. This method allows to preserve the kinematic condition (2.131) at the free surface but the mass conservation of the water is not ensured. Note that, we caption this method in the figures by "characteristic".
Secondly, we consider also a numerical method based on the free surface Navier–Stokes equations with pressure decomposition (2.128-2.131). The numerical strategy to solve the hydrostatic predictor step is based on the decoupled approach (see Subsection 2.6.2) and the numerical one to solve the non-hydrostatic step is based on the coupled method of the Darcy equations (2.206-2.207) (see Subsection 2.6.1). As a consequence, we recall that the free surface is computed through a wave equation (2.214). This numerical method allows to preserve the global mass conservation of the water but the kinematic condition (2.131) at the free surface is not satisfied. We caption this method in the figures by "Hydro/No-hydro".

Thirdly, we consider the latter numerical method in which we solve the kinematic free surface equation (2.131) at the end of the algorithm in order to satisfy this condition, as referred to Subsection 3.5.2. This equation is solved by using the current scheme for the free surface, i.e. a first order forward Euler scheme in time with a Finite Element symmetric stabilization term. This method allows then to preserve the global mass conservation of the water and the kinematic condition (2.131) at the free surface. We caption this method in the figures by "Hydro/No-hydro + Kinematic".
Fourthly, we consider a numerical method based on the free surface Navier–Stokes equations with pressure decomposition (2.128-2.131). The numerical strategies in time of the hydrostatic predictor step and non-hydrostatic corrector step are based on the decoupled approaches (see Section 2.4.5). First, the hydrostatic predictor step is based on a wave equation on the free surface (2.159). Then, the non-hydrostatic corrector step is based on a pressure Poisson equation on the dynamic pressure (2.161). In order to ensure the free divergence condition of the velocity field of the fluid, we compute an alternative conservative velocity $\mathbf{u}^c$ which is divergence free. For this purpose, we compute a vertical velocity w^c from the continuity equation as done in Telemac-3D (see equation (3.39) of Subsection 3.4.3). The last numerical method is the closest one to the algorithm of Telemac-3D (in this decoupled numerical approach). This method allows then to preserve the global mass conservation of the water. We caption this method in the figures by "T3D-like".

The numerical test cases are performed on a 2D vertical domain (x, z) in order to perform computation on fine meshes and to decrease the computational cost. For the sake of simplicity, we keep the same notations in the sequel of this part. We consider $\mathbb{P}_1$ Lagrangian Finite Element space for the free surface and the Lagrangian pair of Finite Element space $\mathbb{P}_1$-bubble $\times\, \mathbb{P}_1$ for the velocity and the pressure, which is inf-sup stable.

4.5.1 Sloshing wave

The test case deals with non-breaking waves resulting for a relatively large ratio of total depth h to the wave length L_0. For this purpose, we consider a closed basin of length $L = 10\text{m}$ with a water depth at the rest $H = 10\text{m}$. The amplitude of the wave is $\eta_0 = 0.1\text{m}$ and the wave number is $k = \frac{\Pi}{L}$. The bottom is assumed to be flat and fixed to $z = -H$. Starting with zero initial velocity, the flow is driven by an initial free surface

$$\eta(x, 0) = \eta_0 \cos[k\, x]. \tag{4.125}$$

The density of the fluid is $\rho = 10^3 \text{kg} \cdot \text{m}^{-3}$. We neglect the bottom friction and the fluid viscosity ($\mu = 0$). The fluid is only under the influence of the gravity and it puts itself to slosh. The oscillations are periodic since there is no dissipation of energy in the model when η_0 is very small compared to L. A good approximation of the solutions is provided

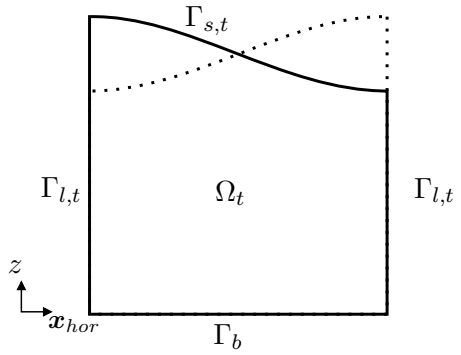

Figure 4.1: Representation of the sloshing test case

by the small amplitude wave theory for the linearized equations, see [43], and is given by:

$$\begin{cases} \eta_{ref} = \eta_0 \cos[k\,x] \cos[\omega t], & (4.126) \\ u_{ref} = \omega\,\eta_0 \dfrac{\cosh[k\,(z+H)]}{\sinh[k\,H]} \sin[k\,x] \sin[\omega\,t], & (4.127) \\ w_{ref} = -\omega\,\eta_0 \dfrac{\sinh[k\,(z+H)]}{\sinh[k\,H]} \cos[k\,x] \sin[\omega\,t], & (4.128) \end{cases}$$

with $\omega^2 = g\,k\,\tanh[k\,H]$. Notice that this reference solution is not a solution of the Euler equations.

We study the convergence of the numerical methods for simulations performed over $T =$ 10s. By an abuse of notations, the reference mesh $\widehat{\mathcal{T}}_h^{3D}$ is built by choosing successively the space steps Δx and Δz equal to 1m, 0.75m, 0.5m, 0.25m and 0.1m. The mesh $\{\mathcal{T}_h^{n,3D}\}_{n=0,\cdots,T-1}$ is built by distributing the vertical layers of $\widehat{\mathcal{T}}_h^{3D}$ using the ALE-Sigma transformation. The time step is chosen in order to satisfy the CFL condition (4.105): it is successively equal to 0.2s, 0.15s, 0.1s, 0.05s and 0.02s. The L^2-norms in time and space of the free surface E_η and the velocity $E_{\mathbf{u}}$ are computed through:

$$E_\eta^2 = \Delta t \sum_{n=0}^{T-1} \int_\omega |\eta_{ref}(t^n) - \eta_h^n|^2 \, dy\, dx, \tag{4.129}$$

$$E_{\mathbf{u}}^2 = \Delta t \sum_{n=0}^{T-1} \int_{\Omega_h^n} |\mathbf{u}_{ref}(t^n) - \mathbf{u}_h^n|^2 \, d\boldsymbol{x}. \tag{4.130}$$

Table 4.1 represents E_η according to the different space and time steps. The curves associated to these errors are drawn in Figure 4.2a. The notation "H/NH" (resp. "H/NH+Kin") refers to the method based on the decomposition of the pressure (resp. decomposition of the pressure with a kinematic equation at the end). We observe that the characteristics and alternative methods give significant better results than the methods based on the

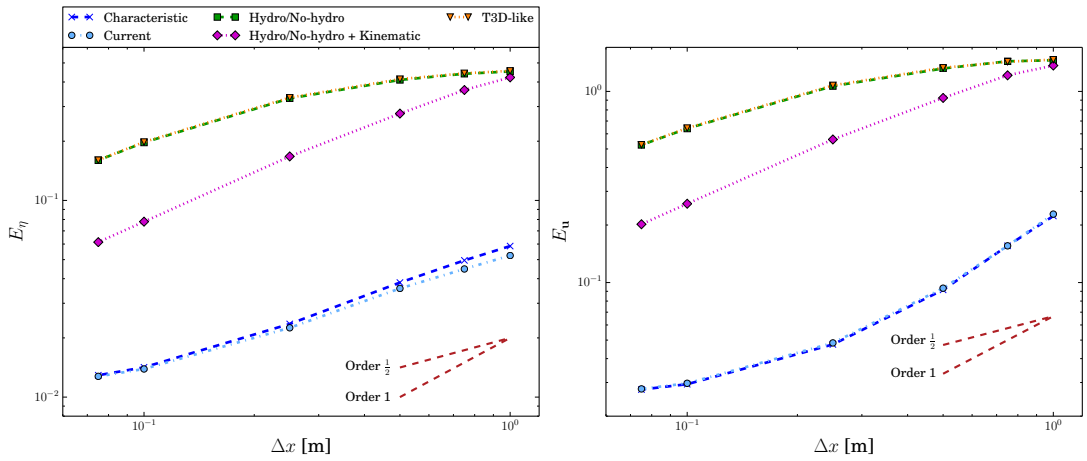

(a) L^2-norm on the free surface E_η (b) L^2-norm on the velocity $E_{\mathbf{u}}$

Figure 4.2: L^2-norms on the free surface and on the velocities with respect to the space step Δx

pressure decomposition. The accuracy of the numerical solution computed with the alternative algorithm is noticeably better. The order of the alternative and characteristics methods is around of size $\mathcal{O}(\Delta x^{\frac{1}{2}})$.

Δx	Δt	Characteristics	Current	H/NH	H/NH+Kin	T3D-like
1	0.2	0.0585	0.0524	0.4525	0.4221	0.4558
0.75	0.15	0.0495	0.0448	0.4404	0.3641	0.4429
0.5	0.1	0.0382	0.0356	0.4098	0.2763	0.4137
0.25	0.05	0.0235	0.0225	0.3302	0.1673	0.3334
0.1	0.02	0.0141	0.0138	0.1969	0.0779	0.1982
0.075	0.015	0.0129	0.0127	0.1600	0.0613	0.1602

Table 4.1: Error E_η at time $T = 10$s

Table 4.2 represents E_u according to the different space and time steps. The curves associated to these errors are drawn in Figure 4.2b. We observe that the characteristics and alternative methods have roughly the same errors. As for the free surface, these methods give significant better results than the numerical methods based on the pressure decomposition. The order of the alternative and characteristics methods is around of size $\mathcal{O}(\Delta x)$. In addition, the order of the algorithm based on the pressure decomposition is of size $\mathcal{O}(\Delta x^{\frac{1}{2}})$. If the kinematic condition is computed at the end of the algorithm, we retrieve an order of size $\mathcal{O}(\Delta x)$ but the error is more important than the ones of the alternative and characteristics methods.

Δx	Δt	Characteristics	Current	H/NH	H/NH+Kin	T3D-like
1	0.2	0.2230	0.2280	1.4555	1.3658	1.4661
0.75	0.15	0.1556	0.1556	1.4374	1.2139	1.4307
0.5	0.1	0.0915	0.0934	1.3179	0.9245	1.3298
0.25	0.05	0.0474	0.0483	1.0663	0.5606	1.0761
0.1	0.02	0.0293	0.0297	0.6393	0.2584	0.6433
0.075	0.015	0.0275	0.0277	0.5247	0.2018	0.5261

Table 4.2: Error E_u at time $T = 10$s

The evolution in time of the free surface and of the velocity components at $x = 0.25$m are represented in Figures 4.3a, 4.4a and 4.5a. Note that the velocity components has been taken at the free surface such that $z = \eta_h^n(0.25)$. The curves correspond to simulation performed with $\Delta x = \Delta z = 0.1$m and $\Delta t = 0.02$s for $T = 10$s. We remark that the numerical solutions computed with the alternative and characteristics algorithms are similar to the analytic solution for all graphes. Notice that we can see a slight diffusion effect for the horizontal velocity. The loss of accuracy for the "Hydrostatic/No-hydro" and "T3D-like" methods observed in Tables 4.1 and 4.2 is due to an important numerical diffusion. It can be observed that the numerical solution is reduced if the kinematic free surface equation is solved at the end, see "Hydrostatic/No-hydro+Kin".

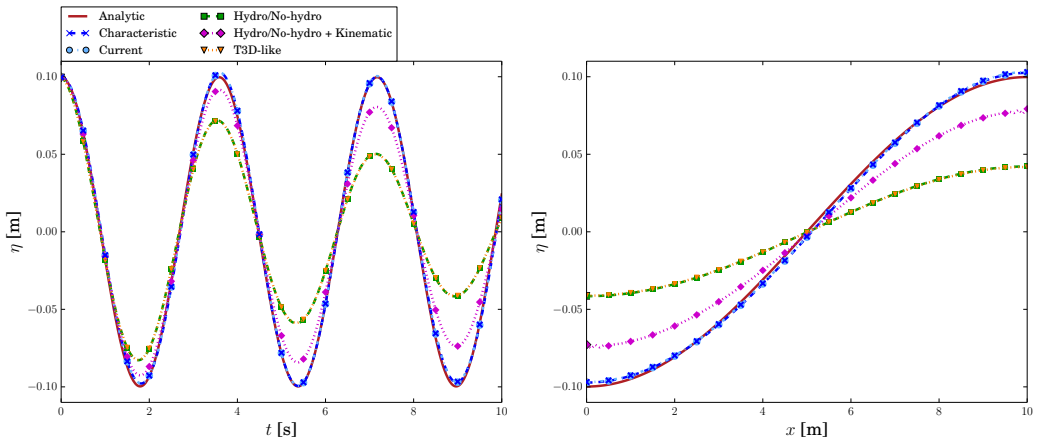

(a) Time evolution at $x = 0.25$m (b) At time $t = 9$s

Figure 4.3: Free surface η for the sloshing test case

The time evolutions (over $T = 10$s) of the free surface and of the velocity at the free surface are represented on the left-hand side in Figures 4.3b, 4.4b and 4.5b. The final profile of the free surface (at time $t = 9$s) is represented in the right-hand side in Figure 4.3b and the ones of the velocity at the free surface (at time $t = 8$s) are represented in 4.4b and 4.5b. As previously mentioned, we observe that the numerical solutions

computed with the alternative and characteristics algorithms reproduced correctly the analytical solutions. Besides, we observe that the numerical solutions computed with the algorithms based on the pressure decomposition are subjected to an important numerical diffusion. For all the numerical solutions, we remark a slight translation to the right with respect to the symmetry point.

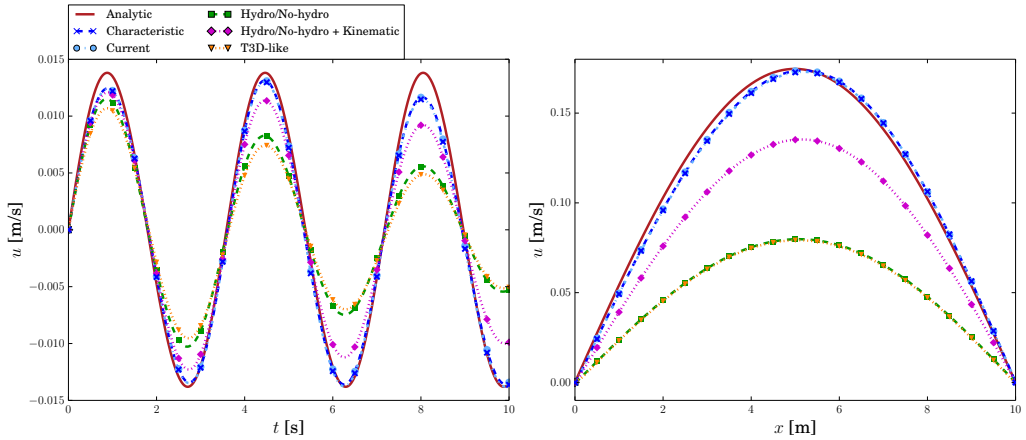

(a) Time evolution at $x = 0.25$m (b) At time $t = 8$s

Figure 4.4: Horizontal velocity u for the sloshing test case

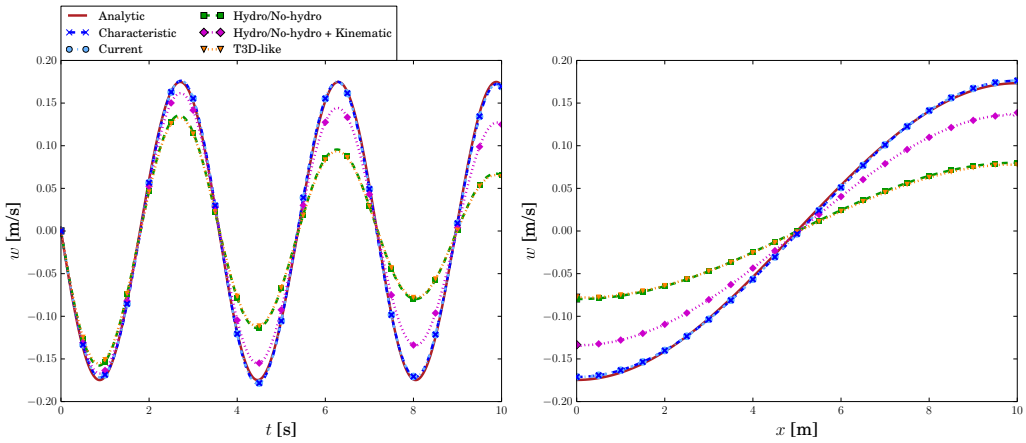

(a) Time evolution at $x = 0.25$m (b) At time $t = 8$s

Figure 4.5: Vertical velocity w for the sloshing test case

We also check the mass conservation for each method. The initial mass is equal to 100m^2. In agreement with the theoretical proofs, the simulations confirm that the current method as well as the methods based on the pressure decomposition exactly ensure the conservation of the mass. For simulations performed with $\Delta x = \Delta z = 0.25$m and $\Delta t = 0.05$s over $T = 10$s, we exhibit that the characteristics algorithm suffers from a slight

loss of mass that increases in time. Indeed, at the final time $t = 10$s, the mass of the water quantity is 99.9952m^2, which remains relatively small here but it could become non negligible for computations on large domains and for long time.

4.5.2 Wave separation

This test case corresponds to the propagation and the reflection of water waves in a closed basin. We consider a square basin with side of $L = 10$m and with a water depth at the rest $H = 1$m. The basin is filled by a fluid whose the initial free surface is a Gaussian shape function of amplitude $\eta_0 = 0.5$m given by:

$$\eta(x,0) = H + \eta_0 \exp\Big[-0.5 \Big(x - \frac{L}{2}\Big)^2 \Big]. \tag{4.131}$$

The peak of the Gaussian function is located at the center of the domain. We assume a flat bottom located at $z = -H$. At the initial time, the velocity field is assumed to be zero. The density and the viscosity of the fluid are respectively $\rho = 10^3\text{kg} \cdot \text{m}^{-3}$ and $\mu = 10^{-1}\text{kg} \cdot (\text{m} \cdot \text{s})^{-1}$. Under the influence of the gravity, the initial free surface separates into two water waves which propagate to the extrema of the basin. At time $t = 3$s, the water waves reflect against the side walls and go back to the center of the basin.

The simulation of the propagation of the water wave is performed over $T = 10$s. The reference mesh $\widehat{\mathcal{T}}_h^{3D}$ is built by choosing the space steps Δx and Δz equal to 0.1m. The mesh $\{\mathcal{T}_h^{n,3D}\}_{n=0,\cdots,T}$ is built by distributing the vertical layers of $\widehat{\mathcal{T}}_h^{3D}$ using the ALE-Sigma transformation. The time step is chosen in order to satisfy the CFL condition (4.105): it is equal to 0.02s. The reference solution for this test case is computed numerically with $\Delta x = \Delta z = 10^{-2}$m and $\Delta t = 10^{-2}$s.

We begin by checking the mass conservation for each method. The initial mass is equal to 11.2533m^2. As mentioned previously, the current method as well as the methods based on the pressure decomposition exactly ensure the conservation of the mass and the characteristics algorithm suffers from a slight loss of mass that increases in time. Here, at the final time $T = 3.5$s, the mass of the water is 11.1786m^2.

Figures 4.6 (see next page) represents the evolution of the free surface at different times. We observe that the numerical solutions of the characteristics and alternative methods match with the reference numerical solutions. We remark that the current method gives the closest numerical solutions to the reference ones. As previously mentioned, we can see that the numerical solutions computed with the methods based on the pressure decomposition suffer from a non negligible numerical diffusion.

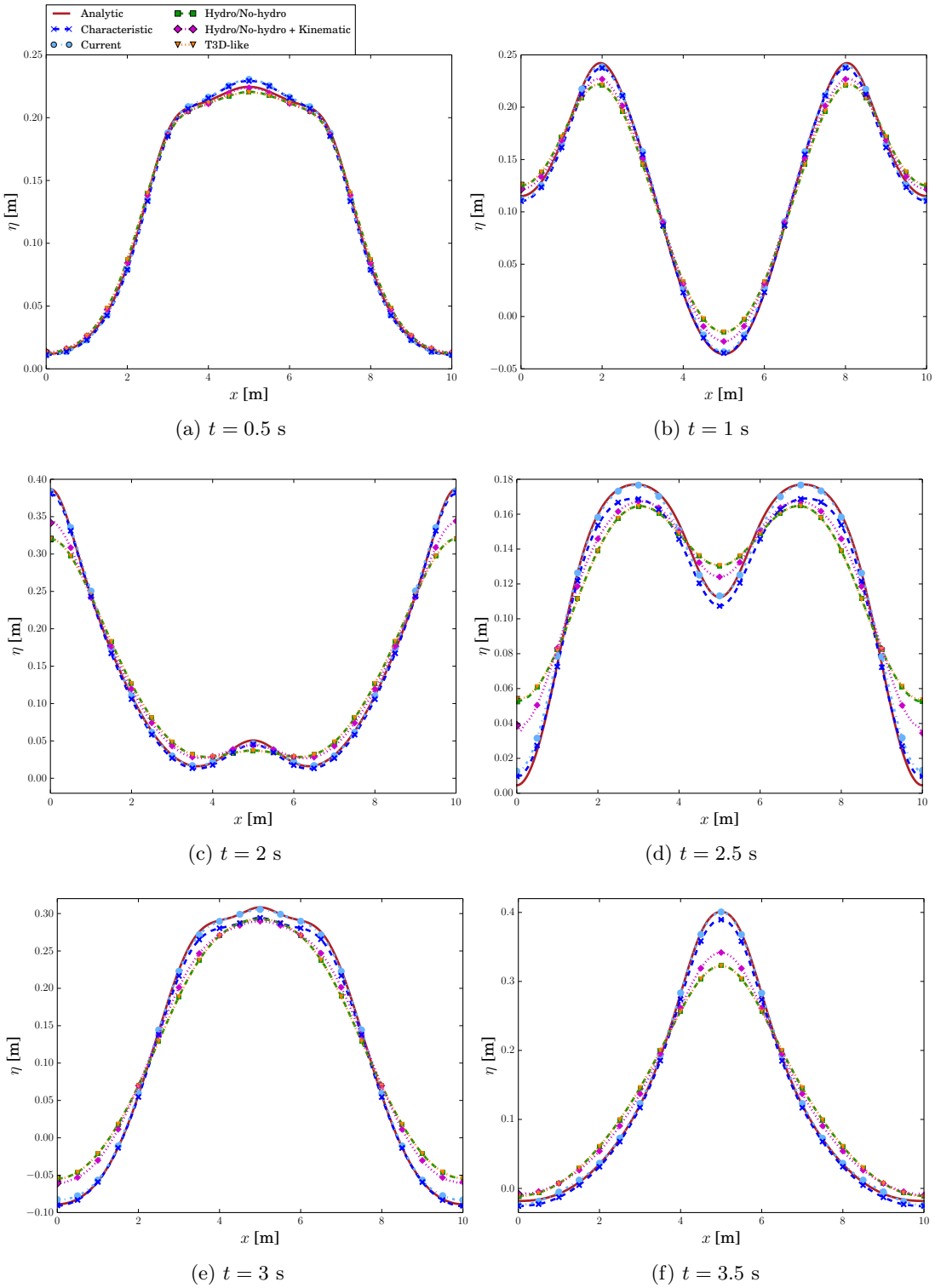

(a) $t = 0.5$ s (b) $t = 1$ s

(c) $t = 2$ s (d) $t = 2.5$ s

(e) $t = 3$ s (f) $t = 3.5$ s

Figure 4.6: Evolution of the free surface for the wave separation test case

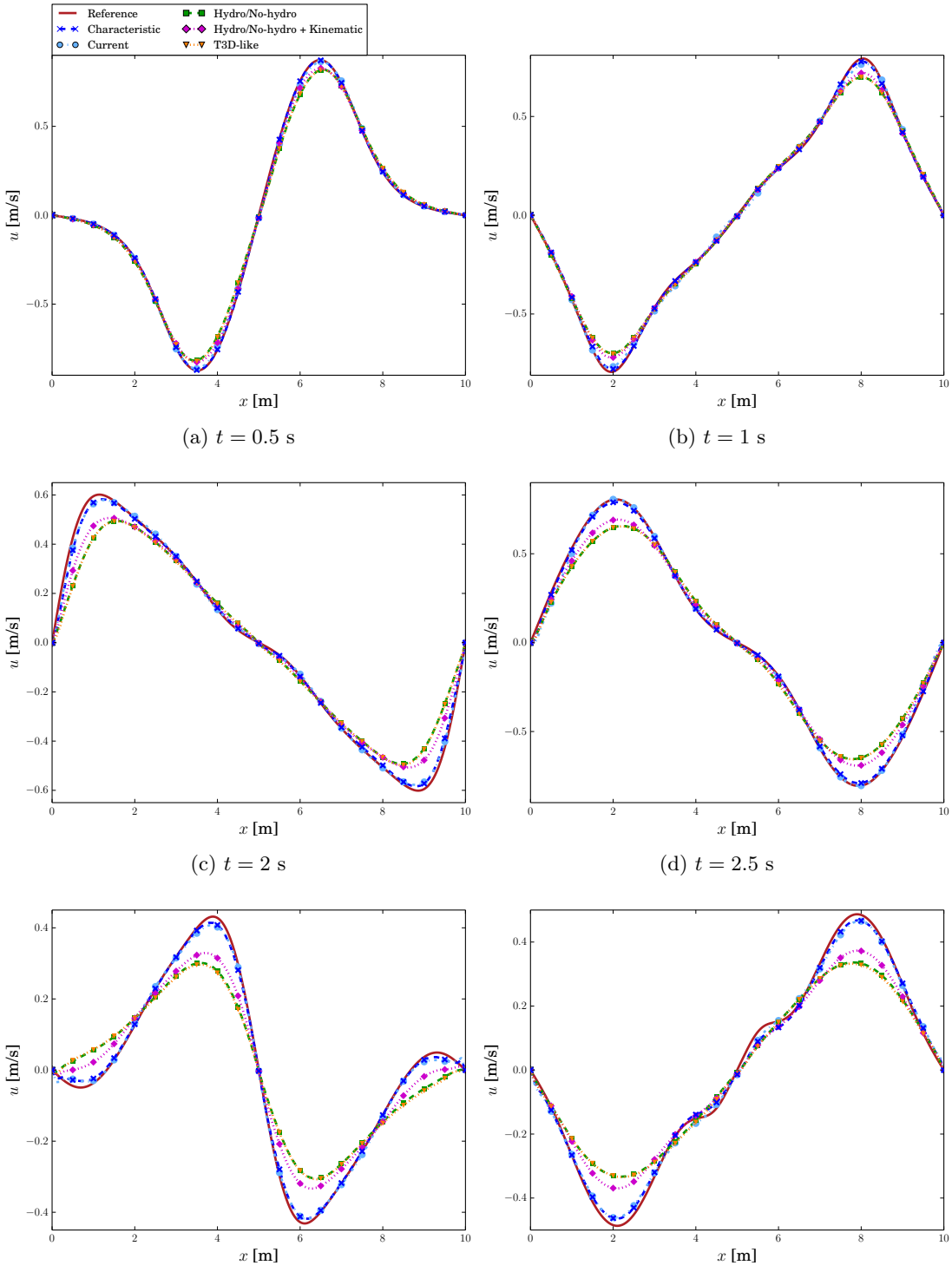

(a) $t = 0.5$ s (b) $t = 1$ s

(c) $t = 2$ s (d) $t = 2.5$ s

(e) $t = 3$ s (f) $t = 3.5$ s

Figure 4.7: Evolution of the horizontal velocity at the free surface for the wave separation test case

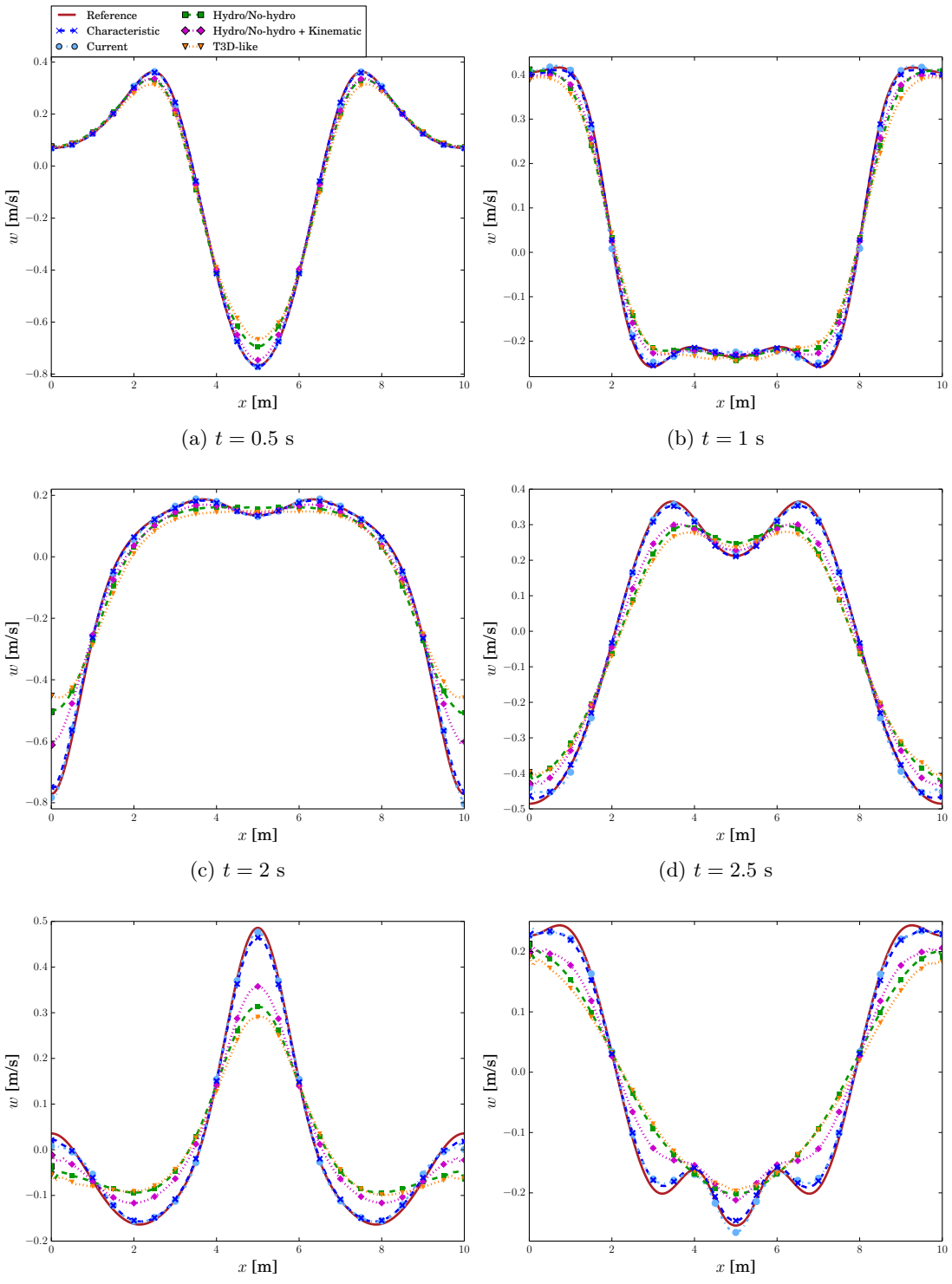

(a) $t = 0.5$ s (b) $t = 1$ s

(c) $t = 2$ s (d) $t = 2.5$ s

(e) $t = 3$ s (f) $t = 3.5$ s

Figure 4.8: Evolution of the vertical velocity at the free surface for the wave separation test case

Figures 4.7 and 4.8 represent respectively the evolution of the horizontal and vertical velocities at the free surface for different times. As observed for the numerical solutions of the free surface, we can see that the characteristics method produces good numerical solutions. We remark that the horizontal velocity computed with the current method does not exactly match to the reference solution. Furthermore, we can observe negative effect on the numerical solutions near the wall. The numerical solution of the characteristics method are better but the same problem near the wall can be observed. As previously mentioned, the methods based on the pressure decomposition suffer from a slight diffusion.

4.5.3 Solitary wave

This case represents the propagation of a solitary wave in a closed basin of length $L = 150\text{m}$ and depth $H = 1\text{m}$. We assume a flat bottom located at $z = -H$. The density is $\rho = 10^3 \text{kg} \cdot \text{m}^{-3}$ and we neglect the viscosity terms. A solution of the solitary wave for the Euler equations can be efficiently approximated by the numerical model of Clamond and Dutykh [39]. At the initial time, the solitary wave is initialized by an initial free surface deformation of amplitude $\eta_0 = 0.5\text{m}$ and horizontal and vertical velocity profiles. During its propagation, the wave keeps its shape and moves with only constant velocity $\|\boldsymbol{u}^{hor}_{h|_{z=\eta_h}}\|_\infty = \sqrt{g\,(H+\eta_0)}$.

The simulation is performed to a final time $T = 20\text{s}$ and we expect that the solitary wave moves over around 76m. The reference mesh $\widehat{\mathcal{T}}_h^{3D}$ is built by choosing successively the space steps Δx and Δz equal to 0.1m. The mesh $\{\mathcal{T}_h^{n,3D}\}_{n=0,\cdots,T}$ is built by distributing the vertical layers of $\widehat{\mathcal{T}}_h^{3D}$ using the ALE-Sigma transformation. The time step is chosen in order to satisfy the CFL condition (4.105): it is equal to $\Delta t = 0.01\text{s}$.

We begin by checking the mass conservation for each method. The initial mass is equal to 151.791m^2 at time $t = 0\text{s}$. In agreement with the theory, the current method enables to preserve the water quantity contrary to the characteristics method. Indeed, for this latter, the mass at time $t = 20\text{s}$ is equal to 151.331m^2. Note that the loss of water quantity for the characteristic algorithm is approximatively of 1%. As expected, the method based on the decomposition of the pressure preserve also the water quantity.

Figure 4.9 corresponds to the free surface profile at different times. Inside each figure, a zoom around the solitary wave is shown. Contrary to the two previous cases, we observe that the methods have difficulties to simulate the propagation of the solitary wave. We can see that they suffer from numerical diffusion, since the amplitude of the wave decreases and its position is deviated to the left. However, at the final time, we remark that the amplitude of the numerical free surface computed with the current method is slightly better than the others one. Furthermore, we can observe that the level of the free surface behind the solitary wave is raised in comparison with the reference curve. Notice also that some oscillations appear behind the solitary wave.

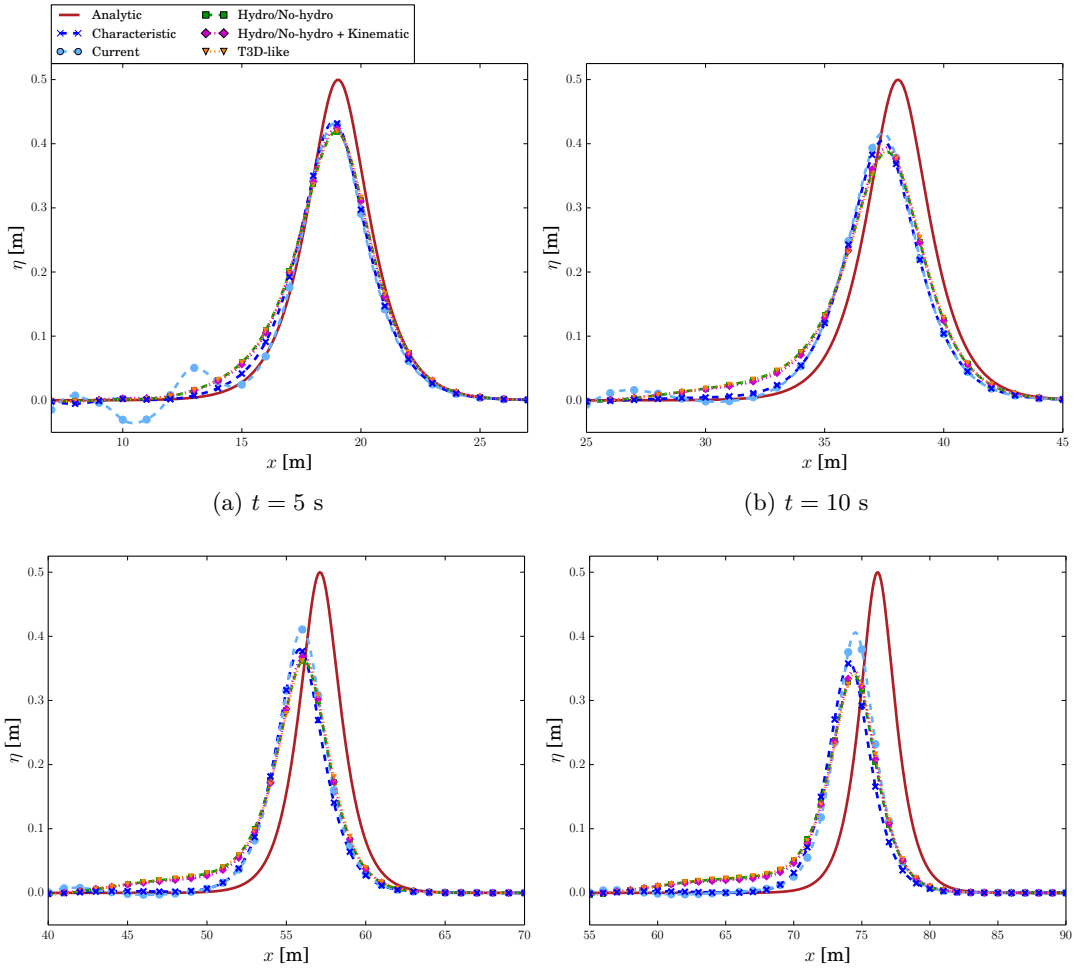

(a) $t = 5$ s (b) $t = 10$ s

(c) $t = 15$ s (d) $t = 20$ s

Figure 4.9: Evolution of the free surface for the solitary wave test case

4.6 Conclusion

In this Chapter, we proposed and analyzed a Finite Elements method for the free surface Navier–Stokes equation in the ALE framework.
On the one hand, the free surface equation is solved by a first order forward Euler scheme in time with a symmetric stabilization term in space. We shown that this scheme allows to preserve the global mass conservation of the water quantity at the discrete level. Besides, we demonstrated the conditional stability under the CFL condition (4.105) and the regularity condition given by $\mathbf{u}_h^n \in W^{1,\infty}(\Omega_h^n)$.
On the other hand, we studied an alternative ALE formulation of the Navier–Stokes equations. In this formulation, the skew symmetric term is adopted and is rewritten with respect to the ALE framework. After discretization in time, this allows to obtain a numerical scheme that is unconditionally stable, independently of the mesh velocity and of an exact divergence free discrete velocity. We demonstrated this stability result under the Lipschitz regularity condition on the free surface and the hypothesis that the mass conservation of the water quantity is preserved in time.
Finally, we performed numerical test cases and we compared the current method to other numerical methods. In agreement with the theory, we verified numerically that the current method ensures the global mass conservation. Besides, this method is around of size $\mathcal{O}(\Delta x^{\frac{1}{2}})$ on the free surface and of size $\mathcal{O}(\Delta x)$ on the velocity. The numerical results are close to the ones computed by a characteristics ALE method. These both methods produce better results than the numerical methods based on the pressure decomposition. Nevertheless, the alternative method does not ensure the positivity of the water quantity. A perspective of improvement will be to ensure this property and can be relied on the work of Burman [24].

4.7 Appendix

In this Appendix, we describe the numerical methods used in the numerical Section 4.5 and the method of characteristic.

4.7.1 Method of characteristics

Let us consider the following advection equation in $\Omega_t \times [0,T]$:

$$\left.\frac{\partial \mathbf{u}}{\partial t}\right|_{\widehat{\Omega}} + (\mathbf{u}-\mathbf{c})\nabla\mathbf{u} = 0. \tag{4.132}$$

The method of characteristics consists in computing the pathlines of the flow. We consider the characteristic $\boldsymbol{X}_\tau(\boldsymbol{x},\cdot) : \mathbb{R}^+ \to \Omega_\tau$ defined on the domain Ω_τ. It is a solution of the following Cauchy problem:

$$\begin{cases} \dfrac{\partial \boldsymbol{X}_\tau(s)}{\partial s} = (\mathbf{u}_\tau - \mathbf{c}_\tau)(\boldsymbol{X}_\tau(s)), & (4.133) \\ \boldsymbol{X}_\tau(\boldsymbol{x}) = \boldsymbol{x}. & (4.134) \end{cases}$$

At each time step $s \in \mathbb{R}^+$, we can define:

$$\boldsymbol{X}_\tau(s;\tau,\boldsymbol{x}) = \widehat{\mathcal{A}}_s \circ \widehat{\mathcal{A}}_\tau^{-1} \circ \boldsymbol{X}_\tau(\boldsymbol{x},s), \tag{4.135}$$

where $\widehat{\mathcal{A}}_t$ is the mapping between the reference domain $\widehat{\Omega}$ and the current domain Ω_t. The relation (4.135) expresses the position $\boldsymbol{x} = \widehat{\mathcal{A}}_t \circ \widehat{\mathcal{A}}_s^{-1}(\boldsymbol{x}_\tau)$ of a pseudo-particle advected by the velocity $\mathbf{u}-\mathbf{c}$ at time t.

The total derivative on the velocity $\mathbf{u}$ reads:

$$\begin{aligned} \frac{d}{dt}\mathbf{u}_\tau(\boldsymbol{x}_\tau(t),t) &= \frac{\partial \mathbf{u}_\tau}{\partial t}(\mathbf{X}_\tau(t),t) + \frac{\partial \mathbf{X}_\tau(t)}{\partial t}\cdot\nabla\mathbf{u}_\tau(\mathbf{X}_\tau(t),t) \\ &= \left.\frac{\partial \mathbf{u}}{\partial t}\right|_{\widehat{\Omega}}(\mathbf{X}_\tau(t),t) + \frac{\partial \mathbf{X}_\tau(t)}{\partial t}\cdot\nabla\mathbf{u}_\tau(\mathbf{X}_\tau(t),t). \end{aligned} \tag{4.136}$$

At $t=\tau$, the advection equation in the ALE framework is:

$$\begin{aligned} \frac{d}{dt}(f_\tau(\mathbf{X}_\tau(t),t) &= \left.\frac{\partial f}{\partial t}\right|_{\widehat{\Omega}} + (\mathbf{u}_\tau - \mathbf{c}_\tau)\cdot\nabla f_\tau(\boldsymbol{x},t) \\ &= 0. \end{aligned} \tag{4.137}$$

Discretized in time at the first order, the equation (4.135) becomes:

$$\frac{\mathbf{u}_n^{n+1}\circ\mathbf{X}_n^{n+1} - \mathbf{u}^n}{\Delta t} = 0, \tag{4.138}$$

where $\mathbf{X}_n^{n+1}$ is the solution at time $t=t^n$ of the following Cauchy problem, defined on the domain Ω^n:

$$\begin{cases} \dfrac{\partial \mathbf{X}_n(t)}{\partial t} = (\mathbf{u}^n - \mathbf{c}^n)(\mathbf{X}_n(t)), & (4.139) \\ \mathbf{X}_n(t^n) = \boldsymbol{x}. & (4.140) \end{cases}$$

4.7.2 Characteristics ALE method for the free surface Navier–Stokes equations

In this Subsection, we recall the fully discrete formulation of the characteristics ALE method for the free surface Navier–Stokes, proposed by Maury [100]. We consider $0 = t^0 < t^1 < ... < t^T = T$ the decomposition of the time interval $[0, T]$ into T equal time intervals. We denote the uniform time step by $\Delta t = t^{n+1} - t^n$, where $0 \leq n \leq T-1$. As previously defined, we consider $\mathcal{T}_h^{2D}$ the triangulation of the horizontal domain ω. The discrete domain is $\omega_h = \omega$. We denote by $\widehat{\mathcal{T}}_h^{3D}$ the triangulation of the reference domain $\widehat{\Omega}$. The triangulation of the domain Ω^n is denoted by $\mathcal{T}_h^{n,3D}$. This triangulation is built from $\widehat{\mathcal{T}}_h^{3D}$ through the discrete ALE mapping $\mathcal{A}_{h,n}$, as introduced in Subsection 2.2.4. The discrete domain of Ω^n at time t^n is denoted Ω_h^n. We consider $\mathcal{V}_{0,h}^n$ and $\mathcal{Q}_h^n$ the discrete functional spaces on the velocity and the pressure, given in (4.81) and (4.80), respectively. The discrete functional space on the free surface is $\mathcal{M}_h(\omega) \subset L^2(\omega)$. We denote by $(\mathbf{u}_h^n, p_h^n, \eta_h^n)$ the semi-discrete in space solution of $(\mathbf{u}(\boldsymbol{x}, t), p(\boldsymbol{x}, t), \eta(x, y, t))$. By analogy, we denote by $\mathbf{c}_h^n$ the mesh velocity between Ω_h^n and Ω_h^{n+1}, defined in Ω_h^n.

We suppose that at time t^n, solutions $\eta_h^n \in \mathcal{M}_h(\omega)$ and $(\mathbf{u}_h^n, p_h^n) \in \mathcal{V}_{0,h}^n \times \mathcal{Q}_h^n$ are known. The free surface function η_h^{n+1} is computed by the characteristics method such that:

$$\eta_h^{n+1} = \eta_h^n(x - \Delta t\, \boldsymbol{u}_{h|_{z=\eta_h^n}}^{n,hor}, z - \Delta t\, w_{h|_{z=\eta_h^n}}^n). \tag{4.141}$$

Once the new free surface is known, the mesh is updated. Afterwards, we compute the velocity $\mathbf{u}_h^{n+1}$ and the pressure p_h^{n+1} by solving the following discrete variational problem:

$$\begin{cases} \text{Find } (\mathbf{u}_h^{n+1}, p_h^{n+1}) \in \mathcal{V}_{h,0}^{n+1} \times \mathcal{Q}_h^{n+1} \text{ such that } \forall (\mathbf{v}_h^{n+1}, q_h^{n+1}) \in \mathcal{V}_{h,0}^{n+1} \times \mathcal{Q}_h^{n+1} \\ \\ \displaystyle\int_{\Omega^{n+1}} \mathbf{u}_h^{n+1} \cdot \mathbf{v}_h^{n+1} + \nu \Delta t \int_{\Omega^{n+1}} \nabla \mathbf{u}_h^{n+1} : \nabla \mathbf{v}_h^{n+1} - \frac{\Delta t}{\rho} \int_{\Omega^{n+1}} p_h^{n+1} \nabla \cdot \mathbf{v}_h^{n+1} \\ \qquad = \displaystyle\int_{\Omega^{n+1}} \Pi_{\mathcal{V}_h}(\mathbf{u}_{h,n+1}^n) \circ \mathbf{X}_{h,n+1}^n \mathbf{v}_h^{n+1} - \Delta t \int_{\Omega^{n+1}} \mathbf{g} \cdot \mathbf{v}_h^{n+1} \qquad (4.142) \\ \\ \displaystyle\int_{\Omega^{n+1}} q_h^{n+1} \nabla \cdot \mathbf{u}_h^{n+1} = 0 \qquad (4.143) \end{cases}$$

where $\mathbf{X}_n^{n+1}$ is the ALE characteristic function which is solution of the Cauchy problem (4.140). The interpolation operator associated to the Finite Element space $\mathcal{V}_h$ is denoted by $\Pi_{\mathcal{V}_h}$.

Chapter 5

Mild-slope equation

Contents

This Chapter is the result of a collaboration with Emmanuel Audusse, Olivier Lafitte and Benjamin Melinand. The Section named "Approximate analytical solution for the mild-slope equation" is extracted from a proceeding conference paper [7] written in collaboration with Emmanuel Audusse, Olivier Lafitte, Agnès Leroy, Benjamin Melinand and Chi-Tuân Pham.

5.1 Introduction

Following an initial goal about comparisons between the Telemac-3D and Artemis (another software developed by EDF R&D), we take an interest in the study of the mild-slope equation. Let us precise that Artemis allows to simulate linear water waves in harbor or coastal areas by solving this equation numerically. More precisely, we are interested by the derivation and the validity domain of the mild-slope equation. These studies are presented in this Chapter.

The study of the propagation of water waves presents a major interest for academic and industrial applications. The water waves are subject to diffraction or refraction phenomena in coastal and harbor area. These effects are caused respectively by the presence of islands or structures and by the gradual variation of the topography. The mild-slope equation is a classical model developed by Berkhoff [10, 11], which combines the representation of these effects for slowly varying bottoms without restrictions on the water depth.

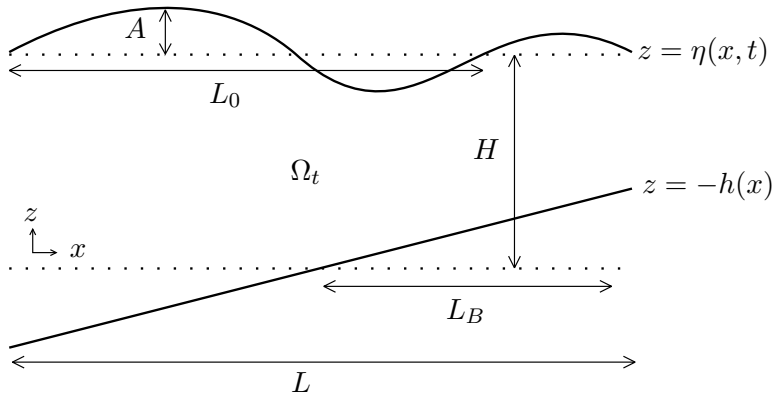

Figure 5.1: Typical scale and domain Ω_t

In this Chapter, we model the sea by an inviscid and homogeneous fluid (of constant density ρ) under the influence of the gravity $\mathbf{g} = -g\,\mathbf{e}_z$ and bounded from below by a non-flat topography and from above by a free surface η such that

$$\begin{aligned} \eta :]0, L[\times \mathbb{R}^+ &\to \mathbb{R} \\ (x,t) &\mapsto \eta(x,t), \end{aligned} \tag{5.1}$$

with L the length of the domain. We neglect the surface tension and the atmospheric pressure is assumed to be constant. The flow is supposed to be irrotational and incompressible. We assume that the bottom and the free surface are single-valued functions. We denote by $x \in \mathbb{R}$ the horizontal variable and $z \in \mathbb{R}$ the vertical variable. The characteristic water depth is denoted by H. The water depth at rest is h such that

$$\begin{aligned} h :]0, L[&\to \mathbb{R}^+ \\ x &\mapsto h(x), \end{aligned} \tag{5.2}$$

and the non-flat topography is defined by $z = -h$. Throughout this chapter, we assume that

$$\exists\, h_{min}, h_{max} > 0, \quad h_{min} \leq h \leq h_{max}, \tag{5.3}$$

and

$$\exists\, M_1, M_2 > 0, \ \|d_x h\| \leq M_1 \ \text{ and } \ \|d_{xx} h\| \leq M_2. \tag{5.4}$$

The water depth is $h + \eta$. At time t, the water occupies the domain $\Omega_t = \{(x, z) \in \mathbb{R}^2 \mid 0 < x < L, \ -h(x) < z < \eta(x, t)\}$. We denote by $\mathbf{u}$ the velocity of the fluid and Φ the velocity potential such that

$$\begin{aligned} \mathbf{u} :\ \Omega_t \times \mathbb{R}^+ &\to \mathbb{R}^2 \qquad \text{and} \qquad \Phi :\ \Omega_t \times \mathbb{R}^+ \to \mathbb{R} \\ (x, z, t) &\mapsto \mathbf{u}(x, z, t), \qquad\qquad (x, z, t) \mapsto \Phi(x, z, t). \end{aligned} \tag{5.5}$$

Notice that from Hodge's theorem and the irrotationality of the fluid velocity there exists a function Φ such that $\mathbf{u} = \nabla\Phi$. Based on this equality, the equations governing the motion of the fluid are the free surface Bernoulli equations (deduced from the momentum and continuity equations):

$$\begin{cases} \partial_t \Phi + \dfrac{1}{2} |\nabla\Phi|^2 + g\, z = -\dfrac{1}{\rho}\, p, & \text{in } \Omega_t, \qquad (5.6) \\ \Delta\Phi = 0, & \text{in } \Omega_t, \qquad (5.7) \end{cases}$$

where p is the pressure in the fluid domain. Since p is defined up to a constant in an incompressible model, we assume that the atmospheric pressure is zero in the following. The boundary conditions are:

$$\begin{cases} \partial_t \eta - \partial_x \Phi\, \partial_x \eta + \partial_z \Phi = 0, & \text{on } z = \eta, \qquad (5.8) \\ \partial_z \Phi + d_x h\, \partial_x \Phi = 0, & \text{on } z = -h. \qquad (5.9) \end{cases}$$

They model the fact that the fluid particles do not cross the bottom or the surface.

The knowledge of the free surface elevation η and the trace of the velocity potential at the free surface $\psi = \Phi_{|_{z=\eta}}$ fully define the flow (see Lannes [90]). The velocity potential Φ is recovered with (5.7) and (5.9).

$$\begin{cases} \Delta\Phi = 0, & \text{on } \Omega_t, \qquad (5.10) \\ \Phi_{|_{z=\eta}} = \psi, & \text{at } z = \eta \qquad (5.11) \\ \partial_z \Phi + d_x h\, \partial_x \Phi = 0, & \text{at } z = -h. \qquad (5.12) \end{cases}$$

The free surface elevation η and the trace of the velocity potential at the free surface $\psi = \Phi_{|_{z=\eta}}$ are computed from the following two scalar evolution equations at $z = \eta$:

$$\begin{cases} \partial_t \eta - \partial_x \Phi \, \partial_x \eta + \partial_z \Phi = 0, & (5.13) \\ \partial_t \psi + \dfrac{1}{2} |\nabla \psi|^2 + g \, \eta = 0. & (5.14) \end{cases}$$

These equations are too complicated to solve in many physical applications. Linearizing the problem, Airy [3] and Stokes [123] developed the linear wave theory in order to simplify the problem. It leads to studying the following problem:

$$\begin{cases} \Delta \Phi = 0, \quad \text{on } \Omega, & (5.15) \\ \partial_{tt} \Phi + g \, \partial_z \Phi = 0, \quad \text{at } z = 0, & (5.16) \\ \partial_z \Phi + d_x h \, \partial_x \Phi = 0, \quad \text{on } z = -h, & (5.17) \end{cases}$$

where $\Omega = \{(x, z) \in \mathbb{R}^2 \mid 0 < x < L, \ -h(x) < z < 0\}$, as represented on Figure 5.2.

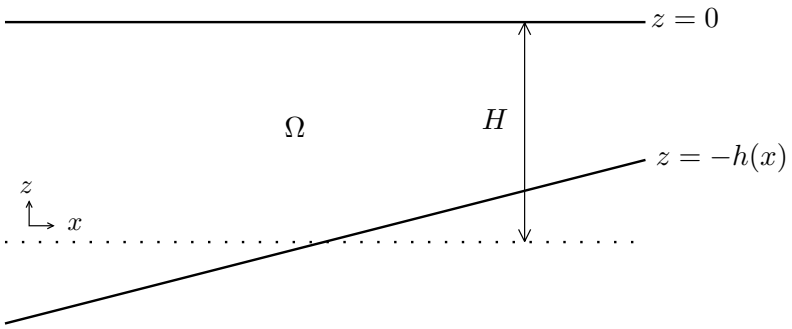

Figure 5.2: Domain Ω

Notice that one can derive this equation after adimensionalizing the equations and assuming that the parameter $\frac{A}{H}$ is small, where A is the amplitude of the wave (see Chapter 1 of [90] and Figure 5.1).

In this chapter, we are interested in travelling waves. We assume in the sequel that

$$\Phi = \phi \, \cos[\omega \, t], \tag{5.18}$$

where ω is the wave pulsation and ϕ a real potential function such that

$$\begin{aligned} &\phi : \ \Omega \to \mathbb{R} \\ &(x, z) \mapsto \phi(x, z). \end{aligned} \tag{5.19}$$

Substituting this expression in (5.15-5.17), we get:

$$\begin{cases} \Delta\phi = 0, & \text{on } \Omega, \quad (5.20) \\ \partial_z\phi - \dfrac{\omega^2}{g}\,\phi = 0, & \text{at } z = 0, \quad (5.21) \\ \partial_z\phi + d_x h\ \partial_x\phi = 0, & \text{at } z = -h(x). \quad (5.22) \end{cases}$$

When $h = h_0$ is constant, a solution of the system (5.20-5.22) is :

$$\phi(x,z) = Z(z,h_0)\ \cos[k_0\,x] \tag{5.23}$$

with

$$\begin{aligned} Z :]-h_0, 0[&\to \mathbb{R}^+ \\ z &\mapsto Z(z) = \frac{\cosh[k_0(z+h_0)]}{\cosh[k_0\,h_0]}, \end{aligned} \tag{5.24}$$

and where k_0 is the unique positive solution of the following dispersion relation:

$$\omega^2 = g\ k_0 \tanh[k_0\,h_0]. \tag{5.25}$$

Define by analogy, where h is general,

$$\begin{aligned} k :]h_{min}, h_{max}[&\to \mathbb{R}^+ \\ h &\mapsto k(h), \end{aligned} \tag{5.26}$$

the unique positive solution of the dispersion relation

$$\omega^2 = g\ k(h) \tanh[k(h)\,h]. \tag{5.27}$$

The function Z is in a general case such that

$$\begin{aligned} Z :]-h, 0[\times]h_{min}, h_{max}[&\to \mathbb{R}^+ \\ (z,h) &\mapsto Z(z,h) = \frac{\cosh[k(h)(z+h)]}{\cosh[k(h)\,h]}, \end{aligned} \tag{5.28}$$

For a slowly varying bottom (i.e. $d_x h \ll 1$), Berkhoff [10, 11] assumed that

$$\begin{aligned} \frac{\phi}{Z} : \mathbb{R}^2 &\to \mathbb{R} \\ (x,z) &\mapsto \frac{\Phi(x,z)}{Z(z,h(x))}, \end{aligned} \tag{5.29}$$

has a small dependence on the vertical coordinate z and then searched for an approximate solution of (5.20-5.22) similar to (5.23), of the form:

$$\begin{aligned} \phi_{app} : \Omega &\to \mathbb{R} \\ (x,z) &\mapsto \phi_{app}(x,z) = Z(z,h(x))\,\varphi(x), \end{aligned} \tag{5.30}$$

where φ is a function from $]0, L[$ to $\mathbb{R}$. After algebraic manipulations (integration in z) and approximations that will be detailed hereafter (see Subsection 5.2.1), the author showed that φ has to satisfy an simplified equation on φ, called the mild-slope equation:

$$d_x\big(T\, d_x\varphi\big) + k^2\, T\, \varphi = 0, \quad \text{in }]0, L[, \tag{5.31}$$

where

$$\begin{aligned} T :\,&]0, L[\to \mathbb{R} \\ &x \mapsto T(x) = \int_{-h(x)}^{0} \big[Z(z, h(x))\big]^2\, dz \\ &\qquad = \frac{1}{2\cosh[k(h(x))\, h(x)]^2} \left(h(x) + \frac{\sinh[2\, k(h(x))\, h(x)]}{2\, k(h(x))}\right). \end{aligned} \tag{5.32}$$

Historically, the mild-slope equation in the case of shallow waters has been proposed by Eckart [50]. Independently, Berkhoff [10, 11] derived this equation without restriction on the water depth. Many authors studied the derivation and the validity of the mild-slope equation. For example, Mei et al. [101], Dingemans [47] proposed a derivation using an Hamiltonian variational principle. An alternative derivation based on Luke's variational principle was proposed by Booij [16]. Tsay and Liu [128] studied the validity of the mild-slope equation and showed that it produces accurate results for bottom slopes up to 1:1 when waves are propagating perpendicularly to the bathymetry contour lines. For general directions of wave propagation, Booij [17] showed that the accuracy of results is acceptable for bottom profiles with slopes up to 1:3, which is often enough for practical applications. In the shallow water regime, it has been observed in [16, 96] that a solution of the mild-slope equation is close to a solution of the linear shallow water equation. Conversely, in deep water regime, it is also known that a solution of the mild-slope equation is close to a solution of the Helmholtz equation [11].
This chapter is devoted to the study of the mild-slope equation. We revisit the derivation and the validity domain of the mild-slope equation in different regimes through asymptotic and numerical studies. In the numerical part, we study the numerical solutions for numerical test cases in which the regime is transitory (i.e. from deep to intermediate waters and from intermediate to shallow waters). Additionally, we exhibit an analytical approximate solution of the mild-slope equation for a family of slopes depending on two parameters: the mean slope and the characteristic water depth. Through quantitative and qualitative studies, we examine the order of accuracy and the validity of these approximate analytical solutions.

This chapter is organized as follows: in Sections 5.2 and 5.3, we begin by considering the mild-slope equation in different asymptotic regimes. Then, in Section 5.4, we present the analytical approximate solution of the mild-slope equation and we study its order of accuracy.

5.2 Derivations of linear asymptotic models

This part is devoted to asymptotic derivations of the mild-slope equation, the linear shallow water equation and the Helmholtz equation. If φ is a solution of one of these equations, we show that ϕ (given by (5.30)) is a solution of the linear water wave equations with an order that we will identify. In order to derive these asymptotic models from the linear water wave equation, we introduce some dimensionless parameters linked to the physical scales of the system. The first one is the ratio between the water depth H and the characteristic wave length L_0 at the free surface. We denote by $\sigma = \frac{H}{L_0}$ the shallowness parameter. The second one is the ratio between H and the characteristic wave length of the bottom L_B. We denote by $\alpha = \frac{H}{L_B}$. In practice, we define L_B such that α is the mean slope of the bottom. In the following, we make the assumption that α is not large (typically $\alpha \leq 1$). We denote by $\delta = \frac{\omega^2}{g} L_0$. As represented in Figure 5.1, we also adimensionalize the variables by

$$x = L_0\,\tilde{x}, \quad x = L_B\,\widehat{x}, \quad z = H\,\tilde{z}. \tag{5.33}$$

The functions are adimensionalized by:

$$\begin{aligned} \tilde{h} : \Big]0, \frac{L}{L_B}\Big[&\to \mathbb{R} \\ \widehat{x} &\mapsto \tilde{h}(\widehat{x}) = \frac{1}{H}\, h\big(L_B \widehat{x}\big), \end{aligned} \tag{5.34}$$

and

$$\begin{aligned} \tilde{k} : \Big]\frac{h_{min}}{H}, \frac{h_{max}}{H}\Big[&\to \mathbb{R}^+ \\ \tilde{h} &\mapsto \tilde{k}(\tilde{h}) = L_0\, k\big(H\tilde{h}\big). \end{aligned} \tag{5.35}$$

Notice that in (5.34) and (5.35), we choose to adimensionalize the horizontal variation by L_B rather than L_0 in order to bring out α in the adimensional equations. In the asymptotic derivations, we use the fact that $\widehat{x} = \dfrac{L_0}{L_B}\tilde{x} = \dfrac{\alpha}{\sigma}\tilde{x}$

The linear water wave equation (5.20-5.22) becomes in dimensionless form:

$$\begin{cases} \sigma^2\, \partial_{\tilde{x}\tilde{x}}\tilde{\phi} + \ \partial_{\tilde{z}\tilde{z}}\tilde{\phi} = 0, & \text{on } \tilde{\Omega}, \quad (5.36) \\ \partial_{\tilde{z}}\tilde{\phi} - \delta\,\sigma\,\tilde{\phi} = 0, & \text{at } \tilde{z} = 0, \quad (5.37) \\ \partial_{\tilde{z}}\tilde{\phi} + \sigma\,\alpha\, d_{\widehat{x}}\tilde{h}\ \partial_{\tilde{x}}\tilde{\phi} = 0, & \text{at } \tilde{z} = -\tilde{h}, \quad (5.38) \end{cases}$$

where $\tilde{\Omega} = \{(\tilde{x}, \tilde{z}) \in \mathbb{R}^2 \mid 0 < \tilde{x} < \frac{L}{L_0}, \ -\tilde{h}\big(\frac{\alpha}{\sigma}\tilde{x}\big) < \tilde{z} < 0\}$.

Notice that the dispersion relation (5.27) writes in dimensionless form:

$$\delta = \tilde{k}\tanh\big[\sigma\tilde{h}\,\tilde{k}\big] \tag{5.39}$$

$$\Leftrightarrow \quad \delta\,\sigma\,\tilde{h} = \sigma\tilde{k}\tilde{h}\tanh\big[\sigma\tilde{k}\tilde{h}\big]. \tag{5.40}$$

This relation can be rewritten as follows:

$$\frac{\delta}{\sigma} = \left(\frac{\omega\, L_0}{\sqrt{g\, H}}\right)^2 = \frac{\tilde{k}}{\sigma}\tanh\left[\sigma\tilde{k}\tilde{h}\right]. \tag{5.41}$$

The numerator $(\omega\, L_0)$ expresses the velocity of the incident wave and the denominator $(\sqrt{g\, H})$ is the velocity of the surface wave in shallow water case. On the one hand, we have that in shallow water regime $\frac{\delta}{\sigma} = 1$. On the other hand, we have that in deep water regime $\frac{\delta}{\sigma} = \mathcal{O}(1)$. We then consider only cases where $\frac{\delta}{\sigma} = \mathcal{O}(1)$. In the case where $\frac{\delta}{\sigma} \gg \mathcal{O}(1)$ is considered, the adimensionalization of the wave number k has to be changed since $\tilde{k} \sim \mathcal{O}(\sigma^{-\frac{1}{2}})$.

Let us denote $I_{\tilde{x}} =]0, \frac{L}{L_0}[$, $I_{\tilde{z}} =]-\tilde{h}\big(\frac{\alpha}{\sigma}\tilde{x}\big), 0[$ and $I_{\tilde{h}} =]\frac{h_{min}}{H}, \frac{h_{max}}{H}[$. The operators of the Laplace equation (5.36) and of the equations at $\tilde{z} = 0$ and at $\tilde{z} = -\tilde{h}$ are respectively denoted by $\tilde{\mathsf{L}}$, $\tilde{\mathsf{S}}$ and $\tilde{\mathsf{Bo}}$ such that

$$\begin{aligned}\tilde{\mathsf{L}} : C^2\big(I_{\tilde{x}} \times I_{\tilde{z}}\big) &\to C^0\big(I_{\tilde{x}} \times I_{\tilde{z}}\big)\\ \tilde{f} &\mapsto \tilde{\mathsf{L}}(\tilde{f}) = \sigma^2\, \partial_{\tilde{x}\tilde{x}}\tilde{f} + \partial_{\tilde{z}\tilde{z}}\tilde{f},\end{aligned} \tag{5.42}$$

$$\begin{aligned}\tilde{\mathsf{S}} : C^2\big(I_{\tilde{x}} \times I_{\tilde{z}}\big) &\to C^0\big(I_{\tilde{x}}\big)\\ \tilde{f}_{|\tilde{z}=0} &\mapsto \tilde{\mathsf{S}}\big(\tilde{f}_{|\tilde{z}=0}\big) = \big(\partial_{\tilde{z}}\tilde{f}\big)_{|\tilde{z}=0} - \delta\,\sigma\,\tilde{f}_{|\tilde{z}=0},\end{aligned} \tag{5.43}$$

$$\begin{aligned}\tilde{\mathsf{Bo}} : C^2\big(I_{\tilde{x}} \times I_{\tilde{z}}\big) &\to C^0\big(I_{\tilde{x}}\big)\\ \tilde{f} &\mapsto \tilde{\mathsf{Bo}}\big(\tilde{f}\big) = \big(\partial_{\tilde{z}}\tilde{f}\big)_{|_{\tilde{z}=-\tilde{h}}} + \sigma\,\alpha\, d_{\tilde{x}}\tilde{h}\,\big(\partial_{\tilde{x}}\tilde{f}\big)_{|_{\tilde{z}=-\tilde{h}}}.\end{aligned} \tag{5.44}$$

5.2.1 Intermediate water regime

In this Subsection, we assume an intermediate depth with a slowly varying bottom such that $\alpha \ll \sigma < 1$.

Mild-slope equation

We first derive the mild-slope equation leading to an approximate solution of a depth-average version of the Laplace equation (5.36). We prove that this approximate solution is of order $\mathcal{O}(\sigma\,\alpha^2)$. In adimensionalized quantities, (5.30) rewrites:

$$\begin{aligned}\tilde{\phi}_{app} : \tilde{\Omega} &\to \mathbb{R}\\ (\tilde{x}, \tilde{z}) &\mapsto \tilde{\phi}_{app}(\tilde{x}, \tilde{z}) = \tilde{Z}(\tilde{z}, \tilde{h}(\frac{\alpha}{\sigma}\tilde{x}))\,\tilde{\varphi}(\tilde{x}),\end{aligned} \tag{5.45}$$

where $\tilde{Z}$ is the function (5.28) in dimensionless form such that

$$\begin{aligned}\tilde{Z} : I_{\tilde{z}} \times I_{\tilde{h}} &\to \mathbb{R}\\ (\tilde{z}, \tilde{h}) &\mapsto \tilde{Z}(\tilde{z}, \tilde{h}) = \frac{\cosh\left[\sigma\,\tilde{k}(\tilde{h})\,(\tilde{z} + \tilde{h})\right]}{\cosh\left[\sigma\tilde{h}\,\tilde{k}(\tilde{h})\right]}.\end{aligned} \tag{5.46}$$

In view of the asymptotic derivation and using the fact that $\widehat{x} = \dfrac{L_0}{L_B}\tilde{x} = \dfrac{\alpha}{\sigma}\tilde{x}$, the partial derivatives of $\tilde{Z}$ according to $\tilde{x}$ can be rewritten as follows:

$$\begin{cases} \partial_{\tilde{x}}\tilde{Z} = \alpha\, d_{\widehat{x}}\tilde{h}\, \partial_{\tilde{h}}\tilde{Z}, & (5.47) \\ \partial_{\tilde{x}\tilde{x}}\tilde{Z} = \alpha^2\,(d_{\widehat{x}}\tilde{h})^2\,\partial_{\tilde{h}\tilde{h}}\tilde{Z} + \dfrac{\alpha^2}{\sigma}\, d_{\widehat{x}\widehat{x}}\tilde{h}\, \partial_{\tilde{h}}\tilde{Z}. & (5.48) \end{cases}$$

We replace the approximate solution $\tilde{\phi}_{app}$ in (5.36-5.38) yielding:

$$\begin{cases} \tilde{\mathsf{L}}(\tilde{\phi}_{app}) = \sigma^2\big(\tilde{Z}\, d_{\tilde{x}\tilde{x}}\tilde{\varphi} + 2\,\alpha\, d_{\widehat{x}}\tilde{h}\, d_{\tilde{x}}\tilde{\varphi}\, \partial_{\tilde{h}}\tilde{Z} + \tilde{k}^2\,\tilde{Z}\,\tilde{\varphi}\big) + O(\sigma\,\alpha^2), \ \text{ on } \tilde{\Omega}, & (5.49) \\ \tilde{\mathsf{S}}(\tilde{\phi}_{app}) = 0, \qquad \text{at } \tilde{z} = 0, & (5.50) \\ \tilde{\mathsf{Bo}}(\phi_{app}) = \sigma\,\alpha\,\dfrac{d_{\tilde{x}}\tilde{\varphi}\; d_{\widehat{x}}\tilde{h}}{\cosh[\sigma\,\tilde{k}\,\tilde{h}]} + O(\sigma\,\alpha^2), \qquad \text{at } \tilde{z} = -\tilde{h}. & (5.51) \end{cases}$$

From (5.49), Berkhoff proposed to solve

$$\tilde{Z}\, d_{\tilde{x}\tilde{x}}\tilde{\varphi} + 2\,\alpha\, d_{\widehat{x}}\tilde{h}\, d_{\tilde{x}}\tilde{\varphi}\, \partial_{\tilde{h}}\tilde{Z} + \tilde{k}^2\,\tilde{Z}\,\tilde{\varphi} = 0. \tag{5.52}$$

This equation can be rewritten as follows:

$$d_{\tilde{x}\tilde{x}}\tilde{\varphi} + \tilde{k}^2\,\tilde{\varphi} = -2\,\alpha\,\frac{\partial_{\tilde{h}}\tilde{Z}}{\tilde{Z}}\, d_{\widehat{x}}\tilde{h}\, d_{\tilde{x}}\tilde{\varphi}. \tag{5.53}$$

Since the term on the left-hand side does not depend on $\tilde{z}$, contrary to the term on the right-hand side, this equation has no solution with the exception of 0. A way to obtain a well-posed problem is to integrate (5.49) over the vertical component $\tilde{z}$. Before doing that we may multiply (5.49) by $\tilde{Z}$ in order to obtain a conservative term. We will see that we then retrieve the mild-slope equation (5.31). Following this strategy, we denote by $\tilde{\mathcal{L}}(\tilde{\phi}_{app})$ the operator such that

$$\begin{aligned} \tilde{\mathcal{L}} : C^2\big(I_{\tilde{x}} \times I_{\tilde{z}}\big) &\to C^0\big(I_{\tilde{x}}\big) \\ \tilde{f} &\mapsto \tilde{\mathcal{L}}(\tilde{f}) = \int_{-\tilde{h}(\frac{\alpha}{\sigma}\tilde{x})}^{0} \tilde{Z}\Big(\tilde{z}, \tilde{h}\Big(\frac{\alpha}{\sigma}\tilde{x}\Big)\Big)\, \tilde{\mathsf{L}}(\tilde{f})\, d\tilde{z}. \end{aligned} \tag{5.54}$$

We denote by $\tilde{T}$ the dimensionless form of the function T defined in (5.32). Developing (5.54) yields:

$$\begin{aligned} \tilde{\mathcal{L}}(\tilde{\phi}_{app}) &= \sigma^2\left(\tilde{T}\, d_{\tilde{x}\tilde{x}}\tilde{\varphi} + \alpha\,\left(\int_{-\tilde{h}}^{0} \partial_{\tilde{h}}\tilde{Z}^2\, d\tilde{z}\right)\, d_{\tilde{x}}\tilde{\varphi}\, d_{\widehat{x}}\tilde{h} + \tilde{k}^2\,\tilde{T}\,\tilde{\varphi}\right) + O(\sigma\alpha^2) \\ &= \sigma^2\left(\tilde{T}\, d_{\tilde{x}\tilde{x}}\tilde{\varphi} + \alpha\, d_{\tilde{h}}\tilde{T}\, d_{\tilde{x}}\tilde{\varphi}\, d_{\widehat{x}}\tilde{h} + \tilde{k}^2\,\tilde{T}\,\tilde{\varphi}\right) - \sigma\ \tilde{Z}\Big|_{\tilde{z}=-\tilde{h}}\, \tilde{\mathsf{Bo}}(\tilde{\phi}_{app}) + O(\sigma\alpha^2). \end{aligned}$$

(5.55)

The condition (5.51) at $\tilde{z} = -\tilde{h}$ gives that

$$\sigma \ \tilde{Z}\Big|_{\tilde{z}=-\tilde{h}} \tilde{\mathsf{Bo}}(\tilde{\phi}_{app}) = \mathcal{O}(\sigma^2\alpha). \tag{5.56}$$

As a consequence, (5.55) can be rewritten as follows

$$\tilde{\mathcal{L}}(\tilde{\phi}_{app}) = \sigma^2\Big(\frac{d}{d\tilde{x}}(\tilde{T}\ d_{\tilde{x}}\tilde{\varphi}) + \tilde{k}^2\,\tilde{T}\,\tilde{\varphi}\Big) + O(\sigma^2\,\alpha). \tag{5.57}$$

Then, if φ is solution of the mild-slope equation (5.57), the remainder term in $\tilde{\mathcal{L}}(\tilde{\phi}_{app})$ is of order $\mathcal{O}(\sigma^2\,\alpha)$.

5.2.2 Shallow water regime

In this Subsection, we consider a shallow water regime, i.e. $\sigma \ll 1$ and $\alpha \sim \sigma$. From the linear theory, the linear shallow water equation can be derived in this regime. Several derivations can be found in the literature. In particular, a derivation from the non-linear shallow water equation exists in [137] and in [90]. It consists in deriving the shallow water equation and then to linearize it. In [10], Berkhoff proposed a derivation from the linear water wave equation. In addition, Lozano and Meyer [96] derived the linear shallow water equation from the mild-slope equation. The authors showed the adequacy between the mild-slope equation and the linear shallow water equations. From the linear water wave equation, we derive the linear shallow water equation, which yields an approximate solution to (5.36-5.38) of order $\mathcal{O}(\sigma^3)$.

Let us note $X = \sigma\tilde{k}\tilde{h}$, the dispersion relation (5.39) writes:

$$\sigma\delta\tilde{h} = X\ \tanh\big[X\big]. \tag{5.58}$$

For $|X| \leq 1$, we have:

$$\begin{aligned}\sigma\delta\tilde{h} &= X^2 + \mathcal{O}(X^4),\\ &= \big(\sigma\tilde{k}\tilde{h}\big)^2\big(1 + \mathcal{O}\big((\sigma\tilde{k}\tilde{h})^2\big)\big).\end{aligned} \tag{5.59}$$

Therefore, in shallow water regime, the dispersion relation (5.39) reads:

$$\frac{\omega^2}{g}L_0 = \sigma\,\tilde{k}^2\,\tilde{h}\,\Big(1 + \mathcal{O}\big((\sigma\tilde{k}\tilde{h})^2\big)\Big), \tag{5.60}$$

We assume that an approximate solution $\tilde{\phi}_{app}$ of the linear water wave equation (5.36-5.38) can be written as follows

$$\begin{aligned}&\tilde{\phi}^{sw}_{app} : \tilde{\Omega} \to \mathbb{R}\\ &\quad(\tilde{x},\tilde{z}) \mapsto \tilde{\phi}^{sw}_{app}(\tilde{x},\tilde{z}) = \tilde{Z}\big(\tilde{z},\tilde{h}(\frac{\alpha}{\sigma}\tilde{x})\big)(\tilde{\varphi_0}(\tilde{x}) + \sigma^2\ \ \tilde{z}^2\,\tilde{\varphi_2}(\tilde{x})) + \mathcal{O}(\sigma^3),\end{aligned} \tag{5.61}$$

where $\tilde{\varphi}_0$ and $\tilde{\varphi}_2$ are functions defined from $]0, \frac{L}{L_0}[$ to $\mathbb{R}$. The expression (5.61) comes from the power series of $\tilde{\phi}^{sw}_{app}$ in $\tilde{z}$.

We replace the solution $\tilde{\phi}^{sw}_{app}$ in (5.36-5.38) leading to:

$$\begin{cases} \tilde{\mathsf{L}}(\tilde{\phi}^{sw}_{app}) = \sigma^2\Big(\tilde{Z}\; d_{\tilde{x}}\tilde{\varphi}_0 + 2\,\tilde{Z}\,\tilde{\varphi}_2 + \tilde{k}^2\,\tilde{Z}\,\tilde{\varphi}_0\Big) + \mathcal{O}(\sigma^3), \quad \text{on } \tilde{\Omega}, & (5.62)\\ \tilde{\mathsf{S}}(\tilde{\phi}^{sw}_{app}) = 0, \qquad \text{at } \tilde{z} = 0, & (5.63)\\ \tilde{\mathsf{Bo}}(\tilde{\phi}^{sw}_{app}) = \dfrac{\sigma^2}{\cosh[\sigma\,\tilde{k}\,\tilde{h}]}\Big(d_{\tilde{x}}\tilde{\varphi}_0\, d_{\tilde{x}}\tilde{h} - 2\,\tilde{h}\,\tilde{\varphi}_2\Big) + \mathcal{O}(\sigma^3), \qquad \text{at } \tilde{z} = -\tilde{h}. & (5.64) \end{cases}$$

From (5.64), we deduce that the remainder term $\tilde{\mathsf{Bo}}(\tilde{\phi}_{app})$ is of order $\mathcal{O}(\sigma^2)$ if

$$\tilde{\varphi}_2 = \frac{1}{2\,\tilde{h}}\, d_{\tilde{x}}\tilde{\varphi}_0\; d_{\tilde{x}}\tilde{h} + \mathcal{O}(\sigma). \tag{5.65}$$

We replace $\tilde{\varphi}_2$ in (5.62) yielding:

$$\tilde{\mathsf{L}}(\tilde{\phi}^{sw}_{app}) = \sigma^2 d_{\tilde{x}}\tilde{\varphi}_0 + \sigma^2\,\frac{1}{\tilde{h}}\, d_{\tilde{x}}\tilde{h}\, d_{\tilde{x}}\tilde{\varphi}_0 + \sigma^2\,\tilde{k}^2\,\tilde{\varphi}_0 + \mathcal{O}(\sigma^3), \quad \text{on } \tilde{\Omega}. \tag{5.66}$$

Then, the remainder term in $\tilde{\mathsf{L}}(\tilde{\phi}^{sw}_{app})$ is of order $\mathcal{O}(\sigma^3)$ if $\tilde{\varphi}_0$ satisfies the linear shallow water equation, which writes in dimensional form:

$$d_x\big(h\; d_x\varphi_0\big) + \frac{\omega^2}{g}\,\varphi_0 = 0, \quad \text{on }]0, L[\tag{5.67}$$

Adequacy with the mild-slope equation:
Let us check the adequacy with the mild-slope equation. In shallow water regime, the function T of the mild-slope equation is (in dimensionless form):

$$\tilde{T} = H\,\tilde{h} + \mathcal{O}(\sigma^3). \tag{5.68}$$

Therefore, a solution of the mild-slope equation approximates a solution of the linear shallow water equation with an accuracy of order $\mathcal{O}(\sigma^3)$.

5.2.3 Deep water regime

In this Subsection, we assume a deep water regime and a slowly varying bottom. We assume that $1 \ll \sigma$ and $\alpha < 1$. From the linear water wave equation, we derive the Helmholtz equation, which yields an approximate solution to (5.36-5.38) of order $\mathcal{O}\big(\frac{\alpha}{\sigma}\big)$. In the deep water regime, the bottom has no influence on the water waves. Let us note $X = \sigma\tilde{k}\tilde{h}$, the dispersion relation (5.39) writes:

$$\sigma\delta\tilde{h} = X\,\tanh\big[X\big]. \tag{5.69}$$

For $X \geq X_0 > 0$, we have:

$$\begin{aligned} \sigma\delta\tilde{h} &= X\big(1+\mathcal{O}\big(e^{-2\,X}\big)\big), \\ &= \sigma\tilde{k}\tilde{h}\big(1+\mathcal{O}\big(e^{-2\,\sigma\tilde{k}\tilde{h}}\big)\big). \end{aligned} \tag{5.70}$$

Therefore, in deep water regime, the dispersion relation (5.39) reads:

$$\frac{\omega^2}{g}\,L_0 = \tilde{k}\Big(1+\mathcal{O}\big(e^{-2\,\sigma\tilde{k}\tilde{h}}\big)\Big), \tag{5.71}$$

We remark that the function $\tilde{k}$ is constant. In this case, we consider travelling wave and we assume an approximate solution $\tilde{\phi}_{app}$ of the linear water wave equation of the form

$$\begin{aligned} &\tilde{\phi}^{helm}_{app} : \tilde{\Omega} \to \mathbb{R} \\ &\qquad (\tilde{x},\tilde{z}) \mapsto \tilde{\phi}^{helm}_{app}(\tilde{x},\tilde{z}) = e^{\sigma\tilde{k}\tilde{z}}\,\tilde{\varphi}(\tilde{x}). \end{aligned} \tag{5.72}$$

We start by dividing the Laplace equation (5.36) by σ^2 and the equations (5.37) (at $\tilde{z}=0$) and (5.38) (at $\tilde{z}=-\tilde{h}$) by σ and we obtain we obtain:

$$\begin{cases} \partial_{\tilde{x}\tilde{x}}\tilde{\phi} + \dfrac{1}{\sigma^2}\;\partial_{\tilde{z}\tilde{z}}\tilde{\phi} = 0, \quad \text{on } \tilde{\Omega}, & (5.73) \\ \dfrac{1}{\sigma}\,\partial_{\tilde{z}}\tilde{\phi} - \delta\,\tilde{\phi} = 0, \quad \text{at } \tilde{z}=0, & (5.74) \\ \dfrac{1}{\sigma}\,\partial_{\tilde{z}}\tilde{\phi} + \alpha\, d_{\tilde{x}}\tilde{h}\,\partial_{\tilde{x}}\tilde{\phi} = 0, \quad \text{at } \tilde{z}=-\tilde{h}. & (5.75) \end{cases}$$

In this part, we denote respectively by $\tilde{\mathsf{L}}_\sigma$, $\tilde{\mathsf{S}}_\sigma$ and $\tilde{\mathsf{Bo}}_\sigma$ the operators of the Laplace equation (5.36) and of the equations at $\tilde{z}=0$ and at $\tilde{z}=-\tilde{h}$ such that

$$\begin{aligned} &\tilde{\mathsf{L}}_\sigma : C^2\big(I_{\tilde{x}}\times I_{\tilde{z}}\big) \to C^0\big(I_{\tilde{x}}\times I_{\tilde{z}}\big) \\ &\qquad\qquad \tilde{f} \mapsto \tilde{\mathsf{L}}_\sigma(\tilde{f}) = \partial_{\tilde{x}\tilde{x}}\tilde{f} + \frac{1}{\sigma^2}\;\partial_{\tilde{z}\tilde{z}}\tilde{f}, \end{aligned} \tag{5.76}$$

$$\begin{aligned} &\tilde{\mathsf{S}}_\sigma : C^2\big(I_{\tilde{x}}\times I_{\tilde{z}}\big) \to C^0\big(I_{\tilde{x}}\times I_{\tilde{z}}\big) \\ &\qquad\qquad \tilde{f} \mapsto \tilde{\mathsf{S}}_\sigma(\tilde{f}) = \frac{1}{\sigma}\left(\partial_{\tilde{z}}\tilde{f}\right)_{|_{\tilde{z}=0}} - \delta\,\tilde{f}_{|_{\tilde{z}=0}}, \end{aligned} \tag{5.77}$$

$$\begin{aligned} &\tilde{\mathsf{Bo}}_\sigma : C^2\big(I_{\tilde{x}}\times I_{\tilde{z}}\big) \to C^0\big(I_{\tilde{x}}\times I_{\tilde{z}}\big) \\ &\qquad\qquad \tilde{f} \mapsto \tilde{\mathsf{Bo}}_\sigma(\tilde{f}) = \frac{1}{\sigma}\left(\partial_{\tilde{z}}\tilde{f}\right)_{|_{\tilde{z}=-\tilde{h}}} + \alpha\, d_{\tilde{x}}\tilde{h}\left(\partial_{\tilde{x}}\tilde{f}\right)_{|_{\tilde{z}=-\tilde{h}}}. \end{aligned} \tag{5.78}$$

We replace the expression (5.72) in these equations yielding:

$$\begin{cases} \tilde{\mathsf{L}}_\sigma(\tilde{\phi}^{helm}_{app}) = (d_{\tilde{x}\tilde{x}}\tilde{\varphi} + \tilde{k}^2\,\tilde{\varphi})\,e^{\sigma\tilde{k}\tilde{z}} + \alpha\, d_{\tilde{h}}\tilde{k}\, f_1\, d_{\tilde{x}}\tilde{\varphi} & (5.79) \\ \qquad\qquad + \Big(\dfrac{\alpha^2}{\sigma}\, d_{\tilde{h}\tilde{h}}\tilde{k}\, f_1 + \alpha^2\,(d_{\tilde{h}}\tilde{k})^2\, f_2\Big)\,\tilde{\varphi}, & (5.80) \\ \tilde{\mathsf{S}}_\sigma(\tilde{\phi}^{helm}_{app}) = \mathcal{O}(e^{-2\sigma\tilde{k}\tilde{h}}), & (5.81) \\ \tilde{\mathsf{Bo}}_\sigma(\phi^{helm}_{app}) = \tilde{k}e^{-\sigma\tilde{k}\tilde{h}}\tilde{\varphi} + \mathcal{O}\big(\alpha\, e^{-\sigma\tilde{k}\tilde{h}}\big). & (5.82) \end{cases}$$

where

$$f_1 :]-\tilde{h}(\tilde{x}), 0[\to \mathbb{R}$$
$$\tilde{z} \mapsto f_1(\tilde{z}) = \tilde{z}\ e^{\sigma\tilde{k}\tilde{z}}, \tag{5.83}$$

and

$$f_2 :]-\tilde{h}(\tilde{x}), 0[\to \mathbb{R}$$
$$\tilde{z} \mapsto f_2(\tilde{z}) = \tilde{z}^2\ e^{\sigma\tilde{k}\tilde{z}}. \tag{5.84}$$

We have that $|f_1| \leq \dfrac{1}{\sigma\tilde{k}}e^{-1}$ and $|f_2| \leq \dfrac{2}{\sigma\tilde{k}}e^{-2}$ for all $-\tilde{h} < \tilde{z} < 0$. We use these inequalities in (5.80) and we get:

$$\tilde{\mathsf{L}}_\sigma(\tilde{\phi}^{helm}_{app}) = (d_{\tilde{x}\tilde{x}}\tilde{\varphi} + \tilde{k}^2\,\tilde{\varphi})\, e^{\sigma\tilde{k}z} + \mathcal{O}\Big(\frac{\alpha}{\sigma}\Big), \quad \text{on } \tilde{\Omega}. \tag{5.85}$$

We deduce that the remainder term (5.80) is of order $\mathcal{O}(\frac{\alpha}{\sigma})$ if φ satisfies the Helmholtz equation, which writes in dimensional form:

$$d_{xx}\varphi + k^2\,\varphi = 0, \quad \text{on }]0, L[\tag{5.86}$$

Adequacy with the mild-slope equation:
We show the adequacy with the mild-slope equation. In deep water regime, the function T of the mild-slope equation is (in dimensionless form):

$$\tilde{T} = \frac{g}{\omega^2}L_0 + \mathcal{O}\Big(\frac{\alpha}{\sigma}\Big). \tag{5.87}$$

Therefore, a solution of the mild-slope equation approximates a solution of the Helmholtz equation with an accuracy of order $\mathcal{O}\big(\frac{\alpha}{\sigma}\big)$.

5.3 Numerical test cases

This section is devoted to numerical comparisons between the solutions of the different linear equations. In the literature, the mild-slope equation has been originally solved with the Finite Element method by Berkhoff [10, 11]. The Finite Difference method was also used by Li and Anastasiou [95] and Panchang and Pierce [109]. These methods present a common drawback: open and partially reflecting boundary conditions are difficult to represent. These deficiencies have been studied by many authors such as [36, 37].

We consider a case representing a water wave which propagates in a harbor. The water wave incomes from $x_0 = 0$ and propagates over a distance $L \in \mathbb{R}_+^*$ above a varying bottom, before reflecting on a wall at $x_L = L$. The initial and final water depths are denoted by h_0 (at x_0) and h_L (at x_L), respectively. Let introduce x_1 and x_2 such that $x_0 \leq x_1 \leq x_2 \leq x_L$. The topography is assumed to be horizontal on the intervals $[x_0, x_1]$

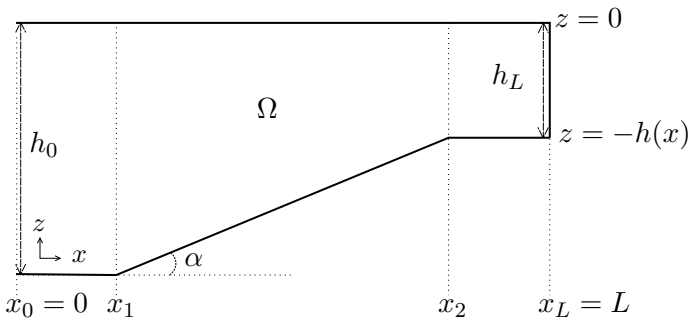

Figure 5.3: Domain Ω for the numerical test cases

and $[x_2, x_L]$. We assume that on $[x_1, x_2]$, the topography varies linearly from h_0 to h_L. In the following, we adapt the values of x_1 and x_2 in order to study different slopes, see Figure 5.3.

We consider the polygonal domain Ω defined by

$$\Omega = \{x \in]0, L[\ , \ z \in]-h(x), 0[\}, \tag{5.88}$$

where the continuous function $h(x)$ is

$$h(x) = \begin{cases} h_0 & \text{if} \quad x \leq x_1, \\ -\alpha\,(x - x_1) + h_0 & \text{if} \quad x_1 < x < x_2, \\ h_L = h_0 - \alpha\,(x_L - x_0) & \text{if} \quad x \geq x_2. \end{cases} \tag{5.89}$$

To model a wave in a harbor, we consider a Dirichlet boundary condition at $x = x_0$ of the form

$$\phi(x_0, z) = Z(z, h(x_0)). \tag{5.90}$$

With this assumption, we assume that the wave corresponds to a wave that travels over a flat bottom. Other open sea boundary conditions are possible [11, 16]. Additionally, we impose at $x = x_L$ that

$$\partial_x \phi(x_L, z) = 0, \tag{5.91}$$

which expresses a reflection on a wall.

For the 1D asymptotic models, these boundary conditions become

$$\varphi(x_0) = 1, \quad \text{and} \quad d_x \varphi(x_L) = 0. \tag{5.92}$$

The numerical studies are performed using Finite Elements method and the numerical solutions of the linear equations are approximated by $\mathbb{P}_1$ Lagrangian Finite Elements basis functions. The continuous and discrete variational formulations of the linear water wave and set of asymptotic equations (i.e. mild-slope equation, Helmholtz equation and linear shallow water equation) are given in Appendix 5.6.

In the sequel of this Section, we use the numerical solution of the linear water wave equation as a reference solution for our comparisons. This numerical solution is denoted by ϕ_h and it is captioned by "Laplace" in the figures. Besides, the numerical solutions of the asymptotic equations are respectively denoted by: φ_h^B for the mild-slope equation, φ_h^{LSW} for the linear shallow water equation and φ_h^H for the Helmholtz equation. Notice that we rescale all the numerical solutions by their respective L^∞-norm. In all the figures, we caption them by the own name of the equations. Afterwards, in the figures, the vertical dashed-lines represent the transition points x_1 and x_2 between the horizontal and varying bottoms.

5.3.1 Characterization of the regimes

In order to consider intermediate water regime, we want to identify approximatively an interval on σ. Usually, the shallow water and deep water regimes are considered when $\sigma \ll 1$ and $\sigma \gg 1$, respectively. In our case, we choose a different characterisation of these regimes. For this purpose, we now consider that $\overline{\sigma} = \dfrac{\sigma}{2\,\pi}$. On the one hand, we assume that the deep water regime is valid when

$$|1 - \tanh[2\,\pi\,\overline{\sigma}]| < 5.10^{-2}. \tag{5.93}$$

We choose then $2\,\pi\,\overline{\sigma} > 2$. On the other hand, we assume that the shallow water is valid when

$$\frac{|\tanh[2\,\pi\,\overline{\sigma}] - 2\,\pi\,\overline{\sigma}|}{2\,\pi\,\overline{\sigma}} < 5.10^{-2}. \tag{5.94}$$

We choose then $2\,\pi\,\overline{\sigma} < 0.2$. Notice that a factor 2π is considered because in practical in the physical studies : $k = \frac{2\,\pi}{L_0}$. As a consequence, we will consider an intermediate regime for $\overline{\sigma} \in]\frac{0.1}{\pi}, \frac{1}{\pi}[$, see Figure 5.4.

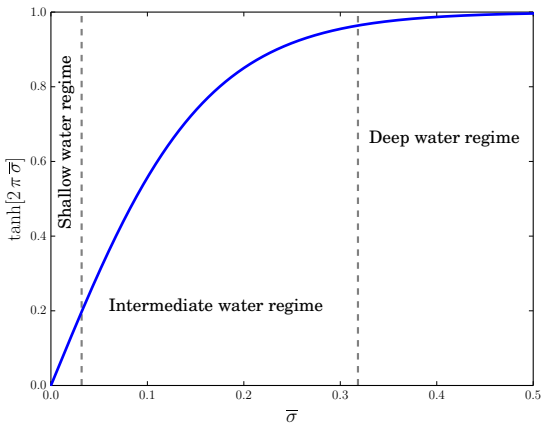

Figure 5.4: Regimes according to the water depth

5.3.2 Shallow water regime

In this Subsection, we consider a water wave of pulsation $\omega = 0.2\text{rad.s}^{-1}$ propagating over a distance $L = 2020\text{m}$. The initial and final water depths are respectively $h_0 = 4\text{m}$ and $h_L = 2\text{m}$. Therefore, we have $kh = 0.13\text{rad}$ at $x = x_0$ and $kh = 0.09\text{rad}$ at $x = x_L$. The characteristic water depth is $H = 3\text{m}$ and the characteristic wave length at the free surface is $L_0 = 170\text{m}$. As a consequence, the shallowness parameter is $\overline{\sigma} \in]0.01, 0.02[$ and its average is $\overline{\sigma}_{moy} \sim 0.015$. We perform a first test case in the shallow water regime when $\alpha \sim \overline{\sigma}_{moy}$ (see Figures 5.5a and 5.5b). Then, we study the effect of the slope on the numerical solutions with $\alpha \sim \frac{\overline{\sigma}_{moy}}{10}$ (see Figure 5.5c) and $\alpha \sim 10\,\overline{\sigma}_{moy}$ (see Figure 5.5d).

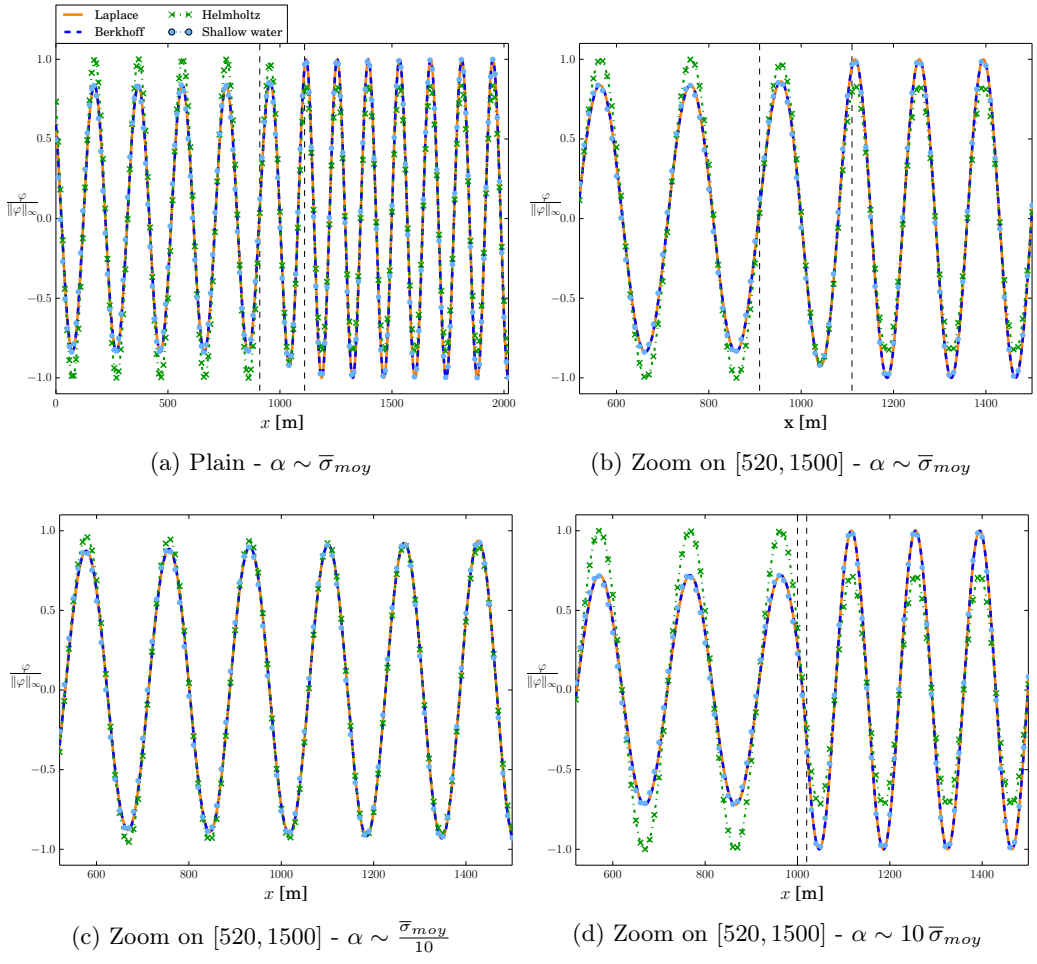

(a) Plain - $\alpha \sim \overline{\sigma}_{moy}$

(b) Zoom on $[520, 1500]$ - $\alpha \sim \overline{\sigma}_{moy}$

(c) Zoom on $[520, 1500]$ - $\alpha \sim \frac{\overline{\sigma}_{moy}}{10}$

(d) Zoom on $[520, 1500]$ - $\alpha \sim 10\,\overline{\sigma}_{moy}$

Figure 5.5: Shallow water regime

On Figure 5.5, we observe that φ_h^B and φ_h^{LSW} are close to $\phi_{h|_{z=0}}$. In the case where $\overline{\sigma}_{moy} \sim \alpha$, this result is in agreement with the theory of Subsection 5.2.2. Nonetheless, we can see that these numerical solutions are also close to $\phi_{h|_{z=0}}$ when $\alpha \sim \frac{\overline{\sigma}_{moy}}{10}$ or

$\alpha \sim 10\,\overline{\sigma}_{moy}$. Notice that the numerical solution of the Helmholtz equation does not match with the other numerical solutions. Its phase is correct but its amplitude decreases instead of increasing.

5.3.3 Intermediate water regime

In this Subsection, we consider a water wave of pulsation $\omega = 1\text{rad.s}^{-1}$ propagating over a distance $L = 600\text{m}$. The initial and final water depths are respectively $h_0 = 10\text{m}$ and $h_L = 2\text{m}$. Therefore, we have $kh = 1.22\text{rad}$ at $x = x_0$ and $kh = 0.47\text{rad}$ at $x = x_L$. The characteristic water depth is $H = 6\text{m}$ and the characteristic wave length at the free surface is $L_0 = 43\text{m}$. As a consequence, the shallowness parameter is $\overline{\sigma} \in]0.07, 0.19[$ and its average is $\overline{\sigma}_{moy} \sim 0.13$. We perform a first case in the intermediate water regime, i.e. $\alpha \ll 0.2 < 2\,\pi\,\overline{\sigma}_{moy} < 2$ (see Figure 5.6c). Then, we study the effect of the slope with $\alpha \sim \frac{\overline{\sigma}_{moy}}{10}$ see Figures 5.6a and 5.6b) and $\alpha \sim 10\,\overline{\sigma}_{moy}$ (see Figure 5.6d).

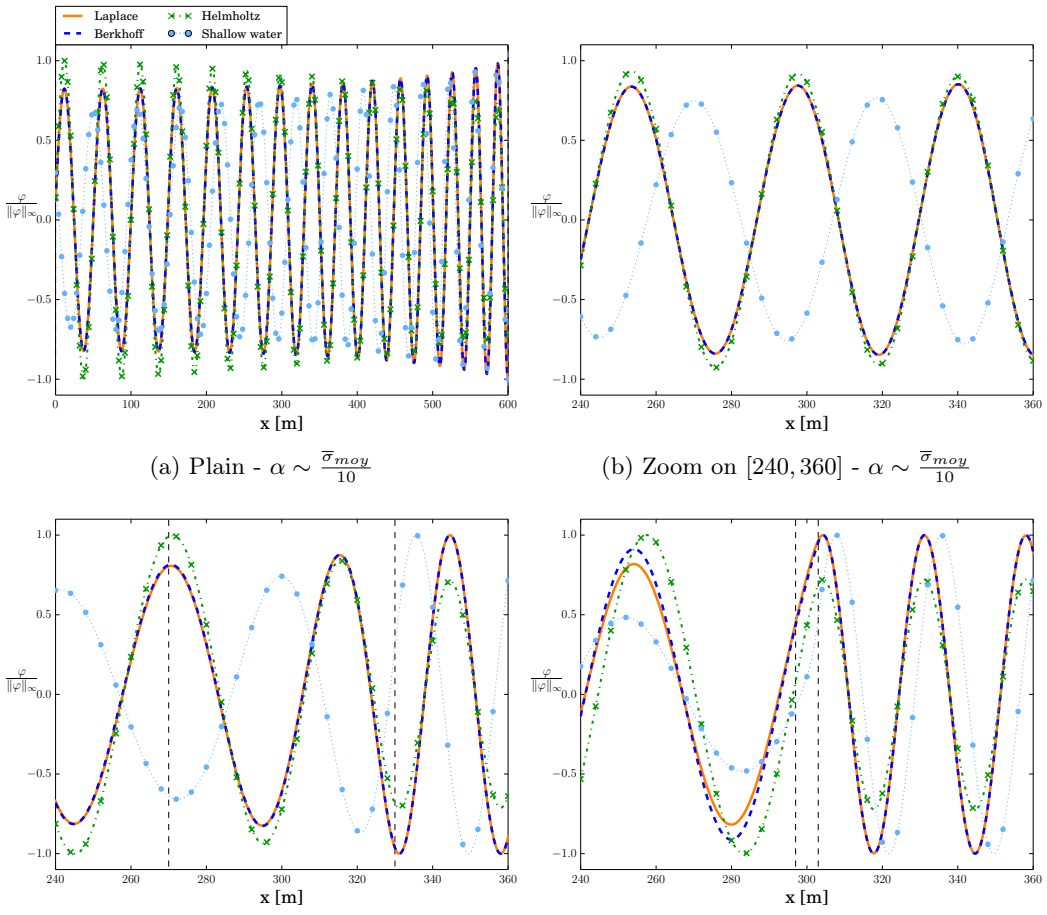

(a) Plain - $\alpha \sim \frac{\overline{\sigma}_{moy}}{10}$

(b) Zoom on $[240, 360]$ - $\alpha \sim \frac{\overline{\sigma}_{moy}}{10}$

(c) Zoom on $[240, 360]$ - $\alpha \sim \overline{\sigma}_{moy}$

(d) Zoom on $[240, 360]$ - $\alpha \sim 10\,\overline{\sigma}_{moy}$

Figure 5.6: Intermediate water regime

On Figure 5.6, we observe that φ_h^{LSW} is not similar to $\phi_{h|_{z=0}}$ since the regime is not shallow water. As expected from the theory, φ_h^B matches with $\phi_{h|_{z=0}}$ when $\alpha \sim \frac{\overline{\sigma}_{moy}}{10}$. We can remark that φ_h^B is still close to $\phi_{h|_{z=0}}$ when $\alpha \sim \overline{\sigma}_{moy}$. Nevertheless, a slight gap begins to appear on the left of the domain between these both numerical solutions when $\alpha \sim 10\,\overline{\sigma}_{moy}$. Afterwards, we observe that φ_h^H is in phase with $\phi_{h|_{z=0}}$. However, as in shallow water regime, the amplitude of φ_h^H decreases while the one of $\phi_{h|_{z=0}}$ increases. In the intermediate regime and for a rising bottom, the mild-slope equation is the only asymptotic model that takes into account the compression and the increasing amplitude of the wave (the so-called refraction phenomenon).

5.3.4 Deep water regime

In this Subsection, we consider a deep water regime. For this purpose, we consider that $2\,\pi\,\overline{\sigma} > 2$. We consider a water wave of pulsation $\omega = 2\text{rad.s}^{-1}$ propagating over a distance $L = 100\text{m}$. The initial and final water depths are respectively $h_0 = 12\text{m}$ and $h_L = 8\text{m}$. Therefore, we have $kh = 4.89\text{rad}$ at $x = x_0$ and $kh = 3.27\text{rad}$ at $x = x_L$. The characteristic water depth is $H = 10\text{m}$ and the characteristic wave length at the free surface is $L_0 = 15\text{m}$. As a consequence, the shallowness parameter is $\overline{\sigma} \in]0.5, 0.8[$ and its average is $\overline{\sigma}_{moy} \sim 0.65$. We consider two cases which are distinguished by the slope of the bottom: $\alpha \sim \frac{\overline{\sigma}_{moy}}{10}$ and $\alpha \sim \overline{\sigma}_{moy}$.

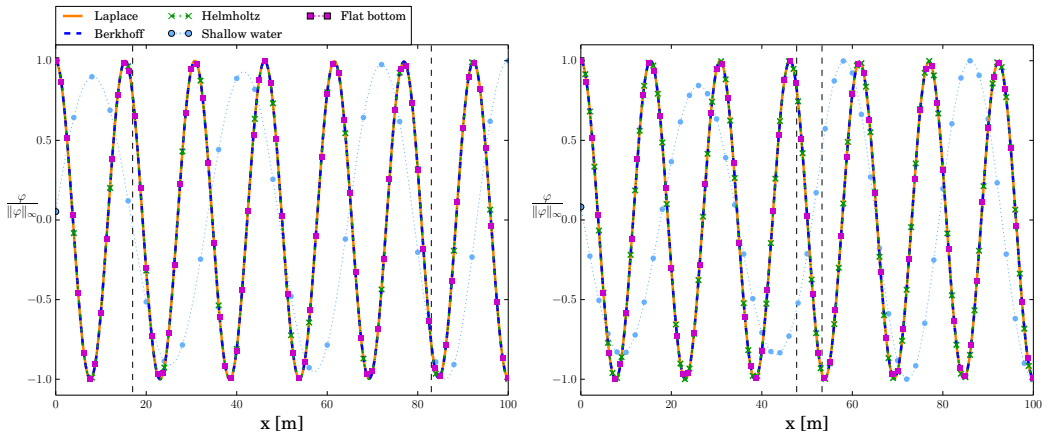

(a) $\alpha \sim \frac{\overline{\sigma}_{moy}}{10}$ (b) $\alpha \sim \overline{\sigma}_{moy}$

Figure 5.7: Deep water regime

On Figure 5.7, we observe that φ_h^{LSW} is not similar to $\phi_{h|_{z=0}}$ since the regime is not shallow water. Moreover, we can see that φ_h^B and φ_h^H are very close to $\phi_{h|_{z=0}}$. In both Figures, we add the solution for a flat bottom. We can see that these numerical solutions are very close to a solution on a flat bottom. It is expected since the water wave is not influenced by the bottom, independently of its profile and its slope.

5.3.5 Deep water to intermediate water regimes

In this Subsection, we consider a wave propagating from a deep water regime to an intermediate water regime. We consider a water wave of pulsation $\omega = 2\text{rad.s}^{-1}$ propagating over a distance $L = 270\text{m}$. The initial and final water depths are respectively $h_0 = 9\text{m}$ and $h_L = 1\text{m}$. Therefore, we have $kh = 3.67\text{rad}$ at $x = x_0$ and $kh = 0.69\text{rad}$ at $x = x_L$. The characteristic water depth is $H = 5\text{m}$ and the characteristic wave length at the free surface is $L_0 = 15\text{m}$. As a consequence, the shallowness parameter is $\overline{\sigma} \in]0.1, 0.6[$ and its average is $\overline{\sigma}_{moy} \sim 0.35$. We choose a slope $\alpha \sim \frac{\overline{\sigma}_{moy}}{10}$ which corresponds to the hypothesis of the asymptotic derivation of the mild-slope equation ($\alpha \ll \overline{\sigma}_{moy}$).

On Figure 5.8, we observe that φ_h^B is the only numerical solution close to $\phi_{h|_{z=0}}$. The numerical solution φ_h^H is in agreement with $\phi_{h|_{z=0}}$ as long as the regime is deep water, but fails to reproduce the correct behavior on the right of the domain. We retrieve that the amplitude of φ_h^H decreases whereas the amplitude of $\phi_{h|_{z=0}}$ increases.

5.3.6 Intermediate regime to shallow water regimes

In this Subsection, we consider a wave propagating from an intermediate water regime to a shallow water regime. We consider a water wave of pulsation $\omega = 0.25\text{rad.s}^{-1}$ propagating over a distance $L = 820\text{m}$. The initial and final water depths are respectively $h_0 = 50\text{m}$ and $h_L = 1$. Therefore, we have $kh = 0.6\text{rad}$ at $x = x_0$ and $kh = 0.08\text{rad}$ at $x = x_L$. The characteristic water depth is $H = 25.5\text{m}$ and the characteristic wave length at the free surface is $L_0 = 386\text{m}$. As a consequence, the shallowness parameter is $\overline{\sigma} \in]0.02, 0.1[$ and its average $\overline{\sigma}_{moy} \sim 0.07$. We choose a slope $\alpha \sim \overline{\sigma}_{moy}$.

On Figure 5.9, we observe that φ_h^B is the only numerical solution close to $\phi_{h|_{z=0}}$. Moreover, the shallow water equation becomes relevant when $kh < 0.3$ ($x > 450$ on Figure 5.9).

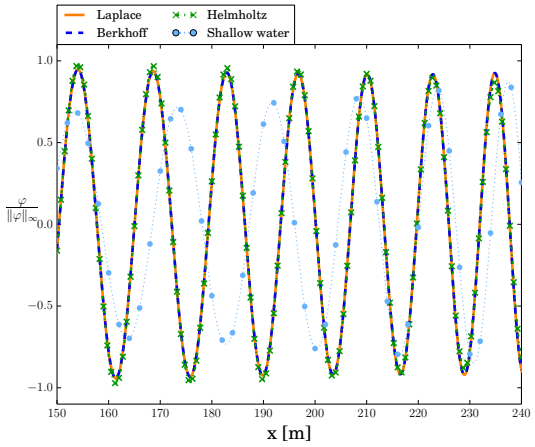

Figure 5.8: Deep water regime to intermediate water regime - On [150,240]

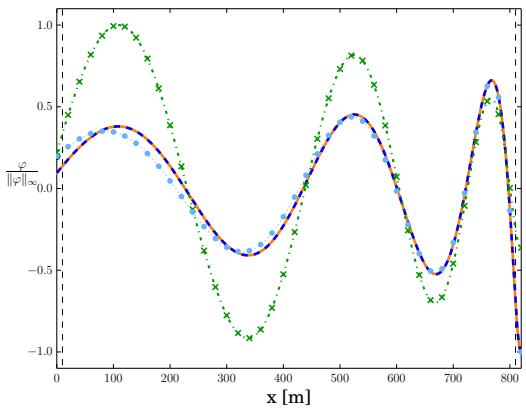

Figure 5.9: Intermediate water regime to shallow water regime

5.4 Approximate analytical solution for the mild-slope equation

This Section is extracted from the proceeding paper [7]. We exhibit an analytical approximate solution of the mild-slope equation for a family of slopes depending on two parameters: the slope and the characteristic water depth evaluated on the middle of the domain. We evaluate various norms for this solution. This study is performed for a two-

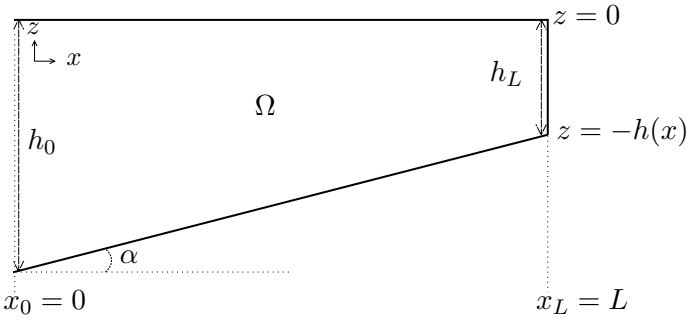

Figure 5.10: Domain Ω for the tests of the approximate analytical solution

dimensional domain $\Omega = \{(x, z) \in \mathbb{R}^2 \mid x \in]0, L[\text{ and } -h(x) < z < 0\}$ where $L \in \mathbb{R}_+^*$ is a constant. The domain Ω is represented on Figure 5.10. We restrict ourselves to the case where the function $kh(x)$ is linear. Notice that in this case, the function $h(x)$ is not linear. This particular form is the key tool for obtaining an analytical approximate solution of the mild-slope equation, in particular, an exact expression of the phase is given in (5.102).

Let us define $\mathsf{L}(\varphi)(x, z) = 0$ the operator of the Laplace equation (5.20), $\mathsf{Bo}(\varphi)(x, z = 0) = 0$ the operator of the equation (5.22) and $\mathsf{Be}(\varphi)(x, z = -h) = 0$ the operator of the mild-slope equation (5.31). For the approximate solution φ_{app}, we study $\mathsf{Be}(\varphi_{app})$, $\mathsf{L}(\varphi_{app})$ and $\mathsf{Bo}(\varphi_{app})$ representing the remainder terms in the corresponding equations. We will show that:

$$\|\mathsf{Be}(\varphi)\|_\infty \leq c_1 \left\|d_x h\right\|_\infty^2, \tag{5.95}$$

$$\|\mathsf{L}(\varphi)\|_\infty \leq c_2 \left\|d_x h\right\|_\infty, \tag{5.96}$$

$$\|\mathsf{Bo}(\varphi)\|_\infty \leq c_3 \left\|d_x h\right\|_\infty, \tag{5.97}$$

where $\{c_i\}_{i=1,\cdots,3}$ are constants. Furthermore, a numerical quantitative study enforces the results.

We begin by introducing the treatment of the dispersion relation (5.27) in order to compute the wave number k. Based on the geometrical optics method [117], we then derive the approximate analytical solution, given in (5.101). Finally, we perform qualitative and quantitative studies.

5.4.1 Treatment of the dispersion relation

The computation of an explicit solution of the mild-slope equation is not easy because the wave number k and then the function T are known implicitly through the dispersion relation (5.27). In the literature, several authors studied the dispersion relation and found explicit approximation of the wave number k. These works include the approximation of Hunt [82], Eckart [50], Nielsen [106] and Venezian [131]. Notice that a review of these different approximations has been made by Fenton and McKee [54].

For our approach, we assume that the bottom profile varies slowly and that the product of the wave number k and the water height h is defined such that

$$(kh)(x) = k(0)h(0) + \frac{k(L)h(L) - k(0)h(0)}{L}x. \tag{5.98}$$

where $k(0)$ and $k(L)$ are given. From the dispersive relation (5.27), the water depth h is then

$$h(x) = \frac{g}{\omega^2}\left(k(0)h(0) + \frac{k(L)h(L) - k(0)h(0)}{L}x\right) \tanh\left[k(0)h(0) + \frac{k(L)h(L) - k(0)h(0)}{L}x\right], \tag{5.99}$$

and the wave number k reads:

$$k(x) = \frac{\omega^2}{g}\frac{1}{\tanh[k(0)h(0) + \frac{k(L)h(L)-k(0)h(0)}{L}x]}. \tag{5.100}$$

Notice that for small slopes $\alpha = \frac{h(L)-h(0)}{L}$ the water depth is very close to its linear approximation.

5.4.2 Approximate analytical solution

We describe the strategy to find an approximate analytical solution at the order 0 for the mild-slope equation. This comes from the geometrical optics method, see for example the book of Rauch [117] for a complete description.

Proposition 5.1. *Let us consider the mild-slope equation* (5.31)*. An approximate explicit solution is:*

$$\varphi_{app}(x) = \frac{a_0}{\sqrt{k(x)T(x)}}\cos[\theta(x) + C], \tag{5.101}$$

where a_0 and C are constants, chosen according to the Dirichlet and Neumann conditions at the boundaries. The function θ is

$$\theta(x) = \frac{\omega^2}{g\ d_x(kh)(x)}\log\left(\frac{\sinh\left[kh(L)\right]}{\sinh\left[kh(x)\right]}\right). \tag{5.102}$$

Proof. We consider the mild-slope equation depending on a small parameter ϵ in the following form:

$$T\, d_{xx}\varphi_\epsilon + d_x T\, d_x\varphi_\epsilon + \frac{k^2}{\epsilon^2}\, T\, \varphi_\epsilon = 0. \tag{5.103}$$

A classical method to derive an asymptotic solution at the order 0 is to assume that:

$$\varphi_\epsilon(x) = a(x)\cos\left[\frac{\theta(x)}{\epsilon} + C\right]. \tag{5.104}$$

We replace the expression of (5.104) in the equation (5.103) and we obtain:

$$\begin{aligned}
&\frac{1}{\epsilon^2}\big(k^2(x) - d_x\theta(x)^2\big)\, T(x)\, a(x)\, \cos\left[\frac{\theta(x)}{\epsilon} + C\right] \\
&-\frac{1}{\epsilon}\Big(2\, a(x)\, T(x)\; d_x\theta(x) - a(x)\; d_x\big(d_x\theta(x)\, T(x)\big)\Big)\sin\left[\frac{\theta(x)}{\epsilon} + C\right] \\
&+\big(T\; d_{xx}a(x) + d_x a(x)\; d_x T(x)\big)\cos\left[\frac{\theta(x)}{\epsilon} + C\right] = 0.
\end{aligned} \tag{5.105}$$

As mentioned, we aim to find an approximate solution at the order zero according to $\frac{1}{\epsilon}$. Therefore, we search θ and a such the terms in $\frac{1}{\epsilon}$ and $\frac{1}{\epsilon^2}$ are zero. The terms in $\frac{1}{\epsilon^2}$ lead to:

$$d_x\theta(x)^2 = k^2. \tag{5.106}$$

Furthermore, the terms in $\frac{1}{\epsilon}$ yield:

$$d_x\left(a^2(x)\, T(x)\, k(x)\right) = 0 \quad \Leftrightarrow \quad a(x) = \frac{a_0}{\sqrt{k(x)T(x)}}. \tag{5.107}$$

We remark that the equation (5.103) is reduced to the mild-slope equation (5.31) when $\epsilon = 1$. As a consequence, the relation (5.104) with $\epsilon = 1$ defines an approximate analytical solution of the mild-slope equation. ■

Proposition 5.2. *If $a(x)$ and $\theta(x)$ satisfy respectively* (5.107) *and* (5.106)*, then the remainder term induced by the approximate explicit solution* (5.101) *is*

$$\mathsf{Be}(\varphi_{app}) = d_x\left(T(x)\; d_x a(x)\right)\cos\left(\theta(x) + C\right). \tag{5.108}$$

Proof. The idea of the proof consists in replacing the approximate solution (5.101) in the mild-slope equation (5.31) and in computing the remainder term. We have:

$$d_x\Big(T(x)\; d_x\big(a(x)\cos[\theta(x) + C]\big)\Big) + k(x)^2\, T(x)\, a(x)\; \cos[\theta(x)] = 0. \tag{5.109}$$

We use (5.107) and (5.106) to rewrite the first term as follows:

$$\begin{aligned}
d_x\Big(T(x)\; d_x\big(a(x)\cos[\theta(x) + C]\big)\Big) &= \partial_x\big(T(x)\; d_x a(x)\big)\cos[\theta(x) + C] \\
&\quad - k^2(x)\, T(x)\, a(x)\; \cos[\theta(x)].
\end{aligned} \tag{5.110}$$

Plugging the expression (5.110) in (5.109) leads to the remainder term (5.108). That concludes the proof. ■

5.4.3 Quantitative study

In this Subsection, we perform a quantitative study of the approximate analytical solution (5.101). We study the respective order of magnitude of the remainder terms: $\mathsf{L}(\varphi_{app})$, $\mathsf{Bo}(\varphi_{app})$ and $\mathsf{Be}(\varphi_{app})$. The study is performed for different slopes α and pulsations ω. As previously, we consider a test case representing a harbor. The water wave incomes from $x_0 = 0$m and propagates over the distance $L = 30$m, above a varying bottom. At $x = L$, the water wave reflects on a wall. As a consequence, we consider a Dirichlet condition at $x = 0$ and a Neumann condition at $x = L$ such that:

$$\begin{cases} \varphi(0) = 1, & (5.111) \\ d_x\varphi(L) = 0. & (5.112) \end{cases}$$

The initial and final water depths are $h(0)$ and $h(L)$, respectively. The approximate analytical solution (5.101) reads:

$$\varphi^B_{app}(x) = \frac{a_0}{\sqrt{k(x)T(x)}}\cos[\theta(x)] + \frac{b_0}{\sqrt{k(x)T(x)}}\sin[\theta(x)], \tag{5.113}$$

where the phase is

$$\theta(x) = \int_L^x k(s)ds = \frac{\omega^2}{g}\frac{L}{kh(L) - kh(0)}\ln\left(\frac{\sinh[kh(L)]}{\sinh\left[kh(x)\right]}\right). \tag{5.114}$$

Using the boundary conditions (5.113), we deduce that

$$\begin{cases} a_0 = \dfrac{\sqrt{kT(0)}}{\left(\cos[\theta(0)] + \dfrac{1}{2}\dfrac{d_x(kT)(L)}{T(L)\,k^2(L)}\sin\left[\theta(0)\right]\right)}, & (5.115) \\ b_0 = \dfrac{1}{2}\dfrac{d_x(kT)(L)}{(kT(L))^{\frac{3}{2}}}\dfrac{\sqrt{k(L)T(L)}}{k(L)}\,a_0. & (5.116) \end{cases}$$

In addition, we compare the orders of magnitude of the remainder terms with φ^B_{app} with the ones for a classical solution of the mild-slope equation for a flat bottom, which is:

$$\varphi_f(x) = \cos[k(0)\,x] + \frac{\sin[k(0)\,L]}{\cos[k(0)\,L]}\sin[k(0)\,x]. \tag{5.117}$$

Figures 5.11a-5.11b and 5.11c-5.11d represent respectively cases with $\omega = \sqrt{0.1\,g}\,\mathrm{rad.s}^{-1}$ and $\omega = \sqrt{g}\,\mathrm{rad.s}^{-1}$. The slopes are respectively equal to $\alpha = 0.1$ on the left-hand side and to $\alpha = 0.01$ on the right-hand side. The curves represent φ^B_{app}, $1000 \times \mathsf{Be}(\varphi^B_{app})$, φ_f and ϕ_{num}, a numerical solution of the the linear water wave problem. This numerical solution is has been computed by the Finite Elements method, see Subsection 5.3.

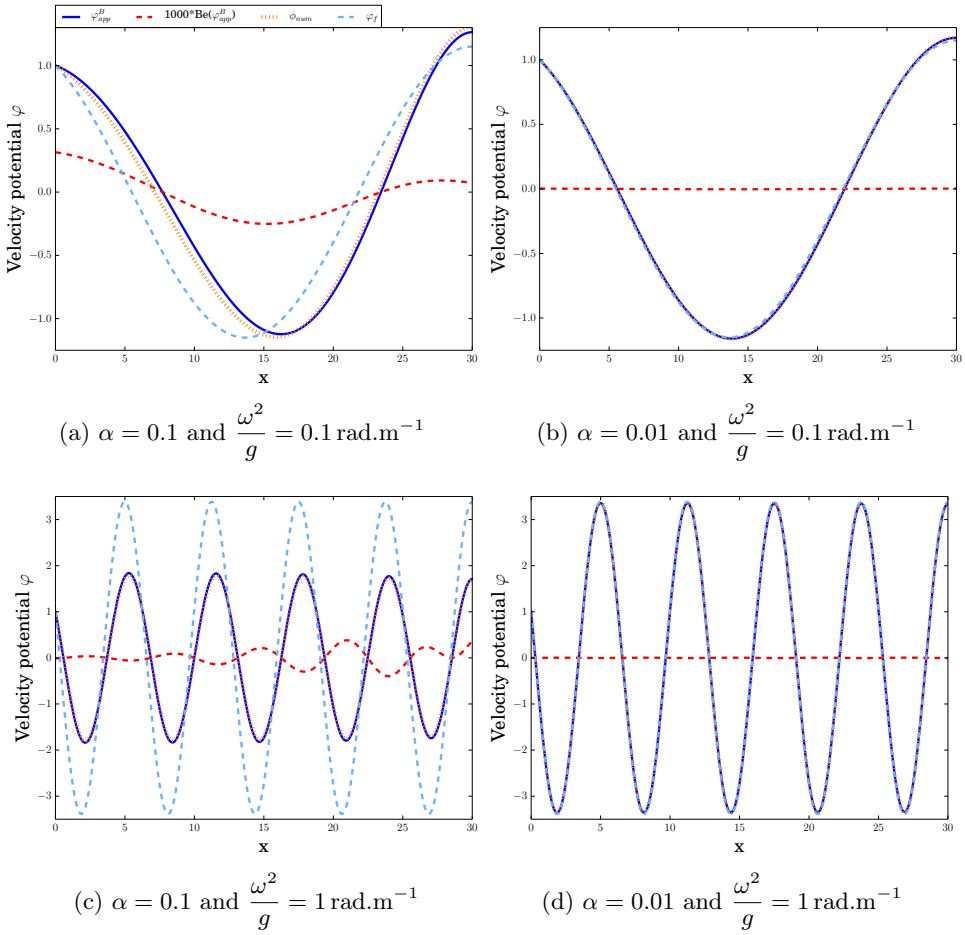

(a) $\alpha = 0.1$ and $\dfrac{\omega^2}{g} = 0.1\,\text{rad.m}^{-1}$

(b) $\alpha = 0.01$ and $\dfrac{\omega^2}{g} = 0.1\,\text{rad.m}^{-1}$

(c) $\alpha = 0.1$ and $\dfrac{\omega^2}{g} = 1\,\text{rad.m}^{-1}$

(d) $\alpha = 0.01$ and $\dfrac{\omega^2}{g} = 1\,\text{rad.m}^{-1}$

Figure 5.11: Numerical solutions for different slopes and wave pulsations

We can observe that φ^B_{app} is close to the linear water wave problem. Indeed, the approximate solutions φ^B_{app} are close to the numerical solutions of the linear water wave equation. We remark that the classical solution φ_f does not match with the other numerical and approximate solutions with $\alpha = 0.1$. When the slope decreases, φ_f matches with the numerical solution of the linear water wave equation. This is coherent since a fundamental solution of the linear wave problem with flat bottom writes as (5.23). We remark that the remainder term $\mathsf{Be}(\varphi^B_{app})$ is small with respect to x. In addition, we remark that the functions $-\mathsf{Be}(\varphi^B_{app})$ and φ^B_{app} have approximatively the same phase. These results are coherent with the expression of the remainder term (5.108) for which we can prove that the order is $\mathcal{O}(\alpha^2)$ as described below.

We now study the L^2-norm of $\mathsf{Be}(\cdot)$, $\mathsf{L}(\cdot)$ and $\mathsf{Bo}(\cdot)$ applied to φ^B_{app} and φ_f for different slopes. On the one hand, Tables 5.1 and 5.2 show the L^2-norms in the case where $\frac{\omega^2}{g} = 0.1\,\text{rad.m}^{-1}$. On the other hand, Tables 5.3 and 5.4 show the L^2-norms in the case

where $\frac{\omega^2}{g} = 1\,\mathrm{rad.m}^{-1}$.

Slope	$\|\mathsf{Be}(\varphi^B_{app})\|_{L^2}$	$\|\mathsf{L}(\varphi^B_{app})\|_{L^2}$	$\|\mathsf{Bo}(\varphi^B_{app})\|_{L^2}$
10^{-1}	9.20×10^{-4}	4.67×10^{-2}	7.68×10^{-2}
10^{-2}	9.85×10^{-6}	4.19×10^{-3}	7.64×10^{-3}
10^{-3}	9.81×10^{-8}	4.16×10^{-4}	7.58×10^{-4}
10^{-4}	9.80×10^{-10}	4.16×10^{-5}	7.58×10^{-5}
10^{-5}	9.80×10^{-12}	4.16×10^{-6}	7.57×10^{-6}

Table 5.1: Remainder terms in L^2-norm compared to slopes with φ^B_{app} - $\dfrac{\omega^2}{g} = 0.1\,\mathrm{rad.m}^{-1}$

Slope	$\|\mathsf{Be}(\varphi_f)\|_{L^2}$	$\|\mathsf{L}(\varphi_f)\|_{L^2}$	$\|\mathsf{Bo}(\varphi_f)\|_{L^2}$
10^{-1}	1.08×10^{-1}	8.20×10^{-2}	7.66×10^{-2}
10^{-2}	1.02×10^{-2}	6.61×10^{-3}	7.59×10^{-3}
10^{-3}	1.02×10^{-3}	6.52×10^{-4}	7.58×10^{-4}
10^{-4}	1.02×10^{-4}	6.48×10^{-5}	7.58×10^{-5}
10^{-5}	2.31×10^{-5}	1.46×10^{-5}	7.57×10^{-6}

Table 5.2: Remainder terms in L^2-norm compared to slopes with φ_f - $\dfrac{\omega^2}{g} = 0.1\,\mathrm{rad.m}^{-1}$

Slope	$\|\mathsf{Be}(\varphi^B_{app})\|_{L^2}$	$\|\mathsf{L}(\varphi^B_{app})\|_{L^2}$	$\|\mathsf{Bo}(\varphi^B_{app})\|_{L^2}$
10^{-1}	9.22×10^{-4}	1.25×10^{-1}	1.21×10^{-1}
10^{-2}	1.72×10^{-5}	1.65×10^{-2}	1.29×10^{-2}
10^{-3}	1.72×10^{-7}	1.67×10^{-3}	1.30×10^{-3}
10^{-4}	1.72×10^{-9}	1.66×10^{-4}	1.30×10^{-4}
10^{-5}	1.72×10^{-11}	1.66×10^{-5}	1.30×10^{-5}

Table 5.3: L^2-norm compared to slopes with φ^B_{app} - $\dfrac{\omega^2}{g} = 1\,\mathrm{rad.m}^{-1}$

We observe that $\mathsf{Be}(\varphi^B_{app})$ is of size $\mathcal{O}(\alpha^2)$ in L^2-norm. This result is coherent with the expression of the remainder term (5.108) for which we can prove the same order. In addition, we remark that the remainder term $\mathsf{Be}(\varphi_f)$ is of size $\mathcal{O}(\alpha)$. For both solutions, the remainder terms $\mathsf{L}(\cdot)$ and $\mathsf{Bo}(\cdot)$ are of size $\mathcal{O}(\alpha)$. However, we observe that $||\mathsf{L}(\varphi^B_{app})||_{L^2} < ||\mathsf{L}(\varphi_f)||_{L^2}$ and $||\mathsf{Bo}(\varphi^B_{app})||_{L^2} \sim ||\mathsf{Bo}(\varphi_f)||_{L^2}$.

Slope	$\|\mathsf{Be}(\varphi_f)\|_{L^2}$	$\|\mathsf{L}(\varphi_f)\|_{L^2}$	$\|\mathsf{Bo}(\varphi_f)\|_{L^2}$
10^{-1}	3.12×10^{-1}	5.13×10^{-1}	2.27×10^{-1}
10^{-2}	1.13×10^{-2}	2.32×10^{-2}	1.30×10^{-2}
10^{-3}	1.10×10^{-3}	2.29×10^{-3}	1.30×10^{-3}
10^{-4}	1.12×10^{-4}	2.31×10^{-4}	1.30×10^{-4}
10^{-5}	2.15×10^{-5}	3.47×10^{-5}	1.30×10^{-5}

Table 5.4: L^2-norm compared to slopes with φ_f - $\dfrac{\omega^2}{g} = 1\,\mathrm{rad.m}^{-1}$

In this quantitative study, the L^2-norm of the remainder terms $\mathsf{L}(\cdot)$ and $\mathsf{Bo}(\cdot)$ applied to the approximate analytical solution and a classical solution for flat bottom are equivalent. However, one observes in the next section that the functions obtained do not have the same qualitative behavior.

5.4.4 Qualitative study

In this Subsection, we perform a qualitative study of the approximate analytical solution (5.101). As previously done, we compare the behavior of the approximate solution with the one of a classical solution of the mild-slope equation on flat bottom. For this purpose, we consider a water wave which propagates in a harbor and above a slowly varying bottom. The water wave incomes from $x_0 = 0$m and reflects over a wall located at $x = L = 70$m. The initial and final water depth are $h(0) = 0.95$m and $h(L) = 0.25$m leading to a characteristic water depth $H = 0.6$m. We choose the slope of the bottom equal to 0.01 and the wave pulsation satisfies $\frac{\omega^2}{g} = 0.5\,\mathrm{rad.m}^{-1}$. We consider a Dirichlet condition at $x = 0$ and a Neumann condition at $x = L$ such that:

$$\begin{cases} \varphi(0) = \dfrac{1}{\sqrt{k(0)\,T(0)}}, & (5.118) \\ d_x\varphi(L) = 0. & (5.119) \end{cases}$$

The approximate analytical solution (5.101) reads:

$$\varphi^B_{app}(x) = \frac{1}{\sqrt{k(x)\,T(x)}}\cos[\theta(x)], \tag{5.120}$$

The classical solution of the mild-slope equation on flat bottom located at $z = -h_0$ is defined by

$$\varphi_f(x) = \frac{1}{\sqrt{k(0)\,T(0)}}\cos[k_0\,x]. \tag{5.121}$$

Let us define the free surface functions:

$$\begin{cases} \eta^B_{app}(x,t) = \mathsf{Re}\big(i\dfrac{\omega}{g}\varphi^B_{app}(x)\mathrm{e}^{i\omega t}\big), & (5.122) \\ \eta_f(x,t) = \mathsf{Re}\big(i\dfrac{\omega}{g}\varphi_f(x)\mathrm{e}^{i\omega t}\big). & (5.123) \end{cases}$$

Figure (5.12) represents $\eta_{2,b}(x, 10)$ (line) and $\eta_{2,f}(x, 10)$(cross) with respect to x. In the case of the approximate analytical solution, the phase evolution due to the variation of the bottom is correctly taken into account and the amplitude of the solution increases. These two phenomena are closer to the experimental observations.

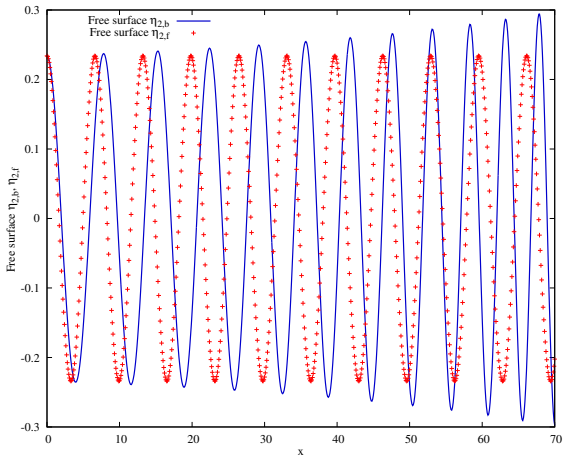

Figure 5.12: Free surface $\eta_{2,b}$ and $\eta_{2,f}$ at time $t = 10$

5.5 Conclusion

In this Chapter, we studied the mild-slope equation that allows to model the refraction and diffraction phenomena of water waves in harbor or coastal areas. Through an asymptotic and numerical studies, we saw that a solution of the mild-slope equation is close to one of the linear water wave equation (resp. Helmholtz equation) in shallow water regime (resp. deep water regime). Besides, we observed that the mild-slope equation is the only one to produce a solution similar to the linear water wave equation when the regime is intermediate or when the regime changes. We also developed an approximate analytical solution deduced from ideas of geometrical optics. From a quantitative and qualitative study, we observed that for an approximate analytical solution φ_{app}, $\mathsf{Be}(\varphi_{app})$ is size of $\mathcal{O}(\alpha^2)$. Nevertheless, the accuracy of the remainder term in the Laplace equation as well as in the relation on $z = -h(x)$ is worse. Qualitatively, we observed that the variations of the amplitude and the phase are correctly taken into account, in agreement with the numerical comparions performed previously and with the physical observations. This implies that an approximate analytical solution of the mild-slope equation is an interesting solution to represent physical phenomena in the case of slowly varying bottom.
A perspective could be to develop a comparative framework between a solution of the mild-slope equation and a solution of the Euler equations. As a consequence, the idea is to compare a solution that is atemporal and defined on a domain where the free surface is located at $z = 0$ and a solution that is temporal and defined on a domain where the free surface is located at $z = \eta(x, y, t)$. This comparative framework will allow to compare

the Telemac-3D and Artemis software.

5.6 Appendix

In this part, we describe the Finite Elements discretizations for the linear equations, which are used in the numerical comparisons of Section 5.3. Let us recall that the linear water wave equation is defined on the polygonal domain Ω, given in (5.88), and the asymptotic equations are defined on the interval ω.

5.6.1 Linear water wave equation

We consider $\mathcal{X}(\Omega)$ the functional space on the potential given by:

$$\mathcal{X}(\Omega) = \{\boldsymbol{v} \in H^1(]0, L[) \ \mid \ \boldsymbol{v} = 1 \text{ at } x = 0\} \tag{5.124}$$

The variational formulation of the linear water wave equation reads: (5.20-5.22):

$$\begin{cases} \text{Find } \phi \in \mathcal{X}(\Omega) \text{ such that } \forall \boldsymbol{v} \in \mathcal{X}(\Omega) \\ -\displaystyle\int_\Omega \nabla\phi \cdot \nabla \boldsymbol{v} \, d\boldsymbol{x} - \int_{-h(0)}^{0} \partial_x\phi(0,z)\, Z(z,h(0))\, dz = 0. \end{cases} \tag{5.125}$$

This variational formulation is well-posed. Afterwards, we consider the $\mathcal{X}_h(\Omega) \subset \mathcal{X}(\Omega)$ the Finite Elements space on the potential ϕ. For the numerical comparisons of Section 5.3, we choose the classical $\mathbb{P}_1$-Lagrange Finite Elements basis functions. We search ϕ_h by solving the following discrete variational problem:

$$\begin{cases} \text{Find } \phi_h \in \mathcal{X}_h(\Omega) \text{ such that } \forall \boldsymbol{v}_h \in \mathcal{X}_h(\Omega) \\ -\displaystyle\int_\Omega \nabla\phi_h \cdot \nabla \boldsymbol{v}_h \, d\boldsymbol{x} - \int_{-h(0)}^{0} \partial_x\phi_h(0,z)\, Z(z,h(0))\, dz = 0. \end{cases} \tag{5.126}$$

5.6.2 Horizontal asymptotic equations

In this Subsection, we denote by φ^B, φ^H and φ^{LSW} the respective solutions of the mild-slope, Helmholtz and linear shallow water equations. We consider $\mathcal{Y}(]0, L[)$ the functional space on the horizontal solutions given by:

$$\mathcal{Y}(]0, L[) = \{v \in H^1(]0, L[) \ \mid \ v = 1 \text{ at } x = 0\}. \tag{5.127}$$

In view of the discrete formulations, we denote by $\mathcal{Y}_h(]0, L[) \subset \mathcal{Y}(]0, L[)$ the Finite Elements space for the approximations of φ^B, φ^H and φ^{LSW}. We choose the classical $\mathbb{P}_1$-Lagrange Finite Elements basis functions.

Mild-slope equation

The variational formulation of the mild-slope equation (5.31) which is well posed reads:

$$\begin{cases} \text{Find } \varphi^B \in \mathcal{Y}(]0, L[) \text{ such that } \forall v \in \mathcal{Y}(]0, L[) \\ -\displaystyle\int_0^L T\, \partial_x\varphi^B\, \partial_x v \, dx + \int_0^L k^2\, T\, \varphi^B\, v \, dx + T(0)\, \partial_x\, \varphi^B(0) = 0. \end{cases} \tag{5.128}$$

Afterwards, we denote by φ_h^B the approximation of φ^B in $\mathcal{Y}_h(]0,L[)$. We search φ_h^B by solving the following discrete variational formulation:

$$\left\{\begin{array}{l} \text{Find } \varphi_h^B \in \mathcal{Y}_h(]0,L[) \text{ such that } \forall v_h \in \mathcal{Y}_h(]0,L[) \\ -\displaystyle\int_0^L T\,\partial_x\varphi_h^B\,\partial_x v_h\,dx + \int_0^L k^2\,T\,\varphi_h^B\,v_h\,dx + T(0)\,\partial_x\,\varphi_h^B(0) = 0. \end{array}\right. \tag{5.129}$$

Linear shallow water equation

The variational formulation of the linear shallow water equation (5.67) which is well posed reads:

$$\left\{\begin{array}{l} \text{Find } \varphi^{LSW} \in \mathcal{Y}(]0,L[) \text{ such that } \forall v \in \mathcal{Y}(]0,L[) \\ -\displaystyle\int_0^L h\,\partial_x\varphi_h^{LSW}\,\partial_x v\,dx + \int_0^L \frac{\omega^2}{g}\,\varphi^{LSW}\,v\,dx + h(0)\,\partial_x\varphi^{LSW}(0) = 0. \end{array}\right. \tag{5.130}$$

Afterwards, we denote by φ_h^{LSW} the approximation of φ^{LSW} in $\mathcal{Y}_h(]0,L[)$. We search φ_h^{LSW} by solving the following discrete variational formulation:

$$\left\{\begin{array}{l} \text{Find } \varphi_h^{LSW} \in \mathcal{Y}_h(]0,L[) \text{ such that } \forall v_h \in \mathcal{Y}_h(]0,L[) \\ -\displaystyle\int_0^L h\,\partial_x\varphi_h^{LSW}\,\partial_x v_h\,dx + \int_0^L \frac{\omega^2}{g}\,\varphi_h^{LSW}\,v_h\,dx + h(0)\,\partial_x\varphi_h^{lsw}(0) = 0. \end{array}\right. \tag{5.131}$$

Helmholtz equation

The variational formulation of the Helmholtz equation (5.86) reads:

$$\left\{\begin{array}{l} \text{Find } \varphi^H \in \mathcal{Y}(]0,L[) \text{ such that } \forall v \in \mathcal{Y}(]0,L[) \\ -\displaystyle\int_0^L \partial_x\varphi^H\,\partial_x v\,dx + \int_0^L k^2\,\varphi^H\,v\,dx + \partial_x\varphi(0) = 0. \end{array}\right. \tag{5.132}$$

Afterwards, we denote by φ_h^H the approximation of φ^H in $\mathcal{Y}_h(]0,L[)$. We search φ_h^H by solving the following discrete variational formulation:

$$\left\{\begin{array}{l} \text{Find } \varphi_h^H \in \mathcal{Y}(]0,L[) \text{ such that } \forall v_h \in \mathcal{Y}_h(]0,L[) \\ -\displaystyle\int_0^L \partial_x\varphi_h^H\,\partial_x v_h\,dx + \int_0^L k^2\,\varphi_h^H\,v_h\,dx + \partial_x\varphi_h(0) = 0. \end{array}\right. \tag{5.133}$$

Bibliography

[1] Abgrall, R. Residual distribution schemes: current status and future trends. *Computers & Fluids 35*, 7 (2006), 641–669.

[2] Adams, R. A., and Fournier, J. J. *Sobolev spaces*, vol. 140. Elsevier, 2003.

[3] Airy, G. B. *Tides and Waves: Extracted from the Encyclopaedia Metropolitana, Tom. V Pag. 241 - 396.* William Clowes and Sons, 1845.

[4] Aris, R. *Vectors, tensors and the basic equations of fluid mechanics.* Courier Corporation, 2012.

[5] Audusse, E. A multilayer saint-venant model: derivation and numerical validation. *Discrete & Continuous Dynamical Systems-B 5*, 2 (2005), 189–214.

[6] Audusse, E., and Bristeau, M.-O. Finite-volume solvers for a multilayer saint-venant system. *International Journal of Applied Mathematics and Computer Science 17*, 3 (2007), 311–320.

[7] Audusse, E., Lafitte, O., Leroy, A., Melinand, B., Pham, C.-T., and Quemar, P. Parametric study of the accuracy of an approximate solution for the mild-slope equation. In *19th International Symposium on Symbolic and Numeric Algorithms for Scientific Computing (SYNASC)* (2017), IEEE, pp. 79–85.

[8] Aydin, M. C. CFD simulation of free-surface flow over triangular labyrinth side weir. *Advances in Engineering Software 45*, 1 (2012), 159–166.

[9] Bell, J. B., Colella, P., and Glaz, H. M. A second-order projection method for the incompressible Navier–Stokes equations. *Journal of Computational Physics 85*, 2 (1989), 257–283.

[10] Berkhoff, J. C. W. Computation of combined refraction-diffraction. In *Coastal Engineering*. 1973, pp. 471–490.

[11] Berkhoff, J. C. W. *Mathematical models for simple harmonic linear water waves: wave diffraction and refraction.* PhD thesis, Delft Hydraulics Laboratory, 1976.

[12] Blumberg, A. F., and Mellor, G. L. A description of a three-dimensional coastal ocean circulation model. *Three-dimensional coastal ocean models 4* (1987), 1–16.

[13] Boffi, D., and Gastaldi, L. Stability and geometric conservation laws for ALE formulations. *Computer methods in applied mechanics and engineering 193*, 42-44 (2004), 4717–4739.

[14] Bonito, A., Guermond, J.-L., and Lee, S. Modified pressure-correction projection methods: Open boundary and variable time stepping. In *Numerical Mathematics and Advanced Applications-ENUMATH 2013*. Springer, 2015, pp. 623–631.

[15] Bonito, A., Kyza, I., and Nochetto, R. H. Time-discrete higher-order ALE formulations: stability. *SIAM Journal on Numerical Analysis 51*, 1 (2013), 577–604.

[16] Booij, N. *Gravity waves on water with non-uniform depth and current*. PhD thesis, Delft University of Technology, 1981.

[17] Booij, N. A note on the accuracy of the mild-slope equation. *Coastal Engineering 7*, 3 (1983), 191–203.

[18] Braack, M., Burman, E., John, V., and Lube, G. Stabilized finite element methods for the generalized Oseen problem. *Computer Methods in Applied Mechanics and Engineering 196*, 4-6 (2007), 853–866.

[19] Brezzi, F. On the existence, uniqueness and approximation of saddle-point problems arising from lagrangian multipliers. *Publications mathématiques et informatique de Rennes*, S4 (1974), 1–26.

[20] Brezzi, F., and Fortin, M. *Mixed and hybrid finite element methods*, vol. 15. Springer Science & Business Media, 2012.

[21] Brooks, A., and Hughes, T. SUPG formulations for convection dominated flows with particular emphasis on the incompressible Navier–Stokes equations. *Comp Methods Appl Mech Eng 32* (1982), 199–259.

[22] Burman, E. A unified analysis for conforming and nonconforming stabilized finite element methods using interior penalty. *SIAM journal on numerical analysis 43*, 5 (2005), 2012–2033.

[23] Burman, E. Consistent supg-method for transient transport problems: Stability and convergence. *Computer Methods in Applied Mechanics and Engineering 199*, 17-20 (2010), 1114–1123.

[24] Burman, E. A monotonicity preserving, nonlinear, finite element upwind method for the transport equation. *Applied Mathematics Letters 49* (2015), 141–146.

[25] Burman, E., Ern, A., and Fernández, M. A. Explicit Runge–Kutta schemes and finite elements with symmetric stabilization for first-order linear PDE systems. *SIAM Journal on Numerical Analysis 48*, 6 (2010), 2019–2042.

[26] Burman, E., and Hansbo, P. Edge stabilization for galerkin approximations of convection-diffusion-reaction problems. *Computer Methods in Applied Mechanics and Engineering 193*, 15-16 (2004), 1437–1453.

[27] Casulli, V. A semi-implicit finite difference method for non-hydrostatic, free-surface flows. *International Journal for Numerical Methods in Fluids 30*, 4 (1999), 425–440.

[28] Casulli, V. A semi-implicit finite difference method for the free-surface Navier–Stokes equations. *Int. J. Numer. Methods Fluids 74*, 605-622 (2014).

[29] Casulli, V., and Cattani, E. Stability, accuracy and efficiency of a semi-implicit method for three-dimensional shallow water flow. *Computers & Mathematics with Applications 27*, 4 (1994), 99–112.

[30] Casulli, V., and Cheng, R. T. Semi-implicit finite difference methods for three-dimensional shallow water flow. *International Journal for numerical methods in fluids 15*, 6 (1992), 629–648.

[31] Casulli, V., and Stelling, G. S. Simulation of three-dimensional, non-hydrostatic free-surface flows for estuaries and coastal seas. In *Estuarine and coastal modeling* (1995), ASCE, pp. 1–12.

[32] Casulli, V., and Stelling, G. S. Numerical simulation of 3D quasi-hydrostatic, free-surface flows. *Journal of Hydraulic Engineering 124*, 7 (1998), 678–686.

[33] Casulli, V., and Walters, R. A. An unstructured grid, three-dimensional model based on the shallow water equations. *International journal for numerical methods in fluids 32*, 3 (2000), 331–348.

[34] Casulli, V., and Zanolli, P. Semi-implicit numerical modeling of nonhydrostatic free-surface flows for environmental problems. *Mathematical and computer modelling 36*, 9-10 (2002), 1131–1149.

[35] Chen, C. M., and Thomée, V. The lumped mass finite element method for a parabolic problem. *The ANZIAM Journal 26*, 3 (1985), 329–354.

[36] Chen, H. Effects of bottom friction and boundary absorption on water wave scattering. *Applied Ocean Research 8*, 2 (1986), 99–104.

[37] Chen, H., and Mei, C. Oscillations and wave forces in a man-made harbor in the open sea. In *Symposium on Naval Hydrodynamics, 10th, Proceedings, Pap and Discuss, Cambridge, Mass, June 24-28, 1974.* (1976), no. Proceeding.

[38] Chorin, A. J. Numerical solution of the Navier–Stokes equations. *Mathematics of computation 22*, 104 (1968), 745–762.

[39] Clamond, D., and Dutykh, D. Fast accurate computation of the fully nonlinear solitary surface gravity waves. *Computers & fluids 84* (2013), 35–38.

[40] Cockburn, B., Karniadakis, G. E., and Shu, C.-W. *Discontinuous Galerkin methods: theory, computation and applications*, vol. 11. Springer Science & Business Media, 2012.

[41] Codina, R. Stabilization of incompressibility and convection through orthogonal sub-scales in finite element methods. *Computer methods in applied mechanics and engineering 190*, 13-14 (2000), 1579–1599.

[42] Codina, R. Stabilized finite element approximation of transient incompressible flows using orthogonal subscales. *Computer Methods in Applied Mechanics and Engineering 191*, 39-40 (2002), 4295–4321.

[43] Dean, R. G., and Dalrymple, R. A. *Water wave mechanics for engineers and scientists*, vol. 2. World Scientific Publishing Company, 1991.

[44] Decoene, A. *Hydrostatic model for three-dimensional free surface flows and numerical schemes*. PhD thesis, Université Pierre et Marie Curie - Paris VI; Laboratoire Jacques-Louis Lions, 2006.

[45] Decoene, A., and Gerbeau, J.-F. Sigma transformation and ALE formulation for three-dimensional free surface flows. *International Journal for Numerical Methods in Fluids 59*, 4 (2009), 357–386.

[46] Decoene, A., and Maury, B. Moving meshes with freefem++. *Journal of Numerical Mathematics 20*, 3-4 (2012), 195–214.

[47] Dingemans, M. W. *Water wave propagation over uneven bottoms*, vol. 13. World Scientific, 1997.

[48] Donea, J., Giuliani, S., Laval, H., and Quartapelle, L. Finite element solution of the unsteady Navier–Stokes equations by a fractional step method. *Computer Methods in Applied Mechanics and Engineering 30*, 1 (1982), 53–73.

[49] Dukowicz, J. K., and Smith, R. D. Implicit free surface method for the Bryan–Cox–Semtner ocean model. *Journal of Geophysical Research: Oceans 99*, C4 (1994), 7991–8014.

[50] Eckart, C. The propagation of gravity waves from deep to shallow water. In *Gravity waves* (1952), p. 165.

[51] EDF R&D. *Telemac Modelling System. Theoretical Note and User Manual. Artemis Software Wave Agitation*, 2010.

[52] Engelman, M., Sani, R., and Gresho, P. The implementation of normal and/or tangential boundary conditions in finite element codes for incompressible fluid flow. *International Journal for Numerical Methods in Fluids 2*, 3 (1982), 225–238.

[53] Ern, A., and Guermond, J.-L. *Theory and practice of finite elements*, vol. 159. Springer Science & Business Media, 2013.

[54] Fenton, J. D., and McKee, W. On calculating the lengths of water waves. *Coastal Engineering 14*, 6 (1990), 499–513.

[55] Flanders, H. Differentiation under the integral sign. *The American Mathematical Monthly 80*, 6 (1973), 615–627.

[56] Fontana, L., Miglio, E., Quarteroni, A., and Saleri, F. A finite element method for 3D hydrostatic water flows. *Computing and Visualization in Science 2*, 2-3 (1999), 85–93.

[57] Formaggia, L., and Nobile, F. A stability analysis for the Arbitrary Lagrangian Eulerian formulation with finite elements. *East-West Journal of Numerical Mathematics 7* (1999), 105–132.

[58] Formaggia, L., and Nobile, F. Stability analysis of second-order time accurate schemes for ALE–FEM. *Computer methods in applied mechanics and engineering 193*, 39-41 (2004), 4097–4116.

[59] Forsythe, G., and Wasow, W. R. *Finite-Difference Methods for Partial Differential Equations, Applied Mathematical Series*. Wiley, New York, 1960.

[60] Fringer, O., Gerritsen, M., and Street, R. An unstructured-grid, finite-volume, nonhydrostatic, parallel coastal ocean simulator. *Ocean Modelling 14*, 3-4 (2006), 139–173.

[61] Ganesan, S., and Srivastava, S. ALE-SUPG finite element method for convection–diffusion problems in time-dependent domains: Conservative form. *Applied Mathematics and Computation 303* (2017), 128–145.

[62] Gary, J. Estimate of truncation error in transformed coordinate primite equation atmospheric models. *J. Atmso. Sci 30* (1973), 223–233.

[63] Ghresho, P., and Chan, S. On the theory of semi-implicit projection methods for viscous incompressible flow and its implementation via finite element method that also introduces a nearly consistent mass matrix. part i and part ii. *Int. J. Numer. Methods Fluids 11* (1990), 587–620.

[64] Girault, V., Nochetto, R. H., and Scott, L. R. Max-norm estimates for Stokes and Navier–Stokes approximations in convex polyhedra. *Numerische Mathematik 131*, 4 (2015), 771–822.

[65] Goda, K. A multistep technique with implicit difference schemes for calculating two-or three-dimensional cavity flows. *Journal of Computational Physics 30*, 1 (1979), 76–95.

[66] Green, A. E., and Rivlin, R. S. On Cauchy's equations of motion. *Zeitschrift für Angewandte Mathematik und Physik (ZAMP) 15*, 3 (1964), 290–292.

[67] Guermond, J., Minev, P., and Shen, J. An overview of projection methods for incompressible flows. *Computer methods in applied mechanics and engineering 195*, 44-47 (2006), 6011–6045.

[68] Guermond, J., P., M., and J., S. Error analysis of pressure-correction schemes for the time-dependent stokes equations with open boundary conditions. *SIAM Journal on Numerical Analysis 43*, 1 (2005), 239–258.

[69] Guermond, J., and Shen, J. On the error estimates for the rotational pressure-correction projection methods. *Mathematics of Computation 73*, 248 (2004), 1719–1737.

[70] Guermond, J.-L. Stabilization of galerkin approximations of transport equations by subgrid modeling. *ESAIM: Mathematical Modelling and Numerical Analysis 33*, 6 (1999), 1293–1316.

[71] Guermond, J.-L. Un résultat de convergence d'ordre deux en temps pour l'approximation des équations de Navier–Stokes par une technique de projection incrémentale. *ESAIM: Mathematical Modelling and Numerical Analysis 33*, 1 (1999), 169–189.

[72] Guermond, J.-L. Subgrid stabilization of galerkin approximations of linear monotone operators. *IMA Journal of Numerical Analysis 21*, 1 (2001), 165–197.

[73] Guermond, J.-L., and Pasquetti, R. A correction technique for the dispersive effects of mass lumping for transport problems. *Computer Methods in Applied Mechanics and Engineering 253* (2013), 186–198.

[74] Guermond, J.-L., and Quartapelle, L. On stability and convergence of projection methods based on pressure poisson equation. *International Journal for Numerical Methods in Fluids 26*, 9 (1998), 1039–1053.

[75] Hecht, F., Pironneau, O., Le Hyaric, A., and Ohtsuka, K. Freefem++ manual, 2005.

[76] Hervouet, J.-M. *Hydrodynamics of free surface flows, modelling with finite element method*. John Wiley & Sons Ltd., 2007.

[77] Hirt, C., Amsden, A., and Cook, J. An arbitrary lagrangian-eulerian computing method for all flow speeds. *J. Comput. Phys. 14(3)*, 227-253 (1974).

[78] Hodges, B. R. Numerical techniques in cwr-elcom (code release v. 1). *CWR Manuscript WP 1422* (2000).

[79] Huerta, A., and Liu, W. K. Viscous flow with large free surface motion. *Computer Methods in Applied Mechanics and Engineering 69*, 3 (1988), 277–324.

[80] Hughes, T. J., Franca, L. P., and Balestra, M. A new finite element formulation for computational fluid dynamics: V. circumventing the babuška-brezzi condition: A stable petrov-galerkin formulation of the stokes problem accommodating equal-order interpolations. *Computer Methods in Applied Mechanics and Engineering 59*, 1 (1986), 85–99.

[81] Hughes, T. J., Franca, L. P., and Hulbert, G. M. A new finite element formulation for computational fluid dynamics: Viii. the galerkin/least-squares method for advective-diffusive equations. *Computer methods in applied mechanics and engineering 73*, 2 (1989), 173–189.

[82] Hunt, J. N. Direct solution of wave dispersion equation. *Journal of the Waterway, Port, Coastal and Ocean Division 105*, 4 (1979), 457–459.

[83] Janjic, Z. Pressure gradient force and advection scheme used for forecasting with steep and small scale topography. *Contrib. Atmos. Phys 50*, 186-199 (1977).

[84] Jasak, H. Openfoam: open source cfd in research and industry. *International Journal of Naval Architecture and Ocean Engineering 1*, 2 (2009), 89–94.

[85] John, V. *Finite element methods for incompressible flow problems*. Springer, 2016.

[86] John, V., and Novo, J. Error analysis of the SUPG finite element discretization of evolutionary convection-diffusion-reaction equations. *SIAM Journal on Numerical Analysis 49*, 3 (2011), 1149–1176.

[87] Kanarska, Y., Shchepetkin, A., and McWilliams, J. Algorithm for nonhydrostatic dynamics in the regional oceanic modeling system. *Ocean Modelling 18*, 3-4 (2007), 143–174.

[88] Ku, H., Hirsh, R., and Taylor, T. A pseudospectral method for solution of the three-dimensional incompressible Navier–Stokes equations. *J. Comput. Phys. 70*, 439-462 (1987).

[89] Lai, Z., Chen, C., Cowles, G. W., and Beardsley, R. C. A nonhydrostatic version of fvcom: 1. validation experiments. *Journal of Geophysical Research: Oceans 115*, C11 (2010).

[90] Lannes, D. *The water waves problem: mathematical analysis and asymptotics*, vol. 188. American Mathematical Soc., 2013.

[91] Lee, S., and Salgado, A. J. Stability analysis of pressure correction schemes for the Navier–Stokes equations with traction boundary conditions. *Computer Methods in Applied Mechanics and Engineering 309* (2016), 307–324.

[92] Leroy, A. *A new incompressible SPH model: towards industrial applications*. PhD thesis, Université Paris-Est, 2014.

[93] Lesoinne, M., and Farhat, C. Geometric conservation laws for flow problems with moving boundaries and deformable meshes and their impact on aerolastic computations. *Comput. Methods Appl. Mech. Eng. 134* (1996), 71–90.

[94] Lesser, G. R., Roelvink, J. v., Van Kester, J., and Stelling, G. Development and validation of a three-dimensional morphological model. *Coastal engineering 51*, 8-9 (2004), 883–915.

[95] Li, B., and Anastasiou, K. Efficient elliptic solvers for the mild-slope equation using the multigrid technique. *Coastal Engineering 16*, 3 (1992), 245–266.

[96] Lozano, C., and Meyer, R. Leakage and response of waves trapped by round islands. *The Physics of Fluids 19*, 8 (1976), 1075–1088.

[97] Luettich Jr, R. A., Westerink, J. J., and Scheffner, N. W. ADCIRC: An Advanced Three-Dimensional Circulation Model forShelves, Coasts, and Estuaries. Report 1. Theory and Methodology of ADCIRC-2DDI and ADCIRC-3DL.DL. Tech. rep., Coastal Engineering Research Center Vicksburg MS, 1992.

[98] Mahadevan, A., Oliger, J., and Street, R. A nonhydrostatic mesoscale ocean model. part ii: Numerical implementation. *Journal of Physical Oceanography 26*, 9 (1996), 1881–1900.

[99] Marshall, J., Adcroft, A., Hill, C., Perelman, L., and Heisey, C. A finite-volume, incompressible Navier–Stokes model for studies of the ocean on parallel computers. *Journal of Geophysical Research: Oceans 102*, C3 (1997), 5753–5766.

[100] Maury, B. Characteristics ale method for the unsteady 3d Navier–Stokes equations with a free surface. *International Journal of Computational Fluid Dynamics 6*, 3 (1996), 175–188.

[101] Mei, C. C., Stiassnie, M., and Yue, D. K.-P. *Theory and Applications of Ocean Surface Waves: Part 1: Linear Aspects Part 2: Nonlinear Aspects*. World Scientific, 1989.

[102] Miglio, E., Quarteroni, A., and Saleri, F. Finite element approximation of quasi-3d shallow water equations. *Comput. Methods Appl. Mech. Engrg 174(3-4)* (1999), 355–369.

[103] Miglio, E., and Saleri, F. *An existence and uniqueness result for the 3D Shallow Water Equations. Internal Report n. 421/P.* Dipartimiento di Matematica Francesco Brioschi, Politecnico di Milano, 2000.

[104] Monaghan, J. J. Smoothed particle hydrodynamics. *Reports on progress in physics 68*, 8 (2005), 1703.

[105] Nakayama, T., and Mori, M. An eulerian finite element method for time-dependent free surface problems in hydrodynamics. *International Journal for Numerical Methods in Fluids 22*, 3 (1996), 175–194.

[106] Nielsen, P. Explicit formulae for practical wave calculations. *Coastal Engineering 6*, 4 (1982), 389–398.

[107] Oliger, J., and Sundstrom, A. Theoritical and practical aspects of some boundary value problems in fluid dynamics. *SIAM J. Applied Mathematics 35* (1978), 419–446.

[108] Paillere, H., and Deconinck, H. Compact cell vertex convection schemes on unstructured meshes. In *Problèmes non linéaires appliqués. Ecoles CEA-EDF-INRIA* (2000), pp. 91–139.

[109] Panchang, V. G., Pearce, B. R., Wei, G., and Cushman-Roisin, B. Solution of the mild-slope wave problem by iteration. *Applied Ocean Research 13*, 4 (1991), 187–199.

[110] Parés, C. Approximation de la solution des équations d'un modèle de turbulence par une methode de lagrange–galerkin. *Rev. Mat. Apl 15*, 2 (1994), 63–124.

[111] Pavan, S. *Nouveaux schémas de convection pour les écoulements à surface libre.* PhD thesis, Université Paris-Est, 2016.

[112] Phillips, N. A coordinate system having some special advantages for numerical forecasting. *J Meteorol 14* (1957), 184–185.

[113] Pironneau, O. On the transport-diffusion algorithm and its applications to the Navier–Stokes equations. *Numerische Mathematik 38*, 3 (1982), 309–332.

[114] Prohl, A. *Projection and quasi-compressibility methods for solving the incompressible Navier-Stokes equations.* Springer, 1997.

[115] Quarteroni, A., and Valli, A. *Numerical Approximation of Partial Differential E Springer Ser. Comput. Math. 23.* Springer-Verlag, Berlin, 1994.

[116] Rannacher, R. On Chorin's projection method for the incompressible navier-stokes equations. In *The Navier-Stokes equations II—theory and numerical methods.* Springer, 1992, pp. 167–183.

[117] Rauch, J. *Hyperbolic partial differential equations and geometric optics*, vol. 133. American Mathematical Soc., 2012.

[118] Reynolds, O., Brightmore, A. W., and Moorby, W. H. *Papers on Mechanical and Physical Subjects: The sub-mechanics of the universe*, vol. 3. The University Press, 1903.

[119] Roos, H.-G., Stynes, M., and Tobiska, L. *Robust numerical methods for singularly perturbed differential equations: convection-diffusion-reaction and flow problems*, vol. 24. Springer Science & Business Media, 2008.

[120] Science, F. *Flow-3d Theory manual.* Los Alamos, NM, 2002.

[121] Shchepetkin, A., and McWilliams, J. The regional ocean model system (ROMS): A split-explicit, free-surface, topography-following coordinate ocean model. *Ocean Modelling 9* (2005), 347–404.

[122] Shen, J. On error estimates of the projection methods for the Navier–Stokes equations: second-order schemes. *Mathematics of Computation of the American Mathematical Society 65*, 215 (1996), 1039–1065.

[123] Stokes, G. G. On the theory of oscillatory waves. *Transactions of the Cambridge Philosophical Society* (1880).

[124] Temam, R. Sur l'approximation de la solution des équations de Navier–Stokes par la méthode des pas fractionnaires ii. *Arch. Ration. Mech. Anal 33*, 377-385 (1969).

[125] Temam, R. *Navier–Stokes Equations: Theory and Numerical Analysis.* North-Holland, Amsterdam, 1984.

[126] Tezduyar, T. E. Stabilized finite element formulations for incompressible flow computations. In *Advances in applied mechanics*, vol. 28. Elsevier, 1991, pp. 1–44.

[127] Timmermans, L., Minev, P., and Van De Vosse, F. An approximate projection scheme for incompressible flow using spectral elements. *International journal for numerical methods in fluids 22*, 7 (1996), 673–688.

[128] Tsay, T.-K., and Liu, P. L. A finite element model for wave refraction and diffraction. *Applied Ocean Research 5*, 1 (1983), 30–37.

[129] Usmani, R. A. Inversion of a tridiagonal jacobi matrix. *Linear Algebra and its Applications 212*, 213 (1994), 413–414.

[130] Van Kan, J. A second-order accurate pressure-correction scheme for viscous incompressible flow. *SIAM J. Sci. Stat. Comput. 7 (3)* (1986), 870–891.

[131] Venezian, G. Direct solution of wave dispersion equation. *Journal of the Waterway Ports Coastal and Ocean Engineering Division ASCE 106*, 4 (1980), 501–502.

[132] Verfürth, R. Finite Element approximations on steady Navier–Stokes equations with mixed boundary conditions. *R.A.I.R.O, Mod Math. Anal. Numer 19* (1985), 461–475.

[133] Violeau, D. *Fluid mechanics and the SPH method: theory and applications.* Oxford University Press, 2012.

[134] Vitousek, S., and Fringer, O. B. Stability and consistency of nonhydrostatic free-surface models using the semi-implicit θ-method. *International Journal for Numerical Methods in Fluids 72*, 5 (2013), 550–582.

[135] Warren, I., and Bach, H. Mike 21: a modelling system for estuaries, coastal waters and seas. *Environmental Software 7*, 4 (1992), 229–240.

[136] Weinan, E., and Liu, J. Projection method I: Convergence and numerical boundary layers. *SIAM J. Numer. Anal. 32* (1995), 1017–1057.

[137] Whitham, G. B. *Linear and nonlinear waves*, vol. 42. John Wiley & Sons, 2011.

[138] Zakharov, V. E. Stability of periodic waves of finite amplitude on the surface of a deep fluid. *Journal of Applied Mechanics and Technical Physics 9*, 2 (1968), 190–194.

[139] Zhang, F. *The Schur complement and its applications*, vol. 4. Springer Science & Business Media, 2006.

[140] Zhang, Y., and Baptista, A. M. Selfe: a semi-implicit Eulerian–Lagrangian finite-element model for cross-scale ocean circulation. *Ocean modelling 21*, 3-4 (2008), 71–96.